

**Characterisation of ASYNAAPTIC 4: a novel
meiotic chromosome axis associated protein in
*Arabidopsis thaliana***

**By
Alice Rose Darbyshire**

A thesis submitted to
the University of Birmingham
for the degree of
DOCTOR OF PHILOSOPHY

School of Biosciences
College of Life and Environmental Sciences
University of Birmingham
August 2019

**UNIVERSITY OF
BIRMINGHAM**

University of Birmingham Research Archive

e-theses repository

This unpublished thesis/dissertation is copyright of the author and/or third parties. The intellectual property rights of the author or third parties in respect of this work are as defined by The Copyright Designs and Patents Act 1988 or as modified by any successor legislation.

Any use made of information contained in this thesis/dissertation must be in accordance with that legislation and must be properly acknowledged. Further distribution or reproduction in any format is prohibited without the permission of the copyright holder.

Abstract

Formation of genetic crossovers (COs) during prophase I of meiosis is essential for faithful segregation of chromosomes at anaphase I. As in many organisms, in *Arabidopsis thaliana*, CO number and distribution is non-random, and thus understanding the factors that influence CO localization is of great interest. One such factor is the chromosome axis: a proteinaceous meshwork that organizes the chromatin into a linear array of loops. Previous work has identified ASY1 and ASY3 (homologues of yeast Hop1 and Red1 respectively) as key constituents of the axis in *A. thaliana*.

In this study, we commence a functional analysis of novel chromosome axis associated protein ASY4, identified via immuno-affinity proteomics with ASY1. Using a range of cytological and molecular techniques including structured-illumination microscopy and CRISPR-Cas9, we confirm that ASY4 is required for normal fertility, CO number and maturation, axis structure, and synapsis in *A. thaliana*. Using both an antibody raised against ASY4 and ASY4 tagged with yellow fluorescent protein, we show that ASY4 is associated with the chromosome axis during prophase I of meiosis. We confirm that ASY4 is a direct interacting partner of core axis protein ASY3, and that this is potentially facilitated through the second coiled-coil domain of ASY4. Combined, this data shows ASY4 to be an essential component of the meiotic chromosome axis in *A. thaliana*, and highlights the importance of the axis structure in crossover formation.

“Education never ends, Watson. It is a series of lessons, with the greatest for the last.”

– Sherlock Holmes in *His Last Bow*, Sir Arthur Conan Doyle (1917).

For Mum & Dad

Acknowledgements

I would like to thank my supervisors, Prof. Chris Franklin and Dr Eugenio Sanchez-Moran, for giving me the opportunity to conduct this research. I am grateful for their expertise and support, and their encouragement to pursue things that interest me both in and out of the lab.

I also thank my lab mates who have been instrumental in helping me develop as a scientist: Allan West, Stefan Heckmann, and Chris Morgan, who taught me all I know about molecular biology and cytology; Marina Martinez-Garcia and Maria Cuacos for their useful conversations and kindness that never failed to brighten my day; and Kim Osman: one of the most patient and kind people I have met, with an extensive knowledge of science and meiosis that I have relied on all too often. I am also grateful to our support staff: Ruth Perry, Steve Price, Karen Staples, Andy Breckles, and the Central Services team. I am especially grateful for Steve's extra help over the final few months – I would have had a Much Less Good Time writing up without him minding the plants.

From outside our lab, I thank Iain Johnston for all his advice with writing, and for his infectious enthusiasm that made our discussions all the more exciting; Kirsten Bomblies for kindly allowing us to use the SIM at the John Innes Centre; Holger Puchta and Amy Whitbread for sharing CRISPR vectors and knowledge; our collaborators, Mathilde Grelon and her lab for sharing data and resources; George Bassel for careers advice and friendly conversation; and James Higgins from the University of Leicester for being a brilliant first supervisor. I also thank the past and present members of the Gibbs, Coates, Bassel, Johnston, Alderwick, and Grainger labs for always ensuring I remained appropriately socialised.

I also wish to thank Abigail Tura from Student Services, whose advice I continue to use every single day.

Finally, I would like to thank my friends and family for putting up with me over these last few years; I am quite sure this was not easy! I thank my parents for their unconditional love and support: my Mum, for always being the voice of reason, and encouraging me to do what I know is best; and my Dad, for sharing his view of space from his telescope, and igniting my desire to understand the universe a little better.

This PhD was funded by the Biotechnology and Biological Research Council (BBSRC) as part of the Midlands Integrative Biosciences Training Partnership (MIBTP).

Table of Contents

| | | |
|-------------|---|-----------|
| 1 | Introduction..... | 2 |
| 1.1 | An Overview of Meiosis | 2 |
| 1.2 | The Stages of Meiosis | 2 |
| 1.3 | Meiotic Recombination..... | 5 |
| 1.3.1 | Double Strand Break Initiation | 7 |
| 1.3.1.1 | Controlling DSB Formation..... | 8 |
| 1.3.1.1.1 | Location and Number of DSBs..... | 9 |
| 1.3.1.2 | DSB Processing and Formation and Single End Invasion | 11 |
| 1.3.2 | DSB Repair: COs and NCOs | 12 |
| 1.3.2.1 | CO/NCO Repair Decision..... | 13 |
| 1.3.2.2 | Crossover Formation..... | 16 |
| 1.3.2.2.1 | The Class I CO Pathway: ZMM Dependent | 16 |
| 1.3.2.2.1.1 | Class I CO Resolution | 20 |
| 1.3.2.2.2 | The Class II CO Pathway..... | 20 |
| 1.3.3 | Control of Meiotic Crossovers | 21 |
| 1.3.3.1 | CO Assurance and Homeostasis..... | 22 |
| 1.3.3.2 | CO Interference: localisation and distribution of COs | 22 |
| 1.3.3.2.1 | CO Hotspots | 22 |
| 1.3.3.2.2 | CO Interference | 24 |
| 1.4 | The Chromosome axis in meiosis | 26 |
| 1.4.1 | Axis Assembly | 29 |
| 1.4.2 | The Synaptonemal Complex and Axis Remodelling..... | 32 |
| 1.4.2.1 | SC Assembly..... | 33 |
| 1.4.3 | The Chromosome Axis and Recombination | 34 |
| 1.4.3.1 | DSBs..... | 34 |
| 1.4.3.2 | Crossovers..... | 35 |
| 1.4.3.2.1 | The Influence of the Axis..... | 35 |
| 1.4.3.2.2 | The Role of the SC | 36 |
| 1.5 | Meiosis Research and Food Security..... | 39 |
| 1.5.1 | The Food Security Crisis..... | 39 |
| 1.5.2 | Meiosis and Plant Breeding | 40 |
| 1.6 | Project Aims..... | 42 |
| 2 | Materials and Methods | 45 |
| 2.1 | Plant Material..... | 45 |
| 2.1.1 | Seed Sterilisation and Plant Selection | 45 |

| | | |
|---------|--|----|
| 2.1.2 | Seed Counts | 45 |
| 2.1.3 | Crossing <i>Arabidopsis thaliana</i> mutant lines..... | 46 |
| 2.2 | Nucleic Acid Extraction and Manipulation | 46 |
| 2.2.1 | DNA Extraction | 46 |
| 2.2.2 | DNA Extraction for Genotyping | 46 |
| 2.2.3 | RNA Extraction | 47 |
| 2.2.4 | Genotyping T-DNA Insertion Lines..... | 47 |
| 2.2.5 | RT-PCR | 48 |
| 2.2.6 | Spectrophotometry | 48 |
| 2.3 | General Cloning | 49 |
| 2.3.1 | Transformation of chemically competent <i>Escherichia coli</i> DH5 α via Heat Shock..... | 49 |
| 2.3.2 | Transformation of electrocompetent <i>Escherichia coli</i> DH5 α via Electroporation..... | 49 |
| 2.3.3 | Transformation of electrocompetent <i>Agrobacterium tumefaciens</i> GV3101 via Electroporation..... | 50 |
| 2.3.4 | Bacterial Selection | 50 |
| 2.3.5 | Colony PCR | 50 |
| 2.3.6 | Plasmid DNA Extraction..... | 51 |
| 2.3.7 | <i>Saccharomyces cerevisiae</i> Transformation via Polyethylene Glycol/Lithium Acetate | 51 |
| 2.3.7.1 | Yeast Media Preparation | 52 |
| 2.4 | Transforming <i>A. thaliana</i> with <i>Agrobacterium tumefaciens</i> via floral dipping | 52 |
| 2.5 | Yeast-2-Hybrid | 53 |
| 2.5.1 | Cloning into pENTR™/D-TOPO® and pDEST vectors..... | 53 |
| 2.5.2 | Yeast-2-Hybrid Assay | 55 |
| 2.6 | Targeted Gene Editing in <i>Arabidopsis thaliana</i> using the <i>Staphylococcus aureus</i> CRISPR-Cas9 system | 55 |
| 2.6.1 | Making the CRISPR-Cas9 ASY4 construct | 56 |
| 2.6.2 | Transforming <i>A. thaliana</i> with CRISPR-Cas9 | 58 |
| 2.6.3 | Selection and Identification of potential mutants | 59 |
| 2.6.3.1 | Genotyping the final asy4-4 mutant line..... | 59 |
| 2.7 | Cytology | 60 |
| 2.7.1 | DAPI Staining of Meioocytes..... | 60 |
| 2.7.2 | Fluorescence <i>in-situ</i> Hybridisation (FISH) of meiotic spreads | 61 |
| 2.7.2.1 | Probe Preparation for FISH | 62 |
| 2.7.3 | Spreading Immunolocalisation using Fresh Material | 63 |

| | |
|--|------------|
| 2.7.3.1 Modified Immunolocalisation protocol for Structured Illumination Microscopy (SIM)..... | 64 |
| 2.7.3.2 Staging buds using Aceto-Orcein | 65 |
| 2.7.4 Immunolocalisation on Acid-Fixed Material (Microwave Technique) | 65 |
| 2.7.5 Microscopy and Image Analysis..... | 66 |
| 2.8 Bioinformatics and Sequencing Analysis..... | 66 |
| 2.9 Statistics | 66 |
| 3 ASYNPATIC 4 is a novel component of the meiotic chromosome axis in <i>Arabidopsis thaliana</i>..... | 68 |
| 3.1 Introduction..... | 68 |
| 3.2 Results..... | 71 |
| 3.2.1 T-DNA insertions in <i>asy4</i> cause a reduction in fertility that correspond with errors during meiosis | 71 |
| 3.2.1.1 <i>asy4-1</i> and <i>asy4-2</i> produce a truncated ASY4 transcript..... | 72 |
| 3.2.1.2 <i>asy4-1</i> and <i>asy4-2</i> have reduced fertility and crossover number | 73 |
| 3.2.1.3 ASY1 localisation is abnormal in <i>asy4</i> | 80 |
| 3.2.1.4 Early recombination events appear normal in <i>asy4-1</i> | 81 |
| 3.2.2 Characterisation of an <i>asy4-1</i> line complemented with ASY4eYFP confirms that ASY4 is associated with the chromosome axis during meiosis..... | 83 |
| 3.2.2.1 An antibody raised against ASY4 suggests axis localisation | 83 |
| 3.2.2.2 Complementation of <i>asy4-1</i> with ASY4eYFP restores fertility, and increases CO number..... | 86 |
| 3.2.2.3 Complementation of <i>asy4-1</i> with ASY4eYFP restores synapsis | 90 |
| 3.2.2.4 ASY4eYFP signal is axis associated | 91 |
| 3.2.2.5 ASY4 loading requires ASY3..... | 93 |
| 3.2.3 ASY4eYFP structure appears abnormal in <i>pch2</i> | 97 |
| 3.2.4 ASY4 directly interacts with ASY3 in Yeast-2-Hybrid | 99 |
| 3.3 Discussion | 103 |
| 3.3.1 ASY4 is required for normal maturation of COs | 103 |
| 3.3.2 ASY4 is an integral component of the meiotic chromosome axis in <i>Arabidopsis thaliana</i> | 105 |
| 3.3.2.1 Immunolocalisation of ASY4 and ASY4eYFP | 105 |
| 3.3.2.2 Protein-Protein Interactions suggest ASY4 physically interacts with the axis..... | 107 |
| 4 Generation of an ASY4 mutant using the CRISPR-Cas9 gene editing system | 110 |
| 4.1 Introduction: Utilisation of the CRISPR-Cas System as a Gene Editing Tool..... | 110 |
| 4.1.1 Discovery and History | 110 |
| 4.1.2 CRISPR-Cas: an RNA-directed nuclease | 111 |

| | | |
|----------|--|------------|
| 4.1.3 | CRISPR-Cas9 in Gene Editing | 114 |
| 4.1.4 | Using CRISPR-Cas9 to generate a meiotic mutant in <i>A. thaliana</i> | 114 |
| 4.2 | Generation and Identification of candidate plant lines | 116 |
| 4.2.1 | Segregation of Cas9 and analysis of the resultant T2 progeny | 121 |
| 4.2.2 | Fertility analysis | 122 |
| 4.3 | CRISPR Line 20 shows a 1.7 kb deletion in ASY4 | 123 |
| 4.4 | Finalising the mutant line at T3 and T4 | 130 |
| 4.5 | Discussion | 132 |
| 4.5.1 | asy4-4 is a knock-out mutant of the ASY4 gene..... | 132 |
| 4.5.2 | CRISPR-Cas9 and Off-targets | 133 |
| 5 | Characterisation of a null-mutant of asy4 generated by CRISPR-Cas9 | 135 |
| 5.1 | Introduction..... | 135 |
| 5.2 | A 1.7 kb deletion in ASY4 results in a reduction in fertility and recombination | 135 |
| 5.2.1 | asy4-4 has reduced fertility but normal vegetative growth..... | 135 |
| 5.2.2 | An allelic test between asy4-1 and asy4-4 reveals the 4-1 and 4-4 insertion and edits affect the same gene | 141 |
| 5.2.3 | asy4-4 has a reduction in the number of chiasmata resulting in aneuploid tetrads | 142 |
| 5.3 | Axis organisation is compromised in asy4-4..... | 146 |
| 5.3.1 | Sister cohesion appears unaffected in asy4-4..... | 146 |
| 5.3.2 | ASY4 is required for normal ASY1 and ASY3 localisation..... | 147 |
| 5.3.3 | Extension of the synaptonemal complex is reduced in asy4-4 | 151 |
| 5.3.4 | ASY1 appears to be depleted from synapsed regions in asy4-4 | 151 |
| 5.3.5 | PCH2 appears to localise normally in asy4-4..... | 154 |
| 5.4 | Reduction in chiasmata in asy4-4 may be due to problems with CO maturation . | 156 |
| 5.4.1 | Early recombination events appear to progress normally in asy4-4..... | 156 |
| 5.4.2 | The number of HEI10 foci is significantly reduced in asy4-4 | 158 |
| 5.5 | An antibody raised against ASY4 gives no proper axis-associated signal in an asy4-null mutant..... | 159 |
| 5.6 | Discussion | 162 |
| 5.6.1 | ASY4 is required for normal fertility | 162 |
| 5.6.2 | Crossover number is reduced in all asy4 mutants | 163 |
| 5.6.3 | ASY4 and the chromosome axis | 164 |
| 5.6.4 | ASY4 is required for CO maturation | 166 |
| 6 | General Discussion | 172 |
| 6.1 | ASY4 as a chromosome axis component..... | 172 |

| | |
|--|------------|
| 6.1.1 ASY4 and axis organisation | 172 |
| 6.1.2 ASY3 and ASY4 as functional homologues of mammalian SYCP2 and SYCP3..... | 174 |
| 6.2 ASY4 and CO maturation..... | 176 |
| 6.3 ASY4 and PCH2 | 177 |
| 6.4 CRISPR-Cas9 is an effective way to produce novel mutations in meiotic genes . | 180 |
| 6.5 Future Research and Applications | 181 |
| 6.6 Summary | 183 |
| References | 185 |
| Appendix | 208 |
| Appendix for Chapter 2: Materials and Methods | 208 |
| Appendix for Chapter 3: ASYNAPTIC 4 is a novel component of the meiotic chromosome axis in <i>Arabidopsis thaliana</i> | 215 |
| Appendix for Chapter 4: Generation of ASY4 mutant lines using the CRISPR/Cas9 gene editing system | 221 |
| Appendix for Chapter 5: Characterisation of a null-mutant of <i>asy4</i> generated by CRISPR-Cas9..... | 224 |
| General Appendix: Presentations, Publications, Outreach, Teaching, and Awards..... | 228 |
| List of Oral Presentations | 228 |
| List of Poster Presentations | 228 |
| List of Publications | 229 |
| List of Teaching Experience..... | 229 |
| List of Outreach Actions | 230 |
| Awards | 231 |

List of Figures

| | |
|---|-----|
| Figure 1. 1 A Brief Overview of the Meiotic Programme | 3 |
| Figure 1. 2 Overview of the process of meiotic recombination..... | 6 |
| Figure 1. 3 The Meiotic Chromosome Axis and Synaptonemal Complex | 27 |
| Figure 1. 4 Proposed model of Axis Assembly | 31 |
| Figure 1. 5 The Tethered-loop model of DSB formation | 35 |
| | |
| Figure 3. 1 ASY4 ClustalW Alignment of ASY3 and ASY4 | 68 |
| Figure 3. 2 ASY4 gDNA Annotation..... | 70 |
| Figure 3. 3 Expression of ASY4 in various <i>Arabidopsis</i> tissues and <i>asy4</i> mutants..... | 73 |
| Figure 3. 4 DAPI stained PMCs from WT | 77 |
| Figure 3. 5 Chiasma number is significantly reduced in <i>asy4-1</i> and <i>asy4-2</i> | 78 |
| Figure 3. 6 Fluorescence <i>in situ</i> hybridisation (FISH) on a metaphase I spread from <i>asy4-1</i> | 79 |
| Figure 3. 7 Immunolocalisation of ASY1 in WT and <i>asy4-1</i> | 81 |
| Figure 3. 8 Immunolocalisation of MSH4 and MSH5 and comparison of number of foci..... | 82 |
| Figure 3. 9 Immunolocalisation of ASY4 relative to the SC and sister cohesion in wild-type <i>Arabidopsis thaliana</i> | 85 |
| Figure 3. 10 Seed Count data from <i>asy4</i> <i>Arabidopsis thaliana</i> mutants transformed with ASY4eYFP..... | 87 |
| Figure 3. 11 Comparison of distribution of chiasma number between Col-0 (WT), <i>asy4</i> :ASY4eYFP, and <i>asy4-1</i> | 88 |
| Figure 3. 12 DAPI-stained PMCs at metaphase I and Telophase II in <i>asy4</i> :ASY4eYFP | 89 |
| Figure 3. 13 DAPI-stained PMCs at Anaphase I. DAPI-stained male meiocytes | 89 |
| Figure 3. 14 Microwave immunolocalisation shows near complete synapsis is achieved in <i>asy4</i> :ASY4eYFP | 90 |
| Figure 3. 15 Spreading immunolocalisation on PMCs from <i>asy4</i> :ASY4eYFP confirms ASY4 is axis-associated during prophase I | 91 |
| Figure 3. 16 Large foci of ASY4eYFP are present on the axis and at the SC in some <i>asy4</i> :ASY4eYFP cells | 92 |
| Figure 3. 17 Immunolocalisation of ASY4eYFP using the anti-GFP antibody in an <i>asy3-1</i> mutant background | 94 |
| Figure 3. 18 Anthers from <i>asy3</i> :ASY4eYFP are fluorescent, confirming expression of the ASY4eYFP construct | 95 |
| Figure 3. 19 Zygote-stage cell from Col-0:ASY4eYFP | 96 |
| Figure 3. 20 Immunolocalisation of PMCs from <i>pch2-1</i> transformed with ASY4eYFP show aggregates of ASY4eYFP and ASY1 signal at the leptotene/zygotene transition | 98 |
| Figure 3. 21 Yeast-2-Hybrid shows ASY4 interacts with ASY3, potentially via its second coiled-coil..... | 102 |
| | |
| Figure 4. 1 Summary of how the CRISPR-Cas9 system produces a double strand break (DSB) in target DNA. | 113 |
| Figure 4. 2 Location of the <i>Staphylococcus aureus</i> CRISPR-Cas9 target sites in the genomic sequence of ASY4. | 117 |
| Figure 4. 3 Flow chart displaying the decisions made to establish the final <i>asy4-4</i> mutant line. | 119 |

| | |
|--|-----|
| Figure 4.4 Selection for lines presenting Mendelian segregation of the CRISPR-Cas9 construct via kanamycin resistance..... | 122 |
| Figure 4.5 Verification of a potential deletion in ASY4 via PCR screening with two sets of primers..... | 124 |
| Figure 4.6 Alignment of genomic ASY4 sequence with intergenic region and sequencing reads from 20.17 and 20.19 showing a ~1.7 kb deletion..... | 126 |
| Figure 4.7 PCR amplification of full-length ASY4..... | 127 |
| Figure 4.8 PCR detection of the ASY4 CRISPR/Cas9 construct in planta. | 128 |
| Figure 4.9 Seed count data for ASY4 CRISPR/Cas9 Line 20..... | 129 |
| Figure 4.10 Expression of ASY4 in wild-type and <i>asy4-4</i> mutant buds. Gel electrophoresis stained with ethidium bromide. Water control. Wild-type (WT). Two <i>asy4-4</i> T3 mutants: 25i and 25ii. Comparison of the 'short' transcript present in <i>asy4-1</i> and <i>asy4-2</i> , the full-length ASY4 transcript (long), and any possible transcript from the third exon through to the stop codon. No ASY4 transcript detectable in either of the <i>asy4-4</i> T3 mutants tested. | 131 |
| | |
| Figure 5.1 Comparison of vegetative growth between WT and <i>asy4-4</i> | 136 |
| Figure 5.2 Seed count and silique length data for WT (Col-0), <i>asy4-1</i> , and <i>asy4-4</i> | 137 |
| Figure 5.3 Seed count data from Col-0 control and three genotypes of <i>asy4-4</i> | 139 |
| Figure 5.4 Alexander Staining of pollen from WT, <i>asy4-1</i> and <i>asy4-4</i> | 140 |
| Figure 5.5 Seed count data from <i>asy4-1</i> , <i>asy4-4</i> , and <i>asy4-1/asy4-4</i> | 142 |
| Figure 5.6 Comparison of the meiotic stages between <i>asy4-4</i> and WT. | 144 |
| Figure 5.7 Chiasma counts in PMCs from WT, <i>asy4-1</i> and <i>asy4-4</i> | 145 |
| Figure 5.8 Immunolocalisation of SMC3 and SYN1 during prophase I in WT and <i>asy4-4</i> | 147 |
| Figure 5.9 Immunolocalisation of ASY1 and ASY3 during prophase I in WT and <i>asy4-4</i> | 148 |
| Figure 5.10 Immunolocalisation of the chromosome axis during prophase I in PMCs from WT and <i>asy4-4</i> | 150 |
| Figure 5.11 Immunolocalisation of the chromosome axis and synaptonemal complex in PMCs from WT and <i>asy4-4</i> | 153 |
| Figure 5.12 Total SC length measurements in WT and <i>asy4-4</i> . (A-D) 3D-rendering of ZYP1 signal in prophase I PMCs | 154 |
| Figure 5.13 Immunolocalisation of PCH2 and ZYP1 in prophase I PMCs from WT and <i>asy4-4</i> | 155 |
| Figure 5.14 Immunolocalisation of DMC1 and comparison of the number of foci. | 157 |
| Figure 5.15 Immunolocalisation of MSH4 and comparison of the number of foci..... | 158 |
| Figure 5.16 Immunolocalisation of HEI10 and comparison of the number of foci.. | 159 |
| Figure 5.17 Immunolocalisation of the chromosome axis with SYN1 and ASY4 in WT and <i>asy4-4</i> | 161 |
| | |
| Figure 6. 1 Chromosome axis assembly and remodelling in WT and two <i>asy4</i> mutants.... | 184 |
| | |
| Figure A 1 Vector maps for pEn-Sa-Chimera (A) and pDe-Sa-Cas9 (B). | 212 |
| Figure A 2 DAPI stained metaphase I cells from <i>asy4-1</i> and <i>asy4-2</i> displaying connections. | 215 |

| | |
|--|-----|
| Figure A 3 Immunolocalisation with ASY4 antibody in two T-DNA insertion mutants for <i>asy4</i> gives a strong axis-associated signal..... | 216 |
| Figure A 4 DAPI stained metaphase I cells from <i>asy4-1</i> displaying chromosome fragments..... | 216 |
| Figure A 5 Locations of Y2H primer sets for the ASY3 coiled-coil domain..... | 218 |
| Figure A6 Replicate plates from the Y2H experiments..... | 220 |
| Figure A 7 Detection of the CRISPR/Cas9 construct <i>in planta</i> via PCR..... | 221 |
| Figure A 8 Seed count data from T2 ASY4 CRISPR-Cas9 lines..... | 222 |
| Figure A 9 The ~1.7 kb deletion in ASY4 should not interfere with genes on the reverse strand..... | 223 |

List of Tables

| | |
|---|-----|
| Table 2. 1 Incubation times for TOPO reactions | 54 |
| Table 2. 2 Components required for the ligation of annealed oligonucleotide pairs into the entry vector, pEN-Sa-Chimera..... | 57 |
| Table 2. 3 Components required for the CRISPR Gateway reaction. | 58 |
| | |
| Table 6. 1 Comparison of several axis mutants in <i>Arabidopsis thaliana</i> | 178 |
| | |
| Table A 1. T-DNA insertion lines used in this study..... | 208 |
| Table A 2. List of primers used for genotyping T-DNA lines..... | 208 |
| Table A 3. Primers used in RT-PCR..... | 209 |
| Table A 4. Primers used in the Yeast-2-Hybrid experiments..... | 210 |
| Table A 5. Concentrations for antibodies used in Western Blotting..... | 211 |
| Table A 6. Oligonucleotide pairs and primers used in CRISPR/Cas9 | 213 |
| Table A 7. Concentrations for antibodies used in immunolocalisation | 214 |
| Table A 8.. Primers used to PCR screen for ASY4 over-expression lines..... | 214 |
| Table A 9. Counts of MSH4/MSH5 foci on <i>asy4-1</i> . Counts were performed using the NIS Elements software..... | 217 |
| Table A 10. Total SC length data for Col-0 (WT) and <i>asy4-4</i> | 224 |
| Table A 11. DMC1 foci data for Col-0 (WT) and <i>asy4-4</i> | 224 |
| Table A 12. MSH4 foci data for Col-0 (WT) and <i>asy4-4</i> | 226 |
| Table A 13. HEI10 foci data for Col-0 (WT) and <i>asy4-4</i> | 227 |

List of frequently used abbreviations**BF** Beam-film model of crossover interference**CO** Crossover**CRISPR** Clustered Regularly Interspaced Short Palindromic Repeats**DNA** Deoxyribonucleic acid**DSB** Double-strand break**eYFP** Enhanced Yellow Fluorescent Protein**HR** Homologous Recombination**IHR** Inter-homologue Repair**NCO** Non-crossover**PMCs** Pollen Mother Cells**PPI** Protein-Protein Interactions**SC** Synaptonemal complex**SIM** Structured-Illumination Microscopy**TF** Transverse filament

Chapter 1

Introduction

1 Introduction

1.1 An Overview of Meiosis

In sexually reproducing organisms, meiosis is an essential cell division responsible for maintaining the ploidy level of the species, and for introducing genetic variation (Kerr *et al.*, 2012). Both are achieved by the process of inter-homolog recombination (IHR), which results in the formation of genetic crossovers (COs) (reviewed in *Arabdiopsis* in Osman *et al.*, 2011).

The meiotic programme is split into two divisions, following one round of DNA replication. Meiosis I is termed the ‘reductional’ division, where homologous chromosomes are separated. The second is the ‘equational’ division, where the sister chromatids, held together since replication, are pulled apart. The products of meiosis are therefore four genetically non-identical haploid gametes. This is in contrast with mitosis, where two genetically identical sister cells are produced (reviewed in McIntosh, 2016).

1.2 The Stages of Meiosis

In common with mitosis, the process of meiosis I is split into several cytologically distinct phases: prophase, metaphase, anaphase, and telophase. In meiosis II, stages consist of a dyad (two-cell) stage, followed by metaphase II, anaphase II, and telophase II, culminating in the formation of the final tetrad of cells.

As in other organisms, in *Arabidopsis thaliana*, prophase I takes the longest time to complete, accounting for c. 30 hours of the total 33 hours it takes to reach the end of meiosis II (Armstrong *et al.*, 2003). Prophase I is divided further into five sub-stages: leptotene, zygotene, pachytene, diplotene, and diakinesis (Figure 1.1).

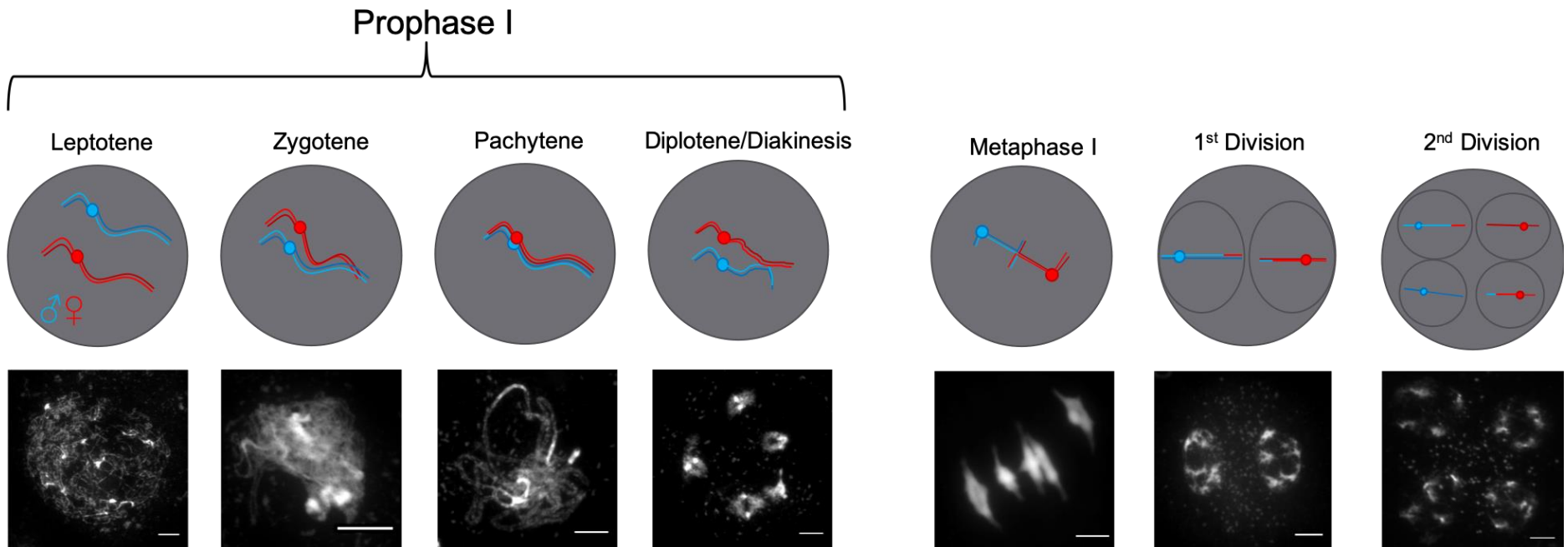


Figure 1.1 A Brief Overview of the Meiotic Programme. DAPI stained meiocytes from *Arabidopsis thaliana* PMCs. Diagrams illustrate the conformation of the chromosomes during each stage shown. Bar = 5 μ m.

Leptotene occurs after S-phase and meiotic G2. During S-phase, the DNA is replicated, resulting in each chromosome consisting of two sister chromatids held together by the cohesin complex. The cohesins form the base of what will become the meiotic chromosome axis, and will continue to hold the sister chromatids together until anaphase II (Cai *et al.*, 2003; Lam *et al.*, 2005; Strunnikov *et al.*, 1993).

As the cells exit G2 and enter leptotene, the meiotic chromosome axis commences extension along the chromosomes. Cytologically, the chromatin begins to appear more discrete than at earlier stages as the chromatin is elaborated into a linear array of loops, constrained at the bases by the axis meshwork (reviewed in: Kleckner, 2006). In *Arabidopsis*, this is characterised by the installation and extension of two key axis-associated proteins, ASY1 and ASY3 (Armstrong *et al.*, 2002; Caryl *et al.*, 2000; Ferdous *et al.*, 2012). As zygotene commences and progresses, the chromosomes that have successfully identified their homologs begin to synapse, as is indicated by the formation of the synaptonemal complex (SC): a tripartite structure comprised of the central transverse filament (TF) protein ZYP1 in *Arabidopsis*, and the axial elements, termed as the ‘lateral elements’ in the context of the SC (Higgins *et al.*, 2005). Once synapsis is complete along all chromosome pairs, the cell is defined as having reached pachytene. This stage is defined by its thick, rope-like chromosomes that represent the paired homologs in close apposition. In immunolocalisation studies, this stage is notable for the presence of a fully extended ZYP1 signal, with ASY1 appearing more diffuse (Armstrong *et al.*, 2002; Higgins *et al.*, 2005; Lambing *et al.*, 2015). From pachytene, further remodelling of the axis occurs with the removal of the SC at diplotene, at which point the homologues are held together at chiasmata. Condensation of the chromatin then compacts the chromosomes down into discrete bivalents which can align on the equatorial plate of the cell at metaphase I. At this

stage, chiasma can be identified and counted (Jahns *et al.*, 2014; Sanchez Moran *et al.*, 2001).

Homologous chromosomes are then pulled apart by the spindle at anaphase I, which eventually results in the two-cell dyad stage. Through a further division in meiosis II, sister chromatids finally separate, and the four resultant daughter cells are visible as a tetrad (Figure 1.1).

This global remodelling of chromosomes during prophase I is contemporaneous with the progression of meiotic recombination: the process by which COs are formed. This process commences with the initiation of pre-programmed double-strand breaks (DSBs) in DNA during leptotene, and their subsequent repair, which is complete by the end of pachytene. The process of recombination is tightly regulated, as will be explored later. High levels of regulation are necessary not only because DSBs are highly genotoxic if they go unrepaired, but also because various meiotic mutant studies have revealed that errors during IHR can lead to chromosomes failing to locate and synapse with their partner, and thus ultimately fail to align correctly at metaphase I. Incorrect alignment at metaphase I may then lead to incorrect separation at anaphase I. This is termed ‘non-disjunction’, and is thought to arise due to the inability of the meiotic spindle to orient chromosomes by a mechanism that senses a tension ‘threshold’ when the bivalents, attached by chiasmata, are correctly aligned (Forejt, 2001; Lampson and Cheeseman, 2011).

The process of meiotic recombination itself will now be discussed in detail.

1.3 Meiotic Recombination

An overview of the process of meiotic recombination is presented in Figure 1.2.

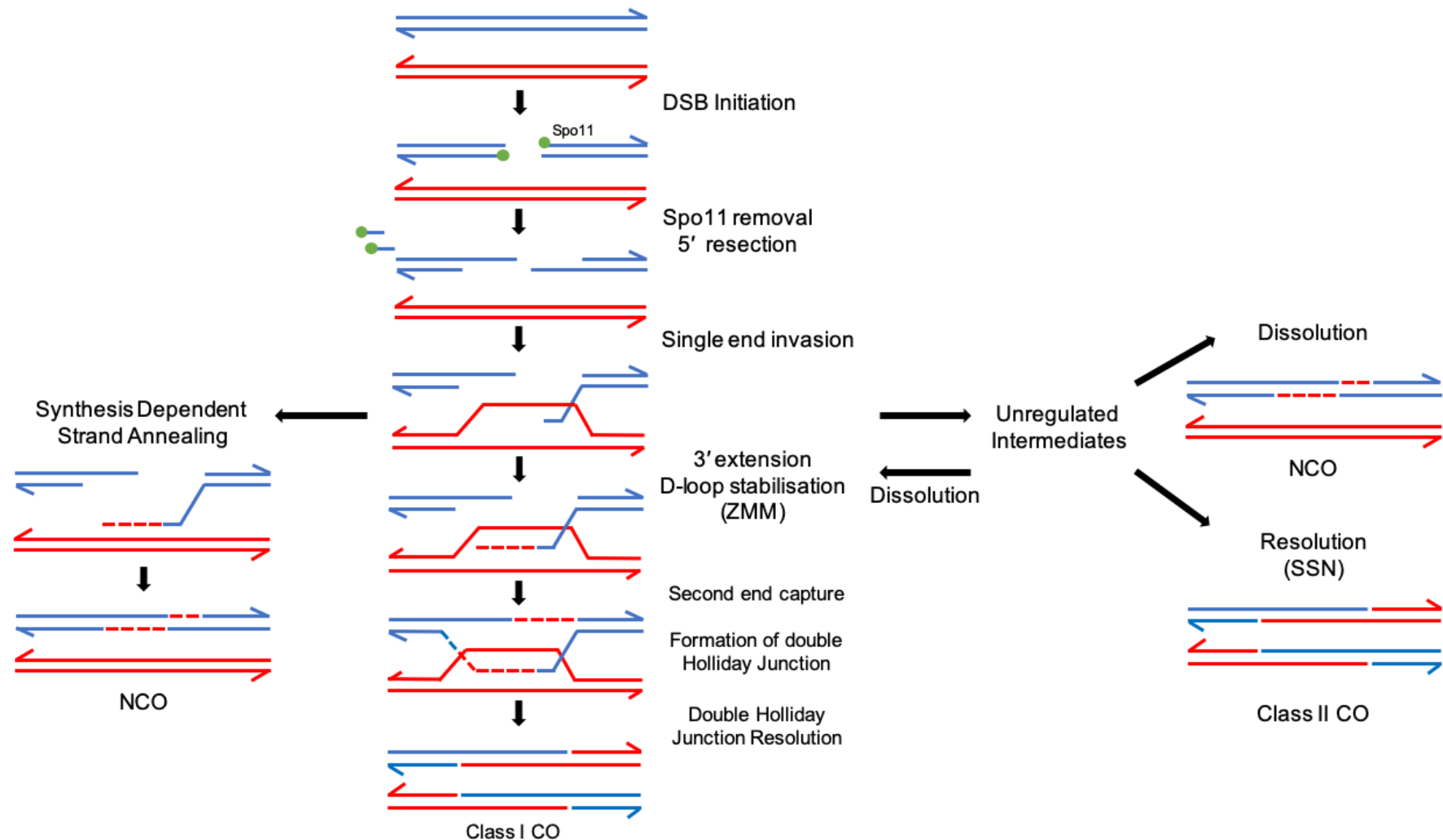


Figure 1.2 Overview of the process of meiotic recombination. Main pathways to resolving pre-programmed double strand breaks in DNA. Modified from Osman et al., 2011.

1.3.1 Double Strand Break Initiation

Inter-homolog recombination commences with the formation of double strand breaks (DSBs) in DNA at pre-programmed locations termed ‘DSB hotspots’ (reviewed in: Petes, 2001). In *Arabidopsis*, between 250 and 300 DSBs are formed per cell (reviewed in: Serrentino and Borde, 2012). DSBs are created by a transesterification reaction, catalysed by Spo11: an archaeal topoisomerase-VI subunit A-like protein (Bergerat *et al.*, 1997; Keeney *et al.*, 1997). In *Arabidopsis*, Spo11 has three non-functionally redundant homologues: SPO11-1, SPO11-2, and SPO11-3 (Grelon *et al.*, 2001; Hartung and Puchta, 2000; Stacey *et al.*, 2006). Whilst SPO11-3 is only required for somatic development, both the active Tyr-103 in SPO11-1 and Tyr-124 in SPO11-2 are required to catalyse DSB formation (Hartung *et al.*, 2007b). The three SPO11 genes are common to all land plants, but only homologues of SPO11-1 are present in animals and fungi (Sprink and Hartung, 2014). The more recent discovery of AtMTOPVIB, which is also essential for DSB induction, has also shown that SPO11-1 and SPO11-2 work in a heterodimer, the formation of which is dependent on AtMTOPVIB (Robert *et al.*, 2016; Vrielynck *et al.*, 2016).

In *Saccharomyces cerevisiae*, Spo11 works with a combination of other proteins, including Mre11, Xrs2, Rad50, Ski8, Rec102, Rec104, Rec114, Mer2, and Mei4 (reviewed in: Borde and de Massy, 2013). As in *S. cerevisiae*, SPO11 does not work alone in initiating DSBs in *Arabidopsis*. The other accessory proteins identified thus far to work with AtSPO11 are: AtPRD1, AtPRD2, AtPRD3, AtDFO, and AtSWI1, some of which have homologs in *S. cerevisiae* (De Muyt *et al.*, 2007; Mercier *et al.*, 2001; Muyt *et al.*, 2009; Zhang *et al.*, 2012). AtPRD1 is a homologue of Mei1 from mammals and yeast; AtPRD2 is a functional orthologue of Mei4; and AtPRD3 is a homologue of OsPAIR1 in rice, and appears to be specific to plants (Nonomura *et al.*, 2004). AtDFO

and AtSWI1 are also specific to plants. AtRAD50, AtMRE11 and a Ski8 orthologue have also been identified in *Arabidopsis*, but are non-essential for DSB formation (Jolivet *et al.*, 2006; Osman *et al.*, 2011).

1.3.1.1 Controlling DSB Formation

Given the toxic nature of DSBs, their timing, location, and number are tightly controlled. DSB formation commences between 1.5 and 2 h after DNA replication in *S. cerevisiae*, and between 1 and 5 h after replication in *A. thaliana* (Borde *et al.*, 2000; Sanchez-Moran *et al.*, 2007). Timing is thought to be controlled in a number of ways.

Firstly, the expression of meiotic genes – including those involved in DSB production – increases during the appropriate stage of meiosis. For example, in *Schizosaccharomyces pombe* and *Caenorhabditis elegans*, Spo11 is only expressed during meiosis (Atcheson *et al.*, 1987; Dernburg *et al.*, 1998; Lin and Smith, 1994). In *A. thaliana*, it appears that whilst SPO11 is transcribed in non-meiotic cells, it is inactive, most likely due to alternative splicing (Sprink and Hartung, 2014), *i.e.*, only during meiosis are meiotic transcripts spliced efficiently such that they can carry out their role. In budding yeast, meiosis specific splicing factors have been identified, and it has been suggested that Mei4 is required to promote efficient splicing of Rem1: a cyclin necessary for normal recombination (Malapeira *et al.*, 2005). It has also been shown that Mer2 is transcribed during meiosis and mitosis, but is only spliced to become active during meiosis, and that this is dependent on Mer1 (Engebrecht *et al.*, 1991). As Mer2 is needed for Spo11 induced DSBs, DSB licencing could only occur once Mer2 had been efficiently spliced at the onset of meiosis. That the meiotic programme is coupled with a large-scale alteration in splicing has also been documented in *Mus musulus* (Schmid *et al.*, 2013), suggesting splicing is a conserved mechanism of controlling the timing of recombination and DSB induction.

Licencing of DSBs in budding yeast also depends on the S-phase cyclin dependent kinases CDK-S, and DDK: a member of the replication fork protection complex (Wan *et al.*, 2008). To become active, Mer2 requires phosphorylation first by CDK-S, and subsequently by DDK. Crucially, CDK-S and DDK are most active after DNA replication, which is when DSBs begin to form during leptotene; this therefore couples DSB induction to DNA replication, and sets the sequence of events to occur one after the other (Wan *et al.*, 2008). In species with larger genomes such as Barley, there is a 2 h delay between replication in the distal regions of the chromosomes, and the more proximal regions (Higgins *et al.*, 2012). The roles of these kinases could therefore provide an efficient method via which DSBs cannot be induced before replication has occurred, and this would be of particular importance in an organism such as Barley. Though, thus far, this particular mechanism of regulation has not been demonstrated in plants.

1.3.1.1.1 Location and Number of DSBs

Where a DSB is formed on the chromosome, and how many are made, is predetermined and non-random. In *S. cerevisiae*, around 160 DSBs are made per meiosis (Panizza *et al.*, 2011). This value remains constant in mutants with elevated levels of Spo11 (Neale *et al.*, 2005). This is via a process termed ‘DSB homeostasis’, and the fact that this buffering exists highlights the importance of forming the correct number of DSBs. In *S. cerevisiae*, DSB homeostasis is at least in part governed by the kinases Tel1 and Mec1, homologs of plant and mammalian ATM/ATR respectively, and are part of the DNA Damage Response (DDR) machinery (Carballo *et al.*, 2013). In *M. musculus* and *Drosophila melanogaster*, it has been demonstrated that once DSBs are formed, the DDR machinery becomes active. Specifically, ATM activity increases, which then phosphorylates its targets, and thereby prevents further DSB formation

(Joyce *et al.*, 2011; Lange *et al.*, 2011). In yeast, one such target is Rec114: part of the RMM complex. Once Rec114 is phosphorylated, its activity decreases, and the formation of more DSBs is restricted (Carballo *et al.*, 2013). This has not been demonstrated in *A. thaliana*, but it is possible that this is still the case, as a Rec114 homolog has been identified (AtPHS1) with having a meiotic role, and *A. thaliana* also possesses ATM/ATR (Ronceret *et al.*, 2009).

As mentioned, DSBs form in locations termed ‘hotspots’: regions of approximately 200 bp in length at GC sites, away from the AT-rich axis-associated sites. Notably, in *S. cerevisiae*, DSBs usually occur within gene promoters (Berchowitz *et al.*, 2009). Gene promoters in *S. cerevisiae* are nucleosome depleted regions (NDRs), marked by the presence of fewer histones, and more open chromatin marks. 88% of *S. cerevisiae* DSBs occur in these NDRs (Berchowitz *et al.*, 2009). Open chromatin marks such as trimethylation of lysine four of histone three (H3K4me3) has been noted to be associated with DSB hotspots in budding yeast (Borde *et al.*, 2009; Pan *et al.*, 2011). In *S. cerevisiae*, H3K4me3 is deposited by Set1, and knocking out the *Set1* gene results in both fewer DSBs, and different DSB localisation (Borde *et al.*, 2009). In *A. thaliana*, H3K4me3 is thought to be deposited by the *SET DOMAIN* group of proteins, including AtSDG2: a protein essential for normal pollen development (Berr *et al.*, 2010). So far, no link has been conclusively proven between loss of SDG2 and any change in DSB localisation or number, but given the recent studies in plants showing no obvious link between DSBs and H3K4me3, this is perhaps unsurprising (Choi *et al.*, 2018; He *et al.*, 2017). Current data does suggest, however, that CO localisation is altered in these *sdg2* knockout lines, which may or may not reflect an alteration in DSB hotspot localisation (West, 2015).

Localisation of DSBs in mammals, however, is different to yeast and plants. Instead of occurring predominantly in promoters, mammalian DSBs occur in intergenic regions, including transcription start sites (TSS). Hotspots are reported to be in some way linked to H3K4me3, but it is proposed that other factors including the genome architecture also need to ‘favour’ the formation of DSBs as H3K4me3 alone is not necessarily a reliable indicator of DSB formation (Lange *et al.*, 2016). Nonetheless, the altered location in mammals compared to plants and yeast is predominantly due to the zinc-finger containing PRDM9: a protein that has the capability to deposit H3K4me3 marks (Baudat *et al.*, 2010). In mouse, 73% of hotspots contain the PRDM9 consensus sequence, and knocking out PRDM9 results in DSBs reverting to a similar location to that in yeast. This suggests that gene promoters are a default location for DSB formation (Baudat *et al.*, 2010; Smagulova *et al.*, 2016).

1.3.1.2 DSB Processing and Formation and Single End Invasion

As it forms the DSB, Spo11 becomes covalently bound to the 5' end of the DNA, and so for the break to be repaired, Spo11 must first be removed, and the DNA resected. In *S. cerevisiae*, the MRX-N complex, containing Mre11, Rad50, and Xrs2/Nbs1, along with Com1/Sae2, completes removal of Spo11 (reviewed in: Lam and Keeney, 2014).

Resection of the overhangs at the break site is conducted by Sgs1-Dna2, and Exo1 (Mimitou and Symington, 2009). The result of DSB resection is a long 3' end tract of single stranded DNA that, in *S. cerevisiae*, is loaded by Replication Protein A (RPA) and Rad52, which protects the ends from degradation (Gasior *et al.*, 1998; Soustelle *et al.*, 2002). In *Arabidopsis*, RPA has five homologs, yet no binding of ssDNA has been demonstrated, and RNAi mutants of AtRAD52 show phenotypes consistent with meiotic defects, but no conclusive role has been determined (Aklilu *et al.*, 2014; Samach *et al.*, 2011; Shultz *et al.*, 2007). In *S. cerevisiae*, RPA and Rad52, along with

accessory proteins Rad54, Tid1/Rdh54, Mei5-Sae3, and Hop2-Mnd1 allow for the loading of the RecA-related recombinases Rad51 and Dmc1, creating a nucleoprotein filament that can commence the search for its homologue (Chan *et al.*, 2014; Cloud *et al.*, 2012; Ferrari *et al.*, 2009; Hayase *et al.*, 2004; Miné-Hattab and Rothstein, 2012; Nimonkar *et al.*, 2012). Successful single end invasion (SEI) of the homologous chromosome by this nucleoprotein filament results in the formation of a nascent displacement loop (D-loop) structure, and the formation of the pre-synaptic filament, which will later be cytologically visible as an inter-axis bridge (Dubois *et al.*, 2019; Gasior *et al.*, 1998; this thesis in *Arabidopsis*). Recombination-associated DNA synthesis may then occur, thus forming an extended D-loop structure. At this point, the second end may go on to be captured, and form a double Holliday junction (dHJ), or could be disrupted by either SRS or Srs2 (discussed below) (Holliday, 1964; Piazza *et al.*, 2019).

In plants, AtDMC1, AtRAD51, AtRAD51C, and AtXRCC3 all appear to have a role in meiotic DSB repair, with DMC1 and RAD51 acting as the essential components for facilitating formation of the nucleoprotein filament, and directing the homology search. Loading of DMC1 and RAD51 appears to be promoted by AtBRACA2, and DMC1 itself may require RAD51 for normal localisation (Kurzbauer *et al.*, 2012; Seeliger *et al.*, 2012; Siaud *et al.*, 2004).

1.3.2 DSB Repair: COs and NCOs

Ultimately, meiotic DSBs will either be repaired as a crossover (CO), resulting in a reciprocal exchange of genetic content, or as a non-crossover (NCO), resulting in the non-reciprocal exchange of DNA.

1.3.2.1 CO/NCO Repair Decision

A key question in meiosis research has related to how the decision of whether to resolve a recombination intermediate as a CO or as an NCO is made. Studies in budding yeast have shed some light on the timing of this process, with many favouring the proposal of an ‘Early CO decision’ (ECD) model (Allers and Lichten, 2001; Börner *et al.*, 2004). This stipulates that the decision of whether to repair a recombination intermediate as a CO or NCO is made prior to dHJ resolution, possibly as early as the point at which a stable single end invasion intermediate is made. This is based on the observation that yeast *zmm* mutants (*mer3*, *msh5*, *zip1*, *zip2*, *zip3*) had reduced levels of COs (following a reduction in the number of stable SEI intermediates and dHJs), but DSB production and NCO resolution was unaffected (Börner *et al.*, 2004). This suggested that the decision to repair a DSB as a CO must come before the establishment of dHJs, in contrast to the previously proposed DNA double strand break repair (DSBR) model. DSBR proposed that the orientation in which a dHJ was resolved could yield either a CO or NCO, and so the CO/NCO decision would be made at this point (Bell and Byers, 1983; Holliday, 1964; Szostak *et al.*, 1983). Later research that led to the proposal of the ECD found that, via physical detection methods of recombination intermediates, the isolated structures did not fit with the idea that a proportion of dHJs were resolved as NCOs. This research went further to propose that, at least in yeast, it is likely that all dHJs are pre-CO intermediates (Allers and Lichten, 2001; Gilbertson and Stahl, 1996; Porter *et al.*, 1993). Furthermore, intermediates analysed from the *zmm* mutants revealed that there was a delay in progression of recombination intermediates post-DSB, but pre-SEI. This led to the conclusion that SEIs are likely CO-specific, and given that NCOs were still produced

normally in these mutants, these DSBs had likely already been designated as COs (Hunter and Kleckner, 2001).

Based on these observations, it was therefore proposed that NCOs arose through a distinct pathway in *S. cerevisiae*, namely, synthesis dependent strand annealing (SDSA) (McMahill *et al.*, 2007; Nassif *et al.*, 1994; Resnick and Martin, 1976). This is where a D-loop is dissolved after a short stretch of DNA has been synthesised, resulting in a non-reciprocal genetic exchange. Whilst yeast appear to primarily utilise the SDSA pathway to resolve its NCOs, this does not appear to be obvious in plants. It is suggested that SDSA could result in gene conversion (GC) tracts, resulting from the non-reciprocal nature of the DSB repair (McMahill *et al.*, 2007). In plants, however, there is no obvious evidence of GC occurring at a detectable level; but it is nonetheless possible that the NCOs in plants merely result in very short GC tracts (Drouaud *et al.*, 2013; Wijnker *et al.*, 2013). This could also be consistent with the idea of the majority of NCOs in plants arising from early dissolution of unregulated joint molecules, or from inter-sister repair, which may also be difficult to detect. Supporting this latter idea, no chromosome fragmentation was observed in IHR-defective *Atdmc1* and *Atasy1* mutants, suggesting that inter-sister repair is actively utilised during *Arabidopsis* meiosis (Couteau *et al.*, 1999; Sanchez-Moran *et al.*, 2007).

The decision to direct a D-loop toward an NCO or a CO in yeast is in part controlled by the STR complex, comprised of Sgs1, Top3, and Rmi1, along with helicases Mph1 (a relative of human FANCM) and Srs2, modulated by Rdh54 (Mazón and Symington, 2013; Mitchel *et al.*, 2013; Piazza *et al.*, 2019; Prakash *et al.*, 2009; Sun *et al.*, 2008; Tang *et al.*, 2015; Tay *et al.*, 2010). It is thought that these proteins can disassemble distinct D-loop structures, including those that may have otherwise been directed down the Class II CO route (such as abnormal joint molecules) to be processed by the

structure specific endonucleases (SSN; **1.3.2.2.2**). Successfully dissolved intermediates may then form an NCO via SDSA, or become a Class I CO if captured and stabilised by the ZMM complex. If the joint molecule persists/escapes this level of regulation, it may be resolved as a Class II CO (see **1.3.2.2.2**) (Kaur *et al.*, 2015).

In *Arabidopsis*, it is not exactly clear at which point the CO/NCO decision is made. An analogous system to yeast does appear to be present, however. The proteins involved in these processes are referred to as ‘anti-recombinases’, and include the RTR complex (AtRMI1/BLAP75, AtTOP3 α , and AtRECQ4A, AtRECQ4B); AtFANCM and its DNA-binding cofactors AtMHF1 and AtMHF2; and AtFIGL1 with its partner AtFLIP (Chelysheva *et al.*, 2008; Crismani *et al.*, 2012; Fernandes *et al.*, 2018; Girard *et al.*, 2014; Hartung *et al.*, 2008, 2007a; Higgins *et al.*, 2011; Knoll *et al.*, 2012; Séguéla-Arnaud *et al.*, 2017, 2015). These factors limit the levels of COs by either acting to unwind particular joint molecules/recombination intermediates (RTR, FANCM, limiting COs produced by the Class II pathway), or by interfering in the process of strand invasion (FIGL and FLIP) (Fernandes *et al.*, 2018; Girard *et al.*, 2015; Séguéla-Arnaud *et al.*, 2015).

In *S. cerevisiae*, phosphorylation of the C-terminal end of the ZMM/TF protein Zip1 also appears to be essential in committing a particular DSB to become a CO (Chen *et al.*, 2015). This data also supports the idea of the ECD, as it was proposed that Zip1 is phosphorylated after DSB formation, but before the action of the other ZMMs. Thus under this model, after DSB initiation, Zip1 becomes directly/indirectly associated with the DSB, and then its phosphorylation designates the site to be repaired by the Class I CO pathway (discussed below) (Chen *et al.*, 2015). Future research would need to be conducted on AtZYP1 to determine if it acts similarly.

1.3.2.2 Crossover Formation

Further to the distinction of whether an intermediate is resolved as a CO or an NCO, COs can be further categorised by the recombinases that are responsible for their formation and resolution. These are referred to as the Class I and Class II pathways.

1.3.2.2.1 The Class I CO Pathway: ZMM Dependent

COs dependent on the Class I pathway of CO resolution are both essential for maintenance of the obligate chiasma necessary for normal disjunction, and interference-sensitive; that is, the presence of one Class I CO decreases the likelihood of another forming nearby, and thus their distribution along the chromosome is non-random (Jones and Franklin, 2006). The proteins responsible for these COs were first comprehensively characterised in budding yeast. These are the ZMMs: Zip1, Zip2, Zip3, Zip4, Msh4, Msh5, Mer3, and Spo16 (Börner *et al.*, 2004). Mutants of these genes present with a reduction in CO numbers, confirming that they are essential for normal levels of CO formation. Notably, they are reduced to a CO level of only 15% of that of WT, therefore suggesting that there they are not required for formation of all COs in yeast (Börner *et al.*, 2004). That the ZMMs all work in the same pathway was shown in double *zmm* mutant experiments, which revealed that the double mutants had a phenotype nearly indistinguishable from that of the single mutants (Börner *et al.*, 2004; Fung *et al.*, 2004; Hunter and Kleckner, 2001).

In *Arabidopsis*, several ZMMs have also been identified. These are AtSHOC1/ZIP2, AtHEI10, AtZIP4, AtMSH4, AtMSH5, AtPTD, and AtMER3/RCK (Chelysheva *et al.*, 2007, 2012; Higgins *et al.*, 2004a, 2008b; Lu *et al.*, 2014; Macaisne *et al.*, 2008; Mercier *et al.*, 2005). Future research could also explore whether a potential *Arabidopsis* homologue of the recently identified rice ZMM HEI10 INTERACTION

PROTEIN 1 (HEIP1) identified via BLAST is also required for Class I CO formation in *Arabidopsis* (Li *et al.*, 2018).

The individual functions of these proteins have been explored, mostly through work conducted in budding yeast. Msh4/Msh5 are homologues of the bacterial MutS proteins, which, like Msh4/Msh5, also form a dimer. In *E. coli*, MutS is an essential component of the mismatch repair (MMR) pathway in responding to DNA damage, but in yeast was shown to be essential for stabilisation of proto-dHj structures (SEI and D-loops) via a ‘sliding clamp’ mechanism that can embrace, and thus stabilise, DNA duplexes (Snowden *et al.*, 2004). Its stability is also further influenced by post-translational modification of at least MSH4 by the protein kinase DDK in yeast, and RNF212 and HEI10 in mouse (He *et al.*, 2018; Qiao *et al.*, 2014). In *Arabidopsis*, MSH4/MSH5 are proposed to execute their role in a similar manner. The *Atmsh4/Atmsh5* mutants were also some of the first to suggest that there was indeed likely two CO resolution pathways in *Arabidopsis*, with each mutant retaining a residual chiasma number of approximately 15% of that of WT, reminiscent of data presented in *S. cerevisiae* (Higgins *et al.*, 2004a, 2008b).

Mer3 is a 5' to 3' DNA helicase conserved across yeast, plants, and mammals (Guiraldelli *et al.*, 2013; Mercier *et al.*, 2005; Storlazzi *et al.*, 2010; Wang *et al.*, 2009). It has been shown to load early in the recombination process, and is proposed to bind to D-loops to promote their stabilisation, thus aiding their transition by other ZMMs into later CO intermediates such as an SEI (Börner *et al.*, 2004; Duroc *et al.*, 2017; Hunter and Kleckner, 2001; Mazina *et al.*, 2004). That *Arabidopsis* AtMER3 is also a ZMM was determined in an *Atmer3* mutant study which revealed a significant reduction in COs, with the residual COs appearing insensitive to interference (Mercier *et al.*, 2005).

Recent studies have determined that Zip2, Zip4, and Spo16 work together in a complex, called the ZZS (Muyt *et al.*, 2018). Zip2-Spo16 (homologues of the XPF/ERCC1 endonucleases) are proposed to direct the ZZS complex to D-loops and Holliday junctions, and Zip2 itself has been identified as the component responsible for the complex's CO promoting role (Arora and Corbett, 2019; Muyt *et al.*, 2018). Zip4 is proposed to, in part, act as a 'scaffold' due to its ability to stabilise Zip2, and interact with both the other ZMMs and the chromosome axis (Muyt *et al.*, 2018).

In *Arabidopsis*, the *shoc1* (*zip2*) mutant presented with a phenotype similar to that of the other *Arabidopsis* *zmm* mutants with a reduction in COs, despite no obvious effect on the levels of DSBs or synapsis, and *shoc1/msh5* double mutant analysis confirmed it acted alongside the ZMMs (Macaisne *et al.*, 2008). This was similarly the case for *Atzip4* (Chelysheva *et al.*, 2007). Though the functions of these ZMMs has not been explored in such detail as in yeast, it is suggested that they possibly work in a similar capacity, further supported by the fact that AtPTD (ERCC1-like) has been shown to interact with SHOC1, and that the formation of this complex is likely necessary for Class I CO formation via stabilisation of dHJs (Lu *et al.*, 2014; Macaisne *et al.*, 2008). Thus, a ZZS-analogous system may also operate in *Arabidopsis*.

The role of Zip3 in the formation of Class I COs has perhaps remained the most elusive. The Zip3 family in meiosis function as either SUMO or ubiquitin E3 ligases, and appear to be recruited as DSB processing commences; that Zip3 is loaded early is supported by the fact that it appears to be required for loading of other ZMMs (Serrentino *et al.*, 2013; Shinohara *et al.*, 2015, 2008). As with the other ZMMs, in budding yeast, Zip3 is required for both Class I CO formation and polymerisation of the SC (Shinohara *et al.*, 2015). Whilst the precise function of Zip3 and its homologues in other organisms remains unclear, there are several theories surrounding its

function. In budding yeast, normal CO formation and SC polymerisation is also reliant on the SUMOylation of axis element component Red1. It has been proposed that this SUMOylation is necessary for the TF protein Zip1 to interact directly with Red1, and thus help promote formation of the SC (Cheng *et al.*, 2006). As with other ZMMs, it is also possible Zip3 is another factor required for stabilisation of Class I CO intermediates. Fitting with this suggestion, in *Arabidopsis*, an antibody raised against the Zip3 homologue HEI10 revealed that HEI10 forms c. 97 small foci across the nucleus during early prophase I, reducing down to c. 8.8 large foci by the end of pachytene. This is consistent with the CO number in WT meiosis, suggesting it has essential roles in CO maturation (Chelysheva *et al.*, 2012). Furthermore, in *M. musculus*, it is suggested that the action of its Zip3 homologues RNF212 and HEI10 may prevent removal of the MutSy MSH4-MSH5 heterodimer from CO sites, and that this is how RNF212 and HEI10 stabilise, and thus promote, CO formation (Qiao *et al.*, 2014).

Lastly, the ZMM Zip1 is both required for normal Class I CO formation, and forms the transverse filament of the SC (Sym *et al.*, 1993). In budding yeast, *zip1* mutants also suffer a reduction in spore viability and a significant reduction in CO number (Tung and Roeder, 1998). In *Arabidopsis*, the two ZYP1 homologues ZYP1a and ZYP1b also present with a reduction in fertility, but also with an inability to correctly regulate CO formation; at metaphase I in a *zyp1a^{T-DNA}/zyp1b^{RNAi}* mutant line, there was an increase in ectopic recombination, resulting in both multivalents and non-homologous bivalents (Higgins *et al.*, 2005). In contrast to budding yeast where Zip1 is absolutely required for Class I COs, the chiasma frequency in *zyp1a^{T-DNA}/zyp1b^{RNAi}* was 80% of that of WT; this would suggest that, in contrast to yeast, ZYP1 is not absolutely required for CO formation *per se*, but rather for properly controlled CO formation/CO fidelity.

Though for future experiments, it would be interesting to produce a completely ZYP1 null mutant, potentially via gene editing, as it could be argued that there is the possibility of these *zyp1* mutants being hypomorphic, *i.e.*, with some protein still being produced. The role of ZYP1 as an SC component is discussed in **1.4.2**.

1.3.2.2.1.1 Class I CO Resolution

The Class I CO dHJ intermediates are then finally resolved by the *E. coli* MutL homologues Mlh1 and Mlh3 in yeast. Mlh3 executes the endonucleolytic role, making single-stranded nicks in DNA, which is thought to be the basis of how it may resolve the dHJ (Al-Sweel *et al.*, 2017; Nishant *et al.*, 2008; Ranjha *et al.*, 2014; Rogacheva *et al.*, 2014; Wang *et al.*, 1999). In *Arabidopsis*, MLH1/MLH3 are also essential for CO formation, with mutants for both presenting with a significant reduction in fertility and homologous recombination (Dion *et al.*, 2007; Jackson *et al.*, 2006). At late prophase I, antibodies raised against MLH1 and MLH3 are used as markers for COs, presenting with around 9 foci per nucleus, corresponding with the WT CO number (Franklin *et al.*, 2006). Furthermore, in *Atmlh3*, MLH1 is unable to localise onto the chromosomes, as has been observed in other systems (Franklin *et al.*, 2006). Therefore, it is proposed that MLH1/MLH3 likely function in a similar manner to yeast and other systems in *Arabidopsis*.

1.3.2.2.2 The Class II CO Pathway

As previously discussed, the ZMMs account for 85% of the total number of COs in both budding yeast and *Arabidopsis*. The remaining 15% are from the Class II CO pathway, characterised by both the distinct manner in which they arise and are processed, and by the fact that they are interference insensitive. Given their stochastic formation along the chromosomes, Class II COs are not primarily responsible for formation of the obligate CO (Zickler and Kleckner, 1999).

Class II COs are thought to arise from the formation of unregulated/abnormal joint molecules. These structures are usually disassembled by STR/Srs2, but some may escape this stage of processing, and thus must be resolved in a different way (de los Santos *et al.*, 2003; Kaur *et al.*, 2015; Oh *et al.*, 2008; Zakharyevich *et al.*, 2012). In *S. cerevisiae*, the resolution of Class II COs is dependent on the structure-specific nucleases (SSN), comprised of Mus81-Eme1/Mms4, Yen1, and Slx1-Slx4 (De Muyt *et al.*, 2012; Zakharyevich *et al.*, 2012).

In *Arabidopsis*, AtMUS81 is thought to be required for the resolution of some, but not all Class II COs, given that the *Atmus81* single mutant has no significant reduction in chiasma frequency, and the *Atmus81/Atmsh4* double mutant still had some residual chiasma, albeit at a reduced level compared to the single *msh4* mutant (Higgins *et al.*, 2008a). More recent work has identified *Fanconi anaemia D2* (AtFANCD2) as a potential key-player in the Class II CO resolution pathway. In *Atfancd2*, CO number is reduced by 14%, consistent with the proposed proportions of Class I/Class II COs. Furthermore, the residual chiasmata are interference sensitive (Kurzbauer *et al.*, 2018). Kurzbauer *et al.* (2018) also suggest that, given that univalents were observed in an *Atfancd2/Atmus81* double mutant, that the Class II pathway may also contribute toward formation of some obligate chiasma. Nonetheless, a *Atfancd2/Atmus81/Atmsh4* triple mutant still formed some bivalents, and thus CO formation was not completely abolished, suggesting the importance of further components of the Class II pathway that are yet to be discovered in *Arabidopsis* (Kurzbauer *et al.*, 2018).

1.3.3 Control of Meiotic Crossovers

Given the importance of genetic COs during meiosis in ensuring timely and accurate segregation of the homologues, COs are subject to several layers of control.

1.3.3.1 CO Assurance and Homeostasis

The first is, as has been previously mentioned, the formation of the ‘obligate CO’, *i.e.*, the one CO necessary per chromosome pair to ensure correct tension on the metaphase I plate. This is true irrespective of chromosome size; both the smallest and largest chromosomes will receive, on average, between 1 and 2 COs (discussed in Jones and Franklin, 2006; Wang *et al.*, 2015). That the obligate CO is maintained even when earlier recombination intermediates are reduced is referred to as CO assurance, and is directly related to CO homeostasis.

CO homeostasis refers to the process by which CO levels are usually protected despite perturbations to the numbers of initial recombination precursors. Therefore, irrespective of increases or decreases in DSB levels, for example, the CO number remains constant. This phenomenon has been experimentally observed in several systems, and in some cases, has been related to the existence of a specific ‘CO assurance checkpoint’ (Cole *et al.*, 2012; Deshong *et al.*, 2014; Hartung *et al.*, 2008; Martini *et al.*, 2006; Mehrotra and McKim, 2006; Xu *et al.*, 1997; Yokoo *et al.*, 2012; Yu *et al.*, 2016).

1.3.3.2 CO Interference: localisation and distribution of COs

1.3.3.2.1 CO Hotspots

Despite COs forming at different sites between meioses, COs nonetheless tend to form in 1 - 10 kb regions known as ‘CO hotspots’ (Choi and Henderson, 2015). Unsurprisingly, these are also usually correlated with the locations of DSB hotspots, though in *S. cerevisiae*, this relationship is not necessarily so clear (Hyppa and Smith, 2010; Smagulova *et al.*, 2016). As previously mentioned in 1.3.1.1.1, there are several factors that correlate with recombination hotspots across species, *e.g.*, NDRs, open

chromatin marks such as H3K4me3 and H3K9ac, and low mDNA (Borde *et al.*, 2009; Choi *et al.*, 2013; Pan *et al.*, 2011; Shilo *et al.*, 2015; Wijnker *et al.*, 2013; Yamada *et al.*, 2013). More recent research has highlighted in plants that recombination hotspots may also be associated with particular types of transposons, including *Stowaway* and *gypsy*: a somewhat unexpected result given previous observations that DSBs tend to be directed away from repetitive sequences which are prevalent in some transposons (Choi *et al.*, 2018; He *et al.*, 2017; Marand *et al.*, 2019, 2017).

In *Arabidopsis*, COs appear to be most concentrated at gene promoter and terminator sequences, and associated with the unstable histone H2A.Z variant (Choi *et al.*, 2013; Drouaud *et al.*, 2013; Yelina *et al.*, 2012). In general, however, the COs in plants are associated with the gene-rich euchromatic regions, and are suppressed within heterochromatic regions (Fu *et al.*, 2001; Li *et al.*, 2015; Saintenac *et al.*, 2009; Yelina *et al.*, 2012). A key phenomenon also noted in plant crop species such as grasses is the tendency for the COs to form at the very distal ends of the chromosomes, visualised by the large ring bivalents that can be observed at metaphase I in barley and wheat (Higgins *et al.*, 2012; Künzel *et al.*, 2000; Osman and Franklin, unpublished). This amounts to in excess of 30% of the genes in wheat occurring in recombination ‘cold-spots’ (Künzel and Waugh, 2002; Mayer *et al.*, 2011). In barley, and potentially wheat, this is thought to be the result of the distal chromosomal ends completing replication, and thus initiating meiotic recombination, well before the pericentromeric regions (Higgins *et al.*, 2012). Indeed, in wheat, IHR-promoting axis protein ASY1 appears to load at the sub-telomeric regions first during early prophase I, and thus the distal ends of the chromosomes have a linearised axis well before the centromere-proximal regions (Osman and Franklin, unpublished). Thus, it is possible that these early COs can establish CO interference.

1.3.3.2.2 CO Interference

CO interference is a long-observed phenomenon first described in the early 1900s (Muller, 1916; Sturtevant, 1915). It is the observation that the formation of one CO reduces the likelihood of another forming nearby. The precise details of how it works are not yet fully understood, but several theories have been suggested.

The first was the ‘polymerisation model’ of CO interference, proposed in 1990 by King and Mortimer. They posited that the interference signal spreads along the chromosome via the polymerisation of a particular protein, having nucleated from an initial CO site. The ‘strength’ of this signal is maintained, never dissipating as it spreads out from the CO. This polymerised element was then proposed to remove pro-CO machinery from other recombination intermediates downstream of the successful CO site, and thus, the machinery was then free to re-attach to other precursors. Evidence contrary to recombination machinery re-binding discounts this model (Muyt *et al.*, 2014; L. Zhang *et al.*, 2014a), as does research suggesting interference weakens over distance (Drouaud *et al.*, 2007; Hou *et al.*, 2013; Petkov *et al.*, 2007; L. Zhang *et al.*, 2014a, 2014b).

The second model was proposed in 1993 by Foss and colleagues, where it was suggested that there was a ‘counting’ mechanism involved; that outward from an original, randomly selected CO site, a fixed-number of recombination precursors would be repaired as NCOs. By this theory, however, increasing the number of initial recombination precursors would result in a distinct difference of the number of COs produced; this is therefore not compatible with data presented in many organisms that suggest the existence of CO homeostasis (Cole *et al.*, 2012; Deshong *et al.*, 2014; Hartung *et al.*, 2008; Martini *et al.*, 2006; Mehrotra and McKim, 2006; Xu *et al.*, 1997; Yokoo *et al.*, 2012; Yu *et al.*, 2016). Thus, the model has also since been discounted.

The most recent, and most convincing, model of CO interference with the most supporting evidence was proposed by Kleckner *et al.* in 2004. This is the ‘beam-film’ (BF) model of CO interference. The BF model proposes that, due to the constraints of the chromosome axis on chromatin as it expands and contracts, the chromosomes experience a high level of mechanical stress. This mechanical strain is proposed to be the main factor promoting CO formation, as in this model, a CO will provide local stress relief, with the signal dissipating over the physical distance of the chromosome. Where the stress reaches a particular ‘threshold’ is where another recombination precursor will be designated as a CO (Kleckner *et al.*, 2004). This fits with observations that interference does indeed act across physical distances rather than genomic or genetic (*i.e.*, over μm , not kb or cM) (Drouaud *et al.*, 2007; Hou *et al.*, 2013; Petkov *et al.*, 2007; L. Zhang *et al.*, 2014a, 2014b). Furthermore, it is compatible with the notion of assuring the obligate CO, given that mechanical stress would always be high enough to ensure at least one CO-designated event. Crucially, it is also compatible with CO homeostasis, as if the stress-relief is spreading over a physical distance, an increase or decrease in DSBs would lead to no change in CO number (more DSBs = more interference signals = no overall increase in COs; fewer DSBs = reduced interference signal = more COs formed in response). Mathematical models derived using the BF hypothesis also fit with observed data (Zhang *et al.*, 2014a, 2014b). What these ‘precursor’ sites may be is not strictly defined within the literature, however, recent work in *Sordaria macrospora* describes the presence of inter-axis bridges during late leptotene when CO patterning is proposed to be imposed (Dubois *et al.*, 2019). These are comprised of both axis components, and those involved in the recombination pathways, thus linking the chromosome axis and SC directly to recombination. These bridges could therefore be the ‘weak-points’ described by Kleckner *et al.* (2004), and

that stress at these particular sites would induce the designation of these intermediates as COs.

Through this BF model of CO patterning, we therefore see the influence of the axis on meiotic recombination, highlighting that they are intrinsically linked. It is possible that through this model, perturbing the structure of the axis in such a way as to alter the mechanical stress it may be able to accumulate could affect CO distribution. In yeast, interference has been linked to a Top2/SUMO/STUbL related pathway, with axis components Top011 and Red1 as targets (L. Zhang *et al.*, 2014b). The authors note, however, that they suspect we have not yet uncovered all of the key-players in this process. Thus, a deeper understanding of the chromosome axis, and all of its constituents and their individual roles, will be necessary if we are to learn how we might manipulate the recombination process.

1.4 The Chromosome axis in meiosis

As discussed, the processes necessary to complete meiosis are tightly regulated, and coincident with the global remodelling of the chromosomes (Blat *et al.*, 2002; Kleckner, 2006; Storlazzi *et al.*, 2008). This includes the formation of the chromosome axis: a proteinaceous meshwork that organises the chromatin into linear, co-oriented dual-loop arrays, conjoined at the loop bases by the axial structural components. The axis appears to be comprised of a structural ‘core’, onto which additional meiosis-specific axis-associated proteins load (Moses, 1956) (Figure 1.3).

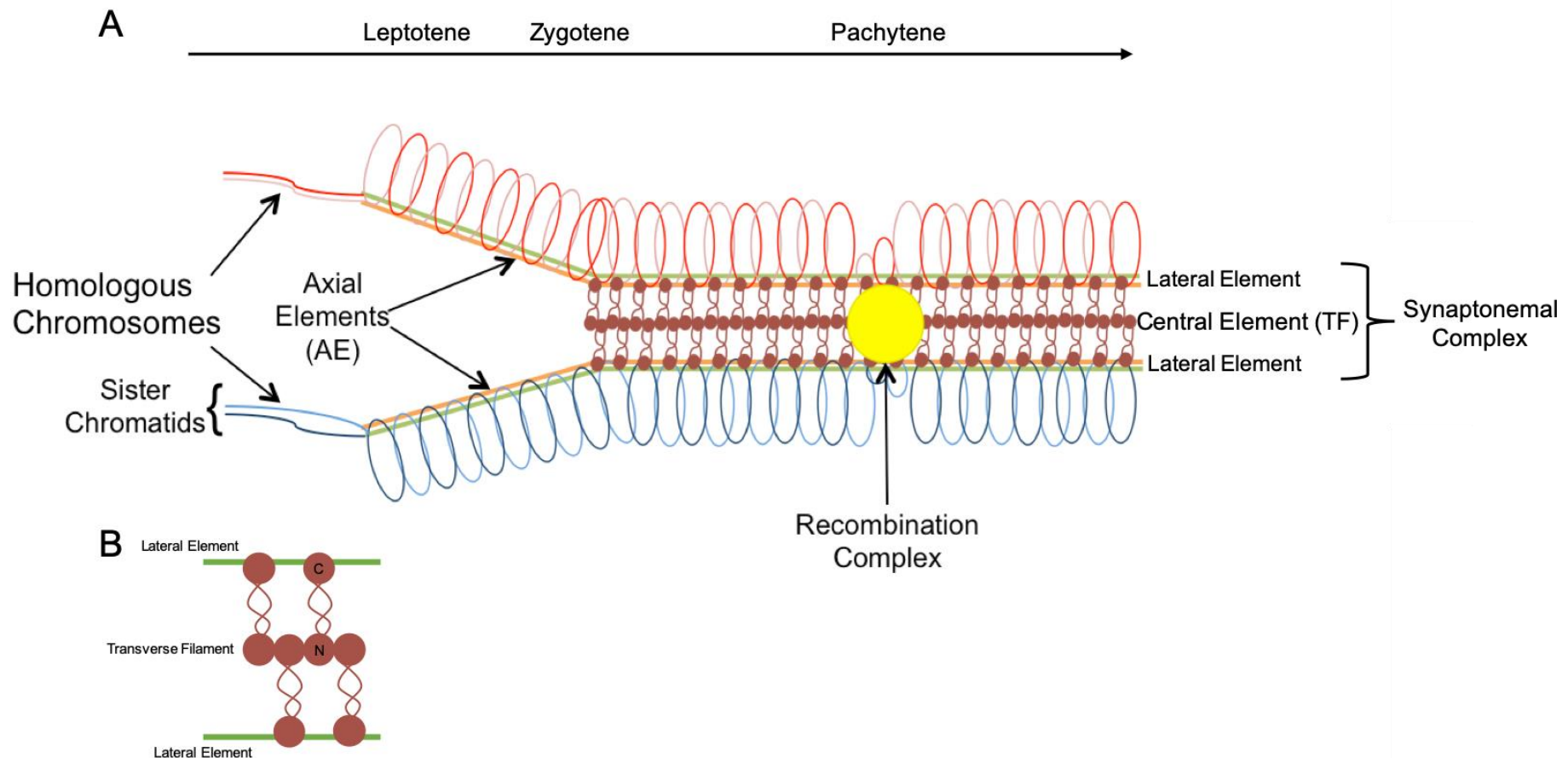


Figure 1. 3 The Meiotic Chromosome Axis and Synaptonemal Complex. (A) The chromosome axis from leptotene through pachytene. Sister chromatids are held together in a dual-loop array by the axial elements. As prophase I progresses, the synaptonemal complex forms, comprised of two lateral elements and a central element region comprised of the transverse filament (TF). A recombination complex is shown, associated with the SC. (B) Close up of the synaptonemal complex structure. Circles represent the globular domains at the N- and C- termini, with coiled-coil regions in-between. Modified from Alberts et al., 1983 and Higgins et al., 2005.

The ‘core’ axis components are the cohesins, which hold the sister chromatids together, and are deposited onto the chromosome during pre-meiotic S-phase. In *S. cerevisiae*, meiotic sister cohesion is maintained by Smc1, Smc3, Scc3, and the kleisin Rec8 (Kim *et al.*, 2010). This core structure is then further elaborated by Hop1, the main yeast HORMAD (HORMA Domain protein; first described in Hop1 Rev1 Mad1), and Red1 (Carballo *et al.*, 2008; Woltering *et al.*, 2000). In *Arabidopsis*, structural and functional homologues have been identified for all of these proteins, as well as some specific to plants. Thus, in *Arabidopsis*, the cohesins are comprised of SMC1, SMC3, SCC3/STAG3 and the kleisin REC8/SYN1/DIF1 (Bhatt *et al.*, 1999; Cai *et al.*, 2003; Chelysheva *et al.*, 2005; Lam *et al.*, 2005; Lambing *et al.*, 2019). Further components of the axis include the HORMADs ASY1 (homologue of Hop1) and ASY2 (no yeast homologue); and two coiled-coil containing proteins, ASY3 (homologue of Red1), and most recently, ASY4 (no known yeast homologue) (Armstrong *et al.*, 2002; Cai *et al.*, 2003; Caryl *et al.*, 2000; Chambon *et al.*, 2018; Ferdous *et al.*, 2012; Osman *et al.*, 2018; this thesis).

Other axis-associated proteins include the AAA+ ATPase Pch2 (PCH2 in *Arabidopsis*, TRIP13 in mammals), and recently characterised in *Arabidopsis*, TOPII (Börner *et al.*, 2008; Lambing *et al.*, 2015; Martinez-Garcia *et al.*, 2018). In *Arabidopsis*, TOPII has a proposed role in interlock resolution (Martinez-Garcia *et al.*, 2018). In yeast, Pch2 is required for proper loading of Hop1 which forms alternating domains of high and low abundance along the axis (Börner *et al.*, 2008). It also appears that the *Arabidopsis* homologue PCH2 is required for normal levels of ASY1 on the axis, given that in the *pch2* mutant, the overall ASY1 signal appeared much dimmer (Lambing *et al.*, 2015; West, 2015). Later during prophase I, PCH2 is involved in the remodelling of the

chromosome axis, removing ASY1 as the SC extends (Lambing *et al.*, 2015). Pch2/TRIP13 are also part of a defined ‘pachytene-checkpoint’ in yeast and mammals, required to detect proper levels of recombination and synapsis (reviewed in: Roeder and Bailis, 2000). This is less clearly defined in *Arabidopsis*, with no direct evidence currently existing for a pachytene-checkpoint. However, in *Atpch2*, a delay of ≤ 8 h in prophase I was detected, suggesting the possibility of such a system (Lambing *et al.*, 2015).

Despite high sequence divergence between some axis components in different species, it appears that their structure, and often, methods of assembly, interactions, and functions are conserved (Bomblies *et al.*, 2015; West *et al.*, 2019), as is discussed below.

1.4.1 Axis Assembly

In *S. cerevisiae*, the axis protein Red1 is proposed to load first, and recruit Hop1 to the axis via a ‘closure motif’: a short peptide series that was first defined in *C. elegans*, and which contains a highly conserved Pro-Tyr-Gly motif necessary for HORMAD self-assembly (Kim *et al.*, 2014; West *et al.*, 2019; Woltering *et al.*, 2000). Red1 also contains a C-terminal coiled-coil domain that is required for its self-assembly onto the axis (Hollingsworth and Ponte, 1997; Woltering *et al.*, 2000). In contrast to *S. cerevisiae*, plants and mammals appear to contain two coiled-coil domain containing axis proteins: ASY3 and ASY4 in *Arabidopsis*, and SYCP2 and SYCP3 in mammals (Chambon *et al.*, 2018; Ferdous *et al.*, 2012; Kouznetsova *et al.*, 2005; Osman *et al.*, 2018; Yang *et al.*, 2006; Yuan *et al.*, 2002, 2000; this thesis). Uniting all three systems, these coiled-coil proteins appear to be required for normal axis formation, loading of the HORMADs, and proper polymerisation of the SC (Chambon *et al.*, 2018; Ferdous *et al.*, 2012; Kouznetsova *et al.*, 2005; Osman *et al.*, 2018; Woltering *et al.*, 2000; Yang

et al., 2006; Yuan *et al.*, 2002, 2000; this thesis). Furthermore, both ASY3/ASY4 and SYCP2/SYCP3 interact via these C-terminal coiled-coil domains, and in mammals, removing the SYCP2 coiled-coil is sufficient to prevent SYCP3 localisation (Ferdous *et al.*, 2012; Shin *et al.*, 2010; West *et al.*, 2019; Yang *et al.*, 2006; this thesis). In yeast, mammals, and plants, the coiled-coils are essential for their self-assembly into a Red1 homotetramer in yeast, and an ASY3/ASY4 and SYCP2/SYCP3 heterotetramer in plants and mammals respectively (West *et al.*, 2019). This therefore highlights the importance of the structure of the axis, given that it has been so well conserved across such diverged species.

The HORMADs appear to rely on their HORMA domains for axial localisation. The HORMA domain itself is ~200 aa in length, and can be split into two functional units of a ‘core’, and a ‘safety-belt’ region at its C-terminus. This safety-belt region can topologically secure protein-protein interactions, and exists in two states: open or closed. Based on evidence in *C. elegans*, these safety-belt interactions allow the proteins to self-assemble, and more recently, have been suggested to allow them to interact with other chromosome axis components such as Red1/ASY3/SYCP2 (Hara *et al.*, 2010; Kim *et al.*, 2014; Luo *et al.*, 2002; Rosenberg and Corbett, 2015; Sironi *et al.*, 2002; West *et al.*, 2019). This led to a proposed, conserved model of axial filament assembly by West *et al.* (2019) (Figure 1.4). Precisely how the meiotic axis-associated proteins interact with the SC and cohesins, however, remains to be determined. Evidence in mammals, however, suggests axis-SC interaction may closely involve the cohesins (Rong *et al.*, 2016).

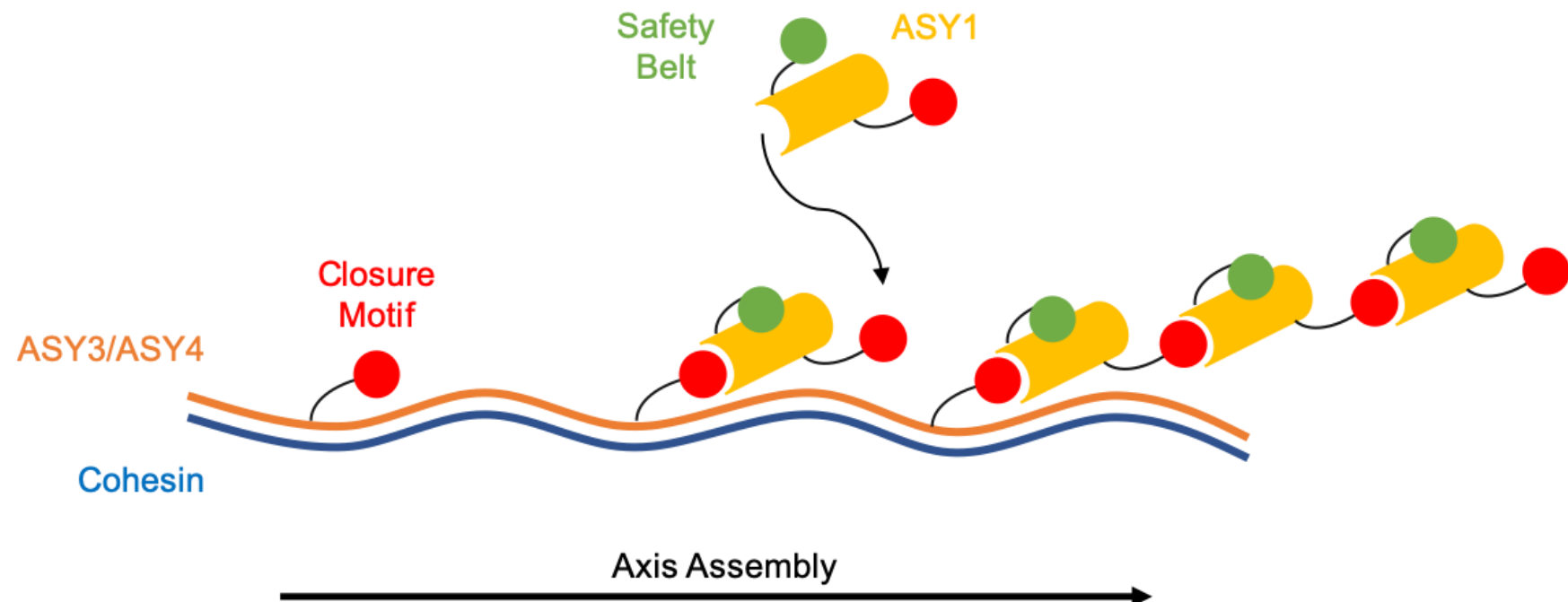


Figure 1.4 Proposed model of Axis Assembly. ASY3/ASY4 self-assemble into head-to-tail heterotetramers, associated with the cohesins. ASY3 recruits ASY1 to the axis via a closure motif that can interact with the ASY1 HORMA domain. ASY1 then assembles via interactions between closure motifs and HORMA domains, secured by the safety belt region. Adapted from Rosenberg and Corbett, 2015; and West *et al.*, 2019.

Another unifying characteristic of the axis proteins is that perturbing them results in a reduction in the number of COs, as well as a disruption to chromatin structure. Knocking out ASY1, for example, reduces the CO number to ~1.39 per nucleus, and in *asy3*, to ~3.3 per nucleus (Armstrong *et al.*, 2002b; Caryl *et al.*, 2000; Ferdous *et al.*, 2012a; Ross *et al.*, 1997). Knocking out SYCP3 in mouse results in a doubling in chromosome axis length, as well as various other meiotic defects (Syrjänen *et al.*, 2014).

Thus, the functions of the axis can be split into two major roles. Primarily, it acts as an organisational unit, holding the chromosomes in the looped-array, and ensuring proper compaction, as illustrated by mutants where the axis structure is in some way disrupted (Fukuda *et al.*, 2014; Novak *et al.*, 2008; Ward *et al.*, 2016). Indeed, in mouse, it is proposed that both SYCP3 and SMC1 β are essential for loop organisation (Novak *et al.*, 2008; Syrjänen *et al.*, 2014). Linked to this, it also acts as a scaffold and landing site for other meiotic proteins. This includes those involved in SC polymerisation, after which, the axis will ultimately comprise the lateral elements of the SC structure. Secondly, the axis promotes formation of DSBs, and is necessary to establish the inter-homologue repair bias necessary for CO formation (see **1.4.3**).

1.4.2 The Synaptonemal Complex and Axis Remodelling

As meiosis progresses, the synaptonemal complex (SC) polymerises between homologous chromosomes. At this point, the axial elements become the ‘lateral elements’, and form one part of the tripartite structure of the SC. Thus, the SC is comprised of two flanking lateral elements, with the transverse filament (TF) protein loaded between them (Figure 1.3 A,B). In yeast, the TF protein is Zip1: also a member of the ZMMs (ZMM role: **1.3.2.2.1**) (Sym *et al.*, 1993). In *Arabidopsis*, the TF is comprised of ZYP1 (Higgins *et al.*, 2005b), and in mouse, SYCP1, SYCE1, SYCE2,

SYCE3 and TEX12 (Costa *et al.*, 2005; Hamer *et al.*, 2006; Schramm *et al.*, 2011). AtZYP1 is, like Zip1 and its mammalian counterparts, predicted to be comprised of a central coiled-coil, flanked by two unstructured globular domains (Higgins *et al.*, 2005b; Page and Hawley, 2004; Sym *et al.*, 1993). In yeast and mouse, it has been demonstrated that the SC TF forms homodimers that align in parallel between synapsing axes. The C-terminal domains are associated with the lateral elements, and the N-terminal domains overlap in the centre, creating the characteristic ‘zipper’ structure in its centre region, as observed via microscopy (Dong and Roeder, 2000; Liu *et al.*, 1996) (Figure 1.3, B).

1.4.2.1 SC Assembly

In *S. cerevisiae*, the SC emanates outward from synapsis initiation sites (SIS) at both the centromeres, and from Class I COs (Chua and Roeder, 1998; Fung *et al.*, 2004; Tsubouchi *et al.*, 2008). In *Arabidopsis*, ZYP1 is seen as c. 25 foci at late leptotene, which later extend into the full SC (Higgins *et al.*, 2005). The polymerisation of the SC in *Arabidopsis*, also appears to require DSBs, and its localisation occurs prior to stable strand invasion; crucially, ZYP1 cannot polymerise when recombination is defective early on, as highlighted by immunolocalization revealing foci, but not extension, of the ZYP1 signal in *Atdmc1* (Higgins *et al.*, 2005). Therefore, it is possible that SC polymerisation in *Arabidopsis* also relies, in part, on the formation of recombination intermediates, although perhaps not necessarily COs. This close association between SC assembly and meiotic recombination could perhaps be attributed in part to a requirement to regulate the structure, ensuring it is more likely to polymerise at the correct time between homologous chromosomes, given the fact it has been observed to self-assemble even without the presence of meiotic chromosomes, forming aberrant structures such as polycomplexes (Ollinger *et al.*, 2005). There is currently no

evidence suggesting that ZYP1 also emanates outward from centromeres in *Arabidopsis* as it does in yeast, but this is not necessarily the case for other plants such as maize (Higgins *et al.*, 2005; Zhang *et al.*, 2013).

Dynamics of the axis and SC can be traced throughout prophase I of meiosis using immunolocalisation with antibodies raised against the key proteins. Thus, we can see that many of the chromosome axis components appear late in G2, before becoming linear structures by the end of leptotene. During zygotene, the SC begins to polymerise, reaching full synapsis by pachytene. At this point, the homologous chromosomes are held together in close apposition of approximately 100 nm: a value conserved across species (Zickler and Kleckner, 2015).

The direct relationships between recombination, the axis and SC, are discussed further below.

1.4.3 The Chromosome Axis and Recombination

1.4.3.1 DSBs

As meiotic recombination occurs within the context of the chromosome axis, it has influence during DSB formation, as well as in CO localisation and number. Data suggests Spo11 loads onto chromatin before the axis, but does not initiate DSBs until the axis has formed (Panizza *et al.*, 2011). Consistent with this, in *Arabidopsis*, SPO11 and ASY1 loading are independent, but the DNA-damage marker γH2AX does not appear until the axis has formed (Sanchez-Moran *et al.*, 2007). Furthermore, DSBs themselves occur in the loop regions, yet the RMM complex – a group of Spo11 accessory proteins including Rec114, Mei4, and Mer2 – is axis associated (Li *et al.*, 2006; Sasanuma *et al.*, 2007). This data has been combined to propose a ‘tethered-loop’ method of DSB induction, where Spp1 located at the axis via an interaction with

Mer2, recognises the histone H3K4me3 mark, and thus brings the future site of DSB cleavage in toward the axis where it can be acted upon by Spo11 and its associated proteins (Panizza *et al.*, 2011; Sommermeyer *et al.*, 2013) (Figure 1.5).

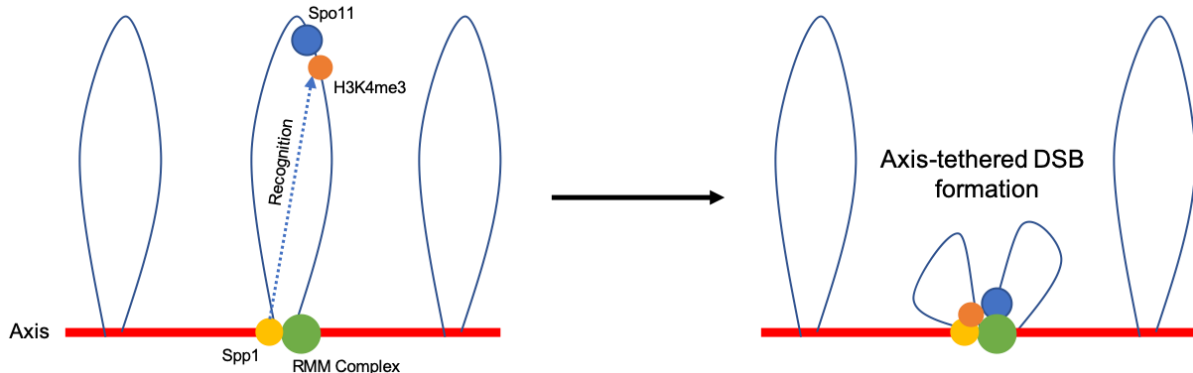


Figure 1.5 The Tethered-loop model of DSB formation. Spp1 interacts with both Mer2 at the axis, and the H3K4me3 mark out in the chromatin loop, thus bringing the loop into the axis. This allows Spo11 and its accessory proteins to initiate DSB formation. Modified from Sommermeyer *et al.*, 2013.

In *Arabidopsis*, a normal axis structure is also essential for WT levels of DSBs; in the axis mutant *asy3-1*, DSB number is reduced to 70% of the WT level (Ferdous *et al.*, 2012a). In contrast to yeast *hop1* mutants, however, no reduction in DSBs was observed in *asy1* (Sanchez-Moran *et al.*, 2007), suggesting some divergence in the roles of these proteins.

1.4.3.2 Crossovers

1.4.3.2.1 The Influence of the Axis

In yeast, it has been shown that phosphorylation of Hop1 is essential for maintenance of the inter-homolog repair (IHR) bias: the preference to repair a DSB via the homologue, rather than the sister. This depends on Hop1, Red1, and the formation of DSBs, which result in the activation of the kinase Mek1. Once it is active, Mek1 can then phosphorylate its targets, including Rad54. Phosphorylation of Rad54 alters its

association with Rad51. Subsequently, there is a reduction in inter-sister DSB repair, and so relative increases Dmc1-mediated inter-homolog repair (Callender *et al.*, 2016; Carballo *et al.*, 2008; Chuang *et al.*, 2012). For Hop1 to activate Mek1, however, Hop1 must already have been phosphorylated by Tel1/Mec1: homologues of ATM/ATR respectively, which are activated by Red1 as DSBs form (Carballo *et al.*, 2008; Lin *et al.*, 2010). IHR can therefore be eradicated in budding yeast by mutating the T-318 residue of Hop1, which is the Tel1/Mec1 phosphorylation target (Carballo *et al.*, 2008; Lin *et al.*, 2010). Axis component Pch2 has also been implicated in this process, with the yeast *pch2Δ* mutant presenting with defects in suppressing inter-sister repair, thus leading to the proposal that Pch2 is required for optimal levels of Mek1 activity, and is thus required for promotion of IHR (Ho and Burgess, 2011; Zanders *et al.*, 2011).

Furthermore, the beam-film model of CO-designation and interference (see 1.3.3.2.2) directly links the chromosome axis to the CO/NCO decision, as well as CO patterning. Interference does not appear to absolutely require the SC, however. This can be inferred from the fact that SIS in yeast and mammals show interference, suggesting it arises before the synapsis initiation complex (SIC) can load, and that the COs in the *Arabidopsis zyp1^{RNAi}* still appeared to be interference-sensitive (Boer *et al.*, 2007; Cole *et al.*, 2012; Fung *et al.*, 2004; Higgins *et al.*, 2005b). The SC appears to have an unclear, but potentially distinct role in recombination, as is discussed below.

1.4.3.2.2 The Role of the SC

As previously mentioned, the polymerisation of the SC in many organisms appears to be linked to meiotic recombination, though how remains elusive. Recent work has strengthened this association between the SC and the progression of recombination further, giving some functional explanation for previously observed phenotypes.

The direct functions of Zip1 as both a ZMM and as an SC component have been most extensively explored in yeast. Work conducted by Voelkel-Meiman *et al.* (2015) revealed that whilst Zip1 itself is required for formation of MutSy-MutLy COs, the fully assembled, mature SC structure is not. More recent work from the same lab found that this could be explained by functionally separate but physically-linked regions of the Zip1 N-terminus. That is, amino acid residues directly next to each other have different roles. These residues are contained within the first 20 amino acids of the protein, with separate regions engaging with pro-CO machinery (such as E3 ligase, Zip3), and pro-synapsis machinery. Thus, this lab propose that Zip1 can physically link recombination to the SC, explaining the observation of SC associated recombination nodules in many species (Anderson *et al.*, 2001, 1997; Carpenter, 1975; Lake *et al.*, 2015; Zickler and Kleckner, 1999). It is also suggested that Zip3 can prevent recombination-independent SC formation, thus further supporting the previously mentioned notion that linking these processes may prevent polycomplex formation (Macqueen and Roeder, 2009; Voelkel-Meiman *et al.*, 2019, 2015). Furthermore, if the SC forming is linked to the progression of recombination, a complete SC could act as a signal to the cell when each homologous pair has likely received the obligate CO (discussed in: Page and Hawley, 2004; Zickler and Kleckner, 1999).

Study of inter-axis bridges in *Sordaria macrospora* also provides a link between the SC and recombination progression. Inter-axis bridges are thought to be sections of DNA, axis/SC proteins, and recombination machinery, that form a physical link between two aligned axes (Albini and Jones, 1987; Dubois *et al.*, 2019). It is proposed that these bridges form when axes are ~400 nm apart, prior to pulling them into ~200 nm co-alignment. Following the assembly of the TF, the homologous axes are thus held at ~100 nm distance. Therefore, bridges are potentially both necessary for pre-

synaptic alignment, and facilitate the movement of recombination complexes from the axis to the SC; they may mediate the initial the axis-association of recombination intermediates, prior to releasing them into the space between co-aligned axes, and finally, promoting SC nucleation from these sites (Dubois *et al.*, 2019).

The particular reason for why it is important for recombination intermediates to become SC associated has been investigated in *C. elegans*. Previous groups have suggested the possibility that the SC may merely provide a stable environment in which COs can be resolved. In favour of this assertion, in *C. elegans*, the SC forms a protective ‘bubble’ around recombination sites, enriching those regions with pro-CO factors (Woglar and Villeneuve, 2018). This would fit together the combined data on SC proteins from other organisms presented above.

Whilst the SC is thus proposed to provide a physical scaffold for recombination, there is also the possibility that it regulates the progression of recombination. In several organisms, it is known that the AAA-ATPase Pch2/PCH2/TRIP13 depletes HORMADs from the axis as the SC polymerises (Joshi *et al.*, 2009; Lambing *et al.*, 2015; Ye *et al.*, 2017, 2015). As previously discussed, HORMADs are known to promote the formation of DSBs (though there is no evidence for this in *Arabidopsis*), and promote the IHR bias (Chuang *et al.*, 2012; Sanchez-Moran *et al.*, 2007). Therefore, it has been proposed that the SC could indirectly regulate the levels of CO formation via a feedback loop where removal of the IHR promoting HORMAD prevents further DSB and CO initiation after synapsis (Börner *et al.*, 2008; Joshi *et al.*, 2009; Lambing *et al.*, 2015; San-Segundo and Roeder, 1999).

Thus, the roles of the axis and SC are tightly coordinated with recombination progression, and thus the two must be thought of almost as one process. This

relationship has also clearly made the axis a target for meiosis research to uncover precisely how the axis and SC influence recombination outcomes, with particular interest in CO localisation. This relates back to the common theme presented in this thesis: the requirement to understand the axis, so that we might ultimately manipulate the recombination process.

Why this is of particular importance is explored below.

1.5 Meiosis Research and Food Security

1.5.1 The Food Security Crisis

In recent years, plant research efforts are increasingly focused on ensuring and creating food security. Food security is defined as all people having ready access to sufficient affordable, safe, and nutritious food at all times (Food and Agriculture Organisation of the United Nations, 2001). In a recent report (2018) from the Food Security Information Network (FSIN), it was estimated that 124 million people across 51 countries are currently facing a food crisis. This is an overall increase of 16 million people since 2017 ("Food Security Information Network (FSIN) Global Report," n.d.). In 23 of these countries, the main factor contributing to the food insecurity is 'climate shocks', predominantly drought.

This problem is predicted to worsen in the upcoming decades. Climate change threatens to alter precipitation patterns, which is expected to increase the likelihood of flooding and droughts, and the prevalence of pests. Global temperatures are rising, as is the concentration of CO₂ in the atmosphere. Furthermore, current predictions envision the declaration of the day of 10 billion to occur by the year 2050, which will require food productivity to be increased on less land (United Nations, 2017). To meet demand, food production needs to increase by 70%, which corresponds to an extra

yield of 1 billion tonnes of cereals. The Food and Agriculture Organisation of the United Nations (FAO) identifies a key area of tackling this problem in protecting biodiversity to maintain the genetic variation that will be available to plant breeders, highlighting the importance of improving the crop production process (Food and Agriculture Organisation of the United Nations, 2009). They also attribute 50% of the global increase in crop productivity over the last century to plant breeding (Global Partnership Initiative for Plant Breeding Capacity Building (FAO), n.d.).

1.5.2 Meiosis and Plant Breeding

Traditional breeding technologies rely on the process of meiosis to introduce genetic variation. During meiosis, the allelic content of the parent is shuffled in the process of meiotic recombination, the product of which is genetic crossovers (COs). Plants displaying ideal characteristics (e.g., increased resistance to drought, pests *et cetera*) are crossed, and the resultant hybrids are screened for these traits. This forms the basis of the development of elite crop varieties.

Where COs form, however, is pre-determined and tightly limited in plants. This is especially pronounced in cereals: one of the most economically important crop groups, which are thought to account for 50% of human caloric intake each day (Awika, 2011). As previously mentioned, it is estimated that in barley and wheat, over 30% of the genes are in recombinatorially ‘cold spots’: areas that rarely receive a CO (Erayman *et al.*, 2004; Künzel and Waugh, 2002; Mayer *et al.*, 2011). One such example of this polarisation is chromosome 3B of the bread wheat *Triticum aestivum* L., where only 13% of the chromosome receives COs (Choulet *et al.*, 2014). The limitations placed on CO localisation thus impede the ability to introduce new, desirable alleles into extant crop varieties. It also contributes to linkage drag: a process by which an undesirable allele/gene is inherited due to its proximity to a desirable allele/gene.

Therefore, research into meiosis and the factors that determine where COs are made are of great importance if we are to increase how quickly new, elite cultivars can be made that will be better suited to the changing climate, and satisfy the demand for high quality, nutritious food (Lambing *et al.*, 2017).

Research councils, government organisations, and private companies are therefore collaborating to support research efforts into the advancement of crop breeding, with emphasis on improving access to recombination cold spots, and utilising gene editing technologies in plants.

1.6 Project Aims

The objective of this thesis is to further elucidate the roles and importance of the chromosome axis during meiosis, and how perturbing its dynamics and organisation affects recombination processes in *Arabidopsis thaliana*. This is with focus on a previously uncharacterised protein, ASY4 (At2G33973).

ASY4 was identified in an immuno-affinity proteomics study with BoASY1 (the homologue of ASY1 in *Brassica oleracea*), and independently by Mathilde Grelon's group (INRA, Versailles) in a BLASTP search with the sequence of ASY3 (Osman *et al.*, 2018; Chambon *et al.*, 2018). It was therefore suggested that ASY4 could be another axis-associated component.

In this project, we first examined the phenotype of two hypomorphic T-DNA insertion mutants for ASY4 to begin to uncover any potential meiotic role. We conducted a range of molecular and cytological experiments to determine if ASY4 was indeed axis-associated, with focus on examining fertility, CO number, and axis formation. To confirm its localisation at the axis, we developed a fluorescently tagged ASY4 line, and investigated potential protein-protein interactions with ASY3: one of the key axis proteins in *A. thaliana* (Ferdous *et al.*, 2012). This work was subsequently published in collaboration with the Grelon lab, and is presented at the end of this thesis (Chambon *et al.*, 2018).

As this analysis was conducted in hypomorphs, we sought to develop a true null mutant for ASY4 using the gene editing technique, CRISPR-Cas9. We then investigated the effects of a complete absence of ASY4 in *A. thaliana* on fertility, meiotic recombination, and axis organisation, including the use of structured-illumination microscopy to observe the axis in more detail. This research therefore

builds on previous knowledge of several axis components, but in particular, ASY1 and ASY3 (Armstrong *et al.*, 2002; Caryl *et al.*, 2000; Ferdous *et al.*, 2012).

As previously discussed, whilst the axis is known to influence COs, its precise role is unclear. Gaining an in-depth understanding of the roles of the chromosome axis during meiosis should shed light on the currently unknown processes that govern CO localisation and number. The ultimate aim of this research is to provide future targets that may facilitate manipulation of homologous recombination with minimal effect on fertility, working toward the ultimate goals outlined above of ensuring and creating food security in the upcoming decades.

Chapter 2

Materials and Methods

2 Materials and Methods

2.1 Plant Material

All *Arabidopsis thaliana* plant material was obtained from the European Arabidopsis Stock Centre (NASC), Nottingham, UK. Columbia (Col-0) ecotype was used as the wild-type control. T-DNA lines used in this study are listed in Appendix Table A1.

Plants were grown under glass in soil-based compost (4 parts M3 compost, 2 parts vermiculite, 1 part Silvaperl soil) with a lighting regime of 16 h light, and 8 h darkness. Temperature was maintained year-round at approximately 20°C.

2.1.1 Seed Sterilisation and Plant Selection

Prior to growth on MS Medium (as in Murashige and Skoog, 1962) for plant selection or germination assay, seeds were sterilised in 20% v/v bleach (Parozone), and then mixed at 200 rpm for 10 min. The bleach was then removed, and the seeds washed 3 x 5 min in sterile, distilled water. The seeds were then plated out in a petri dish on MS medium, and incubated at 4°C for 3 days to vernalise. Plates were then put under a 16 h light and 8 h dark light cycle at 21°C until the first rosettes were established. The plantlets were then transplanted into soil-based compost, and kept under the conditions outlined above.

If the plants had been transformed (as in 2.4), 50 µg/mL Kanamycin was added to the media to select for successful transformants. In the case of plants transformed with the CRISPR/Cas9 construct, a lower concentration of 30 µg/mL Kanamycin was used.

2.1.2 Seed Counts

10 to 15 siliques were taken from the primary stem from plants of a similar size, at either the point where the siliques had immature seeds, or when the plants were

completely dry. The siliques were then measured and dissected under a stereomicroscope, and the seeds counted.

2.1.3 Crossing *Arabidopsis thaliana* mutant lines

Arabidopsis plants were allowed to reach a growth stage where the central stem had become thick and sturdy, and the plants had developed open flower buds. Plants were treated differently depending on whether they were to contribute the egg or the pollen. If the plant was chosen to contribute the female gamete, all siliques and open flowers were removed. At the apical inflorescence, all but several of the largest buds were kept. These were then opened using jeweller's forceps to check if the stigma was at the correct size (large, sticky), and then the buds were emasculated by removing the immature anthers. A single open bud of the correct stage (large, yellow pollen visible) was taken from the plant chosen to contribute the male gamete, and rubbed onto the stigma until it was covered in pollen. Plants were then labelled and allowed to set seed.

2.2 Nucleic Acid Extraction and Manipulation

2.2.1 DNA Extraction

Up to 100 mg of *Arabidopsis* leaf tissue was first collected in sterile 1.5 mL microfuge tubes, selecting the smallest and youngest leaves for optimal DNA yield. Total genomic DNA was extracted using the DNeasy® Plant Mini Kit (Qiagen) as per the manufacturer's instructions.

2.2.2 DNA Extraction for Genotyping

No more than 0.5 cm² of leaf tissue was collected in a sterile 0.5 mL microfuge tube, and placed on ice. 40 µL of extraction buffer (10mM EDTA, 250mM KCl, and 100mM TRIS-HCl at pH 9.5) was added to the tube, and the leaf sample macerated using a 20-200 µL size sterile pipette tip until the buffer became green. The tube was then

incubated at 95°C in a PCR machine for 10 min, and then placed on ice for 2 min. 40 µL of dilution buffer (3% BSA, filter sterilised) was added, and then the sample was spun down in a table-top centrifuge for 1 min at 13,200 rpm. The supernatant was then transferred to a new sterile microfuge tube, taking care not to disturb the pellet. If the samples were not for immediate use, they were stored at -20°C until required.

2.2.3 RNA Extraction

All microfuge tubes, storage jars, and polypropylene pestles were washed overnight in 0.1% DEPC (diethylpyrocarbonate) and autoclaved prior to use to denature any RNases. Up to 100 mg of *Arabidopsis* buds, leaves, flowers, or siliques, were collected in DEPC treated 1.5 mL microfuge tubes, and flash frozen in liquid nitrogen. If the tissues were not used immediately, they were then stored at -80°C until required. RNA was extracted using the RNeasy® Mini Kit (Qiagen) as per the manufacturer's instructions.

To check RNA quality and to give an indication of concentration, 5 µL of sample RNA was added to 15 µL of RNA Sample Buffer (Thermo Fisher Scientific), and incubated at 65°C for 20 min, and subsequently quenched on ice for 2 min. This denatures secondary RNA structure. 20 µL of the sample was then run on a 0.8%-1% (w/v) agarose gel (Invitrogen) alongside HyperLadder™ 1 kb (Bioline).

2.2.4 Genotyping T-DNA Insertion Lines

Genotyping to confirm the presence or absence of a T-DNA was conducted using gene specific (GSP) forward (F) and reverse (R) primers, and a primer to the left border (LB) of the T-DNA. Primers were designed using the T-DNA Primer Design tool (SIGnAL, Salk Institute, available at: <http://signal.salk.edu/tdnaprimers.2.html>). For each plant, two PCR reactions were conducted with the following rationale. GSP F and GSP R

amplify products without a T-DNA insertion. Dependent on the direction of the T-DNA insert, the LB primer was paired with the appropriate GSP to amplify products where the insert is present. If the plant was wild-type for the insert, then only the reaction with GSP F and GSP R would provide a band. If the plant was homozygous for the insert, only the reaction with the GSP and LB would produce a band. Heterozygous plants would have a band visible for both reactions. Primers used are listed in Appendix Table A2.

PCR was conducted using DreamTaq (Thermo Fisher Scientific), as per the manufacturer's instructions. PCR products were visualised via DNA electrophoresis on 0.8%-1% (w/v) agarose gel (Invitrogen) alongside HyperLadder™ 1 kb (Bioline).

2.2.5 RT-PCR

RNA was extracted from *Arabidopsis thaliana* Columbia ecotype plants as described in **2.2.3**. 1st Strand cDNA synthesis was completed using the Invitrogen Superscript II kit, as per the manufacturer's instructions. This is with the exception of the use of RNasin® Ribonuclease Inhibitor (Promega) as opposed to RNaseOUT™ (Invitrogen). Primers for RT-PCR are listed in Appendix Table A3.

2.2.6 Spectrophotometry

Quantification of DNA and RNA concentration (ng/µL) was determined using a NanoDrop® ND-1000 Spectrophotometer. Where a more accurate measure was required, DNA and RNA concentration was determined using the Qubit™ 2.0 Fluorometer (Invitrogen). Protocol was followed as per the manufacturer's instructions for the specific buffer kits provided.

2.3 General Cloning

PCR products amplified using a *Taq*-based polymerase were conducted using the p-GEM®-T Easy kit from Promega, as per the manufacturer's instructions. For cloning PCR products with blunt ends, such as those produced by high-fidelity enzymes (e.g. Phusion), the Zero Blunt® PCR Cloning Kit (Invitrogen) was used, as per the manufacturer's instructions.

2.3.1 Transformation of chemically competent *Escherichia coli* DH5 α via Heat Shock

50 μ L aliquots of *E. coli* DH5 α cells were removed from storage at -80°C, and thawed on ice. Once thawed, the appropriate amount of plasmid DNA (usually between 1 μ L and 10 μ L) was added to the cells, gently swirled to mix, and incubated on ice for 30 min. The cells were then subjected to heat shock by placing the tubes in a 42°C water bath for 90 s, and then returned to ice for 3 min. 900 μ L of lysogeny broth was then added to the tube, and the cells allowed to recover by incubation at 37°C for 1h, horizontally, with 220 rpm shaking.

150 μ L of the mixture was then spread on LB agar (LA) plates with the appropriate antibiotic, and incubated at 37°C for between 16 and 18 h. Concentrations for antibiotics are listed in 2.3.4.

2.3.2 Transformation of electrocompetent *Escherichia coli* DH5 α via Electroporation

10 μ L of the mix containing the plasmid of interest was first dialysed for 45 min on a MF-Milipore™ Nitrocellulose membrane (Merck), floating in ddH₂O in a petri dish. 50 μ L aliquots of cells were removed from storage at -80°C, and allowed to thaw on ice. 10 μ L of dialysed plasmid was then added to the cells, and gently swirled to mix. The

cells and plasmid mix was then pipetted into a chilled electroporation cuvette, and placed into the Electroporator (Bio-Rad) using the 'Ec2' setting. 800 µL of liquid LB was then added to the cuvette. The mix was then transferred into a 2 mL microfuge tube, and incubated horizontally at 37°C for 1 h with 220 rpm shaking.

150 µL of the mixture was then spread on LA plates with the appropriate antibiotic (concentrations **2.3.4**), and incubated at 37°C for between 16 and 18 h.

2.3.3 Transformation of electrocompetent *Agrobacterium tumefaciens* GV3101 via Electroporation

Transformation of electrocompetent *Agrobacterium tumefaciens* (strain GV3101) was as above in **2.7.2**, with the exception of the use of the 'Agr' setting on the Electroporator (Bio-Rad). For the recovery period, cells were incubated horizontally at 28°C with 200 rpm shaking for 2 h. 150 µL of the mixture was then spread on an LA plate, with rifampicin, gentamycin, and the plasmid-specific antibiotic (concentrations **2.3.4**) and incubated at 28°C for at least 48 h.

2.3.4 Bacterial Selection

In all cases, Ampicillin was used for selection at 100 µg/mL; Kanamycin was used at 50 µg/mL; Spectinomycin at 100 µg/mL; Gentamycin at 50 µg/mL; and Rifampicin at 100 µg/mL.

2.3.5 Colony PCR

To confirm the presence of the insert of interest in selected bacterial colonies before growth in liquid media, the individual sample colonies were split in half. Half was used to re-streak onto a fresh LA plate with the appropriate selection antibiotic(s), and half used to inoculate 20 µL of sterile distilled water. 2 µL of the bacterial mix was then

used as DNA template in a PCR reaction using DreamTaq (Thermo Fisher Scientific) as per the manufacturer's instructions.

2.3.6 Plasmid DNA Extraction

Individual selected *E. coli* colonies were used to inoculate 10 mL of liquid LB in a 100 mL conical flask with the appropriate selection antibiotic (concentrations **2.3.4**). Cultures were incubated overnight (16-18 h) at 37°C with 220 rpm shaking. 500 µL of culture was taken to make a glycerol stock (added to 500 µL 50% glycerol, then stored at -80°C). 5 mL of the remaining culture was used for plasmid extraction using the GeneJET Plasmid Miniprep Kit (Thermo Fisher Scientific).

To once more confirm if the plasmid contained the insert, 3 µL of plasmid was digested with the appropriate restriction enzyme(s) to release the insert, and was then imaged on a 0.7% (w/v) agarose (Invitrogen) gel.

2.3.7 *Saccharomyces cerevisiae* Transformation via Polyethylene Glycol/Lithium Acetate

Transformation of *S. cerevisiae* Y2H Gold Competent cells (Clontech/Takara). Yeast Transformation Buffer (YTB) was prepared by combining 400 µL 50% PEG 3350, 200 µL 1M Lithium Acetate, and 4 µL β-Mercaptoethanol (all provided by Sigma). 100 µL of YTB was added to a 2 mL microfuge tube containing 2 µg of each pDEST vector. This was vortexed briefly to mix. One 1 µL loop of yeast was used to inoculate the YTB. The tubes were then incubated at 37°C for 45 min with 200 rpm shaking at a 45° angle. The entire mix was then spread onto Synthetic Defined (SD) /-Leucine/-Tryptophan dropout media (DDO) (as in **2.3.7.1**), and incubated at 30°C for 3 to 5 days.

2.3.7.1 Yeast Media Preparation

All yeast media was prepared by adding a pouch of pre-mixed SD media powder (Takara) to 500 mL of sterile distilled water. The media was then autoclaved. Plated media was stored at 4°C, and liquid media stored at room temperature, in a sterile manner until required.

2.4 Transforming *A. thaliana* with *Agrobacterium tumefaciens* via floral dipping

A. thaliana plants were grown as in 2.1 until the primary stem had bolted. The plants were then cut back to induce an increased number of stems to grow. Once the plants had bolted again and had produced closed buds, they were chosen for transformation via floral dipping (Clough and Bent 1998), performed as below.

Agrobacterium tumefaciens (strain GV3101) was transformed via electroporation, and selected for as described in 2.3.3.

Up to three colonies were then used to inoculate 5 mL LB with rifampicin, gentamycin, and the appropriate marker antibiotic for the plasmid of interest. The cultures were grown for 24 h at 28°C with 200 rpm shaking.

To confirm the presence of the plasmid of interest, an aliquot of the culture was taken forward for PCR. The aliquot was first diluted 1:50 into ddH₂O, prior to amplification with the appropriate primers, as in 2.3.5. Once the presence of the plasmid of interest was confirmed, 1.5 mL of this original 5 mL culture was used to inoculate 500 mL of LB containing the appropriate antibiotics. This culture was grown for 48 h at 28°C with 200 rpm shaking. The cultures were then allowed to cool at room temperature for 15 min. The culture was then halved, and transferred into two sterile 250 mL centrifuge tubes. The tubes were then centrifuged for 10 min at 5000 rpm, at 4°C. Following

centrifugation, the supernatant was removed, and the pellets resuspended in 100 mL of 5% sucrose solution. Following resuspension, a further 150 mL of 5% sucrose solution, and 65 µL of Silwet-77 (Lehle Seeds), was added to each tube. The two tubes were then combined into an autoclaved P1000 tip tray.

Plants were dipped and stirred in the solution for approximately 15 s. The plants were then incubated horizontally overnight under high humidity, and in darkness. The plants were then allowed to dry vertically on the bench top, before being returned to the glasshouse.

2.5 Yeast-2-Hybrid

2.5.1 Cloning into pENTR™/D-TOPO® and pDEST vectors

RNA was extracted from unopened *A. thaliana* flower buds, as described in 2.2.3. Total cDNA synthesis was then conducted using the Tetro™ cDNA Synthesis Kit (Bioline), and the supplied oligo dT₁₈ primer, as per the manufacturer's instructions. The cDNA of interest (ASY4 (full length and halves), ASY3, ASY3 coiled-coil, ASY1) was then amplified using Phusion polymerase (New England Biolabs). Primers used can be found in Appendix Table A4. Importantly, the forward primer contained a CACC addition to the 5' end for TOPO cloning. The product was then cloned into pENTR™/D-TOPO® (Invitrogen) as per the manufacturer's instructions. Incubation times varied dependent on the size of the product to be cloned:

Table 2. 1 Incubation times for TOPO reactions

| Size of Product (kb) | Incubation time at Room Temperature (min) |
|-----------------------------|--|
| >2 | 10 |
| $1 \leq x \leq 2$ | 5 |
| <1 | 0.5 |

The whole reaction mix was then used to transform One Shot™ TOP10 Chemically Competent *E. coli* (Invitrogen), as per the manufacturer's instructions. The bacteria were then incubated overnight on LB agar plates with kanamycin. Colony PCR was performed as per **2.3.5** to confirm the presence and orientation of the insert (primers in Appendix Table A4). Correct colonies were taken forward to inoculate 10 mL of LBB with kanamycin. Cultures were incubated as in **2.3.4**, and the plasmid extracted as in **2.3.6**. Plasmid was then submitted for in-house sequencing.

A Gateway reaction was then performed to shuttle the insert into the pDEST-22 and pDEST-32 vectors (Invitrogen) using the LR Clonase® II Kit, as per the manufacturer's instructions.

The mix was incubated at room temperature for 1 h 30 min. To stop the reaction, 0.5 µL of Proteinase K (Invitrogen) was added, and the mix incubated at 37°C for 10 min before transferring to ice. The whole reaction mix was then used to transform One Shot™ TOP10 Chemically Competent *E. coli* (Invitrogen), as per the manufacturer's instructions. Selection performed as in **2.3.4**. Colony PCR and overnight cultures

performed as for cloning into the entry vector. Primers used are listed in Appendix Table A4.

2.5.2 Yeast-2-Hybrid Assay

After incubation on DDO plates, a discrete single colony selected to inoculate SDW in a 1.5 mL microfuge tube. Different volumes of SDW were used: 100 µL SDW for test samples, and 400 µL for the positive control. This was to account for the fact that the positive control grows significantly faster than the samples. Three colonies were used in total for three replicate plates.

5 µL was taken from each microfuge tube, and plated onto DDO, TDO (SD/-Leucine/-Tryptophan/-Histidine), and QDO (SD/-Leucine/-Tryptophan/-Histidine/-Adenine) plates (preparation as in **2.3.7.1**). Plates were incubated at 30°C for 3-5 days, or until the colonies had reached ~5 mm in diameter. Plates were then photographed using a Nikon D5000 camera.

2.6 Targeted Gene Editing in *Arabidopsis thaliana* using the *Staphylococcus aureus* CRISPR-Cas9 system

The pDe-Sa-Cas9 destination vector and pEn-Sa-Chimera entry vector based on the CRISPR-Cas9 system in *Staphylococcus aureus* were obtained from the Holger Puchta laboratory (Karlsruher Institut für Technologie, Germany; <http://www.botanik.kit.edu/molbio/940.php>). Vector maps can be found in Appendix Figure A1. The following protocol is based on the generation of a CRISPR construct using the *Streptococcus pyogenes* system by Schiml *et al.*, 2016.

Oligonucleotides to target *AtASY4* were designed using the online CCTop tool, with the Protospacer Adjacent Motif (PAM) sequence set to NNGRRT for *S. aureus* (available at: <http://crispr.cos.uni-heidelberg.de/>), and the appropriate overhangs complementary to the sticky ends produced by BbsI digestion added to the 5' ends. The oligonucleotides, and all primers used for this experiment can be found in Appendix Table A6. Oligonucleotides were ordered from Eurofins Genomics, with HPLC purification. pEn-Sa-Chimera was propagated in Bioline α-Select Gold Efficiency cells, as per the manufacturer's instructions. pDe-Sa-Cas9 was propagated in *E. coli* strain DB3.1, transformed by heat shock as in **2.3.1**.

2.6.1 Making the CRISPR-Cas9 ASY4 construct

The *AtASY4* forward and reverse oligonucleotides were diluted to 50 μM each, and 2 μL of each added to 46 μL of SDW. The mix was then heated to 95°C for 5 min to denature, then allowed to anneal at room temperature for 20 min. The oligonucleotides were then stored at -20°C until required.

pEn-Sa-Chimera was prepared for cloning by digestion with BbsI (New England Biolabs) as per the manufacturer's instructions, and purified using MSB® Spin PCRapace kit (Stratec Molecular), as per the manufacturer's instructions. The annealed oligonucleotides were then ligated into the BbsI digested pEn-Sa-Chimera as follows:

Table 2. 2 Components required for the ligation of annealed oligonucleotide pairs into the entry vector, pEN-Sa-Chimera.

| Component | Amount |
|---|--------|
| BbsI Digested pEn-Sa-Chimera (at 5 ng/uL) | 3 µL |
| Annealed Oligonucleotide pair | 4.5 µL |
| T4 Buffer | 1.5 µL |
| T4 Ligase | 1 µL |
| SDW | 5 µL |

The complete ligation mix was then transformed into Bioline α-Select Gold Efficiency cells, as per the manufacturer's instructions. Selection on LA media with Ampicillin was conducted as in **2.3.4**, colony PCR with SS129/ASY4Pair(x)F was performed as in **2.3.5**, and plasmid extraction as in **2.3.6**. The resultant concentration of DNA was then determined using the Qubit (as in **2.2.6**).

Plasmids from three of the successful colonies were then selected, and sequenced using SS42. Once the presence of the correct insert was confirmed, Gateway cloning performed as follows:

Table 2. 3 Components required for the CRISPR Gateway reaction.

| Component | Amount |
|--|--------|
| pEn-Sa-Chimera with ASY4 oligos (at 100 ng/µL) | 2 µL |
| pDe-Sa-Cas9 (at 50 ng/µL) | 3 µL |
| TE Buffer (Tris-EDTA), pH 8 | 4 µL |
| LR Clonase™ II (Invitrogen) | 1 µL |

The reaction mix was then incubated for 3 h at 25°C. The reaction was then stopped by the addition of 1 µL of Proteinase K (Invitrogen), and incubated at 37°C for 10 minutes. The mix was then transformed via heat shock into One Shot OmniMax® 2 T1^R chemically competent cells (Invitrogen), and selected for on LB and 100 µg/mL Spectinomycin plates. Success was determined via colony PCR with SS42 and SS102.

Following miniprep, the resultant plasmid was double digested with AflII and NheI (New England Biolabs), as per the manufacturer's instructions, and run on a 0.8% agarose Ethidium bromide gel. The plasmid was also sequenced using SS42/SS61 for final confirmation that the sequences were correct.

2.6.2 Transforming *A. thaliana* with CRISPR-Cas9

Confirmed CRISPR-Cas9 ASY4 vectors were then used to transform *A. tumefaciens* (as per 2.3.3), and the successful transformants subsequently used to transform Col-0 *A. thaliana* via floral dip (as per 2.4).

2.6.3 Selection and Identification of potential mutants

T0 primary transformants were grown on soil under long day conditions post-dip (as in **2.1**), and allowed to set seed. The subsequent generation (T1) were put to kanamycin MS plates (as per **2.1.1**) to select for plants containing the CRISPR/Cas9 construct. Plants were transplanted to soil after 14 days growth on MS media (as in **2.1.1**), and genotyped for the Cas9 construct using SS42/SS102 to be certain the construct was present. Plants were then allowed to set seed.

The subsequent generation (T2) was then screened on Kanamycin MS plates (as in **2.1.1**) for Mendelian segregation of Kanamycin resistance, as this would confirm that there was only one copy of the CRISPR/Cas9 construct inserted in the genome. For each correctly segregating line, at least 10 seeds were put directly to soil.

Initial PCR screening for novel mutants was conducted using DreamTaq (Thermo Fisher Scientific) on DNA extracted from leaf discs (as in **2.2.2**) with the primers ASY4 CRISPR Check F2/ASY4 CRISPR Check R1, and the products analysed on an ethidium bromide agarose gel. Gel imaging detects band shifts (INDELS), or potential rearrangements (e.g., no band present). If the PCR result proved promising, the primers A4_WHOLE_F1/A4_WHOLE_R2 which amplify ASY4 from the intergenic region through to the 3'-UTR were used. PCR mixes from all plants were purified using MSB® Spin PCRapace (Stratec Molecular) as per the manufacturer's instructions. The purified product was then sent for sequencing by Eurofins Genomics to confirm any mutations.

2.6.3.1 Genotyping the final *asy4-4* mutant line

To check that the *asy4-4* mutant carries the deletion, and has no Cas9, three PCRs are conducted on leaf-discs (as in **2.2.2**), and analysed on an ethidium bromide gel.

The first PCR checks for the INDEL (i.e., a band shift of approximately 1.7 kb) using primers A4 CR F1 and A4 CR F2. This PCR does detect heterozygous plants, but to be certain, the plants are then analysed using ASY4 CRISPR Check F2/ASY4 CRISPR Check R1 to check if there is a WT size band. The final PCR (optional in later generations) will check for the presence of Cas9 using SS42/SS102.

2.7 Cytology

2.7.1 DAPI Staining of Meiocytes

Arabidopsis inflorescence were picked from the plants using sharp forceps, and fixed on ice in 3:1 100% ethanol:glacial acetic acid. The fixative was changed three times in the space of two days, and the fixed material stored between 4°C-10°C until required.

The inflorescences were washed in citrate buffer (at pH 4.5) in a watch glass three times, for five minutes each. During these washes, the opened buds and larger buds containing pollen were removed from the inflorescence, leaving only those that should contain meiocytes. Following the last wash, 300 µL of digestive enzyme mix (0.3% cellulase and 0.3% pectolyase in 10 mM citrate buffer) was added to the watch glass, ensuring all of the buds were completely submerged. The watch glasses were then placed in a humid container, and incubated at 37°C for 1 h 35 min. After this time, the enzyme mix was removed, and replaced with 200 µL of sterile, distilled water to prevent over-digestion. 1-2 buds were then selected based on size (between 400 µm and 500 µm), and picked out with fine-pointed forceps. The chosen buds were then released onto a glass microscope slide, and subsequently macerated with the end of a brass rod until fine. 10 µL of 60% glacial acetic acid was then added to the slide, and the slide was placed on a heated plate set to 45°C for 30s, stirring continuously.

Another 10 µL of 60% acetic acid was added, and the slide heated for a further 30s. After this time, 100 µL of fresh, cold fixative (as above) was used to wash the slide. The slide was then dried using a hairdryer. Once dry, the slides were mounted in 7 µL of 1 µg/mL DAPI (4',6-diamidino-2-phenylindole) in Vectashield mounting medium (Vector Laboratories).

Slides were stored at 4°C thereafter.

2.7.2 Fluorescence *in-situ* Hybridisation (FISH) of meiotic spreads

Slides stained using DAPI (**2.8.1**) were selected based on how many metaphase I spreads they contained, determined via fluorescence microscopy. These slides were then washed in a coplin jar in 100% ethanol for 10 min to dissolve Vectashield, thereby allowing the removal of the coverslips. The slides were then washed for 1 h in 4T (4X SSC (sodium chloride and sodium citrate buffer: for 20x SSC, 3M NaCl, 300 mM trisodium citrate, pH 7)), and 0.05% Tween 20), and then washed for 10 min in 2X SSC at room temperature. Slides were then washed in a pepsin solution (0.01% pepsin in 0.01M HCl at 37°C) for 90 s to destroy the cytoplasm, and then immediately washed in 2X SSC for 10 min to remove debris from the digest. In a fume hood, the slides were then washed in 4% paraformaldehyde (pH 8) for 10 min. To dehydrate the material, the slides were then washed for 2 min each in a series of 70%, 90%, and 100% ethanol. The slides were then drained, and allowed to dry in the fume hood for at least 15 min. 20 µL of labelled probe mix (prepared as in **2.8.2.1**) was added to the slide, and a coverslip gently placed atop it. The coverslip was not pressed down, but sealed onto the slide with rubber solution. The slide was then heated on a hotplate set to 75°C for 4 min. Slides were then incubated overnight in the dark in a humid chamber at 37°C. The rubber solution was then peeled away using a pair of fine-pointed tweezers, and the coverslips removed. Slides were then washed 3 times for 5 min

each in 50% formamide and 2X SSC pre-heated to 45°C. The slides were then washed in 2X SSC at 45°C for 5 min, 4T at 45°C for 5 min, and finally for 5 min in 4T at room temperature. Excess 4T was then drained from the slides, but the slides were not allowed to dry before the addition of the secondary antibodies (anti-Digoxigenin conjugated to FITC (fluorescein isothiocyanate), anti-Biotin (Avidin conjugated to Cy3)). Anti-Digoxigenin was prepared in dioxigenin blocking solution, comprised of 0.25 g of Boehringer Mannheim DIG nucleic acid blocking reagent, diluted in 4X SSC and 0.05% Tween20. Anti-Biotin was diluted in milk blocking solution, comprised of 2.5 g of skimmed milk powder, also diluted in 4X SSC and 0.05% Tween20. 80 µL of the first secondary probe was added to a slip of parafilm cut to the size of a coverslip, which was placed atop the slide. The slides were then incubated in the dark for 30 min at 37°C. The parafilm was then gently removed with tweezers, and the slides washed in the dark 3 times for 5 min each in room temperature 4T. The secondary antibody was then added, and then incubated and washed as was executed for the secondary probe. Slides were then finally washed in a series of 70%, 90% and 100% ethanol for 5 min each at room temperature, and then were left to dry for 15-20 min. 10 µL of DAPI in Vectashield was then added to the coverslip, and the slide pressed gently atop it. The slides were then viewed with an epi-fluorescence microscope (Nikon, 90i).

Slides were stored at 4°C thereafter.

2.7.2.1 Probe Preparation for FISH

The 45s and 5s probes were labelled using the Biotin or DIG-Nick translation mix (Roche, via Sigma Aldrich). Probes were prepared by adding 14 µL of hybridisation master mix (1 mL 20X SSC (as in **2.8.2**), 5 mL deionised formamide, and 1 g dextran sulphate (MW 500,000) in 10 mL SDW, pH 7) to 0.5-2 µL of labelled probe, and then the mix was made up to a final volume of 20 µL with sterile, distilled water. The mix

was then incubated in a PCR machine at 94°C for 10 min to denature the probes. This was then kept on ice until required.

2.7.3 Spreading Immunolocalisation using Fresh Material

Unopened buds from *Arabidopsis* inflorescence were picked using fine-pointed forceps, and immediately transferred to wet filter paper in a petri dish lid. The buds were then picked out from up to 4 inflorescence using fine-pointed forceps and a sharp mounted needle, and arranged by size. Starting with the largest buds (~ 500 µm), the anthers were dissected out, and one anther taken for staging (see **2.8.3.2**). Anthers were placed in a pile on the filter paper. 5 µL of digestion mix (0.4% cytohelicase, 1.5% sucrose, 1% polyvinylpyrrolidone) was added to the centre of a washed glass microscope slide (washed in a series of in 100% acetone, sterile distilled water, and 100% ethanol for five min each), and the anthers placed into it using fine-pointed forceps. The anthers were then macerated with the end of a brass rod for approximately 1 min. A further 5 µL of digestion mix was added, and then the slide was incubated at 37°C in a humid chamber for 2 min. The slide was then removed from the chamber, and 10 µL of 1-1.5% Lipsol added. The mixture was gently stirred with the end of a pipette tip, and spread into a square smaller than the size of a cover slip. In a fumehood, 20 µL of 4% paraformaldehyde was added to fix the cells. The mix was stirred once more, and then the slides were allowed to dry in the fumehood for at least 2 h, taking care to ensure the slides were kept flat. Once dry, 50 µL of the primary antibodies diluted in blocking solution (1% bovine serum albumin (BSA) in PBS) were added to a piece of parafilm (Sigma-Aldrich) cut to the size of a coverslip (3 x 3 cm). Primary antibodies used for immunolocalisation and their dilutions can be found in Appendix Table A7. The slide was briefly dipped into PBST (phosphate buffered saline, 0.1% Triton X₁₀₀), briefly dried, and then placed onto the parafilm. The

slides were then incubated overnight at 4°C in a humid chamber. After overnight incubation, the parafilm was removed, and the slides washed 3 times for 5 min each in PBST. 50 µL of the appropriate secondary antibody (all Alexa Fluor™, Thermo Fisher Scientific) was added to fresh parafilm slips and then added as above. The slides were then incubated for 30 min in a humid chamber at 37°C. Following incubation, the slides were washed 3 times for 5 min each in PBST in the dark to prevent photobleaching. The slides were then dried, and mounted in 7 µL 1 µg/mL DAPI in Vectashield.

Slides were stored at 4°C thereafter.

2.7.3.1 Modified Immunolocalisation protocol for Structured Illumination Microscopy (SIM)

If the slides were for SIM, some alterations were made to the immunofluorescence protocol. These were as follows:

1. Buds were prepared directly onto a high precision coverslip (No. 15, Marienfeld), rather than onto the slide.
2. Slides were pre-blocked by adding 50 µL 3% bovine serum albumin directly to the coverslip, covering with a square of parafilm, and incubating on the bench-top for 5 min before primary antibody incubation.
3. Primary antibodies were added as previous, but were incubated at 37°C in a humid chamber for 45 min. After this time, the coverslips were washed in a petri dish containing PBST as previous. After washing, the coverslip was dipped in sterile distilled water.
4. Secondary antibodies were added as previous. Following washing in PBST, 50 µL of 1 µg/mL DAPI was then added to the coverslip, covered with parafilm,

and incubated at room temperature for 10 min. The coverslips were then washed in PBST 3 times, and then once in sterile distilled water, before finally being mounted in 7 µL Vectashield.

2.7.3.2 Staging buds using Aceto-Orcein

To determine which buds contain meiocytes of the desired stage, one anther was taken from each bud, and placed on a glass microscope slide. A small drop of aceto-orcein was added, and a coverslip pressed atop it. The slide was then viewed via bright-field microscopy. Working back to the largest bud that did not contain pollen provided assurance that all buds smaller should contain meiocytes. This is usually between bud widths of ~350 µm to ~500 µm.

2.7.4 Immunolocalisation on Acid-Fixed Material (Microwave Technique)

As developed by Chelysheva *et al.*, 2010. Slides were prepared as per **2.7.1** with the exception of not adding the DAPI-stain unless the slides had already been stained and imaged. In a coplin jar, coverslips were removed by immersing the slides in 100% ethanol. Citrate buffer (10 mM tri-sodium citrate, adjusted to pH 7 using citric acid) was then heated in a microwave until it began to boil. The slides were then placed in a plastic slide rack, and immersed in the hot citrate buffer for 45 s. The slides were then immediately washed in PBST (as in **2.7.3**) for 5 min. The slides were then blocked using 50 µL of EM block (as in **2.7.3**) added to a piece of parafilm, cut to the size of a coverslip. The slides were placed atop this, and incubated at room temperature for 5 min. Antibody staining was as in **2.7.3**, and antibody concentrations as in Appendix Table A7.

Slides were stored at 4°C thereafter.

2.7.5 Microscopy and Image Analysis

Microscopy was conducted on a Nikon 90i Epifluorescence microscope, and the initial image analysis and editing using the NIS-Elements software (Nikon). Slides for SIM were imaged using the Zeiss ELYRA PS1 at the John Innes Centre, Norwich, UK. Later analysis and processing was conducted within FIJI (ImageJ; available at: <https://imagej.net/Fiji/>).

Measuring of the synaptonemal complex lengths was conducted within FIJI using the 'Simple Neurite Tracer' plugin. Data was then exported to GraphPad Prism 7 for statistical analysis.

2.8 Bioinformatics and Sequencing Analysis

Sequencing analysis, alignments, and vector maps were generated within Geneious 9.1.7 for Mac OS X (available at: <http://www.geneious.com/>). Protein and nucleic acid data was gathered from the SALK Arabidopsis 1,001 Genomes database.

2.9 Statistics

All statistical analysis was carried out using GraphPad Prism 7 for Mac OS X Version 7.0d (available at: <https://www.graphpad.com/scientific-software/prism/>), after ensuring all parameters for each test used had been met.

Chapter 3

**ASYNAPTIC 4 is a novel component
of the meiotic chromosome axis in
*Arabidopsis thaliana***

3 ASYNAPTIC 4 is a novel component of the meiotic chromosome axis in *Arabidopsis thaliana*

3.1 Introduction

As discussed, previous work has identified the main components of the chromosome axis in *A. thaliana* to be ASY1, ASY3, the cohesin complex, including the meiosis specific kleisin, REC8/SYN1, and likely TOPII (Armstrong *et al.*, 2002c; Bai *et al.*, 1999; Cai *et al.*, 2003; Caryl *et al.*, 2000; Ferdous *et al.*, 2012a; Martinez-Garcia *et al.*, 2018; Osman *et al.*, 2018; Sanchez-Moran *et al.*, 2007). To begin to document which other proteins the axis interacts with, Osman and colleagues (2018) conducted an immuno-affinity proteomics (co-IP) study using BoASY1: the ASY1 homologue in *Brassica oleracea*. From a pool of 589 proteins pulled-down with BoASY1, 492 orthologues were identified in *Arabidopsis*. Of these, 11 were of unknown function. Concurrent with this study, one of the genes of unknown function identified by Osman *et al.* (2018) had also been identified by Mathilde Grelon's group (INRA, France) in a BLASTP homology search using the ASY3 sequence, and named ASY4: At2G33793 (Chambon *et al.*, 2018). The Chambon *et al.* (2018) paper is presented at the end of this thesis.

ASY4 is predicted to be a comparatively small protein, composed of only 212 amino acid residues (24.6 kDa). ASY4 has 23.9% identity and 40.1% similarity to ASY3, and aligns to the C-terminal coiled-coil region of ASY3 (Figure 3.1).

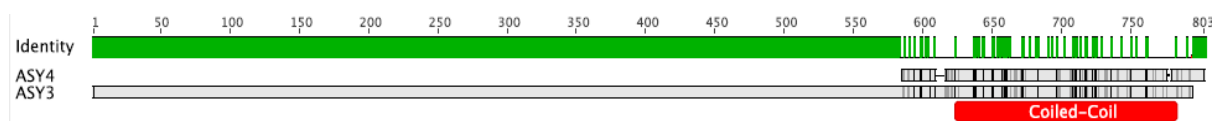


Figure 3.1 ASY4 ClustalW Alignment of ASY3 and ASY4. Greyscale boxes denote areas of identity, from black (100%) through to light grey/white (0%). This information is also shown in the green 'identity' bar. Red coiled-coil label illustrates the coiled-coil region of ASY3 between amino acid residues 623-785.

ASY4 is predicted to contain two coiled-coil domains in the central portion of the protein, separated by 26 amino acid residues (Figure 3.2) (Chambon *et al.*, 2018). Three T-DNA insertion mutant lines were obtained for the gene, with positions in the promoter region (characterised in Osman *et al.*, 2018), the fourth exon (asy4-2), and in the fifth exon (asy4-1) (Chambon *et al.*, 2018) (Figure 3.2).

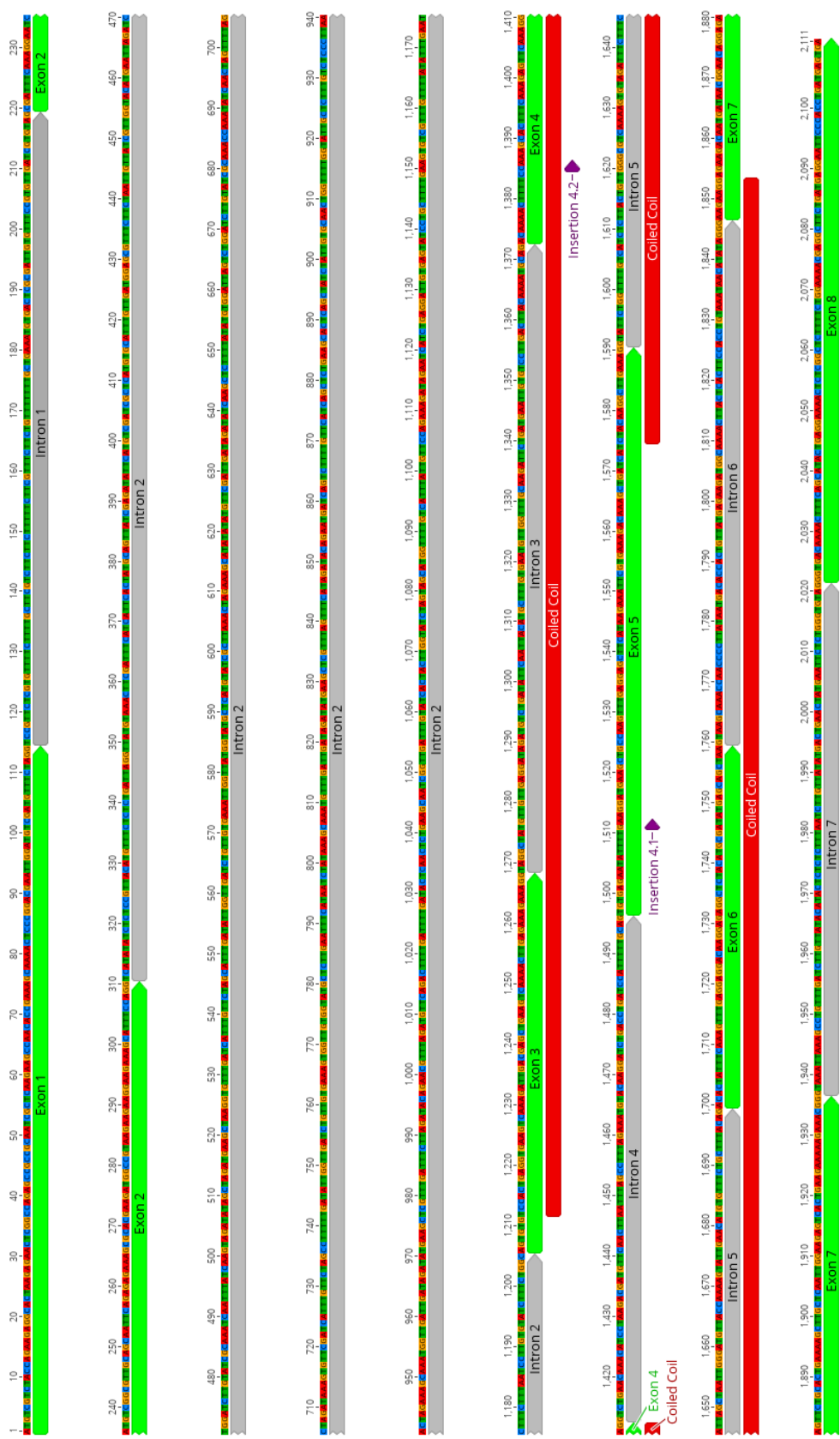


Figure 3.2 ASY4 gDNA Annotation. Green boxes illustrate the exonic sequences. Grey boxes indicate the introns. Red stretches show the regions predicted to be coiled-coil domains. Insertion 4.2 and Insertion 4.1 show the sites of T-DNA insertions.

Outside of plants, this protein appears to have no obvious homologues based on protein BLAST searches; this is not unexpected due to the high sequence divergence observed in meiotic chromosome structural components (Bomblies *et al.*, 2015). It is therefore possible that characterisation will reveal any functional homologues ASY4 may have in other organisms.

In this study, we analysed the two separate T-DNA insertion mutant *asy4* lines to begin to uncover any meiotic role for ASY4. This initially encompassed cytological analysis, and later, complementation with a fluorescently tagged version of ASY4. We have confirmed ASY4 localisation at the chromosome axis during meiosis, and its importance for proper formation of the synaptonemal complex and normal levels of homologous recombination.

Characterisation of the three *asy4* mutant lines was conducted independently by both the Birmingham Franklin/Sánchez-Moran lab, and Mathilde Grelon's lab at the INRA, Versailles, France. All the results presented in this thesis were obtained through my own work unless otherwise stated.

3.2 Results

3.2.1 T-DNA insertions in *asy4* cause a reduction in fertility that correspond with errors during meiosis

Two T-DNA insertion mutant lines for ASY4 were obtained from a private collection and sent to Birmingham by the Grelon lab, further to the initial allele (*asy4-3*) discussed in Osman *et al.* (2018). These are the lines *asy4-1* and *asy4-2*. The locations of the respective T-DNAs are labelled in Fig. 3.2, denoted as 'Insertion 4.1' and 'Insertion 4.2', respectively.

3.2.1.1 *asy4-1* and *asy4-2* produce a truncated ASY4 transcript

To confirm whether the T-DNA insertions had successfully prevented expression of ASY4, I conducted RT-PCR on cDNA obtained from buds from WT, *asy4-1*, and *asy4-2* using two sets of primers: one to amplify the full-length ASY4 product, and one set to amplify from up to the 4.2 T-DNA insertion site (RT-PCR as in **2.2.5**; primers in Appendix Table A3). Furthermore, in WT, I also conducted RT-PCR on cDNA from leaves, siliques, and open flowers to determine whether ASY4 transcription is meiosis specific.

PCR products obtained from the reactions were analysed via gel electrophoresis (Fig. 3.3). In WT, the full-length ASY4 transcript was identified in buds, open flowers, and as a very faint band in siliques (Fig. 3.3 A), suggesting that ASY4 transcription is not meiosis specific. I also show that whilst bands for full-length ASY4 are not present in the *asy4-1* and *asy4-2* mutants, both produce a ~200 bp product from upstream of the T-DNA insertion sites, suggesting these plant lines to be partial knock-outs of ASY4 (Fig. 3.3 B). The Grelon group also obtained this result in an independent experiment with different primers. Based on this result, we propose the *asy4-1* and *asy4-2* mutants are hypomorphic.

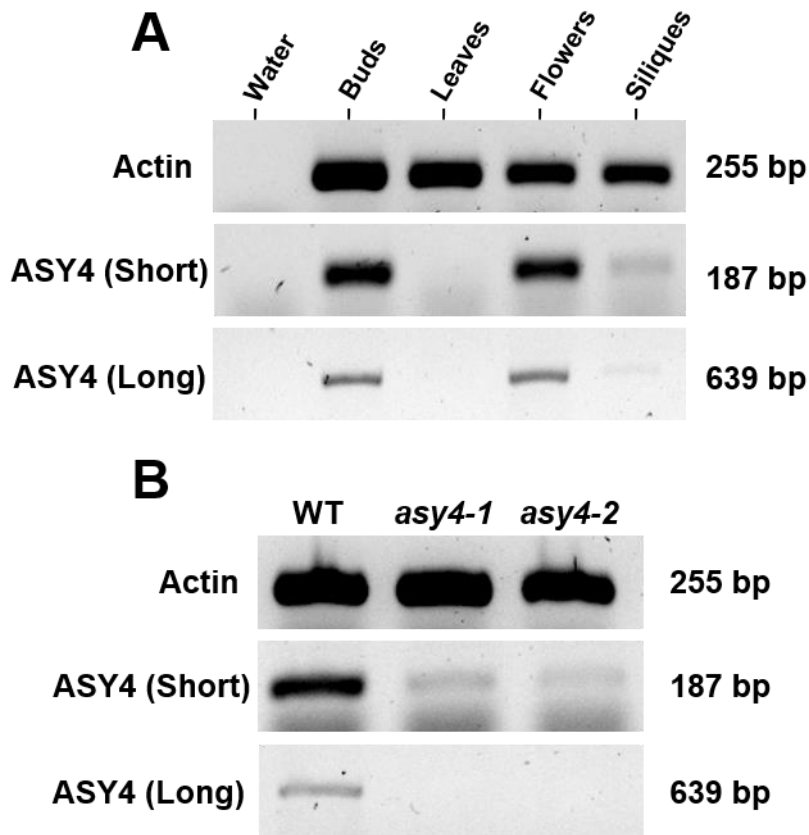


Figure 3.3 Expression of ASY4 in various *Arabidopsis* tissues and *asy4* mutants. Gel electrophoresis imaged using ethidium bromide. **(A)** Analysis of ASY4 transcription in various aerial tissues in WT *A. thaliana*. **(B)** A truncated 187 bp product of ASY4 is present in the *asy4-1* and *asy4-2* mutants.

3.2.1.2 *asy4-1* and *asy4-2* have reduced fertility and crossover number

Initial characterisation of the three *asy4* mutants involved seed counts (as in 2.1.2) to determine if mutating ASY4 conferred any fertility defect. Line *asy4-3* (SAIL_886_D04) was characterised by Osman *et al.* (2018). It displayed a modest yet significant reduction in fertility from an average of 60.54 seeds per siliques in WT to 57.50 seeds in the mutant ($P < 0.001$, $n=50$). Cytological analysis showed that at metaphase I, the mutant produced some univalents (chromosomes that have failed to form a CO with their homologue) (2.3% frequency, $n=130$), and at anaphase I, some bridging (persisting connections between separating chromosomes). As this phenotype was

comparatively mild, characterisation did not extend further than this, and focus was turned to *asy4-1* and *asy4-2*.

The Grelon group reported a significant reduction in fertility compared to WT in both *asy4-1* and *asy4-2*. Seed count data revealed that *asy4-1* displayed a reduction in fertility of approximately 42.65% compared to WT, and *asy4-2* had a 20% reduction in fertility compared to WT (Chambon *et al.*, 2018).

To determine whether the reduction in fertility corresponded with a defect in meiosis, I commenced cytological analysis on DAPI stained PMCs from both *asy4-1* and *asy4-2* (Fig. 3.4). In both lines, there is no obvious defect at leptotene and early zygotene. As the cells progress through zygotene, however, there is a notable issue with condensation and pairing. In WT, the chromatin follows a program of conserved cycles of expansion and contraction during prophase I. During leptotene, the chromatin is expanded and diffuse, prior to contracting down during zygotene, resulting in *Arabidopsis* zygotene cells appearing small and compact (Fig. 3.4 A2). The chromatin then expands again during mid-pachytene, and thus pachytene cells appear larger (Fig. 3.4 A3) (Kleckner *et al.*, 2004). In both *asy4* mutants, the chromatin appears to retain a thinner, thread-like appearance. There does appear to be some alignment and synapsis however; thicker paired regions are apparent, and paired centromeres are also visible in cells that seem to be progressing toward diplotene (Fig. 3.4, B2-B3, C2-C3).

Pachytene is defined as the stage at which the chromosomes have all reached full synapsis, and as such, no pachytene cells have ever been observed in either *asy4-1* or *asy4-2* by myself or the Grelon group. After the cells commence desynapsis at diplotene, condensed bivalents become visible at diakinesis. In *asy4-1* and *asy4-2*,

this appears to progress normally (Fig. 3.4, B5 and C5). As the chromosomes condense further and align on the metaphase I plate, some connections are visible (Fig. 3.4, B6 and C6). For the purpose of this thesis, I define a connection as anything from thin threads of chromatin stretching between adjacent bivalents (telomere ‘stickiness’; entanglements, for example) through to thick sections of chromatin that could potentially be sites of ectopic recombination. With this definition, I observe connections with a frequency of approximately 21.9% in *asy4-1* (16 out of 73 metaphase I images), and 19.4% in *asy4-2* (6 out of 31 metaphase I images) (see Appendix Fig. A2). Connections are not observed in WT. Univalents are also observed at metaphase I, with a frequency of 52% in *asy4-1*, and 43% in *asy4-2*. Univalents are not observed in WT cells. That univalents are present means that *asy4-1* and *asy4-2* are not maintaining the formation of the obligate chiasma. The Grelon group did not report identification of connections.

Later at anaphase I, as the bivalents separate, bridging and laggards (chromosomes delayed in separation) are evident (Fig. 3.4, B7 and C7). This could also be due to connections observed at earlier stages. Potentially also supporting the suggestion that there are connections, I observed fragments in *asy4-1* at both anaphase I and metaphase I. Fragments at anaphase I could be due shearing of the connected chromosomes as they are pulled apart by the spindle, or is the result of unrepaired DSBs. One cell out of the eight anaphase I cells identified had fragments (Figure 3.4, B7). Fragments are observed at metaphase I with a frequency of 2.7% (2 of 73 metaphase I images), which could be explained by unrepaired DSBs (Appendix Figure A3). This was not reported by the Grelon group, however.

To increase the likelihood of obtaining the desired meiotic stage on a slide, bud sizes were measured using a microscope with a graticule lens prior to slide preparation. For

WT meiosis, buds between 400 µm and 500 µm were used, with 400 – 440 µm buds most often yielding cells between leptotene and pachytene, but rarely any further than diplotene/diakinesis. It was therefore notable that in both *asy4* mutants, bud sizes of between 460 µm and 500 µm yielded cells at early prophase I, and furthermore, would often yield cells much later in the meiotic programme; thus, slides containing zygotene through to anaphase II were obtained: a very rare occurrence when preparing slides with measured buds from WT plants. This would therefore suggest that progression through meiosis is potentially delayed in these mutant lines, and furthermore, that there is an asynchrony in timing of meiosis in absence of normally functional ASY4.

Ultimately, these earlier defects in prophase I result in mis-segregation and aneuploidy in the resultant daughter cells.

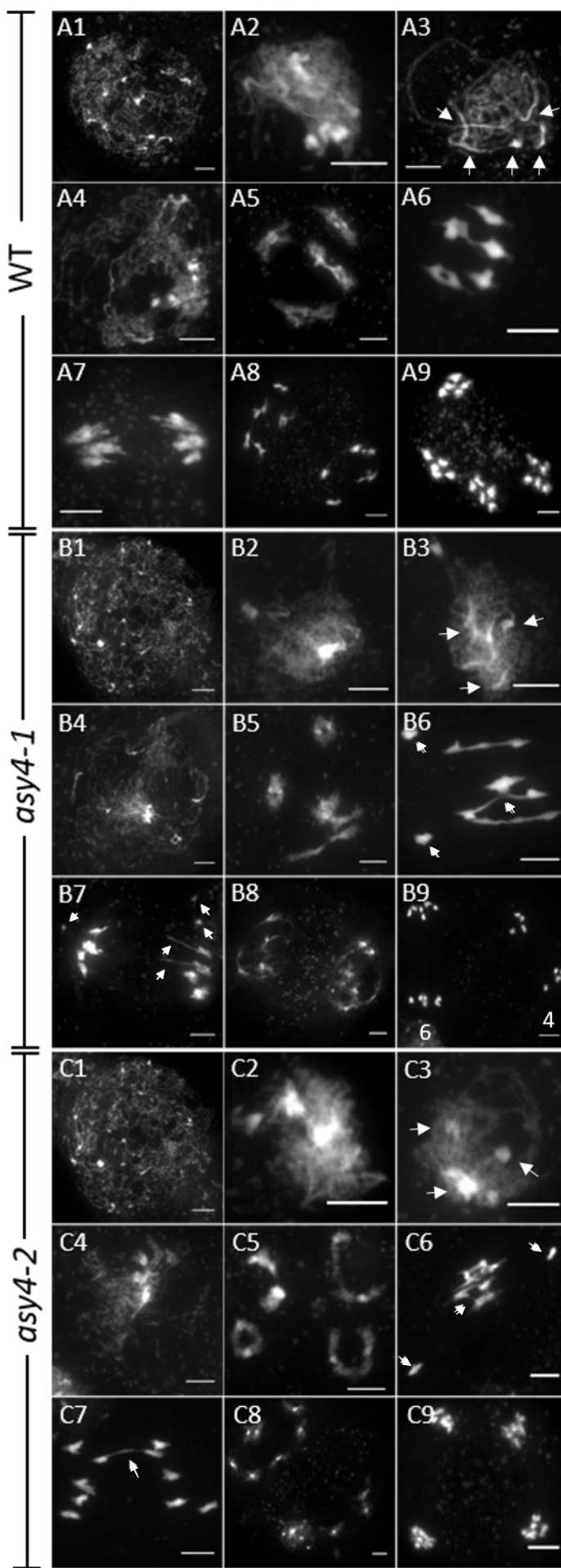


Figure 3.4 DAPI stained PMCs from WT *A. thaliana*, *asy4-1* and *asy4-2*. Spreads from WT (A1-A9), *asy4-1* (B1-B9), and *asy4-2* (C1-C9). (A1, B1, C1) Leptotene. (A2, B2, C2) Zygote/Zygotene-like. (A3, B3, C3) WT image shows pachytene. For *asy4-1* and *asy4-2*, pachytene was not observed; images shown are cells that appear to have paired the most from the sample. Paired centromeres indicated with arrows. (A4, B4, C4) Diplotene. (A5, B5, C5) Diakinesis. (A6, B6, C6) Metaphase I. Arrows indicate univalents and connections. (A7, B7, C7) Anaphase I. Arrows indicate bridges, fragmentation, and laggards. (A8, B8, C8) Dyad. (A9, B9, C9) Tetrad. Bar = 5 μ m.

As univalents were observed in metaphase I cells from both lines, I conducted chiasma counts using the minimum chiasma number (MCN) (Jahns *et al.*, 2014) to determine the severity of the suggested reduction in CO number. In *asy4-1*, there was a reduction in CO number from 8.6 (n=28) in WT, to 6.5 (n=67; P < 0.0001; Mann-Whitney U test, 2 tailed, 5% level). In *asy4-2*, the CO number was also reduced to 6.6 (n=31; P < 0.0001; Mann-Whitney U test, 2 tailed, 5% level). No significant difference was found in the number of chiasma between *asy4-1* and *asy4-2* (P = 0.6942; Mann-Whitney U test, 2 tailed, 5% level) (Figure 3.5).

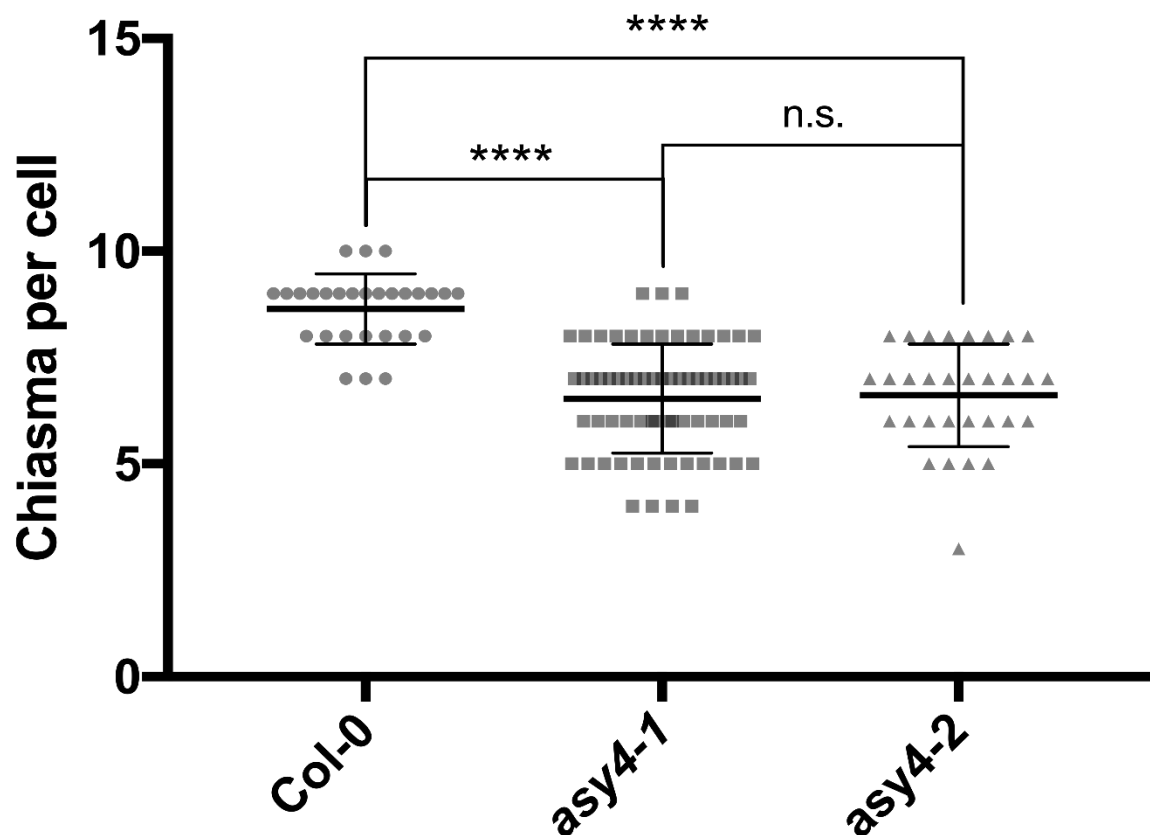


Figure 3. 11 Chiasma number is significantly reduced in *asy4-1* and *asy4-2*.
Data obtained from DAPI stained metaphase I cells from *A. thaliana* PMCs. Each plotted shape represents the chiasma count for one cell. Middle line represents the mean, plotted with the standard deviation. Top bars indicate results of significance testing. *** indicates P<0.0001. N.s. indicates that no significant difference was found.

As discussed, some metaphase I cells appear to show connections between bivalents, as well as fragments. To help determine the nature of these connections (e.g., entanglements or non-homologous recombination events), fluorescence *in situ* hybridisation (FISH) was conducted on the DAPI stained slides using the 45s and 5s rDNA probes (Sanchez-Moran *et al.*, 2002) (as in **2.8.2**). This process labels the chromosomes with a fluorescent marker, thus enabling identification of the chromosome. Based on this, it is possible to determine how many COs we might expect to be present in the bivalent/multivalent due to the shapes they form, given that we know the size of the chromosome arms, and the location of the centromeres.

Of the 67 *asy4-1* cells, 14 were retrieved; of these, only one metaphase appeared to have connections. Of the 30 *asy4-2* cells, only one cell was retrieved. As such, analysis of spreads has been hindered by the number of cells available for analysis. Nonetheless, the cell with possible multivalents retrieved from *asy4-1* confirms evidence of connections, but not necessarily of non-homologous recombination (Fig. 3.6).

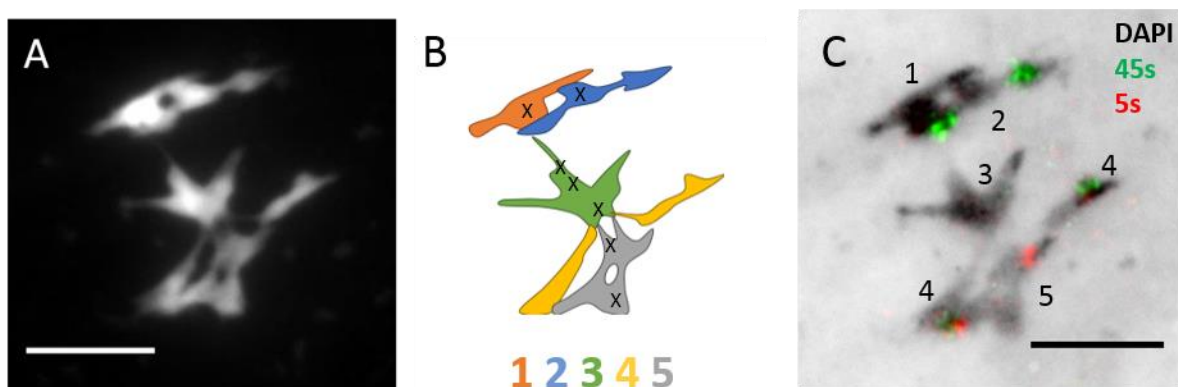


Figure 3.12 Fluorescence *in situ* hybridisation (FISH) on a metaphase I spread from *asy4-1*. **(A)** Original DAPI image. **(B)** Schematic illustrating the conformation of the chromosomes, as revealed by FISH. **(C)** DAPI spread after FISH, labelled with the 45s and 5s rDNA probes. Scale bars = 5 µm.

As illustrated in the schematic presented in Fig. 3.6 B, the threads of chromatin connecting chromosomes 2, 3, and the two univalents of chromosome 4, are rather thin. There is also no obvious evidence of mis-alignment which would suggest improper tension on the spindle caused by an ectopic CO. Furthermore, the shapes of the bivalents formed by chromosomes 3 and 5 are not unexpected if chromosome 3 has three COs, and chromosome 5 has two to three. The simplest explanation for the connections in this cell, therefore, is that they are the result of entangled chromosomes.

3.2.1.3 ASY1 localisation is abnormal in *asy4*

Silver-staining analysis of the chromosome axis by the Grelon group suggests that the underlying structure of the axis is still present in *asy4-1* (Chambon *et al.*, 2018). In *asy3*, ASY1 does not localise to the chromosome axis, instead remaining on the chromatin in foci (Ferdous *et al.*, 2012). To determine whether ASY1 requires ASY4 for normal loading, I conducted immunolocalisation with an antibody against ASY1 to image the axis in *asy4-1*.

In *asy4-1*, ASY1 appears on the axis during leptotene. In WT, the ASY1 signal is strong and linear. In *asy4-1*, however, it takes on a ‘lumpy’ and ‘fuzzy’ appearance, appearing as a series of intense foci close together rather than the continuous signal it appears to form in epi-fluorescence images of cells during leptotene and early zygotene (Fig. 3.7).

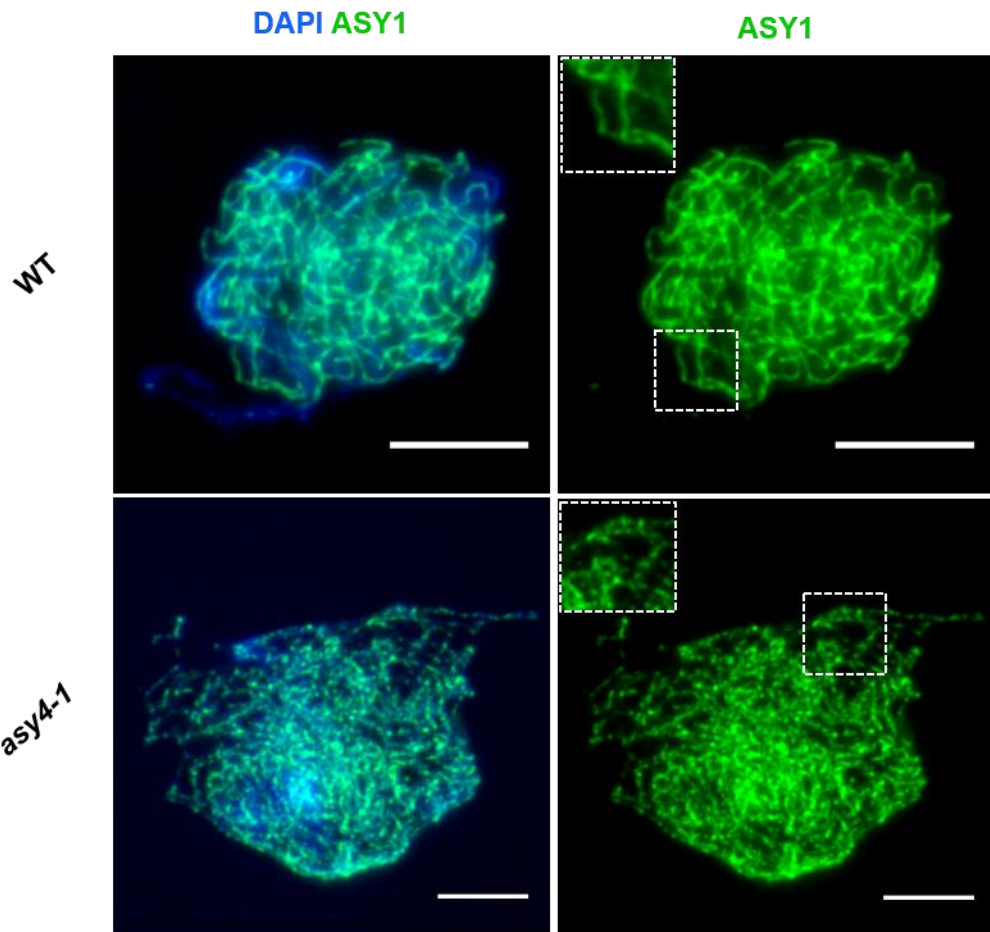


Figure 3.13 Immunolocalisation of ASY1 in WT and *asy4-1*. Top two cells WT Col-0 background. Bottom two cells from *asy4-1*. ASY1 appears more foci-like in *asy4-1*, rather than as a clear linear signal as observed in WT. Scale bars = 5 μ m.

3.2.1.4 Early recombination events appear normal in *asy4-1*

As described in **Chapter 1**, the chromosome axis is required for normal progression of meiotic recombination. To determine at which point recombination is compromised in *asy4*, immunolocalisation was conducted on early prophase I PMCs using antibodies against several early recombinases. The Grelon group confirmed that the levels of DMC1 foci were not significantly different to WT in *asy4*, suggesting that both the number of DSBs is normal, and also, that strand invasion is likely to proceed normally (Chambon *et al.*, 2018).

After strand invasion, D-loop stabilisation and extension, and second end capture, a double Holliday junction (dHj) is established (reviewed in: Wyatt and West, 2014). This is stabilised in *Arabidopsis* by the MutS homologs MSH4 and MSH5: members of the ZMM pathway (Higgins *et al.*, 2008b, 2004; Snowden *et al.*, 2004). Immunolocalisation of MSH4 and MSH5 on PMCs during leptotene to mid-zygote revealed an average of 109.1 ± 20.41 ($n=15$) MSH4 foci, and an average of 121.1 ± 29.55 ($n=15$) MSH5 foci in *asy4-1*. In WT, an average of 120.3 ± 20.8 ($n=15$) was found for MSH4 foci, and an average of 110.9 ± 38.61 ($n=15$) for MSH5. To increase certainty of the foci being genuine, only foci detected as co-localising with the ASY1 signal were counted. Thus, I found no significant difference in the number of MSH4/MSH5 foci between WT and *asy4* (MSH4 $P=0.17$; MSH5 $P=0.3835$. Two-tailed Mann-Whitney U test, 5% level) (Fig. 3.8). This suggests that stable, proto-dHjs are being produced in *asy4*. Data available in Appendix Table A9.

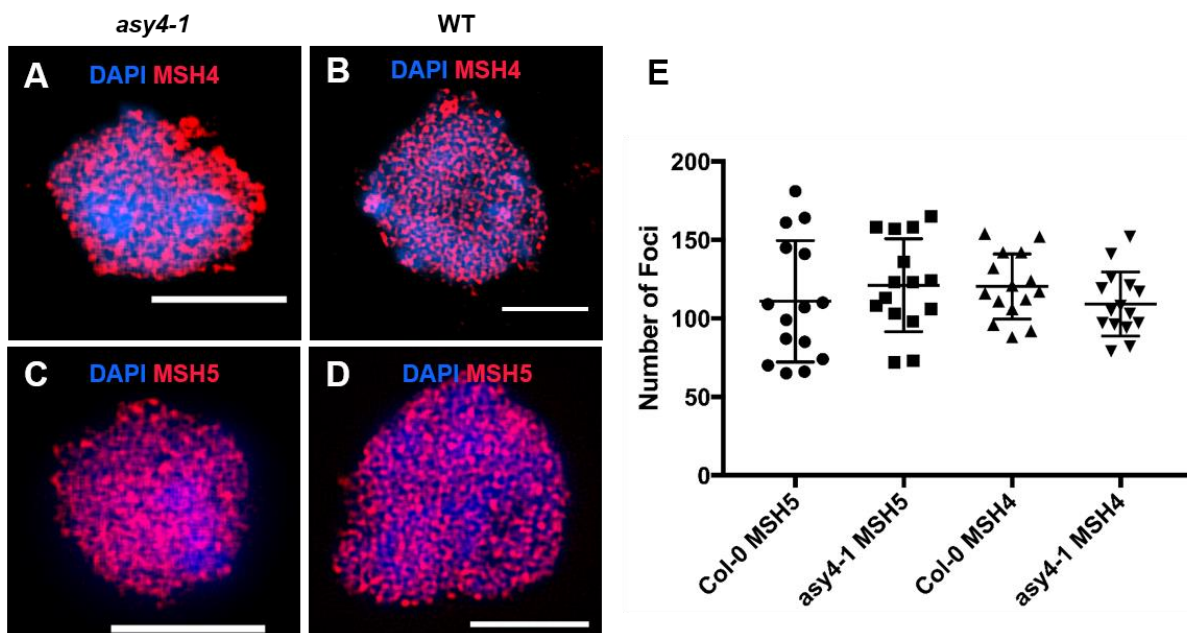


Figure 3.22 Immunolocalisation of MSH4 and MSH5 and comparison of number of foci. Immunolocalisation conducted on early prophase I PMCs. (A, C) Cells from *asy4-1*. (B, D) Cells from WT Col-0 control. (A, B) MSH4 foci shown in red. (C, D) MSH5 foci shown in red. Chromatin in all cells stained with DAPI. All images are a representative single slice from a stack. Texas Red channel processed with Mexican Hat to increase clarity. All scale bars represent 5 μ M. (E) Box and whisker plot to demonstrate the spread of the data between sample groups. Each shape represents the number of foci counted in one cell. Top and bottom lines represent the standard deviation. Middle line represents the mean.

3.2.2 Characterisation of an *asy4-1* line complemented with ASY4eYFP confirms that ASY4 is associated with the chromosome axis during meiosis

3.2.2.1 An antibody raised against ASY4 suggests axis localisation

The co-immunoprecipitation study conducted by Osman *et al.* (2018) suggested that ASY4 was an axis-associated protein, given that it interacts either directly or indirectly with ASY1. Previous studies have used immunocytochemistry to show the localisation of ASY1 and ASY3 on the chromosome axis (Armstrong *et al.*, 2002c; Ferdous *et al.*, 2012a). To conduct a similar study, an antibody was raised in rat against ASY4 by Kim Osman (University of Birmingham).

I conducted immunolocalisation using anti-ASY4 on wild-type Col-0 PMCs. The ASY4 antibody shows signal on the axis during prophase I of meiosis. ASY4 is first observed in late leptotene/early zygotene, and persists into late prophase I (Figure 3.9). It appears to form foci that seem relatively discrete on the chromatin, but forms a more linear signal at the axis. During leptotene, the ASY4 signal appears to co-localise with that of the cohesin SYN1, and later during zygotene through pachytene, with the SC central component ZYP1 (Fig 3.9, A-F). This confirms that ASY4 is present on the axis at both synapsed and unsynapsed regions (Fig. 3.9, D). ASY4 is also visible on the chromatin during all of these stages.

The ASY4 signal appears to be at its strongest and most linear from the commencement of zygotene and polymerisation of the SC, with the ASY4 foci appearing much more abundant in both the chromatin and at the axis where it is co-localising with the ZYP1 signal (Figure 3.9, G-I). At diplotene, the ASY4 signal persists,

but appears to be being depleted as the axis is remodelled, with the signal appearing patchy (Fig 3.9, J-L).

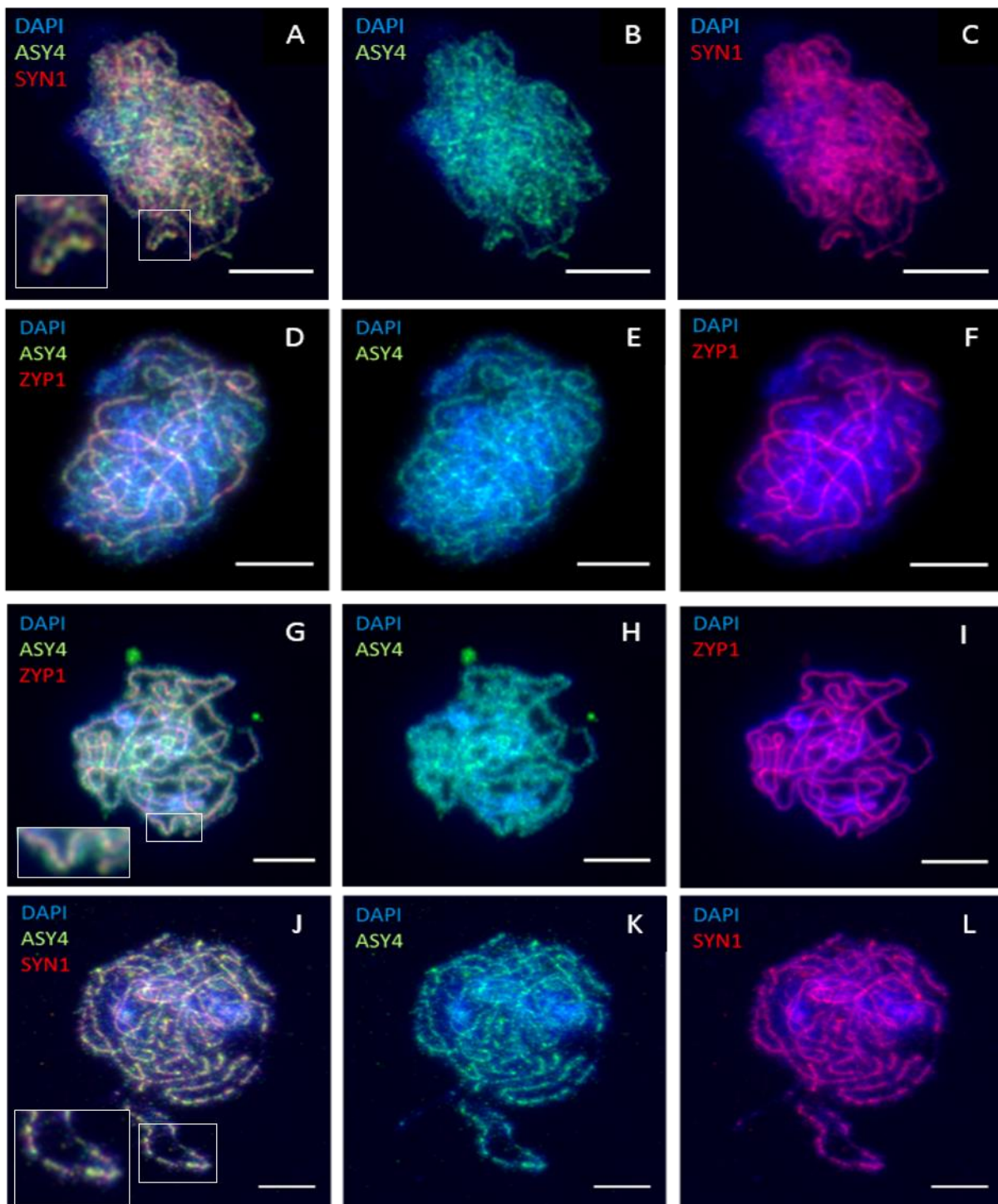


Figure 3.23 Immunolocalisation of ASY4 relative to the SC and sister cohesion in wild-type *Arabidopsis thaliana*. Immunolocalisation conducted on PMCs during prophase I. **(A-C)** Early zygotene stage meiocyte: **(A)** merged image; **(B)** dual localisation of ASY4 (green) and DAPI (blue); **(C)** dual localisation of SYN1 (red) and DAPI (blue). **(D-F)** Mid-zygotene stage meiocyte: **(D)** merged image; **(E)** dual localisation of ASY4 (green) and DAPI (blue); **(F)** dual localisation of ZYP1 (red) and DAPI (blue). **(G-I)** Pachytene stage meiocyte: **(G)** merged image; **(H)** dual localisation of ASY4 (green) and DAPI (blue); **(I)** dual localisation of ZYP1 (red) and DAPI (blue). **(J-L)** Early diplotene meiocyte **(J)** merged image; **(K)** dual localisation of ASY4 (green) and DAPI (blue); **(L)** dual localisation of SYN1 (red) and DAPI (blue). All scale bars represent 5µm. Modified from Darbyshire 2015, p. 30.

3.2.2.2 Complementation of *asy4-1* with ASY4eYFP restores fertility, and increases CO number

Whilst the signal of the ASY4 antibody co-localises with the axis, western blots on total protein from *A. thaliana* inflorescence did not appear to exclusively identify ASY4 (Kim Osman, University of Birmingham, personal communication). Furthermore, signal was still seen on the chromosome axis in the *asy4* mutants, and therefore the antibody could not be verified (Appendix Figure A4, courtesy of Kim Osman, University of Birmingham). Combined with the RT-PCR results in 3.2.1.1, this suggests the presence of a truncated protein in the *asy4-1* and *asy4-2* mutants, confounding antibody verification. To get around this problem, a version of ASY4 tagged with eYFP via triple template PCR was produced by Allan West (University of Birmingham) based on a protocol developed by Tian *et al.* (2004), and modified by Heckmann and Franklin (unpublished). The eYFP tagged ASY4 was then used to complement the *asy4-1* and *asy4-2* mutants via floral dipping.

After selecting for successfully transformed plants on kanamycin plates, I was provided with the resultant plants for analysis by Allan West (University of Birmingham). The success of the complementation was initially determined via seed counts as an indication of fertility. A Kruskal-Wallis test was then conducted to identify those lines that no longer had significantly reduced fertility compared to wild-type. The most fertile T2 generation was considered to be the best complemented line, and was therefore taken forward for further analysis (Figure 3.10). The *asy4*:ASY4eYFP line 165.15 was chosen as the best complemented line (\bar{x} 164.15 = 47; \bar{x} Col-0 = 50; $P > 0.05$), which shall henceforth be referred to as ‘*asy4*:ASY4eYFP’.

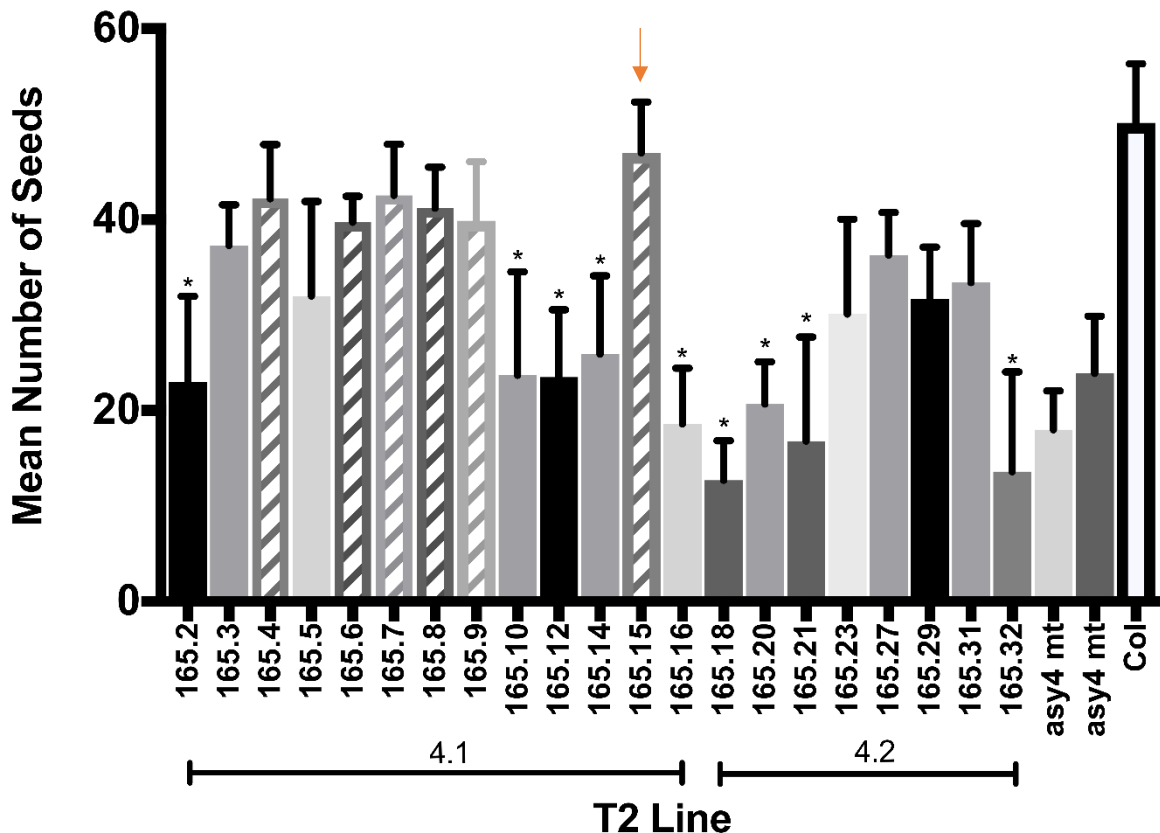


Figure 3.24 Seed Count data from *asy4* *Arabidopsis thaliana* mutants transformed with ASY4eYFP. Asterisks indicate plant lines with a fertility significantly different to the Col-0 WT control at the 5% level in a two-tailed Kruskal-Wallis test. Bars with hashed lines indicated that the plants with the highest fertility, and that were not significantly different to Col-0 in a two-tailed Kruskal-Wallis test ($P>0.05$). Error bars indicate standard deviation. The 4.1 and 4.2 legends denote which T-DNA *asy4* mutant background the plants were from. Selected line indicated with arrow.

I next sought to confirm whether the rescued fertility corresponded with more WT levels of COs. Chiasma counts were conducted on 75 DAPI metaphase I spreads from the T3 generation of plants from the T2 *asy4*:ASY4eYFP line to determine if there was any difference in CO frequency compared to wild-type. Spreads with between 5 and 10 chiasma were observed, with an average chiasma frequency of 7.72. This was significantly different to wild-type ($\bar{x}=8.64$, $n=28$) in a Mann-Whitney U test at the 5% level ($P=0.0002$). However, this result was also significantly different to *asy4-1* ($\bar{x}=6.5$, $n=64$; ($P<0.0001$)) (Figure 3.11).

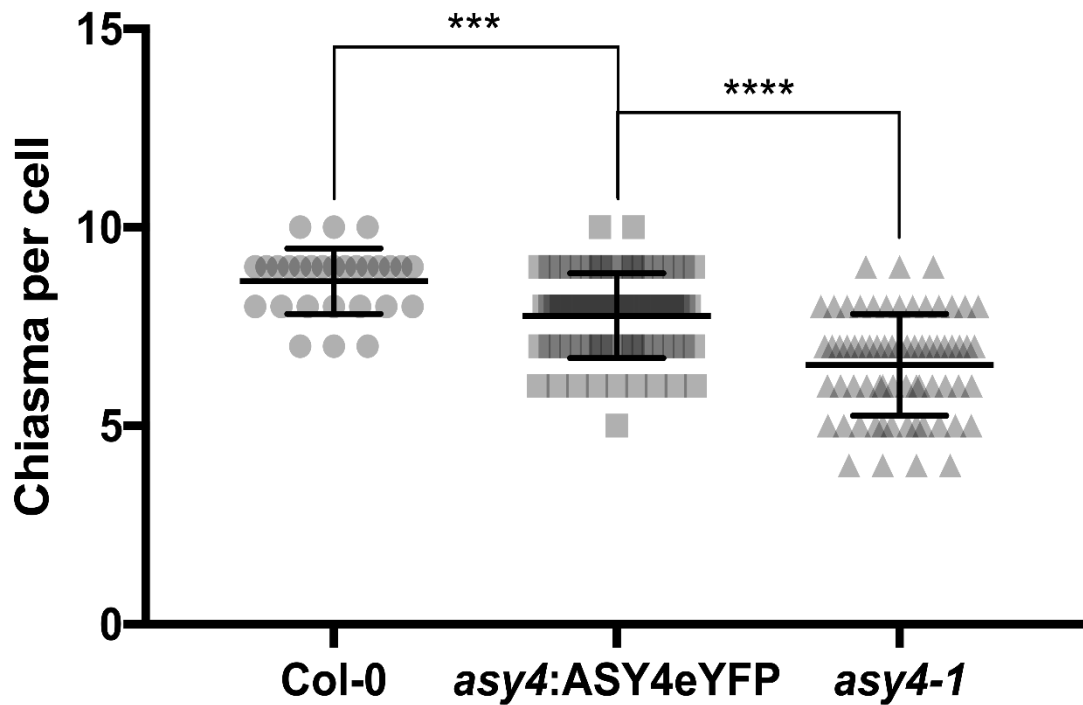


Figure 3.25 Comparison of distribution of chiasma number between Col-0 (WT), asy4:ASY4eYFP, and asy4-1. Grey shapes depict the number of chiasma in individual cells. In black, the mean (central horizontal line) and standard deviations are shown for each plant line. Top bars indicate results of the significance testing. *** illustrates $P=0.0002$. **** denotes $P<0.0001$.

Some meiotic errors were also identified at the MI stage in *asy4:ASY4eYFP*. Crucially, univalents were observed in 2 of the 75 cells (2.6% frequency) (Figure 3.12). There also potentially appears to be a persistent issue with connections, as is observed in the *asy4-1* mutant, suggesting the possible presence of interlocks and entanglements (Fig. 3.12, B).

Aberrations were also observed at anaphase I (Figure 3.13). This included bridges (Fig. 3.13, D), and laggards (Fig. 3.13, C). There also appears to be an issue with segregation between chromosomes that may have been entangled. It appears that a bivalent is separating, but another chromosome is also attached to the pair, connected by a thin thread of chromatin (Fig. 3.13, B).

Mis-segregation was also observed at telophase II, but only one cell was observed displaying this characteristic (Figure 3.13 D).

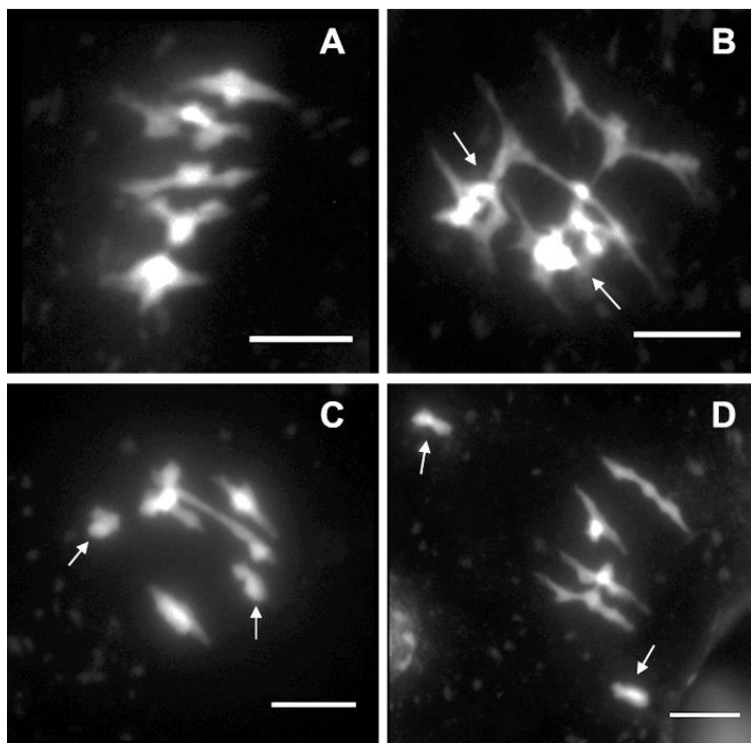


Figure 3.34 DAPI-stained PMCs at metaphase I and Telophase II in *asy4:ASY4eYFP*. (A) WT Metaphase I. (B, C, D) Metaphase I images from T3 generation of *asy4:ASY4eYFP*. (B) Cell displaying a potential interlock and entanglement. (C, D) Cell with univalents. Scale bars = 5 μ m.

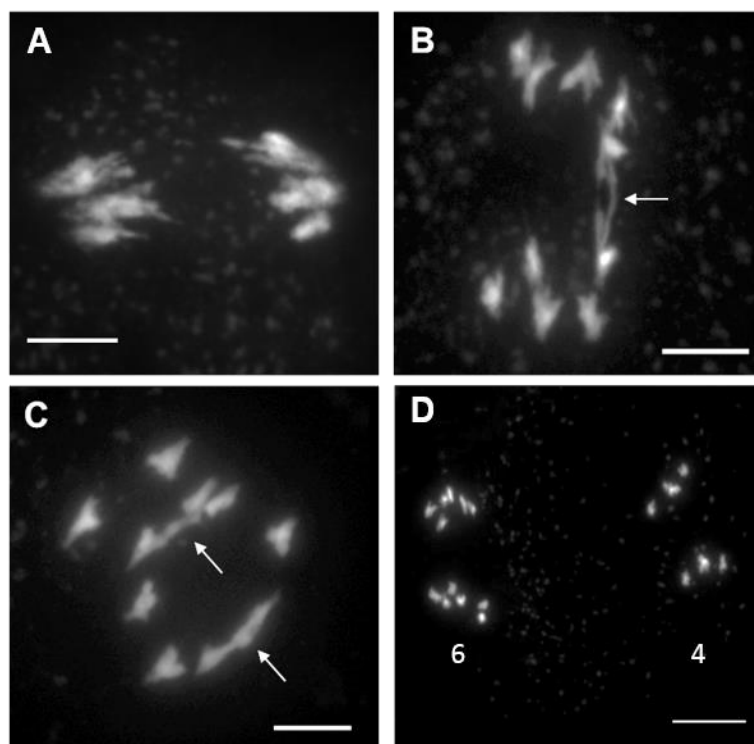


Figure 3.35 DAPI-stained PMCs at Anaphase I. DAPI-stained male meiocytes. (A) WT anaphase 1. (B, C) and anaphase I images from T3 generation of *asy4:ASY4eYFP*. (D) Telophase II. (B) shows bridging, potentially between non-homologous chromosomes. (C) Shows laggards. (D) 6:4 segregation of chromosomes. (A, B, C) Scale bars represent 5 μ m. (D) Scale bar represents 10 μ m.

3.2.2.3 Complementation of *asy4-1* with ASY4eYFP restores synapsis

One significant phenotype in the *asy4* mutant is persistent regions of asynapsis, resulting in apparent absence of a true pachytene stage (Chambon *et al.*, 2018). I thus commenced immunolocalisation on acid-fixed PMCs (**2.8.4**) to investigate whether ASY4eYFP complementation restored synapsis to wild-type levels. As illustrated in Fig. 3.14 B, near complete synapsis is observed in *asy4*:ASY4eYFP, with the ZYP1 signal appearing to extend the full length of the chromosomes. Comparing the images directly to *asy4-1*, it is evident that synapsis extends much further in the ASY4eYFP complemented line than in the homozygous mutant, where only short, aberrant stretches of ZYP1 are visible (Fig. 3.14 C).

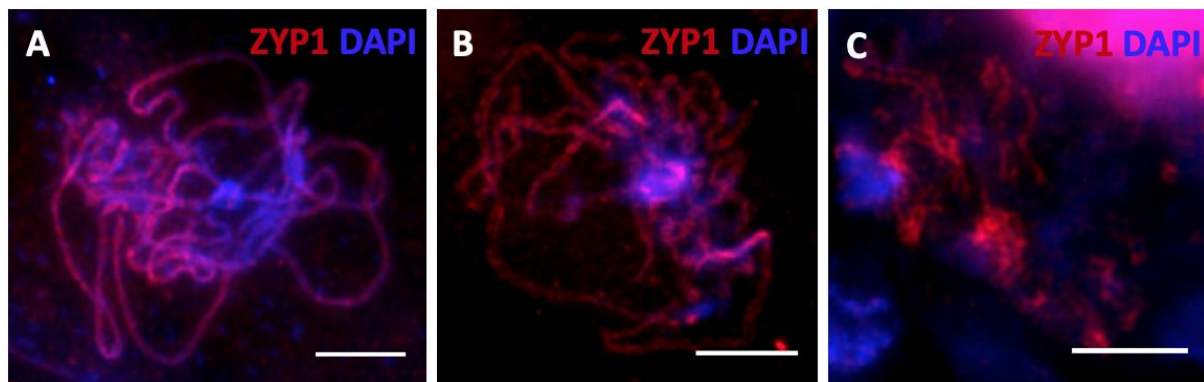


Figure 3.36 Microwave immunolocalisation shows near complete synapsis is achieved in *asy4*:ASY4eYFP. Immunolocalisation conducted on late zygote PMCs from *Arabidopsis*. **(A)** WT. **(B)** *asy4*:ASY4eYFP. **(C)** *asy4-1* homozygote. Chromatin is stained with DAPI. ZYP1 shown in Texas Red. All scale bars represent 5 μ m.

3.2.2.4 ASY4eYFP signal is axis associated

To complete characterisation of this line, I conducted immunolocalisation on chromosome spread preparations from fresh pollen mother cells (PMCs) from the T3 generation of *asy4:ASY4eYFP* to image the axis directly, and finally confirm the axis localisation of ASY4. This showed that the ASY4 signal (eYFP native fluorescence) co-localises at the majority of sites with ASY1 (Fig. 3.15), thereby confirming its presence at the chromosome axis during prophase I of meiosis in *A. thaliana*. Data presented in Chambon *et al.* (2018) suggests that ASY4 loads during leptotene, and persists on both synapsed and unsynapsed regions of the chromosomes, corroborating the result observed in 3.2.2.1.

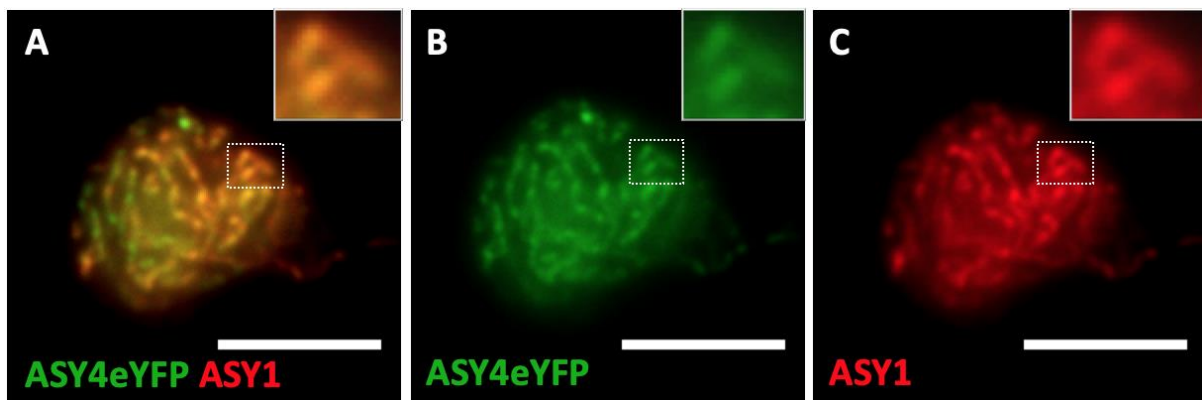


Figure 3.37 Spreading immunolocalisation on PMCs from *asy4:ASY4eYFP* confirms ASY4 is axis-associated during prophase I. Immunolocalisation conducted on zygotene stage PMCs from the T3 of 165.15 *asy4:ASY4eYFP*. (A) Merged image. (B) ASY4eYFP auto-fluorescence imaged in the FITC channel. (C) ASY1 in Texas Red. All scale bars represent 5 μ m.

Some aberrations in ASY4 localisation, however, are apparent in the complemented lines. Large foci of ASY4eYFP are present on the axis, around which, the ZYP1 signal is extending, suggesting the foci are genuine and not an artefact of the immunolocalisation protocol (Fig. 3.16 A). Whilst the more extended ZYP1 signal curves around these foci, interestingly, the points from which ZYP1 seems to be

initially extending are flanked by the large ASY4eYFP foci (Fig. 3.16 B). It was also found that the cells that contained the large ASY4eYFP foci also had large aggregates of ASY1 (Fig. 3.16, C). Some of these ASY1 foci co-localise with ASY4eYFP, but not all. This phenotype is not ubiquitous, only being observed in a subset of cells, but the foci were present in many of the plants screened that had been complemented with ASY4eYFP.

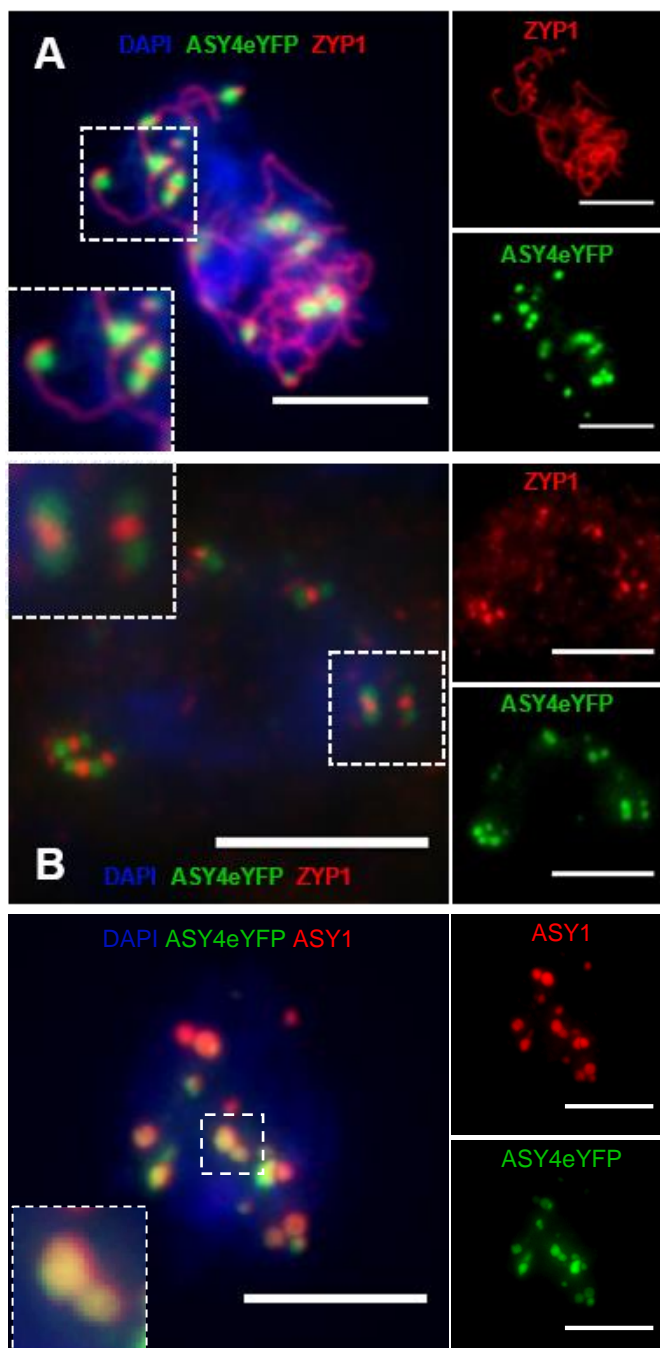


Figure 3.38 Large foci of ASY4eYFP are present on the axis and at the SC in some *asy4*:ASY4eYFP cells. Immunolocalisation conducted on an *asy4-2* line complemented with ASY4eYFP. ASY4eYFP imaged in FITC channel (native fluorescence). ZYP1/ASY1 imaged in Texas Red. Chromatin is stained with DAPI. **(A)** Zygote cell showing ZYP1 curvature around the large ASY4eYFP foci. **(B)** Early zygote cell showing ASY4eYFP foci flanking synapsis initiation sites. **(C)** Early zygote cell showing aggregates of ASY4eYFP and ASY1. Some ASY1 foci co-localise with foci of ASY4eYFP (inlay). All scale bars represent 5 μ m.

3.2.2.5 ASY4 loading requires ASY3

Whilst ASY1 requires ASY3 for proper loading onto the axis, ASY3 does not appear to be dependent on ASY1, as it still localises to the axis in *asy1* (Ferdous *et al.*, 2012a). The Grelon group also reported that ASY3 localisation is disrupted in the *asy4-1* mutant (Chambon *et al.*, 2018).

We next sought to determine whether ASY4, like ASY1, requires ASY3 for localisation to the axis. To do this, the *asy3-1* mutant (Ferdous *et al.*, 2012) was transformed with the ASY4eYFP construct by Allan West (University of Birmingham). Previous work with ASY1eYFP had indicated that whilst this inserts another copy of a gene already present in the plant (albeit with a fluorescent tag), it can still localise to the axis (Heckmann and Franklin, unpublished). Thus, we expected that ASY4eYFP would also be able to localise to the axis. As a control, the WT Col-0 was also transformed with ASY4eYFP by Allan West (University of Birmingham) to determine whether ASY4eYFP can still localise to the axis when native ASY4 is still present.

I commenced immunolocalisation on PMCs during early prophase I when ASY4 is abundant using antibodies against SMC3 (part of the cohesin complex), and GFP (Lam *et al.*, 2005). In the *asy3-1*:ASY4eYFP transformed lines, the ASY4eYFP signal appears as small foci, and no cells with a linear signal have ever been observed in this mutant background (Fig. 3.17). Interestingly, the foci do not appear to be axis-associated, instead appearing next to the SMC3 signal, but not co-localising with it.

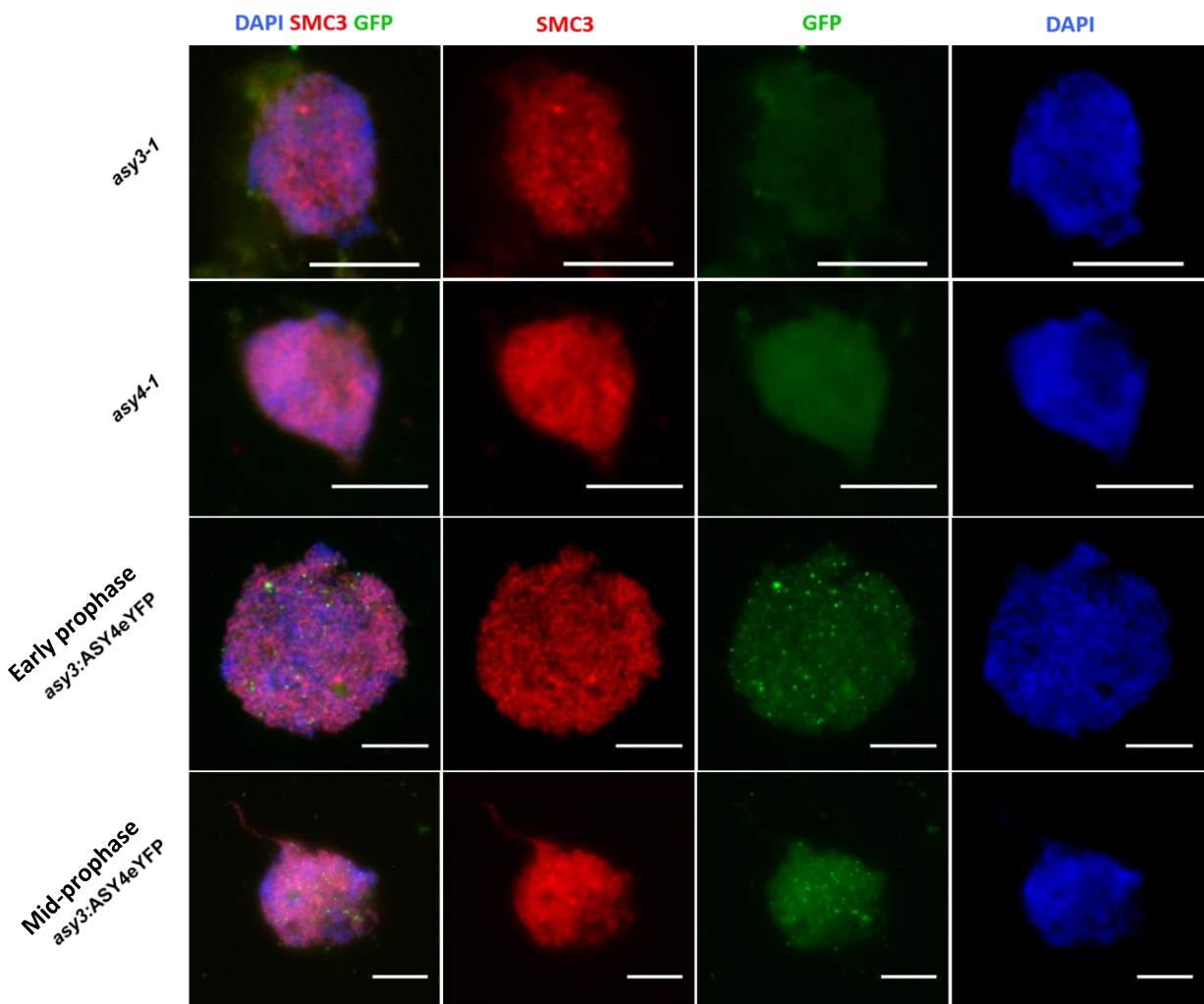


Figure 3.17 Immunolocalisation of ASY4eYFP using the anti-GFP antibody in an asy3-1 mutant background. Chromatin stained with DAPI. Anti-SMC3 in Texas Red. Anti-GFP in FITC. The asy4-1 and asy3-1 images show standard background for the GFP antibody. In asy3:ASY4eYFP, foci of ASY4eYFP are visible in the chromatin and co-localising with the SMC3 signal. Scale bars = 5 μ m.

To confirm that this was not due to an issue with ASY4eYFP expression being silenced, inflorescence were checked for fluorescence in the FITC channel by pressing them under a coverslip onto a slide with DAPI. As is evident in Fig. 3.18, fluorescence localised only to the anthers is present in the plant lines used for immunolocalisation, suggesting that ASY4eYFP being unable to load and polymerise on the axis is likely to be genuine, and not due to a lack of expression.

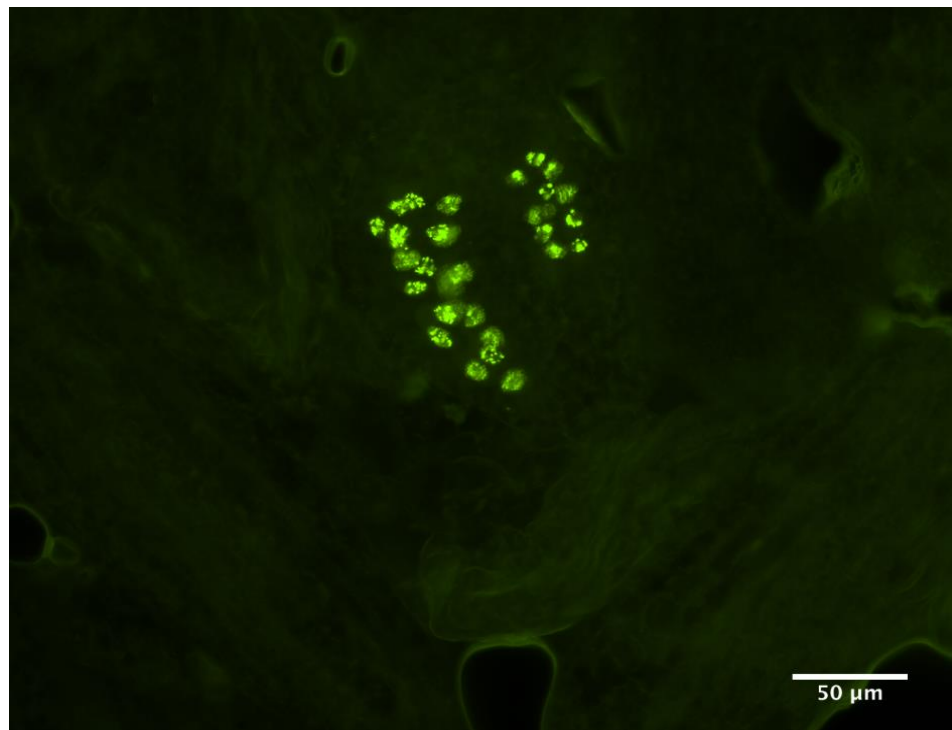


Figure 3.39 Anthers from *asy3:ASY4eYFP* are fluorescent, confirming expression of the ASY4eYFP construct. Whole inflorescence imaged in the FITC channel. Scale bar = 50 μ m.

For the Col-0:ASY4eYFP lines that have been investigated, the ASY4eYFP signal is visible on the axis, but as blobs, similar to what we have observed in **Figure 3.16** (Fig. 3.19). Nonetheless, these large foci are distinct to those seen in the *asy3:ASY4eYFP* lines; in Col-0:ASY4eYFP, the accumulations of ASY4 are far larger and brighter than is observed in *asy3:ASY4eYFP*.

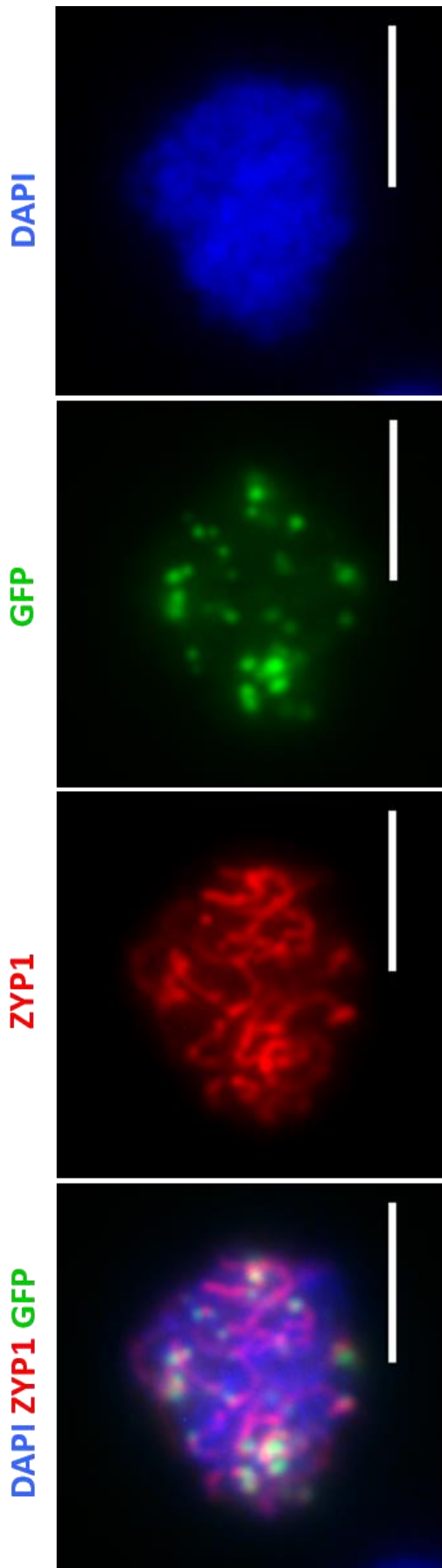


Figure 3.40 Zygote-stage cell from **Col-0:ASY4eYFP**. Chromatin stained with DAPI. ZYP1 shown in Texas Red, GFP in FITC. ASY4eYFP localises to the axis, but appears as large foci. Scale bars = 5 μm .

3.2.3 ASY4eYFP structure appears abnormal in *pch2*

To further our understanding of which proteins might be required for normal loading and/or polymerisation of ASY4eYFP, the *pch2-1* mutant (Lambing *et al.*, 2015) was transformed with the ASY4eYFP construct by Allan West (University of Birmingham). A key phenotype of *pch2* is that it is defective in axis remodelling; the ASY1 signal appears to persist, instead of being depleted, at sites of SC polymerisation (Lambing *et al.*, 2015). The ASY1 signal during prophase I also appears dimmer along the axis in *pch2-1* than in WT (West, 2015). The loading and dynamics of SYN1 and ASY3, however, appear unaffected in *pch2*, and thus the core axis structure is still present. As discussed in 1.4, PCH2 is an AAA+ ATPase. In immunolocalization studies, it was found that the PCH2 signal can be seen as foci during leptotene, but its signal does not extend until zygotene; PCH2 extends exclusively at sites where the SC has commenced polymerisation, and co-localises with ZYP1. Combined, these data suggest that PCH2 is an axis remodeler, as opposed to a crucial, structural component of the axis. It is also not a core component of the SC, as synapsis still occurs in *pch2*, albeit at a reduced level (Lambing *et al.*, 2015). Given that data presented by the Grelon group in Chambon *et al.* (2018) suggests that ASY1 is not depleted from the axis in *asy4-1*, we were curious to see whether there was any clear difference in the behaviour of ASY4eYFP in the *pch2* background.

I conducted immunolocalisation using antibodies raised against GFP, ASY1, and ZYP1, which revealed that ASY4eYFP does indeed load to the axis in *pch2*, but its appearance seems altered to that observed in *asy4*:ASY4eYFP (Fig. 3.20, and 3.2.2.4). Instead of forming the thick, linear signal we see at late leptotene/early zygotene in *asy4*:ASY4eYFP, ASY4eYFP appears much more dotty and irregular (Fig. 3.20, row C). This signal is, however, only seen during leptotene; as zygotene

commences with the extension of the SC, once again, large aggregates of ASY4eYFP become visible (Fig. 3.20, row D). Some of these large ASY4eYFP foci appear to co-localise with ASY1, as was observed in **Figure 3.16**. That ASY1 is co-localising with ASY4eYFP foci was perhaps unexpected, given that ASY1 is not properly remodelled in the absence of PCH2.

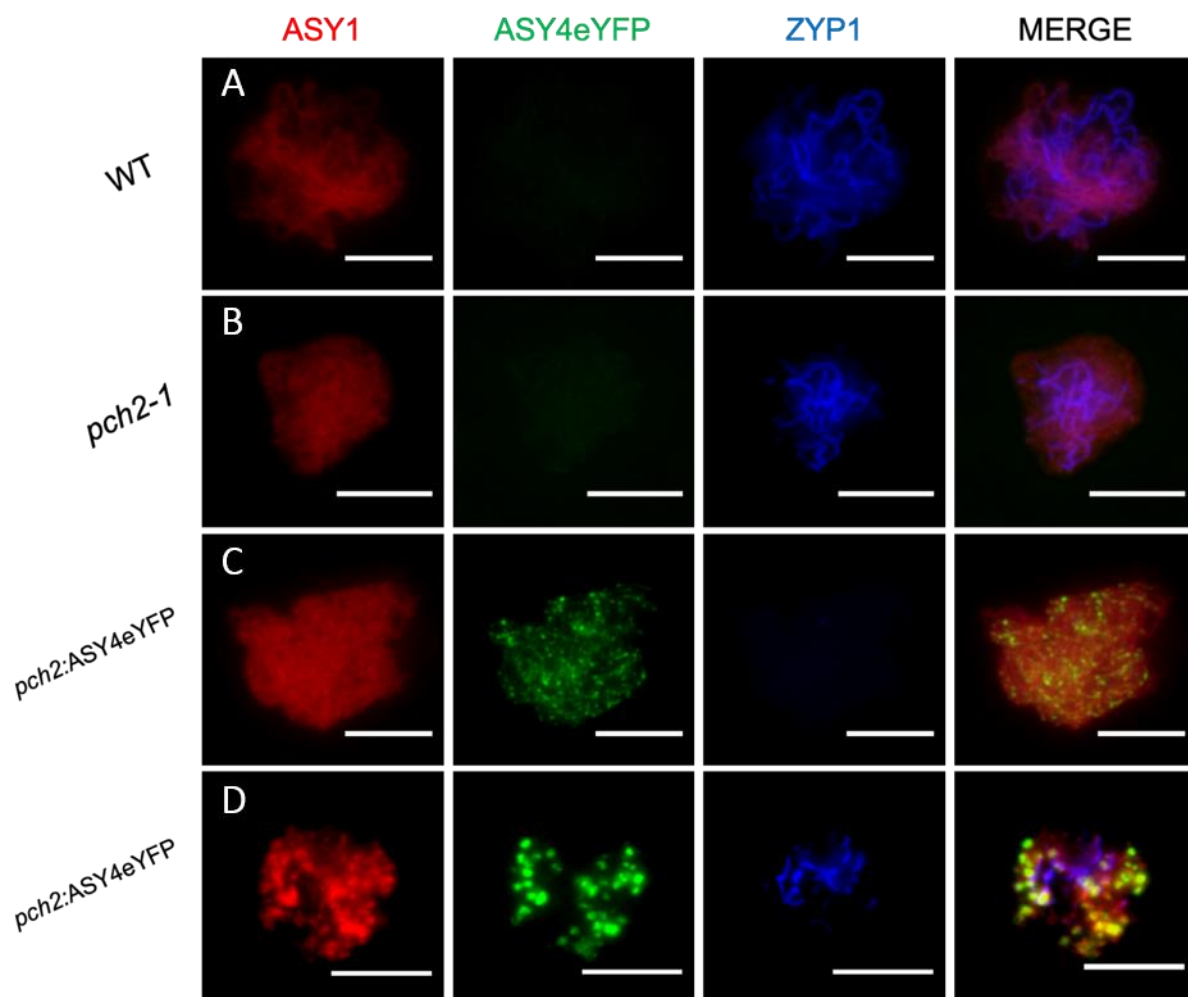


Figure 3.41 Immunolocalisation of PMCs from *pch2-1* transformed with ASY4eYFP show aggregates of ASY4eYFP and ASY1 signal at the leptotene/zygotene transition. ASY1 in Texas Red channel. ASY4eYFP in FITC. ZYP1 shown in DAPI channel. As the SC begins to polymerise in WT and *pch2-1*, the ASY1 signal remains linear. As ZYP1 commences extension in *pch2:ASY4eYFP*, ASY4eYFP and ASY1 form large foci. All scale bars represent 5 μ m.

3.2.4 ASY4 directly interacts with ASY3 in Yeast-2-Hybrid

Yeast-2-Hybrid (Y2H) is a common method used to determine protein-protein interactions. It utilises the modular nature of the Gal4 transcription factor by creating two fusion proteins with the proteins of interest: one fused to the DNA-binding domain (DBD), and one fused to the activation domain (AD). Interaction between the proteins of interest is confirmed via expression of several reporter genes related to the ability of the yeast to produce amino acids and the nucleobase, adenine. In this study, colonies containing DBD and AD fusion proteins that can interact will be able to grow on triple (TDO) and quadruple dropout (QDO) media. TDO lacks leucine (L), tryptophan (T), and histidine (H). QDO is also -LTH, as well as adenine (A) (Y2H system reviewed in: Mehla *et al.*, 2015).

In Osman *et al.* (2018), Chambon *et al.* (2018), and most recently, West *et al.* (2019), ASY4 is shown to interact with ASY3 in Y2H experiments. Previous studies have used Y2H to confirm physical interactions between ASY1 and ASY3 (Ferdous *et al.*, 2012). This interaction was dissected further to reveal that the ASY1/ASY3 interaction requires the presence of the C-terminal coiled-coil region of ASY3, and further, suggested that the coiled-coil domain alone from ASY3 is sufficient to interact with ASY1 (Ferdous *et al.*, 2012). In West *et al.* (2019), it was shown that a HORMA-interacting domain located at the N-terminal of ASY3 (amino acid residues 2-50) is necessary and sufficient for binding of ASY1, suggesting that binding of ASY3 to ASY1 is not entirely reliant on the presence of the ASY3 coiled-coil domain, in contrast to what was published by Ferdous *et al.* (2012).

As discussed, ASY4 is predicted to contain two coiled-coil domains that take up the majority of its central portion, separated by 26 amino acids. To uncover over which regions ASY4 and ASY3 interact, I tested several truncated versions of the proteins

against each other. The first was to determine whether, as with ASY1 and ASY3, the coiled-coil domain of ASY3 was both necessary and sufficient for interaction with ASY4. The second was to test whether either coiled-coil in ASY4 is necessary and/or sufficient for interaction with ASY3. Furthermore, if ASY4 and ASY1 interacted with the same region of ASY3, it could suggest the possibility for competition between the two proteins for ASY3 binding.

To perform the Y2H experiment, I amplified ASY3 and ASY4 from *A. thaliana* bud cDNA. Methodology can be found in **2.5**, and primers in Appendix Table A4. The PCR products were cloned into pDEST-22 (contains the Gal4 activation domain) and pDEST-32 (contains the Gal4 DNA-binding domain) (Invitrogen). Plating transformed *Saccharomyces cerevisiae* onto drop out media (as described in section **2.5**) reveals whether a physical interaction is likely between the two proteins of interest.

As pDEST-22 and pDEST-32 are different vectors than those used in Osman *et al.* (2018), Chambon *et al.* (2018), and West *et al.* (2019), I first tested the interaction between full-length ASY3 and ASY4 using this vector set (Fig. 3.21 A). As this combination grows on the stringent –LTHA media, it suggests ASY3 and ASY4 can interact. Next, I tested whether the coiled-coil domain of ASY3 is necessary and sufficient for interaction with ASY4, as is proposed to be the case in Osman *et al.* (2018). Initially, a primer set used in Ferdous *et al.* (2012) was utilised for cloning the ASY3 coiled-coil (amino acid residues 623-793). However, upon closer inspection, it appears that if the primers published are correct, this would produce an out of frame protein (Appendix Fig. A5). Thus, a different primer set was designed to make a predicted in-frame protein, and subsequently both versions of the coiled-coil domain (C1 ASY3: coil as defined by Ferdous *et al.* (2012); C2 ASY3: coil as defined in this thesis) were tested against ASY4. A truncated version of ASY3 that did not contain

the coiled-coil regions (N-terminal ASY3), and so extended from amino acid residue 1 to 622, was also tested against ASY4 (Fig. 3.21 D).

For both versions of the ASY3 coiled-coil domain, neither were shown to interact with ASY4 in this study (Fig. 3.21 B, C). This is converse to what has been proposed in Osman *et al.*, (2018). It is possible that ASY4 does interact with the coiled-coil of ASY3 as defined in this thesis, but only weakly; it manages to grow on -LTH media. However, there is some uncertainty whether there is some auto-activation as the negative controls for C2 ASY3 also show some growth on the -LTH media. Nonetheless, these results suggest the coiled-coil domain is at least necessary for interaction with ASY4 as the result for ASY4 vs N-terminal ASY3 was negative.

Next, two truncated versions of ASY4 containing only one coiled-coil each (ASY4 H1 (residues 1 to 127) and ASY4 H2 (residues 128 to 212)) were tested against full-length ASY3 (Fig. 3.21 E, F). As there is no growth on -LTH or -LTHA media for the H1 ASY1 vs ASY3 FL interaction, we conclude that, using this method, we cannot show interaction with the first coiled-coil containing region of ASY4 and ASY3. For the second coiled-coil region of ASY4, however, there is growth on -LTH and -LTHA that looks similar to what is seen for the SV40/p53 control vectors, thus suggesting that ASY4 may interact with ASY3 via its second coiled-coil. However, growth on -LTHA was only achieved in one of the two reciprocal reactions; the yeast only grow on -LTHA when ASY4 H2 is in pDEST-22 and ASY3 is in pDEST-32. Explanations for this are explored in the discussion.

Replicate plates for all interactions are presented in Appendix Figure A6.

Thus, in this thesis, the second coiled-coil of ASY4 is likely necessary and sufficient for interaction with ASY3, and so we propose that the interaction with ASY3 is between

amino acid residues 128 and 212 of ASY4. The coiled-coil domain of ASY3 is necessary but potentially not sufficient for interaction with ASY4.

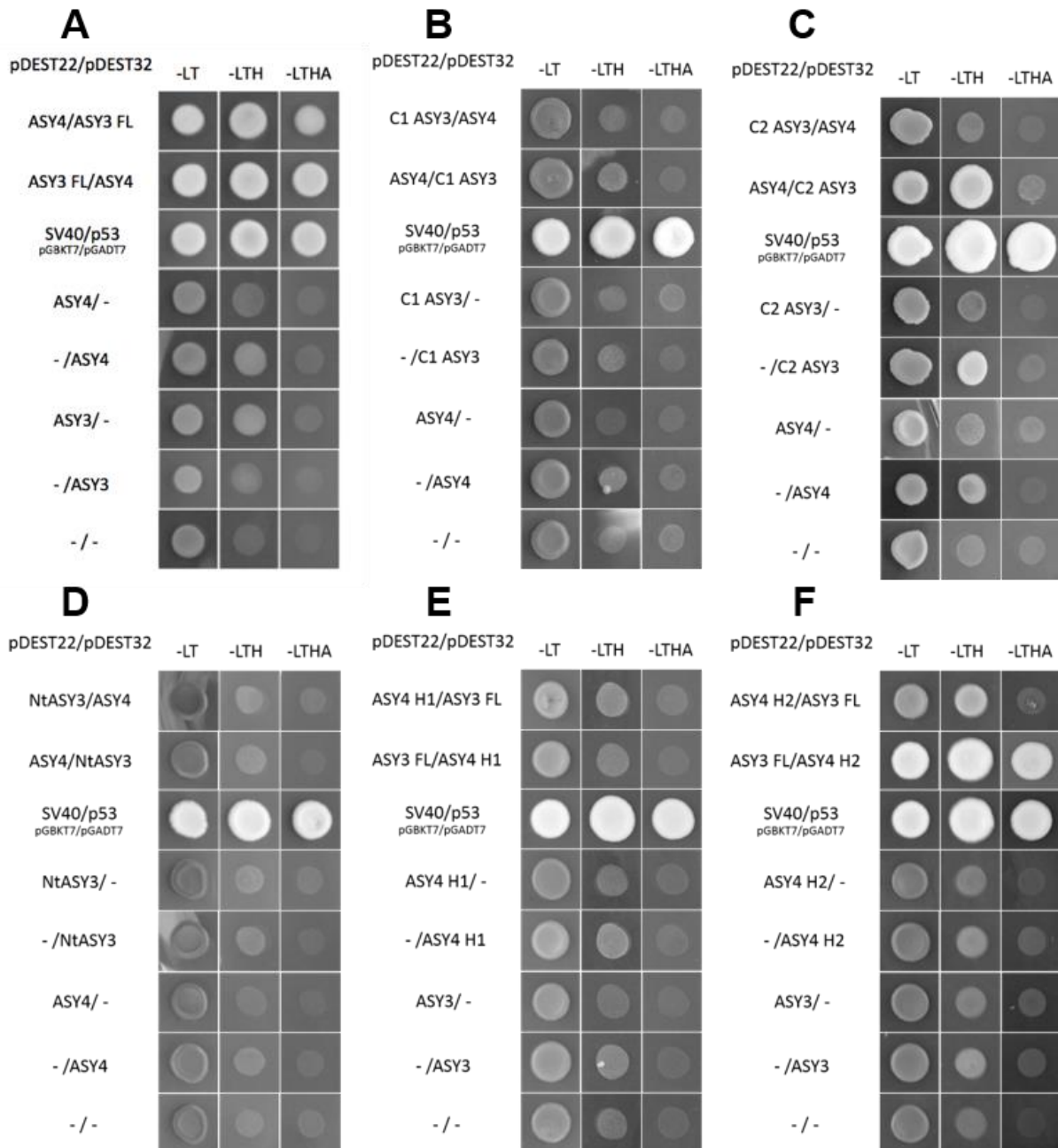


Figure 3.48 Yeast-2-Hybrid shows ASY4 interacts with ASY3, potentially via its second coiled-coil. –LT = selection for presence of Y2H vectors. –LTH = medium stringency. –LTHA = stringent media. (A) ASY4 interaction with full-length ASY3. (B) ASY4 tested against the ASY3 coiled-coil domain as defined in Ferdous et al., (2012). (C) ASY4 tested against the coiled-coil domain of ASY3 as defined in this thesis. (D) ASY4 tested against the ASY3 without its coiled-coil domain. (E) First half of ASY4 tested against full-length ASY3. (F) Second half of ASY4 interaction with full-length ASY3. SV40/p53 interaction is the control for all. Each figure represents the result from one replicate plate. 2nd and 3rd replicate plates can be found in Appendix Figure A5.

3.3 Discussion

In this chapter, we describe a novel component of the chromosome axis in *Arabidopsis thaliana* required for normal fertility, axis structure, synapsis, and CO number: ASYNAPTIC 4 (ASY4). Combined, this body of work has used affinity-proteomics to identify new candidate meiotic proteins, a variety of cytological techniques to analyse mutant lines, yeast-2-hybrid to test potential protein-protein interactions, and a novel triple-template PCR technique to tag proteins for analysis *in planta*.

As in **Chapter 5** we present a novel *asy4* mutant developed by CRISPR-Cas9, a more in-depth discussion regarding ASY4 will be covered in **Chapter 6** for clarity.

3.3.1 ASY4 is required for normal maturation of COs

As has been presented in Chambon *et al.* (2018), the two T-DNA insertion mutants available for *asy4* display a reduction in fertility, along with a reduction in CO number, and defects in chromosome axis formation. Furthermore, there is a reduction in the extent of SC polymerisation. Given that early recombination events appear to progress normally with WT levels of DMC1 foci (Chambon *et al.*, 2019), and MSH4/MSH5 foci, the reduction in CO number could be attributed to a defect in CO maturation. This would indeed appear to be the case, as Chambon *et al.* (2018) reported a reduction in the number of MLH1 and HEI10 foci compared to WT.

The reduction in chiasma number was confirmed independently by both myself at Birmingham, and the Grelon group. Chambon *et al.* (2018) presented a reduction in CO number from 8.9 to 5.9; I report a reduction from 8.6 to 6.5. This discrepancy could be explained by the inherent subjectivity involved in scoring chiasma counts, however, both groups counted using the conservative MCN method, which should make counting more objective (Jahns *et al.*, 2014). There is also a possible environmental

effect, given that the plants would have been grown in different places, and potentially, at different times of year. Nonetheless, both report a significant reduction in CO number, so the conclusion is ultimately the same.

Conversely to what was published in Chambon *et al.* (2018), we found evidence of connections and fragments at metaphase and anaphase I, which would suggest either chromosome shearing due to the connections we observed, or that some DSBs were remaining unrepaired. This could therefore be an issue with RAD51, which is in part responsible for ensuring repair of NCO intermediates off the sister chromatid (Bishop, 1994; Doutriaux *et al.*, 1998; Ines *et al.*, 2013; Li *et al.*, 2004). That this phenotype was only observed by our group means we should be cautious, however, in how this result is interpreted. For example, it is possible that this phenotype is due to the plants being grown in the Birmingham glasshouse conditions rather than those at the INRA, Versailles. There is also the possibility that since the plants have been propagated at Birmingham, they have either accrued mutations, or undergone some form of genetic re-arrangement. To support the evidence that the connections at least are a genuine phenotype, the *asy4-3* hypomorphic line presented by Osman *et al.* (2018) also displayed inter-bivalent connections. To try and solve this problem, we have requested a fresh batch of heterozygous *asy4-1* from the Grelon group with the view to checking if this phenotype still persists.

To try to describe the nature of these connections, FISH was attempted on metaphase I spreads from *asy4-1* and *asy4-2*. As outlined in 3.2.1.2, only a few cells were retrieved after treatment. An obvious conclusion from this would be that there was an issue with the FISH protocol itself, however, nearly all of the Col-0 cells used as a control were identified post-FISH. Therefore, we could speculate that perhaps the nature of the chromatin in *asy4* is somehow affected, resulting in more ‘fragile’

chromosomes. This could account for why spreads from this line were either degraded or washed off the slide. This has also been observed in other axis mutants by other lab members, who noted that it is more difficult to retrieve spreads after FISH from *asy3* and *asy1* (K. Osman and E. Sanchez-Moran, University of Birmingham, personal communication). This could potentially suggest, therefore, some issue with chromosome condensation in *asy4*, but further analysis would need to be conducted to confirm if this is the case.

3.3.2 ASY4 is an integral component of the meiotic chromosome axis in *Arabidopsis thaliana*

Immuno-affinity proteomics with BoASY1 suggested that ASY4 was, directly or indirectly, associated with the chromosome axis (Osman *et al.*, 2018). In this study, immunolocalisation and investigation of protein-protein interactions via yeast-2-hybrid has been used to confirm this suggestion.

3.3.2.1 Immunolocalisation of ASY4 and ASY4eYFP

The antibody raised against ASY4 shows that ASY4 loads onto both the chromatin and the axis during leptotene, and remains on synapsed and unsynapsed regions throughout zygotene and pachytene. Analysis of the *asy4*:ASY4eYFP line also confirms that ASY4 is on the axis during prophase I. ASY4eYFP did not, however, seem to show such a strong signal out in the chromatin. Furthermore, the nature of the signals are slightly different. Using the antibody, the ASY4 signal appears much like that of PCH2: many foci that appear to form linear structures as prophase I progresses (Lambing *et al.*, 2015). In *asy4*:ASY4eYFP, the signal looks less like an amalgamation of foci, and more like the linear signal observed with ASY1 (Chambon *et al.*, 2018).

There are several possible explanations for this. As we were unable to verify the antibody due to its giving signal in the mutant background (discussed in **3.2.2.1**; Appendix Figure A4), it is possible that the antibody could bind to proteins other than ASY4. It is also possible that the antibody is sufficiently specific, and that the signal observed in the mutant background is simply due to the possible presence of a truncated protein. This would appear to be the likely explanation, as the antibody was raised against the first 59 amino acid residues of ASY4. Given that the T-DNA insertions are downstream of this location, if the truncated mRNA transcript were to be translated, it is predicted it would produce a protein that the ASY4 antibody could recognise. Data presented in **Chapter 5** further supports that the ASY4 antibody is sufficiently specific.

The other possibility is that the *asy4*:ASY4eYFP signal looks different to the antibody signal due to the eYFP tag itself altering the dynamics of the protein, or indeed, its regulation. Whilst ASY4eYFP was designed to be under native regulation, ultimately, its expression and behaviour in the plant could be different to how we anticipated. This idea would be supported by the presence of large ASY4eYFP foci in some cells as they enter zygotene. This could be due to eYFP altering the protein's ability to be post-translationally modified, or merely due to the physical properties of the tag itself. Favouring this latter argument, Day and Davidson (2009) discuss the tendency of fluorescent proteins to dimerise and subsequently aggregate, particularly when fused to proteins that form oligomeric structures.

As for the dynamics of ASY4eYFP, its co-localisation with ASY1 may at first suggest dynamics similar to that of ASY1. There are some notable differences, however. During zygotene and pachytene, where the SC has polymerised, ASY1 is depleted from the axis, and appears as foci on the chromatin (Armstrong *et al.*, 2002c; Lambing

et al., 2015; Sanchez-Moran *et al.*, 2007). That ASY1 is depleted from the axis as the chromosomes synapse is in contrast to ASY4, and so in this respect, the dynamics of ASY4 on the axis are more similar to that of ASY3.

The results from *asy3:ASY4eYFP* suggests that ASY4 requires ASY3 to load onto the axis. The inter-relationship between ASY3 and ASY4 will be discussed in **Chapter 6** in light of later experiments conducted in the CRISPR-Cas9 generated mutant, *asy4-4*.

Perhaps most surprising is the result that the ASY4eYFP signal appears patchier in the *pch2:ASY4eYFP* line in leptotene cells. This is in contrast to what has been observed of ASY4eYFP in all other developed ASY4eYFP lines presented in this thesis. A notable phenotype of *pch2* is the persistence of ASY1 on synapsed chromosomes (Lambing *et al.*, 2015). Further to this, ASY1 appears not to load normally onto the axis in the first place, appearing significantly dimmer in *pch2* than in WT (West, 2015). This could suggest a potential early role for PCH2 in axis assembly. As such, it could be possible that ASY4eYFP linearisation has been affected due to this other role of PCH2. Of course, caveats with the eYFP experiments discussed above could also apply here, and it could merely be a consequence of the system used. Thus further experiments such as imaging the ASY4 antibody itself in *pch2* would be useful in determining if this is a genuine interplay between PCH2 and ASY4. This will be discussed further in **Chapter 6**.

3.3.2.2 Protein-Protein Interactions suggest ASY4 physically interacts with the axis

As shown via the yeast-2-hybrid (Y2H) experiments in this chapter, ASY3 and ASY4 can directly interact. This is a fairly robust interaction, as in four sets of Y2H tests

(Osman *et al.*, 2018; Chambon *et al.*, 2018; West *et al.*, 2019; this thesis), the interaction has been positive. It has also been shown via BiFC (Chambon *et al.*, 2018). Some discrepancies with previous work are presented here, however, as neither version of the ASY3 coiled-coil tested were shown to conclusively interact with ASY4 as is presented by Osman *et al.* (2018) and in West *et al.* (2019). This could purely be due to the vector systems used: pDEST-22 and pDEST-32 are noted in the literature as being perhaps one of the most stringent vectors available, and thus is potentially more likely to provide a false-negative result than other vector systems, which are more likely to present false-positives (Rajagopala *et al.*, 2009). Therefore, there are several explanations for this result. One could be that the expression of the two ASY3 coiled-coil proteins is too low to present an interaction. This could be confirmed by probing for the protein on a western blot with antibodies against the Gal4 DBD or AD to see if the proteins are expressed in both vectors. Alternatively, as the amino acid linker between the Gal4 DBD or AD and the protein of interest is relatively short (~14 aa), the yeast component of the fusion protein may cause a topological issue that prevents the bait and prey from being able to interact; this could be one of the sources of the ‘stringency’ of these vectors, as perhaps only the strongest interactions will overcome this issue. Either way, it was not possible to show this interaction in this study. The same reasoning could be applied to ASY4 vs NtASY3, and ASY4 H1 vs ASY3, of course. West *et al.* (2019), however, also presented no detectable interaction between ASY4 and ASY3 without its coil (residues 2-605). To make the conclusions more robust, therefore, other methods would need to be used to test that the interactions are not false negatives. This would also be true for the positive interaction between ASY4 H2 and ASY3, which could be done in a co-immunoprecipitation experiment. This is outside the scope of this thesis, however.

Chapter 4

**Generation of an ASY4 mutant
using the CRISPR-Cas9 gene
editing system**

4 Generation of an ASY4 mutant using the CRISPR-Cas9 gene editing system

4.1 Introduction: Utilisation of the CRISPR-Cas System as a Gene Editing Tool

4.1.1 Discovery and History

CRISPR (Clustered Regularly Inter-Spaced Palindromic Repeats) and the CRISPR-associated (Cas) proteins form a crucial component of an adaptive immune response in many bacteria, and nearly all archaea (reviewed in: Wang *et al.*, 2016). Work to uncover this role, however, spanned over a decade. In 1993, whilst working on the halophile *Haloferax mediterranei*, Mojica *et al.* noted a section of DNA that contained 30 bp stretches of highly conserved sequence that appeared to form a repetitive pattern, now termed as ‘spacers’; a structure that had also been previously identified in bacterial species (Hermans *et al.*, 1991; Ishino *et al.*, 1987). Nine years later, in 2002, a paper by Jansen *et al.* appears to be the first to term these repeats as forming a CRISPR locus. Jansen *et al.* also were the first to identify several Cas proteins that they proposed interact with products of the CRISPR locus in *Streptococcus thermophilus*. Comparative genomics later showed that the non-repetitive sequences between the spacers could be identified in various phage, and extrachromosomal elements (Mojica *et al.*, 2005). Based on this, it was proposed that the CRISPR-Cas system provided a cellular memory of past invasions, and subsequently, that it would target invading foreign DNA. That CRISPR-Cas provided immunity to phage was conclusively shown in 2007 by Barrangou *et al.*, who showed that *S. thermophilus* acquired new spacer sequences post phage invasion, and that altering the spacers could confer or remove immunity to invaders.

4.1.2 CRISPR-Cas: an RNA-directed nuclease

In short, the function of the CRISPR-Cas system is to identify a specific section of DNA (in prokaryote immunity, this will be from an invader such as phage), and to cut it. Its ability to recognise specific sequences of DNA is guided by RNA produced from the CRISPR locus, where its ‘memory bank’ of past invaders is held. Once the Cas protein cuts the invading DNA, the DNA can no longer execute its role, therefore allowing the prokaryote to resist infection (reviewed in: Rath *et al.*, 2015).

Many types of CRISPR-Cas system exist in bacteria and archaea, and are split into two main classes: I and II (reviewed in: Koonin *et al.*, 2017). The most simple, and therefore the system that has been chosen for modification as a gene-editing (GE) tool, is the Class 2 Type II system, CRISPR-Cas9 (reviewed in: Bhaya *et al.*, 2011). In contrast to other systems, CRISPR-Cas9 only requires three components: the Cas9 nuclease and two RNAs. These are the trans-activating RNA (tracrRNA), and an RNA transcribed from the CRISPR locus itself, termed the crRNA. In both prokaryotic immunity and GE, CRISPR-Cas9 functions thus (Fig. 4.1):

1. The tracrRNA and a pre-crRNA are transcribed. The pre-crRNA contains the sequence homologous to a past invader, with a small section of the repeat region. The tracrRNA is transcribed from upstream of the crRNA, and contains homology to the repeat region contained within the crRNA. As such, a pre-crRNA:tracrRNA double stranded RNA hybrid is formed, which can be processed by RNase III, resulting in a mature crRNA:tracrRNA molecule with only one spacer sequence present.
2. The crRNA:tracrRNA is recognised by Cas9 to form the CRISPR-Cas9 ribonucleoprotein (RNP).

3. The CRISPR-Cas9 RNP complex then scans DNA for a Protospacer Adjacent Motif (PAM): a short stretch of DNA sequence. The sequence recognised is specific to the prokaryote species the CRISPR-Cas originates from. This is facilitated by amino acid residues within the Cas9's PAM Interacting (PI) domain.
4. If a PAM is identified, the DNA strand is unwound. If the sequence immediately upstream of the PAM can Watson-Crick-Franklin pair with the specific sequence provided by the crRNA, a RNA:DNA hybrid termed an 'R-Loop' is formed.
5. Cas9 cleaves the DNA. Its HNH domain nicks the strand complementary to the crRNA, and its RuvC domain cleaves the non-complementary strand.

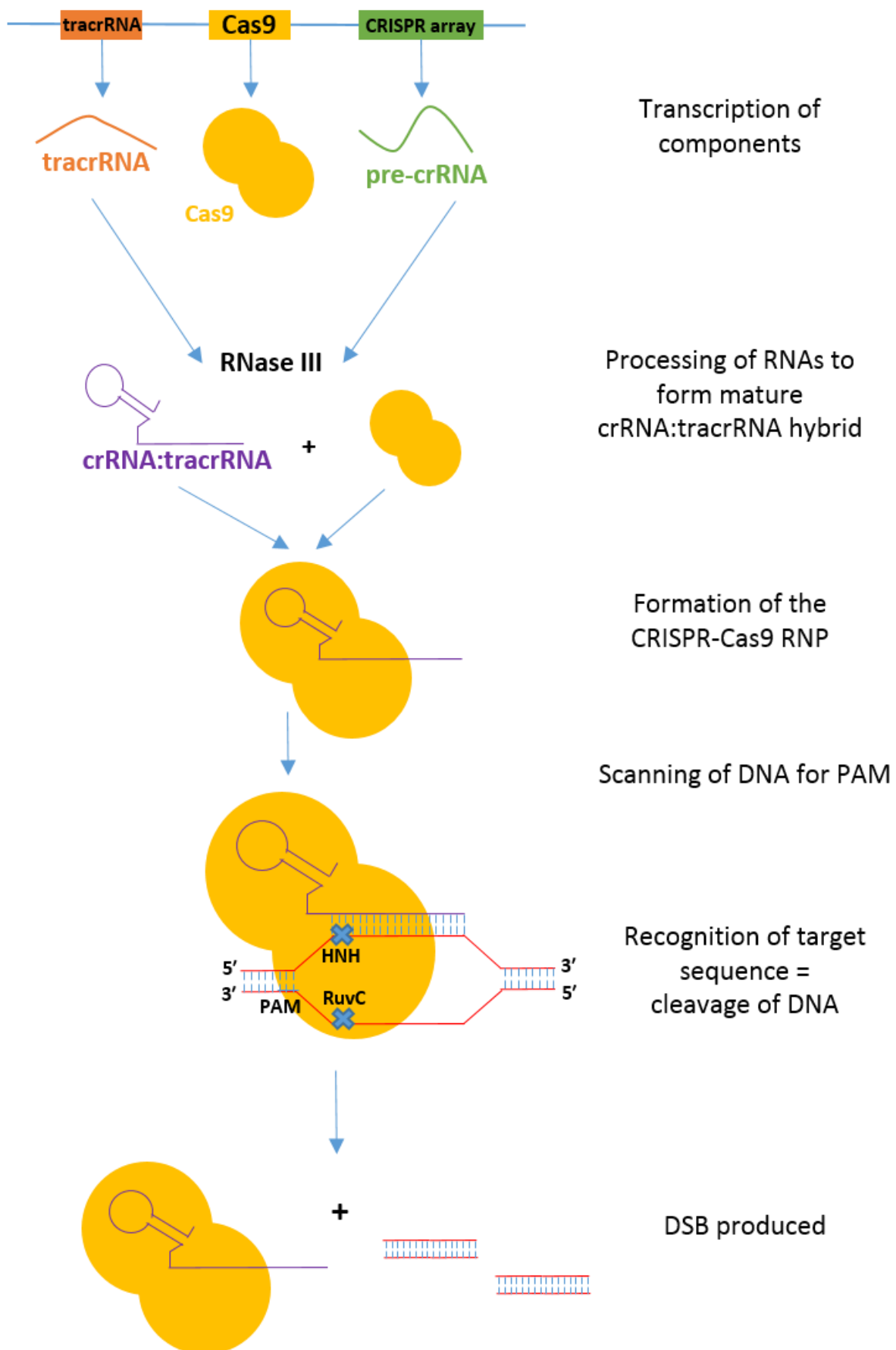


Figure 4.1 Summary of how the CRISPR-Cas9 system produces a double strand break (DSB) in target DNA.

4.1.3 CRISPR-Cas9 in Gene Editing

As previously discussed, the CRISPR-Cas9 system was chosen to be modified as a GE tool as it is the most simplistic of the CRISPR-Cas systems. To simplify the cloning processes further, it was demonstrated that the crRNA and tracrRNA could be combined to form a chimeric single guide RNA that could still successfully guide Cas9 (sgRNA) (Jinek *et al.*, 2012).

The most common CRISPR-Cas9 systems currently come from *Streptococcus pyogenes* (SpCas9) and *Staphylococcus aureus* (SaCas9). As mentioned, the PAM recognised by each CRISPR/Cas9 system is species specific. In SaCas9, the PAM is 5'-NNGRRT-3'. In SpCas9, it is 5'-NGG-3'. Both SpCas9 and SaCas9 are now used with an sgRNA, and have been used to edit DNA in a wide range of organisms, including both model and crop plant species (reviewed in: Bortesi and Fischer, 2015). For each system, the main caveat appears to be that to ensure proper expression of the construct, the codons must first be optimised for the organism they will be editing in, as well as addition of a promoter the system would recognise (Dickinson *et al.*, 2013; Friedland *et al.*, 2013; Shen *et al.*, 2013; for plants reviewed in: Ma *et al.*, 2016).

CRISPR-Cas9 is now a widely established tool for producing precise, heritable mutations, and in contrast to systems such as ZFN and TALENS, with high-throughput applications (Fauser *et al.*, 2014; Feng *et al.*, 2014; H. Zhang *et al.*, 2014).

4.1.4 Using CRISPR-Cas9 to generate a meiotic mutant in *A. thaliana*

As outlined above, the CRISPR-Cas9 system has been harnessed as a precise, high-throughput gene editing tool that can be used in a wide variety of organisms.

Traditional plant mutagenesis techniques include ethyl methanesulfonate (*EMS*) and T-DNA insertions. EMS is a technique that was initially favoured for forward genetic

screens, yet repositories are also available for obtaining a desired mutant. This is also the case for T-DNA insertions, which have traditionally been used for reverse genetics. There is, however, a caveat with these techniques: the mutagenesis program is essentially random. Where a T-DNA is inserted, or where a mutation is induced via EMS, is not determined by the user. T-DNAs may insert into the genome several times, and EMS is not guaranteed to cause a mutation at only one point in the genome (reviewed in: Østergaard and Yanofsky, 2004).

More precise methods of inducing mutants have since been developed, including ZFNs (Zinc Finger Nucleases) and TALENs (Transcription Activator-Like Effector Nucleases), and most recently, CRISPR-Cas (Kim *et al.*, 1996; Miller *et al.*, 2011). Due to ease of production and comparatively lower cost, CRISPR-Cas9 promises to provide precision engineering more cheaply and more quickly, given that the technology has been optimised for the organism of interest. So far in plants, CRISPR-Cas9 has been used in both model and crop systems, including *A. thaliana*, *Nicotiana*, Barley, Rice, and Wheat (Baltes *et al.*, 2014; Lawrenson *et al.*, 2015; Li *et al.*, 2013; Schiml *et al.*, 2016; Shan *et al.*, 2013; Xie and Yang, 2013).

Here, we use the CRISPR-Cas9 system from *Staphylococcus aureus* as described by Schiml *et al.* (2016) and provided by the Puchta laboratory (Karlsruhe Institut für Technologie, Germany) to generate a full knock-out mutant of ASY4. This is desirable as the current *asy4* mutants available appear to produce a truncated transcript (3.2.1.1; Chambon *et al.*, 2018; Osman *et al.*, 2018). An antibody raised against the ASY4 protein also shows signal in the mutant backgrounds, further suggesting production of a truncated protein (discussed in 3.2.2.1).

We present an overview of the methodology used to screen the plants for mutation, culminating in the identification of an *asy4* null mutant.

4.2 Generation and Identification of candidate plant lines

Cloning and transformation of plants was conducted as outlined in **2.6**. Three oligo sets were used, termed ASY4 Pair 1, ASY4 Pair 2, and ASY4 Pair 3. The target sites of each oligo pair are illustrated below (Fig. 4.2).

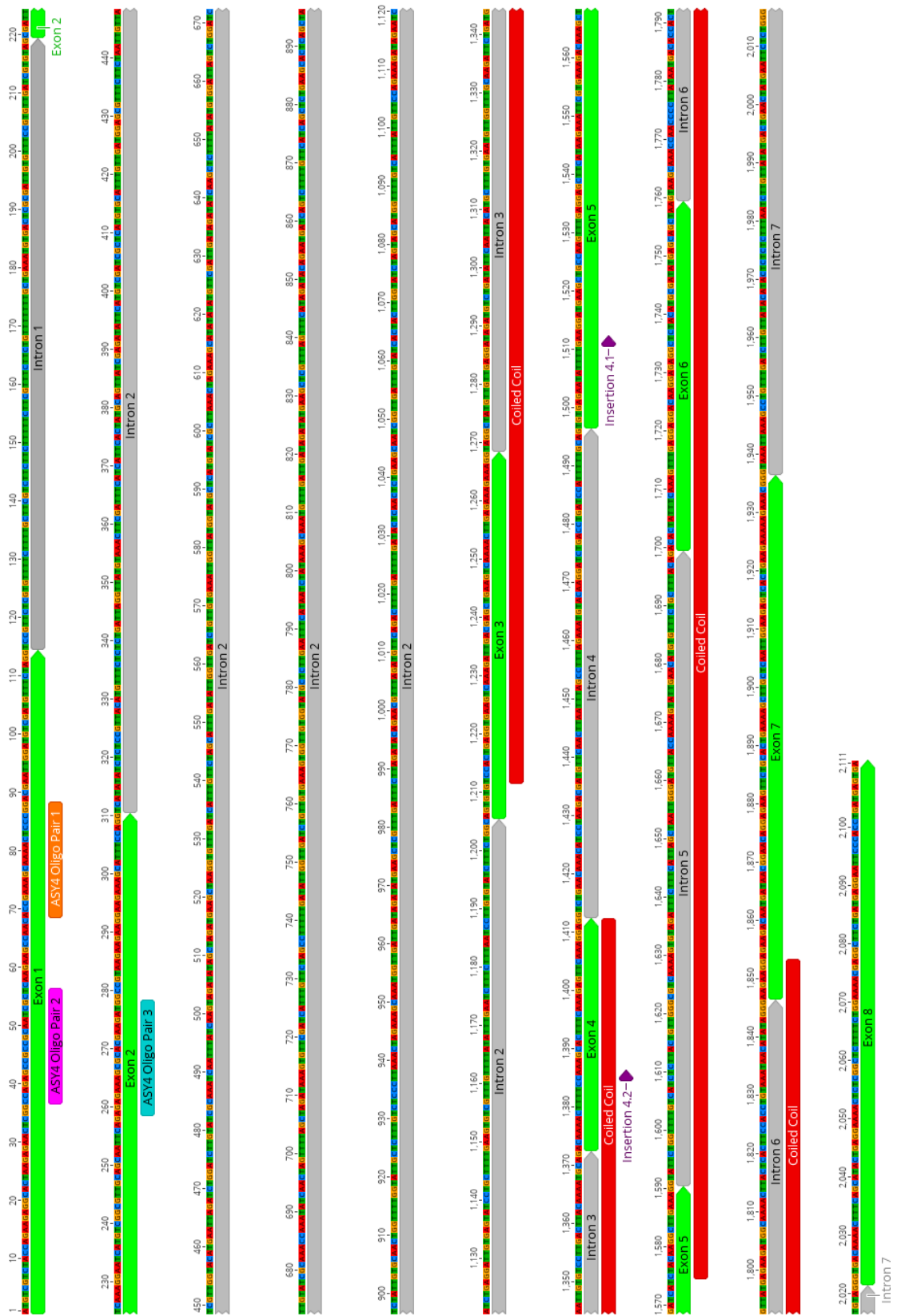


Figure 4.2 Location of the *Staphylococcus aureus* CRISPR-Cas9 target sites in the genomic sequence of ASY4. Green arrows indicate exons. Grey arrows indicate introns. Orange label indicates oligo pair 1; pink oligo pair 2; and blue oligo pair 3. Coiled-coil domains are labelled in red. 4.1 and 4.2 insertions also displayed.

For each oligo pair, five Col-0 WT plants were transformed via floral dip (as in **2.4**), resulting in 15 primary dipped plants (T0). These plants were allowed to set seed. After the seeds had been dried, seeds from the T0 lines were transferred to MS media with 30 µg/mL kanamycin added to select for the plants that contained the Cas9 (**2.1.1**). This yielded a total of 19 primary transformant T1 lines. That these T1 lines contained Cas9 was also verified by PCR using SS102 and SS42. A representative gel showing Cas9 present in T1 transformants is shown in Appendix Figure A7. These lines were once more left to set seed, and taken forward to T2.

To aid clarity, the decision plan of how individual plant lines were selected is presented in Figure 4.3. Furthermore, Table 4.1 outlines the origin of each plant line, and the resultant plants that established the new CRISPR-generated mutant line for *asy4*.

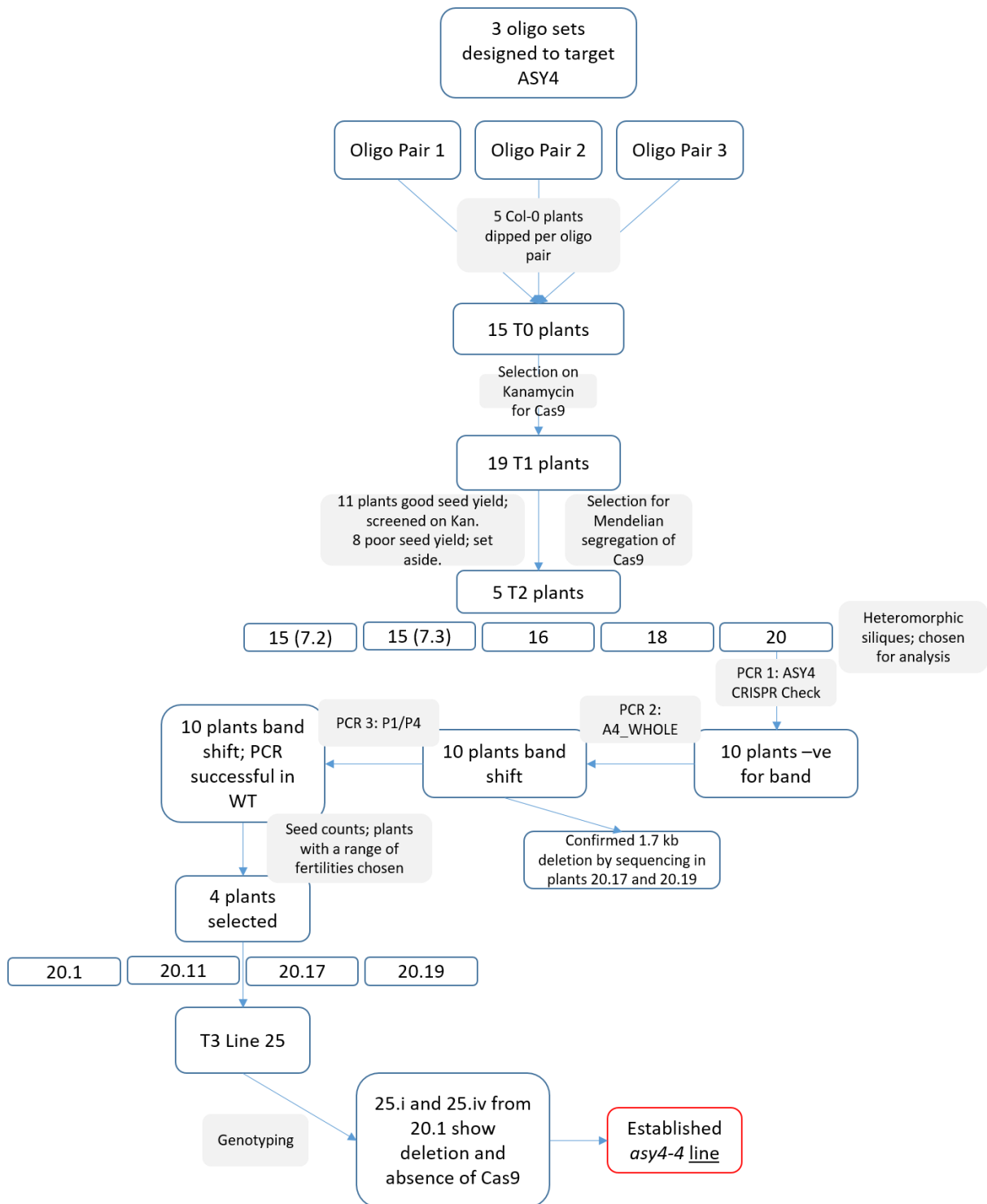


Figure 4.3 Flow chart displaying the decisions made to establish the final *asy4-4* mutant line.

Table 4.1 Description of origin of the 19 ASY4 CRISPR/Cas9 plant lines

| Primary Dipped (T0) | Oligo Set | T1 | T2 | T3 | T4 |
|--------------------------------|------------------|-------------|------------------|-----------------|---------------|
| 1.2 | P1 | 6.16 | - | - | - |
| | | 6.17 | - | - | - |
| | | 6.18 | Line 12 | - | - |
| | | 7.2 | Line 15.21-15.40 | - | - |
| | | 7.3 | Line 15.1-15.20 | - | - |
| | | 7.4 | NON-SEG | - | - |
| | | 7.5 | Line 16 | - | - |
| | | 10.2 | NON-SEG | - | - |
| | | 10.3 | Line 18 | - | - |
| | | 10.9 | - | - | - |
| 1.4 | P1 | 7.1 | NON-SEG | - | - |
| | | 10.8 | NON-SEG | - | - |
| 1.5 | P1 | 10.1 | - | - | - |
| 1.16 | P2 | 10.4 | Line 20 | Line 25, | asy4-4 |
| | | 10.5 | - | - | - |
| | | 10.6 | - | - | - |
| | | 10.7 | NON-SEG | - | - |
| 1.24 | P3 | 6.14 | NON-SEG | - | - |
| | | 6.15 | - | - | - |

4.2.1 Segregation of Cas9 and analysis of the resultant T2 progeny

Segregation of the Cas9 as determined by kanamycin resistance was used to indicate whether the plants were likely to only have one copy of Cas9, or more. Mendelian segregation of the kanamycin resistance would suggest that only one copy was present in the T1 parent line; this is the ideal situation as it is desirable to breed the Cas9 construct out as soon as possible to decrease the likelihood of it repeatedly attempting to cut *ASY4* (thus potentially generating bi-allelic mutants), or indeed, potential off-targets. To do this, T2 plants were screened on MS media with 30 µg/mL kanamycin. A total of 44 seeds were plated for each line; for a true Mendelian ratio of segregation, around 33 would survive, and around 11 would die.

Of the 11 lines screened on plates, 5 showed the correct segregation patterns, and so were put to soil: Line 15 (from plant 7.3), Line 15 (from plant 7.2), Line 16, Line 18 and Line 20. A representative example of correct segregation is shown in Fig. 4.3.

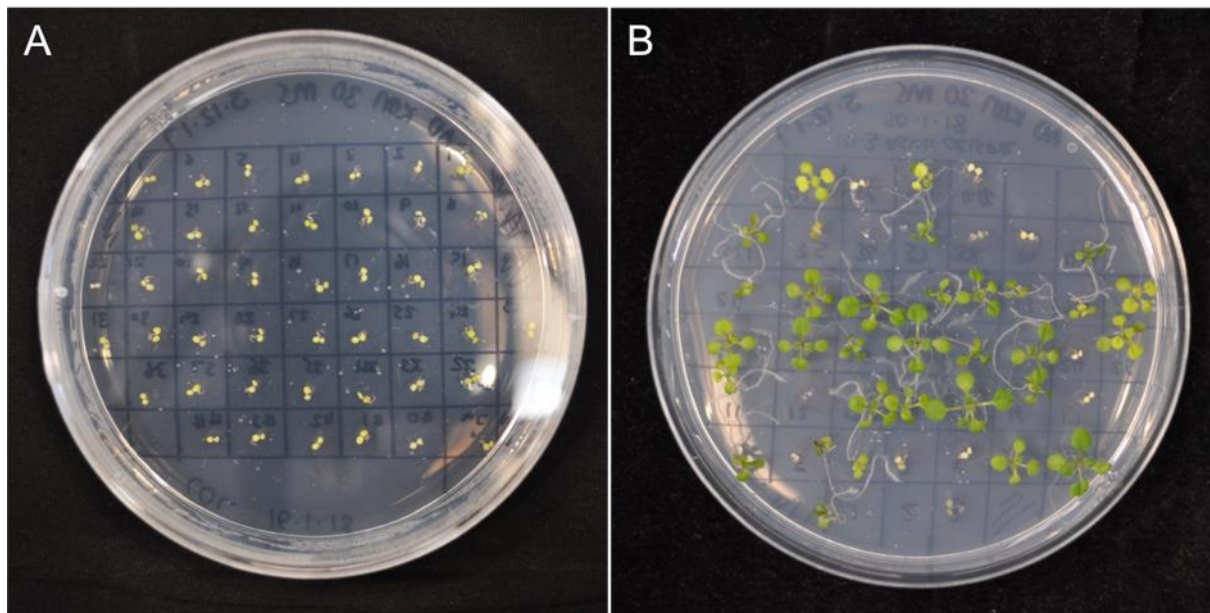


Figure 4.4 Selection for lines presenting Mendelian segregation of the CRISPR-Cas9 construct via kanamycin resistance. Plates photographed after one week on MS media with 30 µg/mL kanamycin. (A) WT seedlings show stunted growth, and subsequently die. (B) Seedlings from T1 CRISPR line 10.3 showing correct segregation: 32 healthy, 12 stunted.

From each correctly segregating line, 5 plants were transplanted to soil from MS media, and 5 were sown directly to soil. The remaining 8 T1 lines produced very little seed; therefore to conserve the seed stock, it was decided to select for these directly on soil via PCR for Cas9 if we did not identify correctly segregating lines with a potential mutation in the 5 lines identified on plates.

4.2.2 Fertility analysis

Seed counts were conducted on the 5 lines showing correct segregation: Line 15 (7.2), Line 15 (7.3), Line 16, Line 18, and Line 20. All plants in Line 15 (7.2), Line 15 (7.3), and Line 16 showed no significant difference in seed number per siliques compared to wild-type in a Kruskal-Wallis test (5% level, two tailed, Dunn's correction for multiple comparisons). Graphs illustrating the seed count data are presented in Appendix Figure A8. Line 20 is presented separately in **4.3**. All plant lines were then screened

for potential INDELS by looking for a band shift in PCR. The PCR used is explained in **4.3.**

4.3 CRISPR Line 20 shows a 1.7 kb deletion in the ASY4 locus

To commence optimisation of the verification process, T2 Line 20 was chosen to be taken forward to go through the entirety of my proposed analysis protocol. It was chosen as the T1 parent line (10.4) showed an unusual phenotype: on some stems, the siliques appeared WT, and on others, they appeared to have reduced fertility. When put to kanamycin, this line showed correct segregation, and so seeds were put to soil.

DNA was extracted from leaf tissue as per **2.2.2**, and a 1037 bp region of ASY4 amplified, spanning from the promoter, into the second intron (ASY4 CRISPR Check primer set, see **2.6** and Appendix Table A6 for sequences). This primer pair was designed to amplify this region as Cas9 is expected to cut around 3 bp upstream of the PAM, thus positioning any potential INDEL/SNP in portion of the ASY4 gene that is predicted to encode the N-terminus of ASY4 (Jinek *et al.*, 2012). Out of 20 plants, 10 did not appear to amplify this section of ASY4 (Fig. 4.4 A). Therefore, another set of primers was designed to amplify the entirety of ASY4 from the intergenic/promoter region, through to the 3'-UTR (A4_WHOLE primer set, see **2.6** and Appendix Table A6). The expected product in WT was 3434 bp. The band produced in the ‘mutants’ however appeared significantly smaller, at around ~1750 bp. (Fig. 4.4 B). This suggested a large deletion in ASY4. Despite several attempts, however, the reaction did not work in WT.

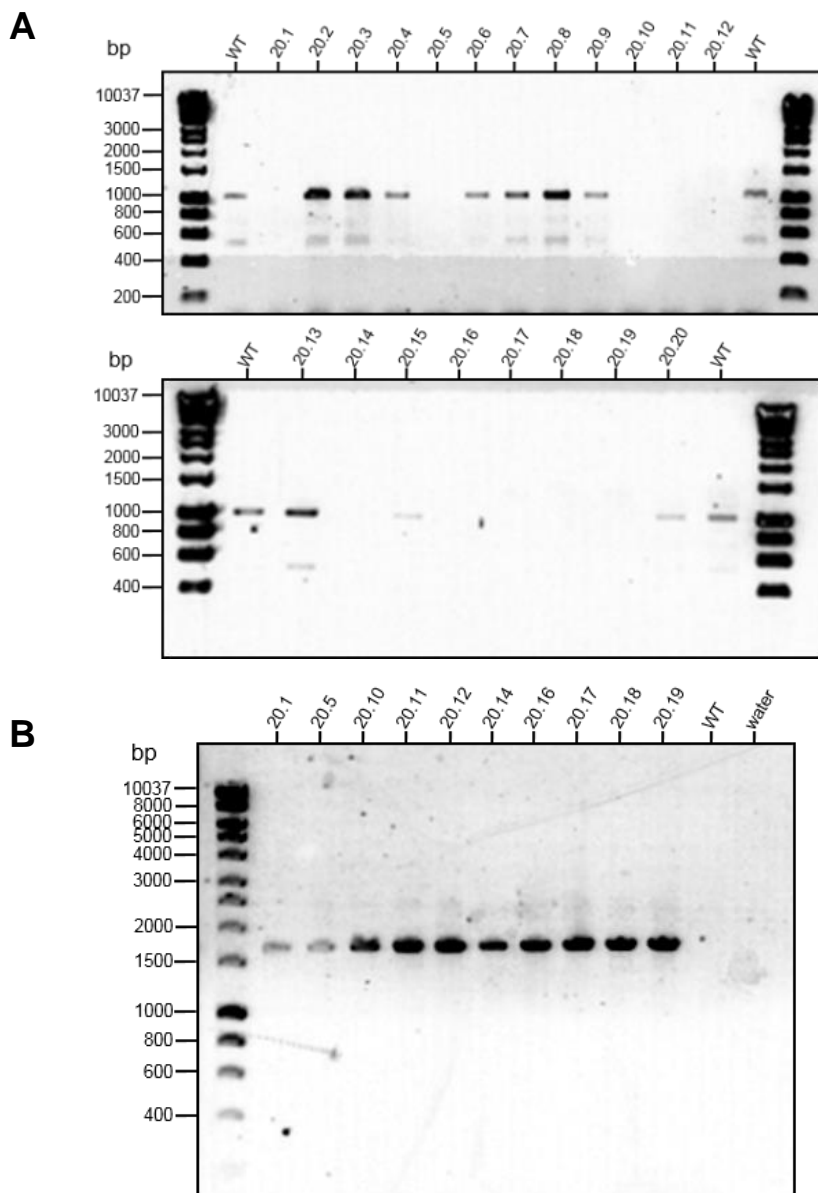


Figure 4.5 Verification of a potential deletion in ASY4 via PCR screening with two sets of primers. (A) Amplification of a ~1 kb region across the expected break site. (B) Amplification of what was expected to be a ~3.4 kb product. Band produced from the selected ASY4 CRISPR/Cas9 plants from Line 20 shows a ~1750 bp product.

The PCR products from Line 20 were therefore purified and sequenced to confirm a deletion in ASY4. High quality sequence was obtained for plants 20.17 and 20.19. Both show the same 1729 bp deletion in ASY4, with a 20 bp region that appears to have been mutated during repair (Fig. 4.5).

The deletion appears to span the intergenic/promoter region (-903, relative to ATG) (whilst not extending into the gene next gene upstream at the 5' end; Appendix Figure A9), through to the middle of the second intron (826, relative to ATG). As all plants are from the same parent, it is suggested that the deletion arose through a single event.

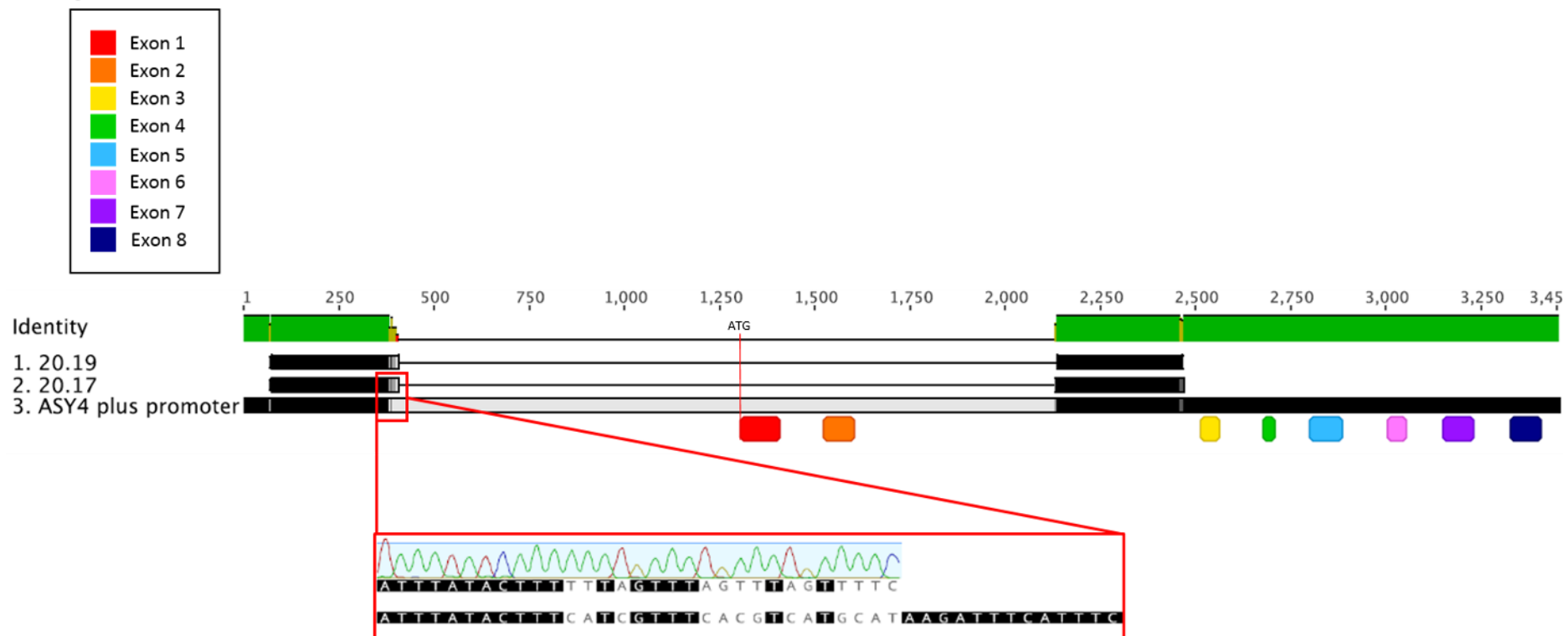
Key:

Figure 4.6 Alignment of genomic ASY4 sequence with intergenic region and sequencing reads from 20.17 and 20.19 showing a ~1.7 kb deletion. Identity bar depicts 100% identity in green, decreasing through yellow. Red indicates low identity. Relative to the ATG start codon, the deletion is between bases -903 (promoter/intergenic region) and 826 (intron 2) of the presented region. Highlighted area shows mutations at the junction between the intergenic region before the deletion and intron 2. Aligned within Geneious R9.

As a product could not be obtained for WT using the A4_WHOLE primer sets, the P1/P4 primers designed for tagging of the ASY4 protein with eYFP were used to amplify from the promoter through to the 3' end of ASY4 (Chambon *et al.*, 2018). This was tested on DNA from plant 20.1, and WT. The gel shows a clear band shift of approximately 1.7 kb (Fig. 4.6).

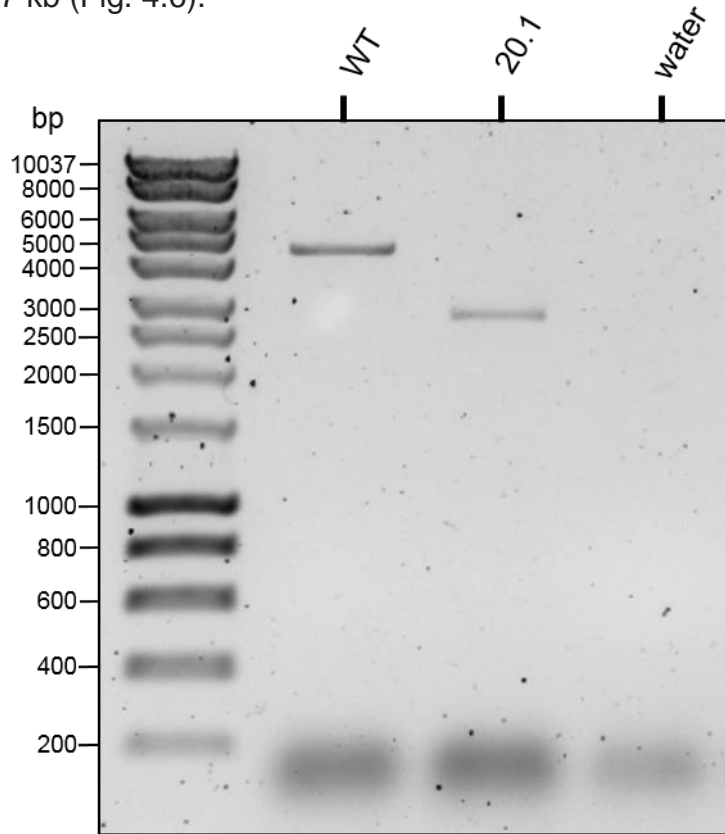


Figure 4.7 PCR amplification of full-length ASY4. PCR products from gDNA on an ethidium bromide stained agarose gel showing a band shift in 20.1 CRISPR/Cas9 *asy4* plant. WT ASY4 product: 4497 bp. 20.1 ASY4: ~2800 bp.

We also checked the reverse strand sequence to ensure no other genes would be interrupted by such a large deletion. That there are no genes in this region on the strand antisense to ASY4 is shown in Appendix Figure A9. Therefore, if we anticipate no off-targets, any phenotype observed should be due to the mutation in ASY4.

To determine which plants still contained Cas9, PCR was conducted using the SS102/SS42 primers. This revealed that plants 20.13, 20.15, and 20.17 appear to

have lost Cas9. Fortunately, 20.17 appeared both mutated, and had lost the Cas9 construct (Fig. 4.7).

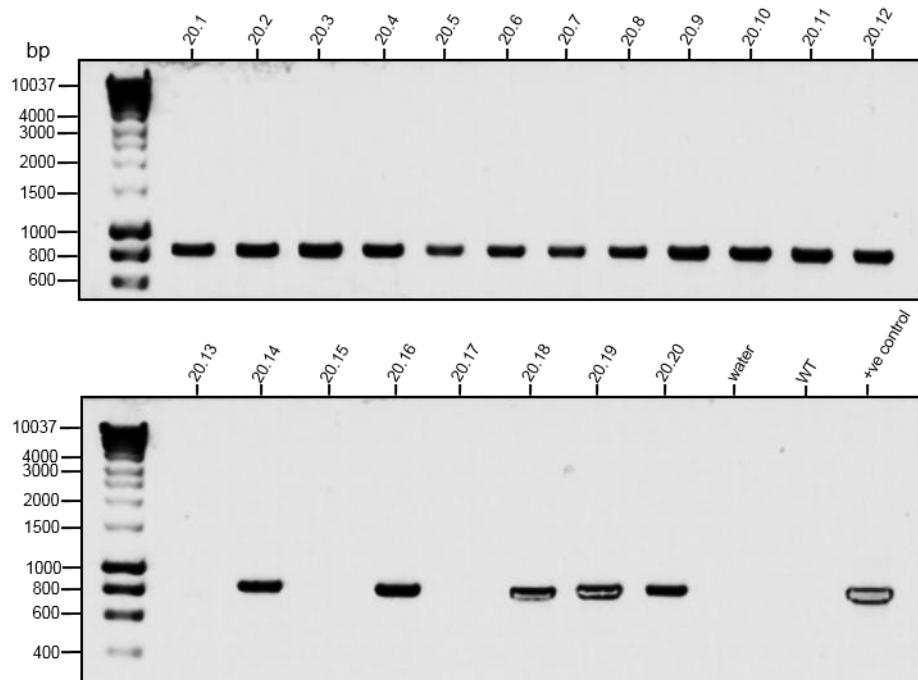


Figure 4.8 PCR detection of the ASY4 CRISPR/Cas9 construct in planta. PCR products analysed via gel electrophoresis, and stained with ethidium bromide. PCR shows a product of the expected size, confirming the ASY4 CRISPR/Cas9 construct to have been lost in 3 of the lines. Positive control is gDNA from a T1 plant confirmed to contain the construct via kanamycin selection.

Finally, seed count data was obtained to determine whether there was a notable fertility defect in the plants expected to carry the deletion. Three plants show a significant reduction in fertility compared to WT: 20.1, 20.9, and 20.11 (Fig. 4.8). Significance was determined in a Kruskal-Wallis test (5% level, two tailed, Dunn's Correction for multiple comparisons), which showed plant 20.11 presents the most severe reduction in fertility ($\bar{x} = 21.8$, $P = 0.0052$), followed by 20.1 ($\bar{x} = 25.6$, $P = 0.0190$). The least significant reduction is seen in 20.9 ($\bar{x} = 28.6$, $P = 0.0377$). Both 20.1 and 20.11 were predicted to contain the deletion, but 20.9 was not.

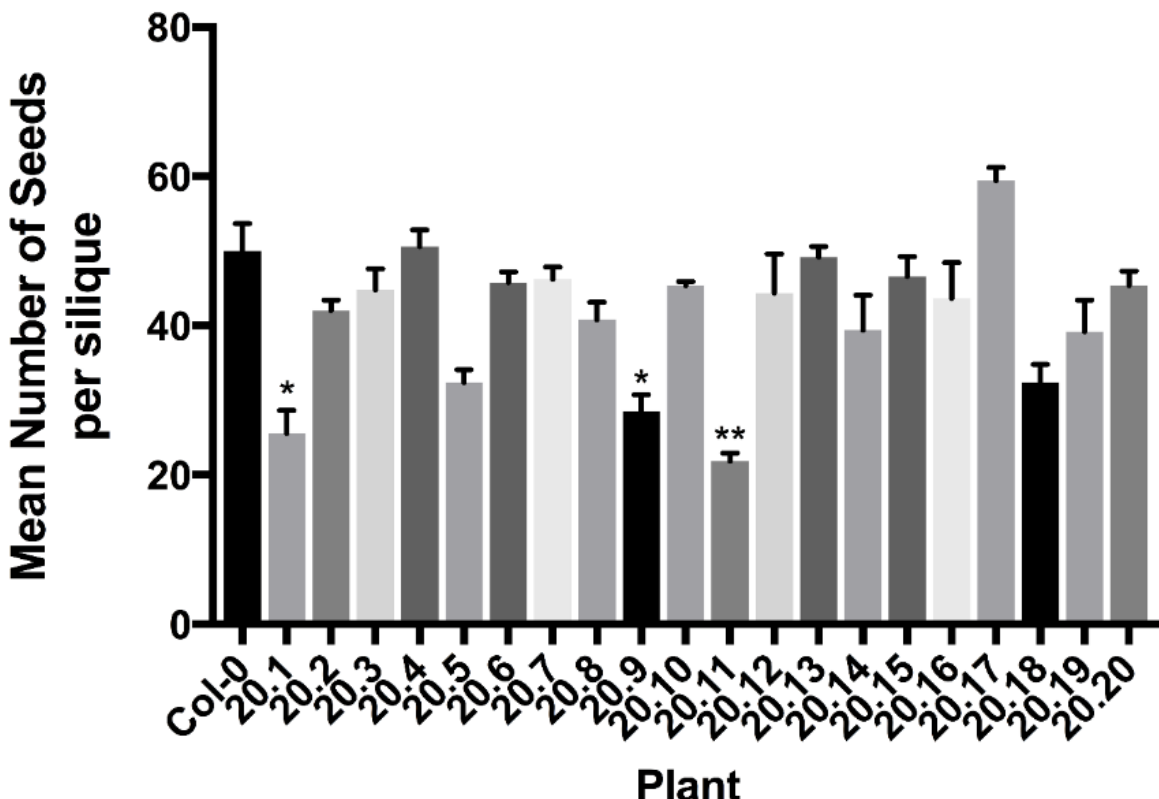


Figure 4.9 Seed count data for ASY4 CRISPR/Cas9 Line 20. Asterisks indicate a significant difference in mean number of seeds per siliques compared to Col-0 WT data in a two-tailed Kruskal-Wallis test at the 5% level. * = $P < 0.05$. ** = $P < 0.01$. Bars represent standard error of the mean. Each bar represents data from 5 siliques.

Thus the final plants selected for propagation to T3 were 20.1, 20.11, 20.17, and 20.19. These plants were selected as they display a range of fertilities. This is because purely selecting for low fertility could lead to inadvertently selecting for plants with other undesirable mutations (unfavourable T-DNA insertion locations, genomic rearrangements etc).

4.4 Finalising the mutant line at T3 and T4

To further develop a homozygous *asy4* mutant with no Cas9, several plants from Line 20 were chosen to proceed to the T3 generation: 20.1, 20.11, 20.17, and 20.19. The resultant T3 plants formed ‘Line 25’. These plants were screened for the deletion via PCR using a final, optimised set of primers: an initial screen with the ASY4 CRISPR Check set which only produces a product if there is a WT copy of the gene present, and the A4 CR set, which amplifies both a WT and mutant band, presenting as a band shift on the gel. Primers are described in Appendix Table A6. Plants at T3 and T4 were also screened for the presence of Cas9 to ensure only Cas9-negative plants were taken forward.

To determine whether the 1.7 kb deletion in ASY4 conferred an absence of expression, RT-PCR was performed on buds from 25.i and 25.iv (from 20.1): two T3 plants that appear homozygous for the deletion. Two primer sets were used: ‘ASY4 Short’ which was used to show a truncated ASY4 transcript was present in the *asy4-1* and *asy4-2* mutants (Chambon *et al.*, 2018), and a pair that amplified from ASY4 exon 3 through to the stop codon in exon 8. This was to determine whether a transcript could still be expressed from the remainder of the ASY4 gene. As is shown in Figure 4.9, no strong band is found in the ASY4 CRISPR plants that would suggest expression of the remaining half of ASY4, satisfying us that using CRISPR-Cas9, we have successfully knocked-out the ASY4 gene. Hereon in, this mutant will be referred to as *asy4-4*.

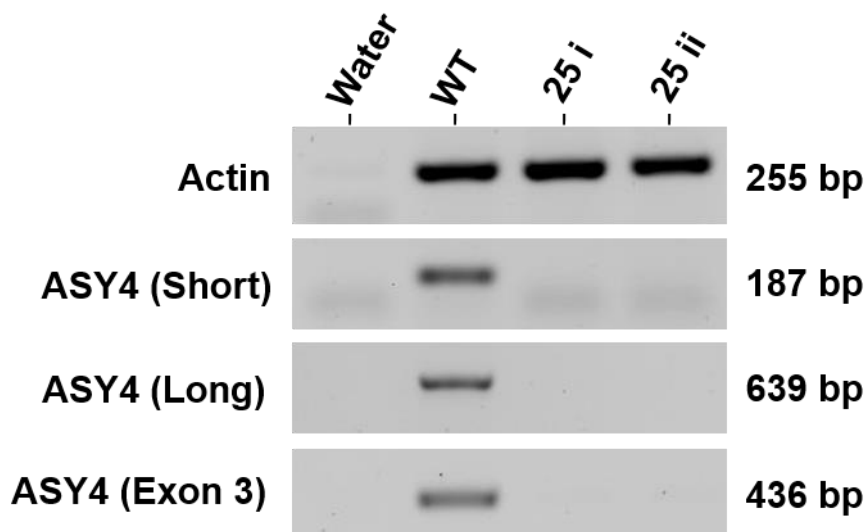


Figure 4.10 Expression of ASY4 in wild-type and *asy4-4* mutant buds. Gel electrophoresis stained with ethidium bromide. Water control. Wild-type (WT). Two *asy4-4* T3 mutants: 25i and 25ii. Comparison of the 'short' transcript present in *asy4-1* and *asy4-2*, the full-length ASY4 transcript (long), and any possible transcript from the third exon through to the stop codon. No ASY4 transcript detectable in either of the *asy4-4* T3 mutants tested.

4.5 Discussion

4.5.1 *asy4-4* is a knock-out mutant of the ASY4 gene

Here we present a CRISPR-Cas9 generated ASY4 mutant line with a deletion of ~1.7 kb in the first half of the gene, and therefore show that we appear to have the *S. aureus* system of CRISPR-Cas9 working in our hands. Generation of this mutant was necessary as the *asy4-1* and *asy4-2* mutants presented in Chambon *et al.* (2018) are likely hypomorphic, possibly producing a truncated version of the ASY4 protein (data presented **Chapter 3**).

That the deletion present is so large is perhaps little unexpected, though in mouse, deletions of up to 9.5 kb have been induced using only a single gRNA (Kosicki *et al.*, 2018). Schiml *et al.* (2016) suggest amplification of a region of 1 kb to check for deletions; it is therefore possible that larger deletions are under-reported in CRISPR-Cas9 data simply because the screening process is biased against them. It is also the case that due to the novel nature of this protocol, we were unsure what to expect.

It is possible that the break in *asy4-4* was repaired by the alternative non-homologous end joining pathway (alt-NHEJ), which could produce the large deletion and 20 bp mutated region observed. Alt-NHEJ is distinct in several ways to canonical NHEJ (c-NHEJ), including that during alt-NHEJ, a strand is resected prior to ligation. Furthermore, it may sometimes rely on identification of microhomologies (microhomology-mediated end joining, MMEJ) to facilitate repair that could be far away from the initial break site. As such, alt-NHEJ is often observed to produce more errors than c-NHEJ, and is more likely to cause deletions (Grabarz *et al.*, 2013; Guirouilh-Barbat *et al.*, 2004; Lee and Lee, 2007; Liang *et al.*, 1996; Rass *et al.*, 2009).

4.5.2 CRISPR-Cas9 and Off-targets

A primary concern with using CRISPR is that of off-target effects: other genes becoming mutagenized due to mis-matches still being recognised by the machinery. Currently in *Arabidopsis*, demonstration of off-target sites is relatively rare; the majority of the literature where off-targets have been sought out shows no off-targets were found, including papers utilising deep sequencing (Feng *et al.*, 2014; Hyun *et al.*, 2015; Li *et al.*, 2013; Peterson *et al.*, 2016; Tsai *et al.*, 2015; Z.-P. Wang *et al.*, 2015; Woo *et al.*, 2015). One notable paper, however, reports a high level of off-targets, and appears to be the only one to date reporting this in *Arabidopsis* (Zhang *et al.*, 2018). To try and minimise the likelihood of off-targets in this experiment, the SaCas9 system was used as its PAM sequence is twice the size of the PAM for the *Streptococcus pyogenes* system (SpCas9 PAM: 5'-NGG-3'; SaCas9 PAM: 5'-NNGRRT-3'), which should make it more specific. Furthermore, the oligos designed to target ASY4 were tested for specificity across free-access tools CCTop, Cas-OFFinder, and EnsemblPlants BLAST. Ultimately, however, *in silico* prediction cannot guarantee what will occur *in vivo*. Thus to be certain any phenotype that is observed in *asy4-4* can be attributed to a lack of ASY4, two further experiments were conducted. First, the fertility of the T4 progeny that are wild-type for ASY4 was determined, having come from a heterozygous *asy4-4* parent. Second, an allelic test was conducted by crossing *asy4-4* with the published T-DNA insertion mutant *asy4-1*. This data is presented in **Chapter 5**.

Chapter 5

Characterisation of a null-mutant of *asy4* generated by CRISPR-Cas9

5 Characterisation of a null-mutant of *asy4* generated by CRISPR-Cas9

5.1 Introduction

As discussed in **Chapter 3**, the two T-DNA insertion mutants for *asy4* appear to be hypomorphic; that is, both still appear to express at least the first 3 exons of the gene. To create a true, null mutant of *ASY4* for analysis, CRISPR-Cas9 gene editing was conducted as is outlined in **Chapter 4**. The result was a plant line with a 1.7 kb deletion in *ASY4* that was shown to be sufficient to prevent expression of any remaining part of the *ASY4* gene (see **4.4**).

In this chapter, we present this novel mutant allele of the *ASY4* gene, denoted hereafter as *asy4-4*. Using a variety of cytological techniques, including structured illumination microscopy (SIM), we confirm that *ASY4* is required for normal fertility, chromosome axis organisation, and recombination in *Arabidopsis thaliana*.

5.2 A 1.7 kb deletion in *ASY4* results in a reduction in fertility and recombination

5.2.1 *asy4-4* has reduced fertility but normal vegetative growth

To determine whether any fertility defect observed in the *asy4-4* lines could likely be attributed to a purely meiotic function, the vegetative growth of the plant line was monitored, observing the growth stages as outlined by TAIR. As is evident in Figure 5.1, the mutant plants appeared to have no obvious defect in vegetative growth at both early and late stages.

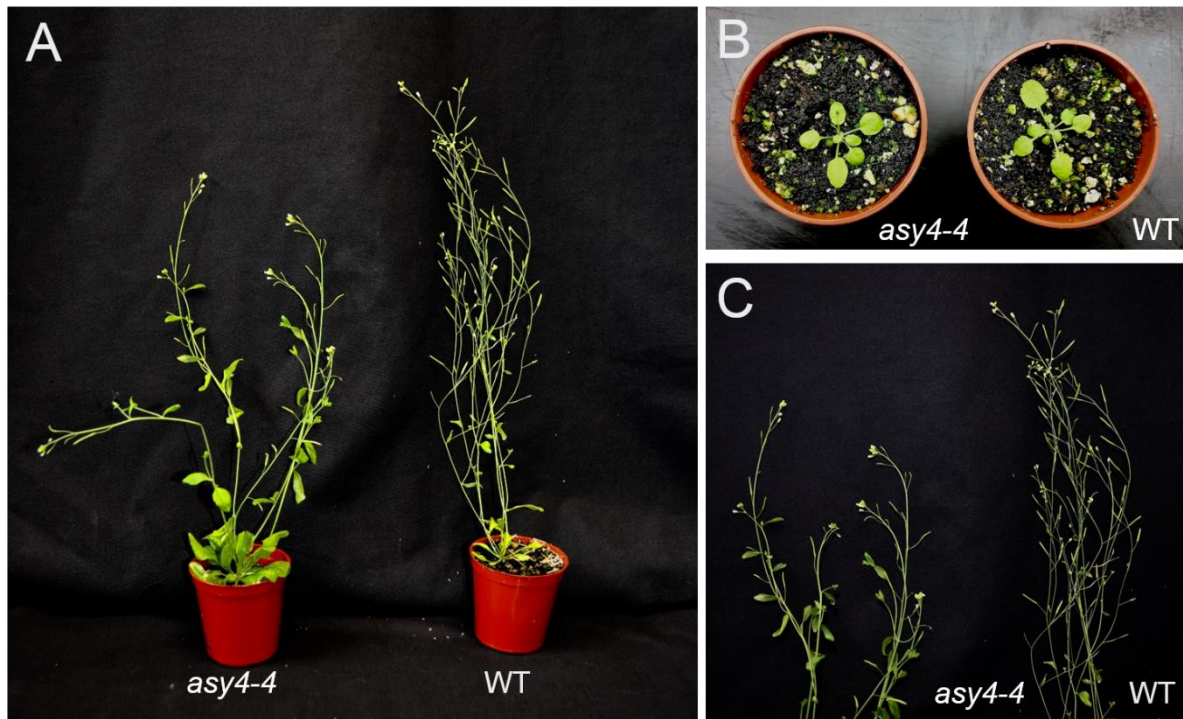


Figure 5.1 Comparison of vegetative growth between WT and *asy4-4*. Vegetative growth of *asy4-4* was observed to be similar to that of WT at both early (**B**) and late (**A**) stages. (**C**) Siliques lengths appeared to differ, with *asy4-4* appearing to have smaller siliques than were observed for WT.

There was, however, an observable difference in the length of the siliques produced by *asy4-4* (Fig. 5.1 C). Thus, seed counts were conducted on *asy4-4*, *asy4-1*, and WT to determine whether fertility was significantly affected by total loss of ASY4. As is presented in Figure 5.2 A, *asy4-4* homozygous plants have a significant reduction in fertility compared to WT, from a mean seed set of 50.3 per siliques in WT ($n=10$), to 22.43 in *asy4-4* ($n=310$; $P<0.0001$, 2-tailed Kruskal-Wallis test, 5% level). This amounts to a reduction in average seed set of ~55.4%. This was also associated with a significant reduction in the length of the siliques produced, from a mean length of 14.7 mm in WT ($n=10$) to 11.18 mm in *asy4-4* ($n=310$; $P<0.0001$; 2-tailed Kruskal-Wallis test, 5% level) (Fig. 5.2 B), and gaps between the seeds (Fig. 5.2 D). No significant difference was found in the number of seeds between *asy4-1* and

asy4-4 (*asy4-1*: $\bar{x} = 22.71$, n= 28; *asy4-4*: $\bar{x} = 22.43$, n=310; P=0.6626, 2-tailed Mann-Whitney test, 5% level) (Fig 5.2 C). Thus for *asy4-1*, we found a reduction in average seed set of 54.9% compared to WT.

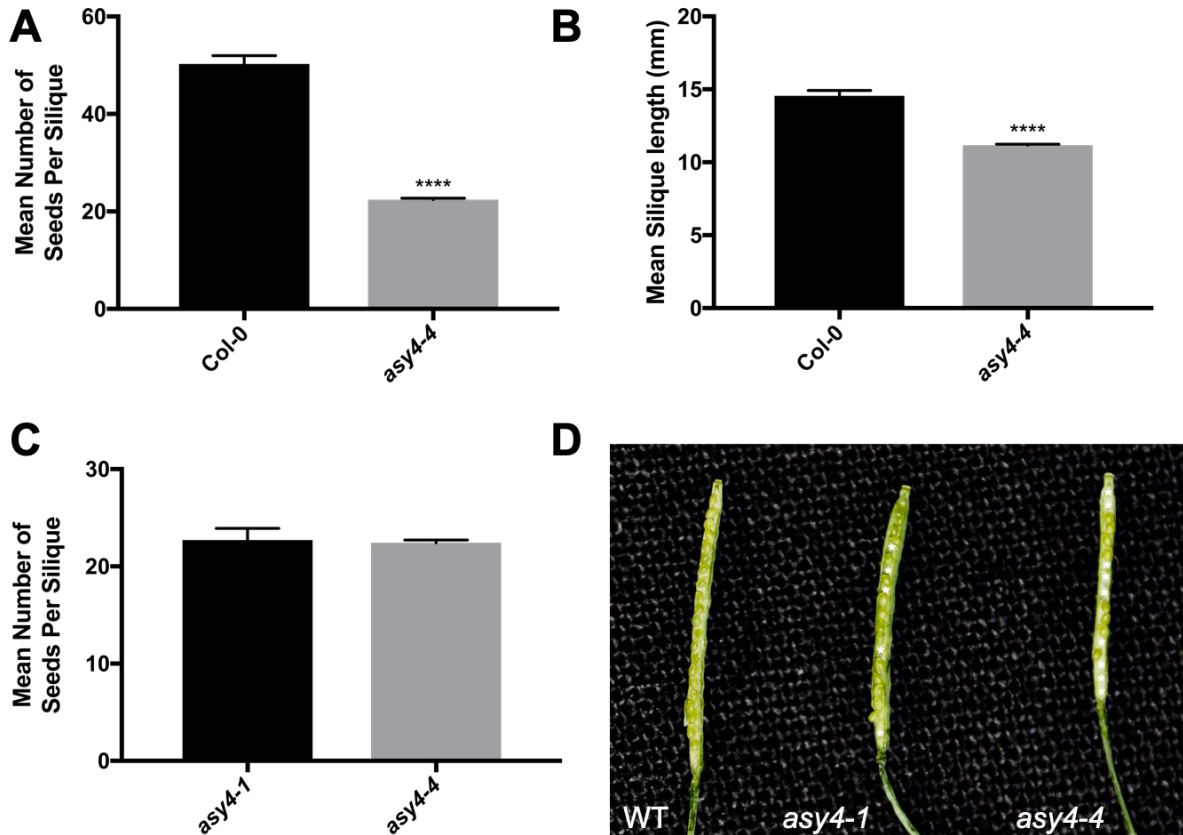


Figure 5.2 Seed count and siliques length data for WT (Col-0), *asy4-1*, and *asy4-4*. All graphs depict mean with SEM error bars. **(A)** Mean number of seeds per siliques is significantly reduced in *asy4-4*. **(B)** Mean siliques length (mm) is significantly reduced in *asy4-4*. **(C)** There is no significant difference in the mean number of seeds per siliques between *asy4-1* and *asy4-4*. **(D)** Mutations in ASY4 result in visible gaps in siliques, as denoted by asterisks. *** = P≤ 0.0001 in a 2-tailed Kruskal-Wallis test at the 5% level.

As previously discussed in **4.5**, off-target effects are a persistent concern in mutants generated via CRISPR-Cas9. To determine whether this decrease in fertility could likely be attributed to the deletion in *ASY4* rather than an off-target, seed counts were also conducted on plants heterozygous for the *asy4-4* allele, as well as plants that had a WT genotype that had segregated out from the heterozygotes. There was no significant difference in seed set between the Het ($\bar{x} = 43.23$, $n = 30$; $P > 0.9999$, 2-tailed Kruskal-Wallis test, 5% level) and WT ($\bar{x} = 45.7$, $n = 40$; $P > 0.9999$, 2-tailed Kruskal-Wallis test, 5% level) compared to the Col-0 WT control ($\bar{x} = 50.3$, $n=10$) (Fig. 5.3 A). Thus, we can conclude that any phenotype observed in *asy4-4* relating to fertility is not likely to be due to an off-target effect.

Furthermore, no significant difference was found when comparing the silique length of the WT genotype ($\bar{x} = 13.63$, $n = 40$; $P = 0.8688$, 2-tailed Kruskal-Wallis test, 5% level) and the Col-0 WT control ($\bar{x} = 14.7$, $n = 10$). A significant difference was discovered between the Het ($\bar{x} = 12.77$, $n = 30$; $P = 0.0456$; two-tailed Kruskal-Wallis test, 5% level) and Col-0 WT control, yet the P value obtained would not be significant at the 1% level, and thus is not a particularly robust conclusion (Fig. 5.3 B).

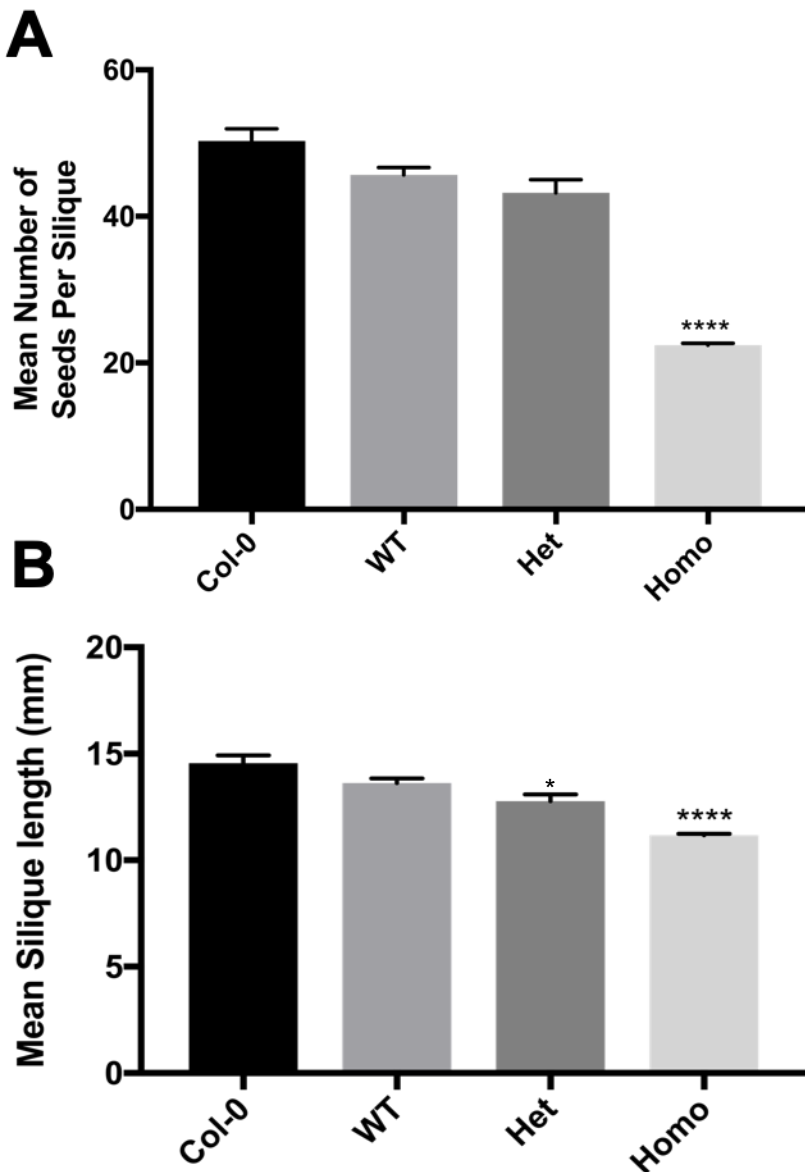


Figure 5.3 Seed count data from Col-0 control and three genotypes of *asy4-4*. All graphs are means plotted with SEM error bars. **(A)** Comparison of mean seed set per silique between the WT control (Col-0), the WT plants segregated from the heterozygous plants for *asy4-4* (WT), heterozygous (Het) plants for *asy4-4*, and the homozygous (Homo) plants. **(B)** Comparison of mean siliques length (mm) between Col-0, the WT plants segregated from the heterozygous plants for *asy4-4*, heterozygous (Het) plants for *asy4-4*, and the homozygous (Homo) plants. Asterisks indicate which plant lines were significantly different to Col-0 in a two-tailed Kruskal-Wallis test at the 5% level. **** = $P \leq 0.0001$; * = $P \leq 0.05$.

Previous research in axis-defective mutants such as *asy1* and *asy3* revealed that they often produce aneuploid tetrads at the end of meiosis (Armstrong *et al.*, 2002; Ferdous *et al.*, 2012). Thus, it would also be expected that a certain proportion of pollen produced from these lines would be inviable as they may have received the incorrect complement of chromosomes. The proportions of viable and inviable pollen in WT, *asy4-1*, and *asy4-4* was therefore determined via Alexander staining (Alexander, 1969).

A significant difference in the number of inviable pollen was recorded for both *asy4-1* (311 viable, 21 inviable; $P = 0.0194$, 2-tailed Fisher's exact test, 5% level) and *asy4-4* (285 viable, 35 inviable; $P < 0.0001$; 2-tailed Fisher's exact test, 5% level) compared to WT (208 viable, 4 inviable). There was also a significant difference between the number of inviable pollen between *asy4-1* and *asy4-4* ($P = 0.0370$; 2-tailed Fisher's exact test, 5% level). This corresponded to a rate of inviable pollen at 6.3% in *asy4-1* and 10.9% in *asy4-4*. Only 1.9% of pollen were inviable in Col-0. This therefore confirms that *asy4-4* has a significant reduction in fertility, and suggests that the phenotype could be related to a defect in male meiosis, as inviable pollen could be the result of mis-segregation at anaphase leading to aneuploidy.

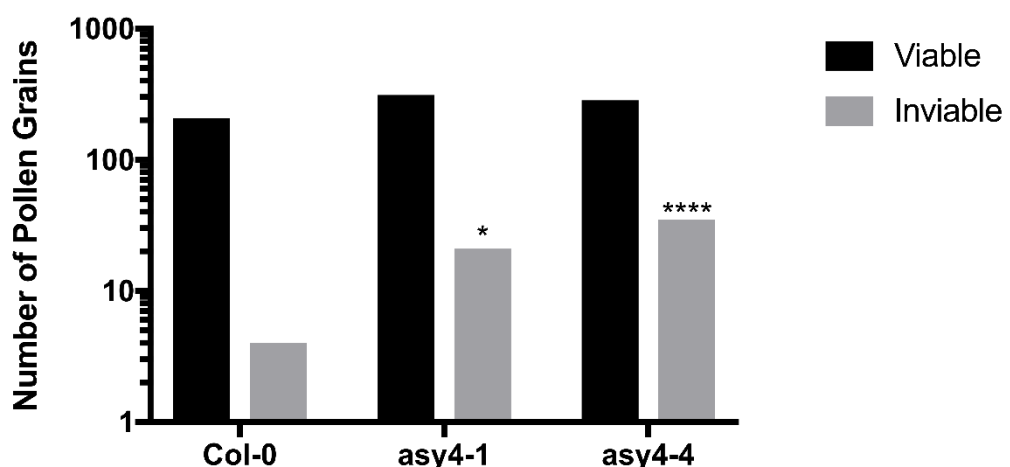


Figure 5.4 Alexander Staining of pollen from WT, *asy4-1* and *asy4-4*. Numbers of viable pollen presented in black, and numbers of inviable pollen counted presented in grey. Both *asy4-1* and *asy4-4* show a significant increase in inviable pollen compared to WT. Fisher's Exact test results: * = $P \leq 0.05$; **** = $P \leq 0.0001$. 2-tailed, 5% level.

5.2.2 An allelic test between *asy4-1* and *asy4-4* reveals the 4-1 and 4-4 insertion and edit affect the same gene

As discussed in **5.5.2**, a consistent concern with mutants generated via CRISPR-Cas9 is the possibility that the observed phenotypes could be due to an off-target effect, where the CRISPR-Cas9 construct causes an edit in a different site to what was intended. To mitigate concerns, further to the results obtained above showing normal fertility in homo and heterozygous plants segregated out from the *asy4-4* mutant line, an allelic test was conducted by crossing *asy4-1* to *asy4-4*. The expectation was that if the mutation is in the same gene, we would see no significant difference in the phenotypes between the *asy4-1/asy4-4* double mutant, and the single mutants of each.

As is observed in Figure 5.5, no significant difference was observed in the average number of seeds per siliques when comparing *asy4-1/asy4-4* to *asy4-1* homozygous (Hm) and *asy4-4* Hm (*asy4-1* ($\bar{x} = 22.71$, n = 28) vs *asy4-1/asy4-4* ($\bar{x} = 21.21$, n = 140), P > 0.9999; *asy4-4* ($\bar{x} = 21.57$, n = 210) vs *asy4-1/asy4-4* ($\bar{x} = 21.21$, n = 140), P > 0.9999; two-tailed Kruskal-Wallis with Dunn's Correction for multiple comparisons, 5% level).

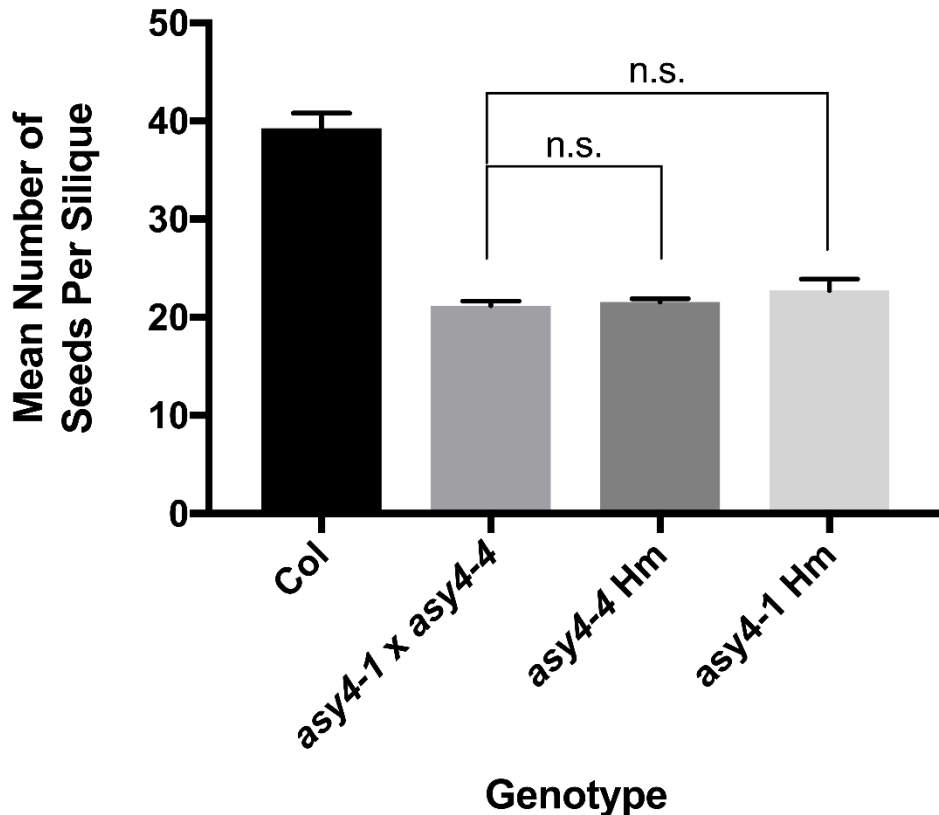


Figure 5.5 Seed count data from *asy4-1*, *asy4-4*, and *asy4-1/asy4-4*. Mean plotted with SEM. No significant difference was found in a two-tailed Kruskal-Wallis test at the 5% level comparing the means number of seeds per siliques between the *asy4-1/asy4-4* double mutant and the two single mutants for the *asy4-1* T-DNA insertion and the *asy4-4* deletion (n.s. = $P > 0.9999$).

5.2.3 *asy4-4* has a reduction in the number of chiasmata resulting in aneuploid tetrads

Given that *asy4-4* presented with a significant reduction in fertility, DAPI spreads of PMCs from both WT and *asy4-4* were analysed to confirm whether this could be attributed to defects in meiosis. In both WT and *asy4-4*, leptotene cells were visible, containing the thin-threads of chromatin characteristic of this stage (Fig. 5.6, A,I).

During mid-prophase I, however, defects become apparent in *asy4-4*. In WT, cells enter zygotene as the SC begins to form between homologues, holding them in close apposition. As such, the chromatin begins to appear thicker, progressing through until pachytene where the full-length of the homologues are synapsed. This is concurrent with an overall condensation of the chromatin (reviewed in: Mercier *et al.*, 2015). In *asy4-4*, the chromatin appears to commence condensation, and pairing of centromeres and some stretches of chromatin is visible, however no nuclei at the pachytene stage were observed in *asy4-4* (Fig. 5.6, B,J). As the cells reached diakinesis and metaphase I, in WT, 5 bivalents became visible (Fig. 5.6, K,L). In *asy4-4*, however, it is clear at metaphase I that some chromosomes have failed to form chiasmata, with univalents appearing in 46.3% of MI nuclei (25 out of 54 cells), thus confirming loss of crossover assurance in this mutant (Fig. 5.6, C,D). This was not significantly different to the proportions of cells with univalents in *asy4-1* ($P = 0.72$; 2-tailed Fisher's Exact test, 5% level). Connections and fragments as discussed in **3.2.1.2** were not observed in *asy4-4*. At anaphase I, bridging and laggards were also observed (Fig. 5.6, E). These defects resulted in mis-segregation (Fig. 5.6, F,G) and aneuploidy in the resultant tetrads (Fig. 5.6, H).

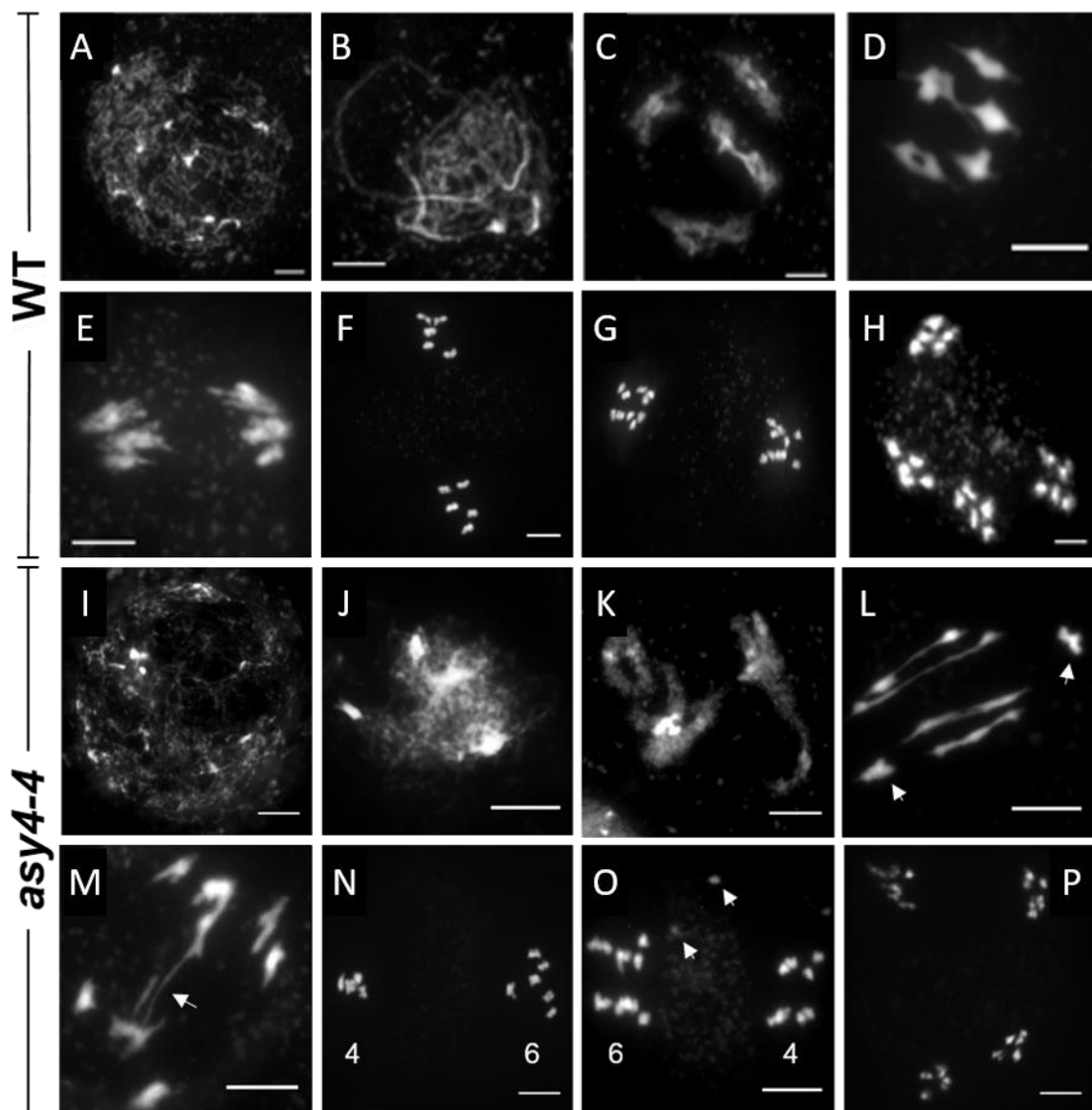


Figure 5.6 Comparison of the meiotic stages between *asy4-4* and WT. DAPI stained PMCs from *A. thaliana*. Spreads from WT (A-H) and *asy4-4* (I-P). (A, I) Leptonene. (B,J) *asy4-4* shows zygotene-like cell, WT shows pachytene; no pachytene cells were observed in *asy4-4*. (C,K) Diakinesis. (D,L) Metaphase I. Arrows indicate univalents. (E,M) Anaphase I. Arrows indicate bridges. (F,N) Metaphase I. Mis-segregation is observed in *asy4-4*. (G, O) Anaphase II. 6:4 segregation observed in *asy4-4*, and two possible fragments. (H,P) Tetrad. Scale bar = 5 μ m.

To determine the severity of the suggested reduction in COs in *asy4-4*, chiasma counts were conducted on metaphase I spreads using the minimum chiasma number (MCN) (Jahns *et al.*, 2014). This revealed a significant reduction in CO number, from 8.6 (n=28) in WT, to 6.3 in *asy4-4* (n=52; P<0.0001, 2-tailed Kruskal-Wallis test 5% level with Dunn's Correction) (Fig. 5.7). No significant difference was found between the number of chiasmata between *asy4-4* and *asy4-1* (*asy4-1*: $\bar{x} = 6.5$, n = 67; P = 0.9179, 2-tailed Kruskal-Wallis test 5% level with Dunn's Correction).

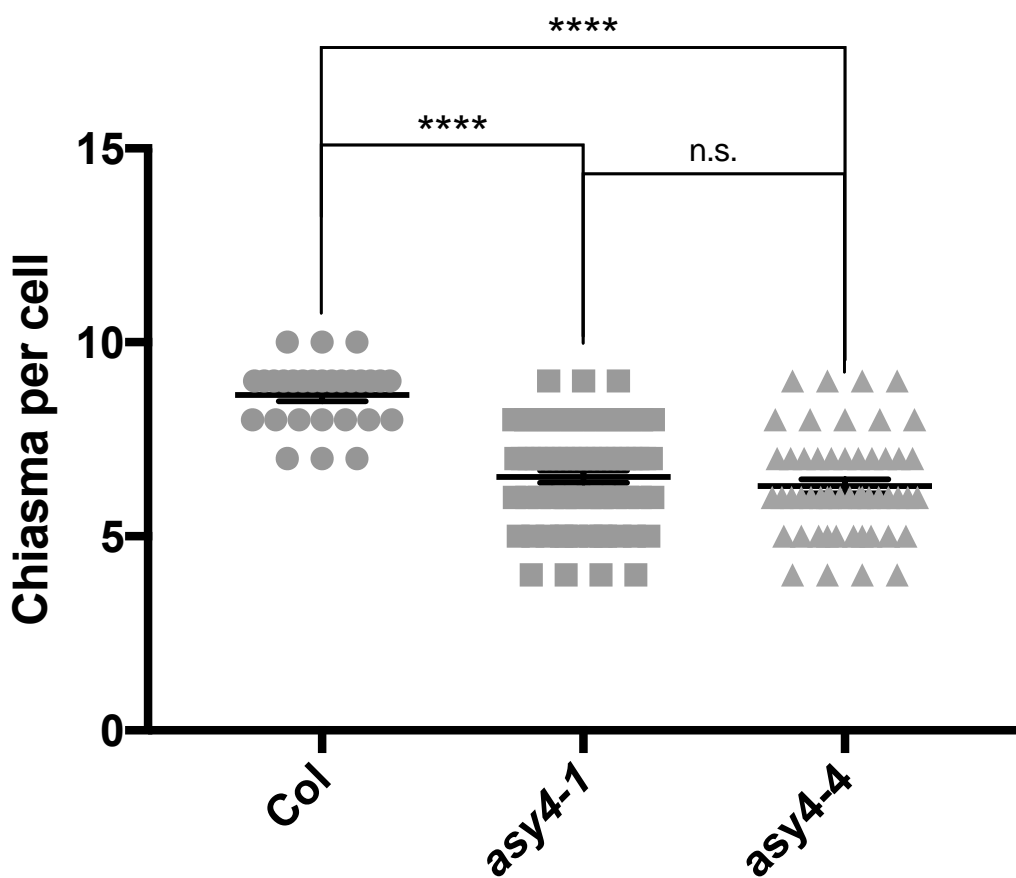


Figure 5.7 Chiasma counts in PMCs from WT, *asy4-1* and *asy4-4*. Comparison of chiasma number between Col-0 WT control and two mutant alleles of ASY4. Each data point represents the number of chiasmata in a single nucleus. Mean plotted with SEM error bars. *** = P≤ 0.0001. n.s. = P > 0.05.

5.3 Axis organisation is compromised in *asy4-4*

Previous experiments using the two T-DNA insertion mutants for *asy4* suggested that ASY4 is required for the normal organisation and remodelling of the chromosome axis, and subsequently, polymerisation of the SC (Chambon *et al.*, 2018; this thesis).

To determine whether these phenotypes are also present in *asy4-4*, immunolocalisation was conducted on prophase I PMCs, and subsequently imaged via structured-illumination microscopy to gain a more detailed insight into the axis structure in this mutant.

5.3.1 Sister cohesion appears unaffected in *asy4-4*

The cohesins, comprised in meiosis in *A. thaliana* of SMC1, SMC3, SCC3 and the kleisin SYN1, are loaded onto sister chromatids after DNA synthesis in the pre-meiotic S-phase (Bai *et al.*, 1999; Cai *et al.*, 2003; Chelysheva *et al.*, 2005; Lam *et al.*, 2005). SYN1 has been shown to be required for ASY3 to successfully localise on the axis (Ferdous *et al.*, 2012). Antibodies against both SMC3 and SYN1 were used to determine whether any defect in axis organisation in *asy4-4* correlated with issues in sister cohesion. As is presented in Fig. 5.8, there was no observable difference in the appearance of the cohesins; both SMC3 and SYN1 signals progress as in WT, from a foci-like stage during early prophase I (Fig. 5.8, A,B), through to a more linear signal by the time the cells reach mid-prophase I (Fig. 5.8, C,D).

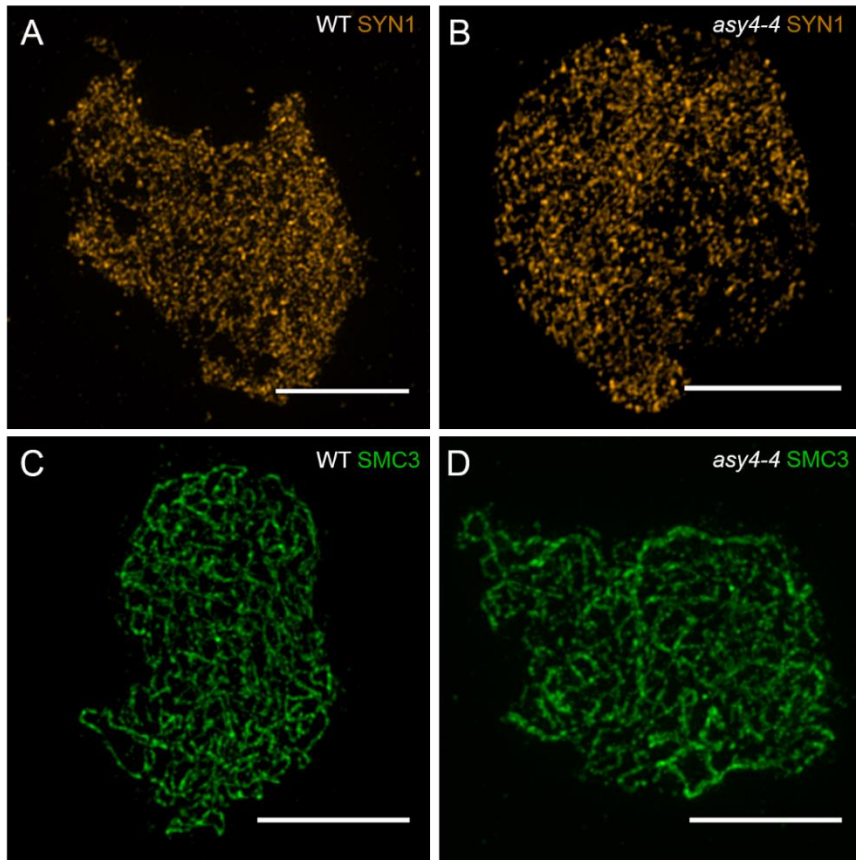


Figure 5.8 Immunolocalisation of SMC3 and SYN1 during prophase I in WT and *asy4-4*. Cells imaged via structured illumination microscopy. SYN1 imaged in 594. SMC3 imaged in 488. **(A)** and **(B)** early prophase I. **(C)** and **(D)** mid-prophase I. **(A,C)** WT. **(B,D)** *asy4-4*. Bar, 5 µm.

5.3.2 ASY4 is required for normal ASY1 and ASY3 localisation

As no obvious defect was observed in sister cohesion, antibodies raised against ASY1 and ASY3 were used to determine if, as was suggested in *asy4-1*, that ASY4 is required for proper loading and organisation of ASY1 and ASY3. In WT, during early-mid prophase I, the ASY1 and ASY3 signals appear linear along the chromosome axis (Fig. 5.9 A, C). In *asy4-4*, whilst ASY1 and ASY3 do indeed appear to load, the signals do not appear to linearise as evenly as in WT, instead appearing patchy and diffuse. Some linear stretches of the ASY1 and ASY3 signals are visible when a single slice

through the Z-stack is examined (Fig. 5.9, B1,D1), however, maximum intensity projections of the cells suggest an overall disorganised structure, where this linear signal is not evenly observed throughout the nucleus (Fig. 5.9, B, D).

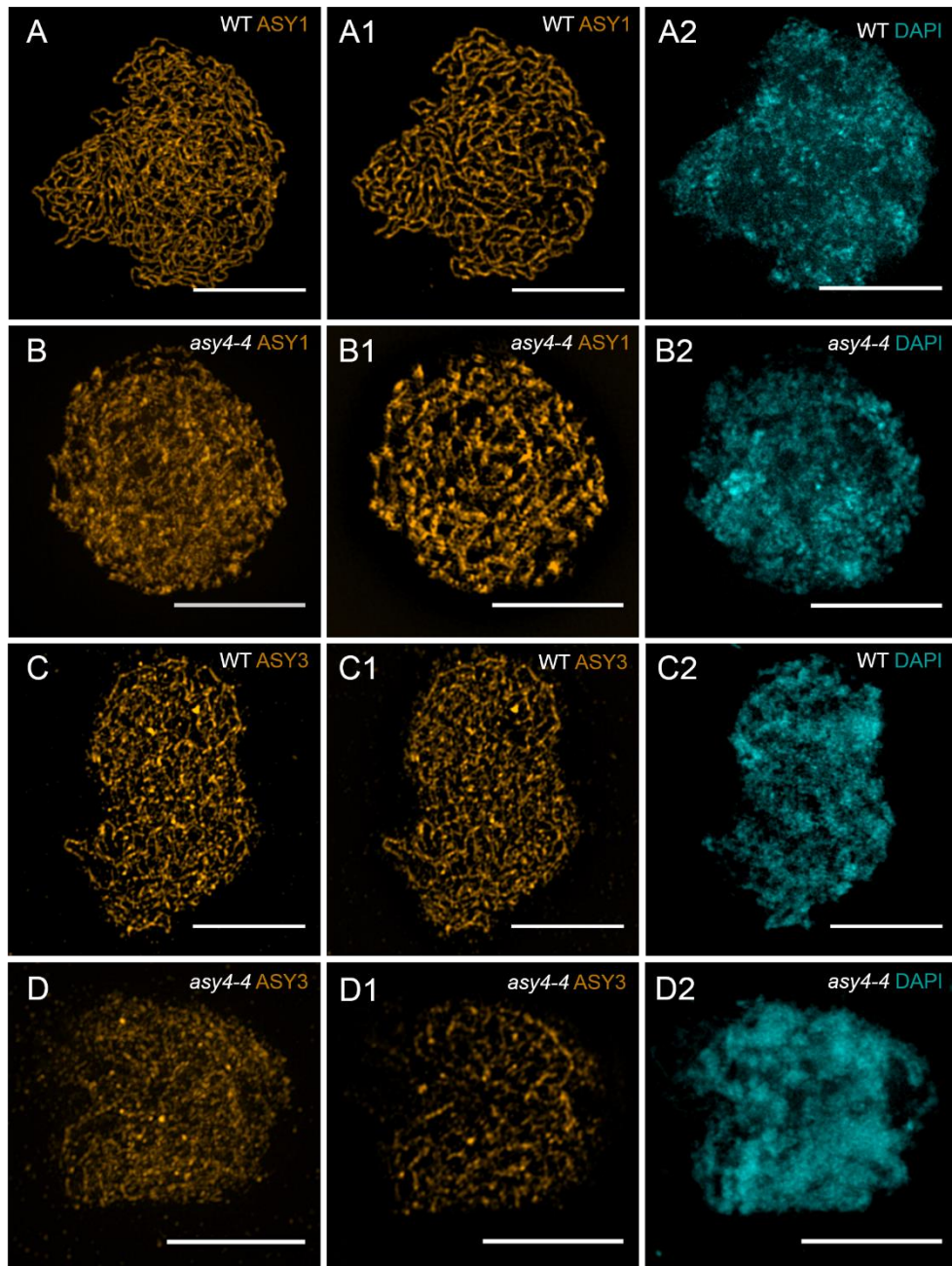


Figure 5.9 Immunolocalisation of ASY1 and ASY3 during prophase I in WT and *asy4-4*. Structured illumination microscopy images of PMCs. ASY1 (rows A,B) and ASY3 (rows C,D) imaged in 594. Chromatin stained with DAPI imaged in 350. Rows A,C = WT. Rows B,D = *asy4-4*. (A,B,C,D) Maximum intensity projection image. (A1,B1,C1,D1) Single slice from a Z-stack. (A2,B2,C2,D2) DAPI to determine approximate stage of cell. All cells in early-mid prophase I. Bar, 5 μ m.

As the cells enter mid-prophase I, there is evidence of chromosome alignment, visible with antibodies against the cohesin SMC3 (Fig. 5.10). In WT, where SMC3 displays a dual signal of the two homologues in alignment, ASY3 also follows this pattern, thus appearing to co-localise with SMC3 (Fig. 5.10, A-F). This is most apparent in cells late in prophase I (Fig. 5.10, A-C), but also in those just entering zygotene (Fig. 5.10, D-F). In *asy4-4*, however, this relationship was not observed, with the ASY3 signal continuing to appear as either short, thin stretches, or as a dotty, patchy signal (Fig. 5.10, G-I). This further suggests that the chromosome axis structure is compromised in *asy4-4*, supporting previous conclusions that ASY4 is necessary for normal axis organisation, but also revealing that its loss does not necessarily affect chromosome alignment.

Interestingly, we also noted the potential presence of inter-axis bridges. These structures form between two aligned chromosome axes, and are thought to be comprised of axis proteins, DNA, as well as other proteins involved in recombination and SC initiation (Dubois *et al.*, 2019). They were first observed in *Allium cepa*, and later in *Homo sapiens*, *Mus musculus*, *Brassica oleracea*, and most recently, in *Sordaria macrospora* (Dubois *et al.*, 2019; Albini and Jones, 1987; Moens *et al.*, 2007; Oliver-Bonet *et al.*, 2007; Holloway *et al.*, 2010; Osman and Franklin, unpublished). In the zoomed panels for SMC3 from both WT (Fig. 5.10, B1 and E1) and *asy4-4* (Fig. 5.10, E1), clear bridges are apparent, suggesting loss of ASY4 does not obviously affect the formation of these structures. To our knowledge, this is the first time inter-axis bridges have been reported in *A. thaliana*.

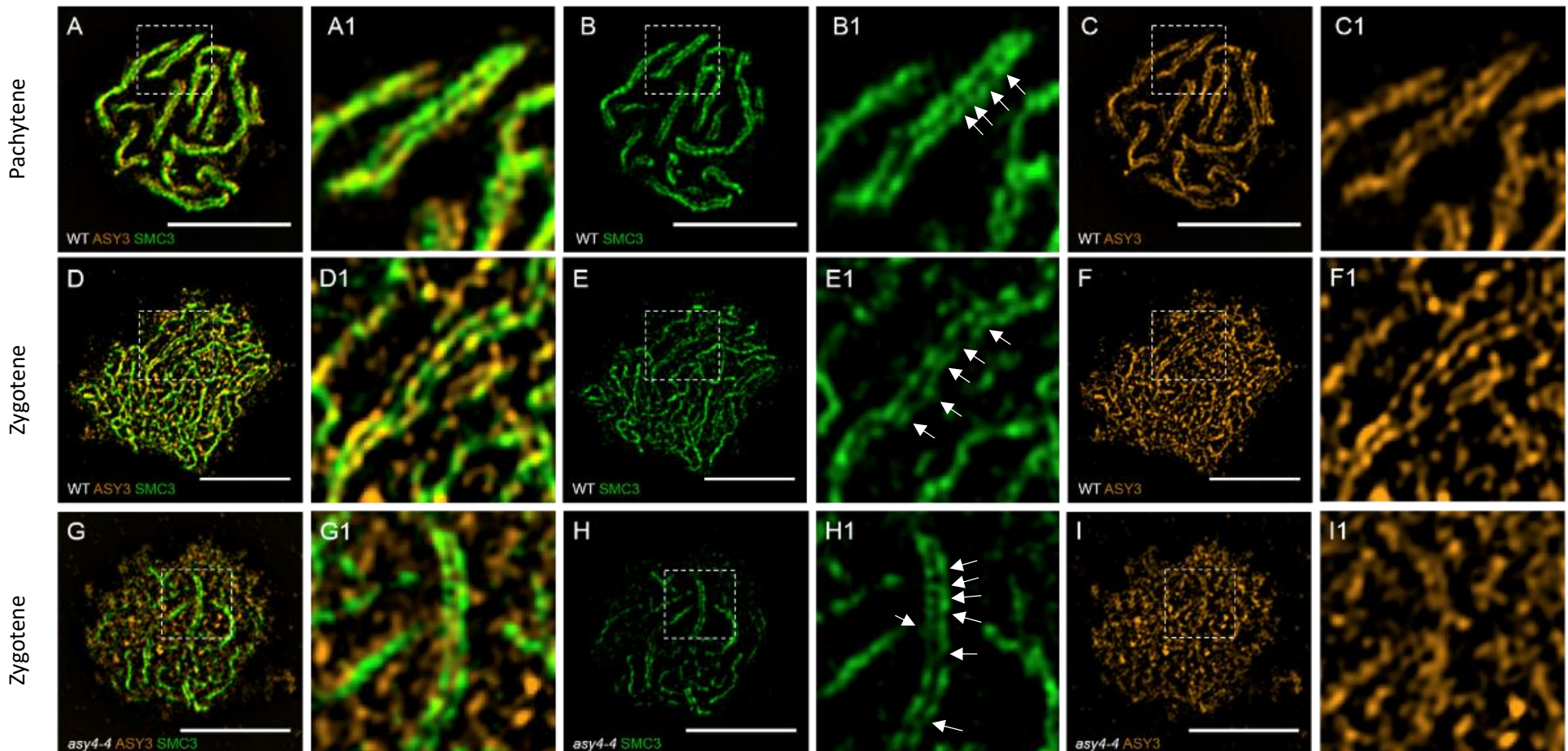


Figure 5.10 Immunolocalisation of the chromosome axis during prophase I in PMCs from WT and *asy4-4*. Structured illumination microscopy images. All images represent a single slice from a Z-stack. ASY3 imaged in 594. SMC3 imaged in 488. **(A-F)** WT. **(G,H,I)** *asy4-4*. **(A,B,C)** late prophase I. **(D-I)** mid-prophase I. Numbered panels = zoomed sections. Arrows indicate potential inter-axis bridges. Bar, 5 μ m.

5.3.3 Extension of the synaptonemal complex is reduced in *asy4-4*

As in other meiotic chromosome axis mutants studied, *asy4-1* had a reduced level of synapsis compared to WT, resulting in a lack of a recognisable pachytene stage (Armstrong *et al.*, 2002; Ferdous *et al.*, 2012; Chambon *et al.*, 2018; this thesis). To confirm whether this was also the case in *asy4-4*, immunolocalisation of the axis and SC was conducted using the ASY1 and ZYP1 antibodies. This revealed that, as suggested by the DAPI spreads presented in Figure 5.6, *asy4-4* is also partially asynaptic, with the ZYP1 signal never appearing to extend along the full length of the homologues (Fig. 5.11, rows C,D) One cell also displayed what appeared to be an unusually thick SC signal, but as this was only observed in 1 out of 12 cells captured by SIM, it was not possible to determine if this was a statistically significant (or indeed, prevalent) phenotype (Fig. 5.11, row D). To quantify any significance in the difference in length of SC extension between WT and *asy4-4*, the total SC lengths of cells at late prophase I were measured (as in: 2.8.5) (Fig. 5.12). For WT, the mean total SC length at late prophase I was 190.4 µm, with values ranging between 79.4 µm and 340.2 µm (n=8). In *asy4-4*, mean total SC length in late prophase-like cells was 74.4 µm, with a range between 16.48 µm and 156.8 µm (n=9). This was found to be significantly different in a 2-tailed Mann-Whitney test at the 5% level ($P = 0.0037$) (Fig. 5.12, E).

Data available in Appendix Table A11.

5.3.4 ASY1 appears to be depleted from synapsed regions in *asy4-4*

A notable phenotype of the *asy4-1* mutant observed by the Grelon group was that, as in *pch2*, the ASY1 signal does not appear to be depleted from the axis as the SC signal extends through the cell (Lambing *et al.*, 2015; Chambon *et al.*, 2018). Immunolocalisation conducted on PMCs from *asy4-4* revealed that, conversely to what has been reported in *asy4-1*, ASY1 does indeed appear to be depleted from the axis

in *asy4-4* (Fig. 5.11, A and C). This is, therefore, a key difference between the mutants, and may also contribute to the evidence suggesting that the *asy4-1* mutant, and likely *asy4-2*, are possibly still producing a truncated protein. It also suggests that, conversely to *pch2* and *asy4-1*, the reduction in polymerisation of the SC observed in *asy4-4* may not be due to the axis being unable to be remodelled.

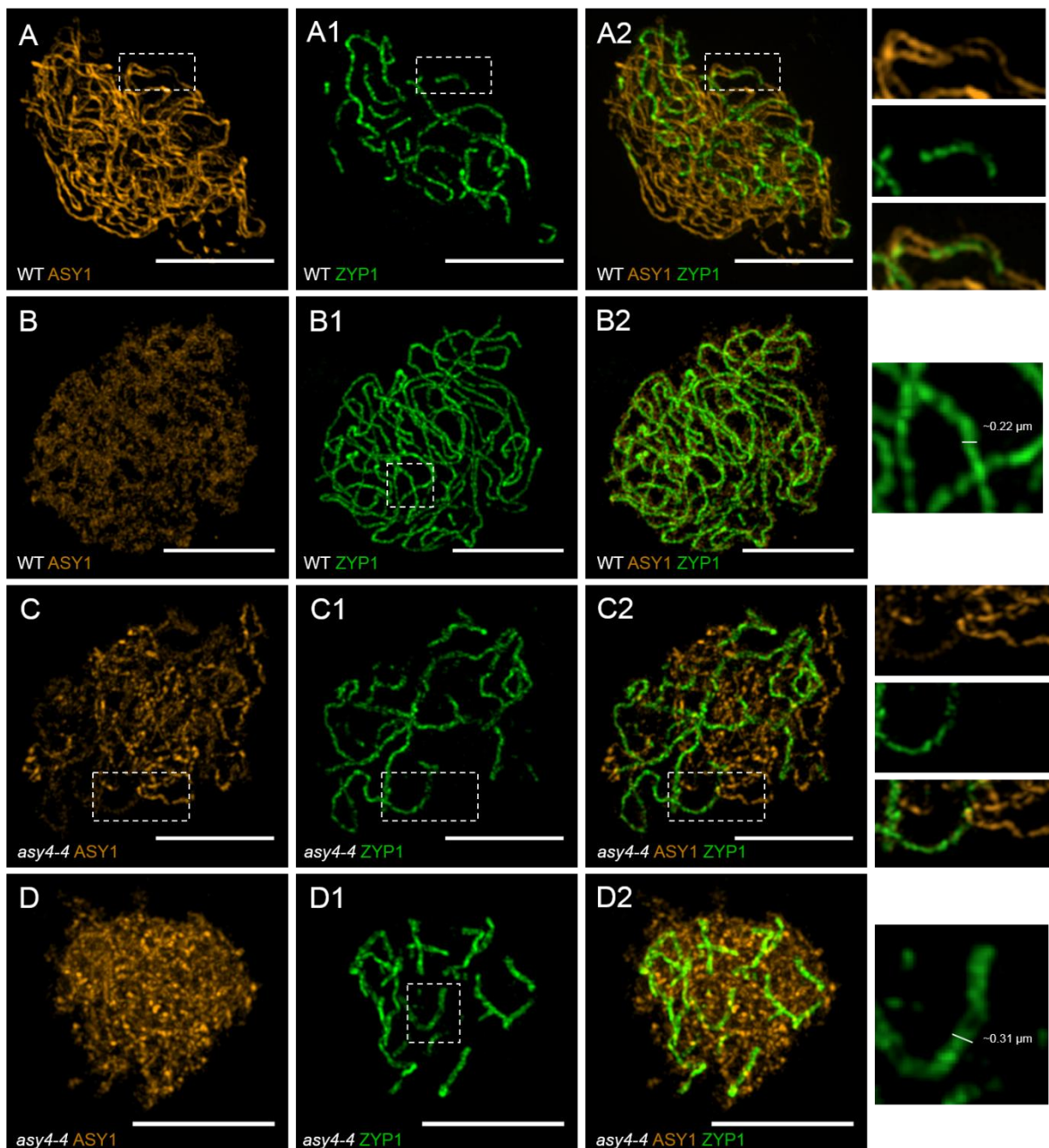


Figure 5.11 Immunolocalisation of the chromosome axis and synaptonemal complex in PMCs from WT and *asy4-4*. Structured illumination microscopy. All images are maximum intensity projections. ASY1 captured in 594. ZYP1 in 488. **(A-B)** WT. **(C-D)** *asy4-4*. **(A,C,D)** mid-prophase I. **(B)** Pachytene. Zoomed panels for rows **A** and **C** show depletion of ASY1 from synapsed regions. Zoomed panels for rows **B** and **D** show width of sections of the SC. Bar = 5 μm.

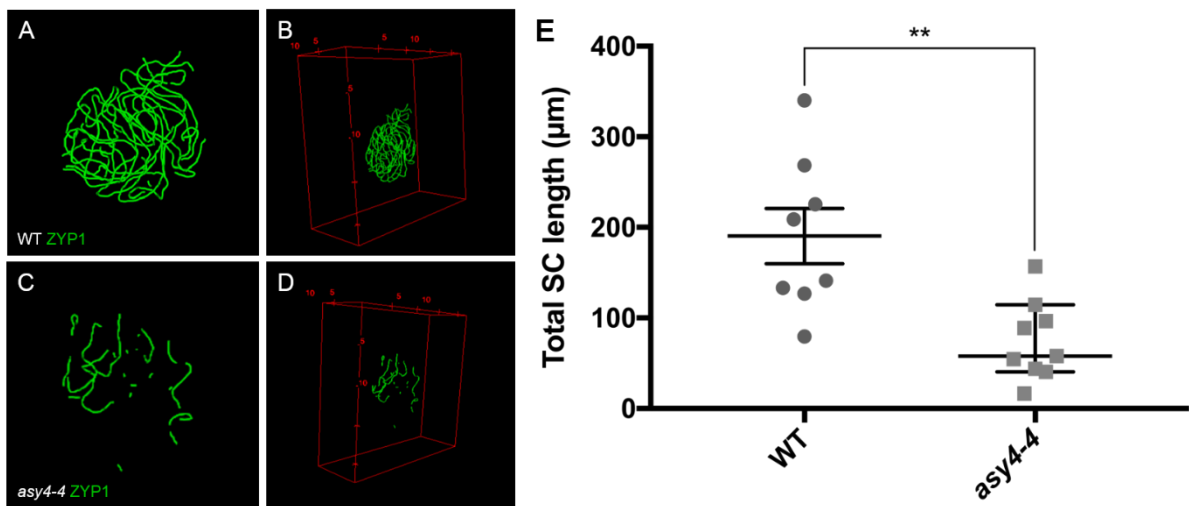


Figure 5.12 Total SC length measurements in WT and *asy4-4*. (A-D) 3D-rendering of ZYP1 signal in prophase I PMCs. (A,B) WT. (C,D) *asy4-4*. (A,C) Front view. (B,D) Side view showing cell depth. (E) Comparison of total SC lengths between WT and *asy4-4*. Each point denotes the total SC length in μm for an individual cell. Means plotted with SEM error bars. ** = $P \leq 0.01$.

5.3.5 PCH2 appears to localise normally in *asy4-4*

Given that ASY1 appears to be successfully depleted from the axis in *asy4-4*, we were curious to see if the axis remodeller PCH2 was therefore localising normally in this mutant. In WT, the PCH2 signal is seen as diffuse and ‘dotty’ through early prophase I, before finally localising as a more linear signal along sites where the SC has extended (Lambing *et al.*, 2015) (Fig. 5.13, row A). In *asy4-4*, PCH2 also seems to co-localise with where the SC has successfully extended (Fig. 5.13, row B). This therefore suggests that PCH2 function, at least in the respect of axis remodelling, and PCH2 localisation, is unaffected by loss of ASY4.

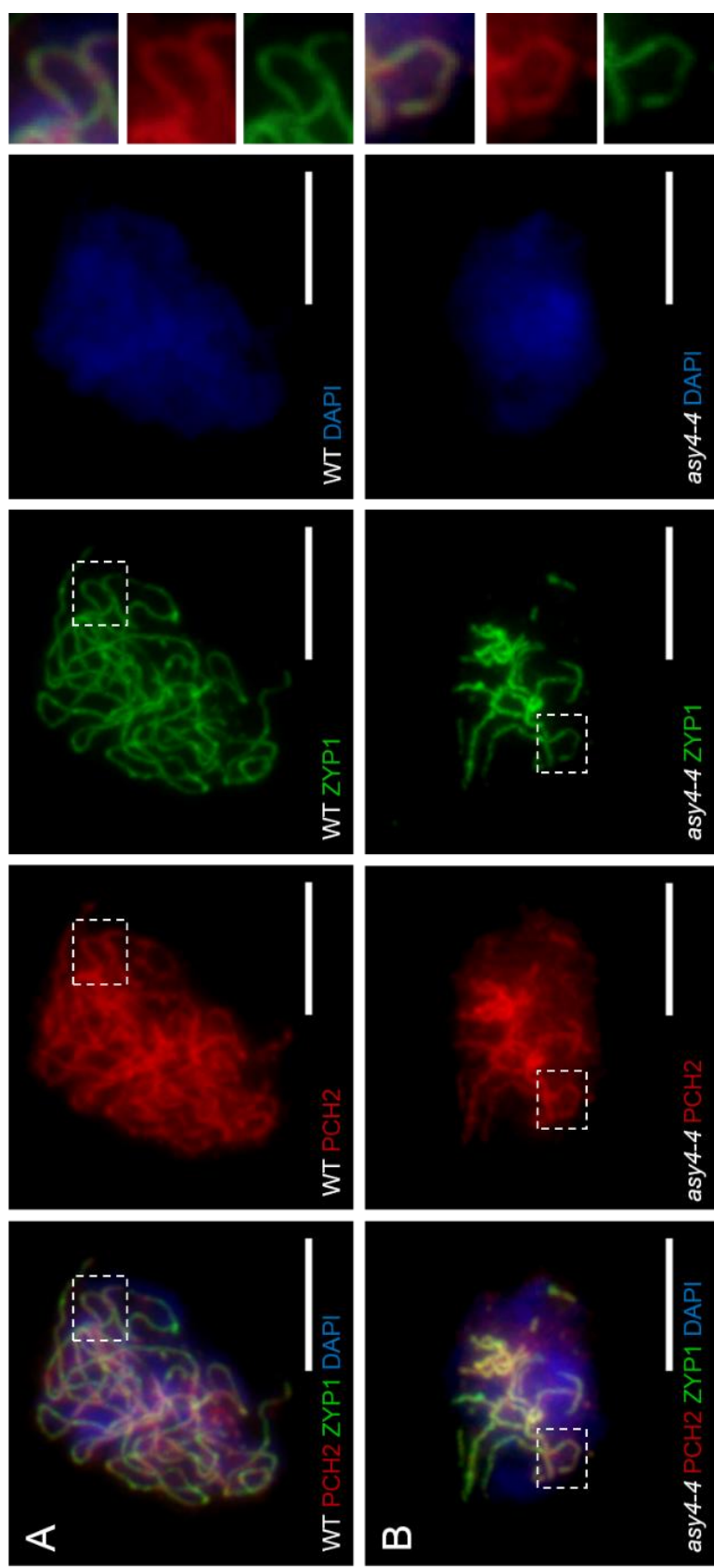


Figure 5.13 Immunolocalisation of PCH2 and ZYP1 in phase I PMCs from WT and *asy4-4*. (A) WT. (B) *asy4-4*. PCH2 in Texas Red. ZYP1 in FITC. Chromatin stained with DAPI. Zoomed panels show co-localisation of PCH2 and ZYP1. Bar = 5 μ m.

5.4 Reduction in chiasmata in *asy4-4* may be due to problems with CO maturation

5.4.1 Early recombination events appear to progress normally in *asy4-4*

Converse to what has been discovered in experiments examining mutants of the yeast HORMAD Hop1, ASY1 in *A. thaliana* does not appear to be required for production of WT levels of DSBs (Sanchez-Moran *et al.*, 2007; Armstrong *et al.*, 2002; Woltering *et al.*, 2000; Mao-Draayer *et al.*, 1996). Instead, in *A. thaliana*, it appears that ASY3 is required for WT-levels of DSB formation (Ferdous *et al.*, 2012). Research conducted by the Grelon group on the *asy4-1* mutant suggested that ASY4 is, like ASY1, also non-essential for DSB production, with WT-levels of DMC1 foci observable during early prophase I (Chambon *et al.*, 2018). Given that the resultant ssDNA either side of a DSB is loaded with the RPA homologues DMC1 and RAD51, DMC1 is considered a proxy for the number of DSBs produced (Ferdous *et al.*, 2012b; Pradillo *et al.*, 2012; Sanchez-Moran *et al.*, 2007). As such, the number of DMC1 foci was counted in early prophase I in WT and *asy4-4* (Fig. 5.14, A-D). In WT, the mean number of DMC1 foci was 185.3 ($n = 23$), and in *asy4-4*, the mean was 187.5 ($n = 27$). As in *asy4-1*, no significant difference was detected in the number of DMC1 foci at early prophase I ($P = 0.8356$; 2-tailed Mann-Whitney test, 5% level), corroborating the result that ASY4 is dispensable for DSB production in *A. thaliana* (Fig. 5.14 E). Data available in Appendix Table A12.

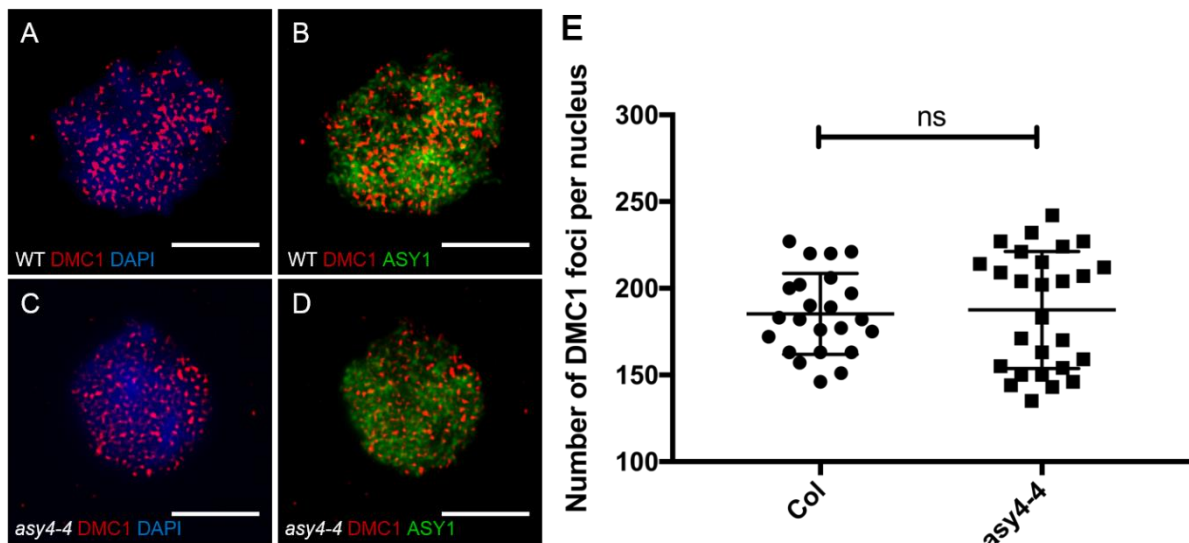


Figure 5.14 Immunolocalisation of DMC1 and comparison of the number of foci.
Early prophase I PMCs. (A,B) WT. (C,D) *asy4-4*. DMC1 in Texas Red. ASY1 in FITC. Chromatin stained with DAPI. Texas Red channel processed using Mexican Hat to improve clarity of foci. Bar = 5 μ m. (E) Each data point = total DMC1 foci in one cell. Means plotted with SEM. n.s. = $P > 0.05$.

Following the loading of DMC1/RAD51 onto resected DNA at the break site, the resultant nucleoprotein filament can commence the search for its homologue (Pradillo *et al.*, 2012). As previously discussed, some of these early recombination intermediates will progress to form a double Holliday junction (dHj), which, in *A. thaliana*, is stabilised by MutS homologs MSH4 and MSH5 (Higgins *et al.*, 2008b, 2004). Immunolocalisation using the MSH4 antibody revealed an average of 155 ($n=15$) in WT, and 151.7 ($n = 18$) in *asy4-4* (Fig. 5.15). There was no significant difference in the number of foci between WT and *asy4-4* ($P = 0.5142$; 2-tailed Mann-Whitney test, 5% level), suggesting that recombination proceeds normally at least as far as stable proto-dHjs (Fig. 5.15, E). Data available in Appendix Table A13.

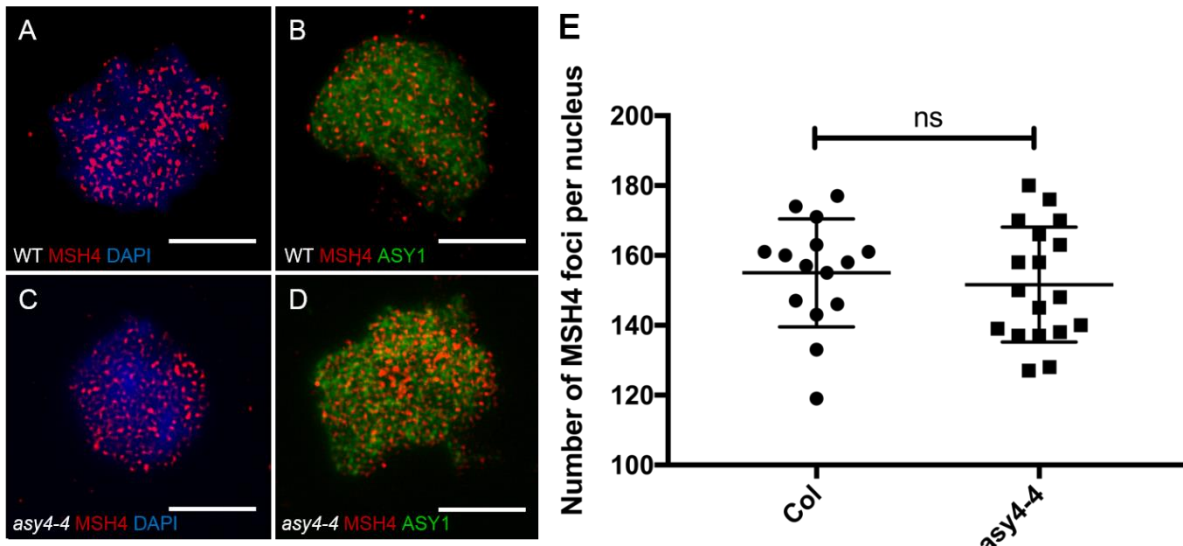


Figure 5.15 Immunolocalisation of MSH4 and comparison of the number of foci.
Early prophase I PMCs. (A,B) WT. (C,D) asy4-4. MSH4 in Texas Red. ASY1 in FITC. Chromatin stained with DAPI. Texas Red channel processed using Mexican Hat to improve clarity of foci. Bar = 5 μ m. (E) Each data point = total MSH4 foci in one cell. Means plotted with SEM. n.s. = P > 0.05.

5.4.2 The number of HEI10 foci is significantly reduced in asy4-4

As early recombination events appeared to be unaffected in asy4-4, we next sought to determine if the reduction in crossover number could be attributed to issues arising later in the process. The E3 ligase HEI10 is a component of the ZMMs in *A. thaliana*, and is homologous to Zip3 in yeast (Chelysheva *et al.*, 2012). It is known cytologically to denote many recombination intermediates during early-mid prophase, and eventually, reduces in number, at which point it is thought to mark only the Class I COs. These larger foci appear to co-localise with both the SC, and MLH1: a homolog of *Escherichia coli* MutL that is also proposed to label Class I CO sites (Chelysheva *et al.*, 2012; Dion *et al.*, 2007; Lhuissier *et al.*, 2007).

At mid-late prophase I in WT, an average of 11.11 ($n = 19$) HEI10 foci were observed. In asy4-4, there was an average of 8.27 ($n = 22$) HEI10 foci per nucleus (Fig. 5.16, A-D). Therefore, there is a significant difference in the number of HEI10 foci at mid-late

prophase I between WT and *asy4-4* ($P = 0.0002$, 2-tailed Mann-Whitney test, 5% level). Combined with the data from DMC1 and MSH4, this suggests that, as in *asy4-1*, there is a potential issue later in recombination in *asy4-4*, confirming that ASY4 is necessary for normal maturation of COs in *A. thaliana*. Data available in Appendix Table A14.

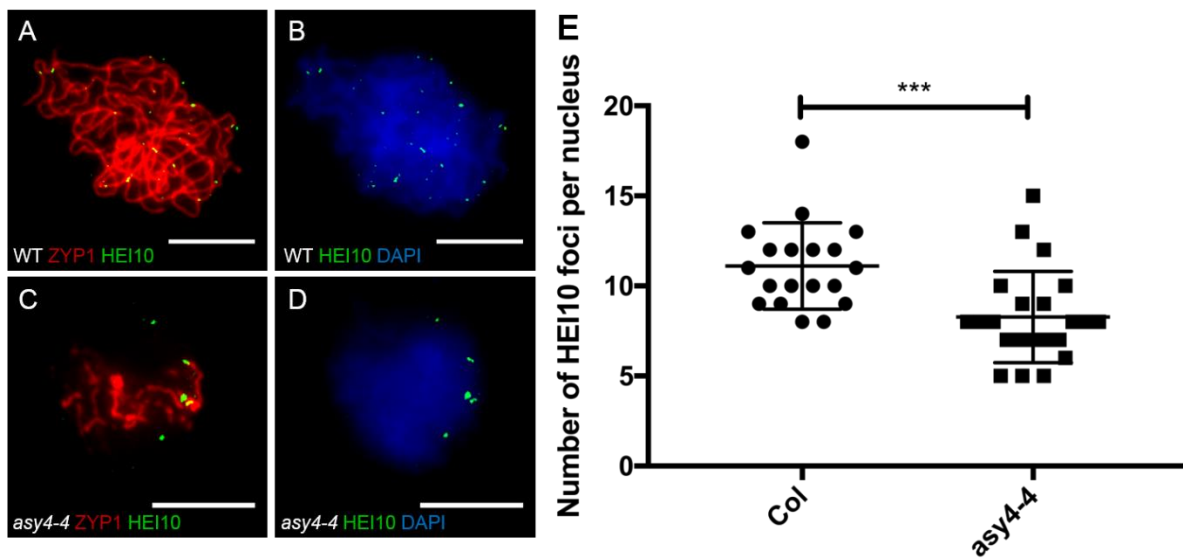


Figure 5.16 Immunolocalisation of HEI10 and comparison of the number of foci. Early prophase I PMCs. **(A,B)** WT. **(C,D)** *asy4-4*. ZYP1 in Texas Red. HEI10 in FITC. Chromatin stained with DAPI. Minimum-IP subtracted from the Maximum-IP in FITC channel to improve clarity of foci. Bar = 5 μ m. **(E)** Each data point = total HEI10 foci in one cell. Means plotted with SEM. *** = $P \leq 0.001$.

5.5 An antibody raised against ASY4 gives no proper axis-associated signal in an *asy4*-null mutant

As was discussed in 3.2.2.2, the antibody raised against ASY4 could not be verified in the *asy4-1* and *asy4-2* mutants as they still gave a strong, axis-associated signal (Kim Osman, University of Birmingham, personal communication; Appendix Figure A4). Thus to attempt to verify this antibody, immunolocalisation with anti-ASY4 and anti-SYN1 was conducted on PMCs from both WT and *asy4-4*. In WT, an axis associated

signal, as previously described in **3.2.2.1**, is observed during mid-prophase I (Fig. 5.17, A-B). As was observed in the epi-fluorescence images presented in Figure 3.10, the ASY4 antibody appears as stretches of foci along the axis, rather than the bright, linear signal we usually observe for ASY1. In *asy4-4*, whilst foci are visible, they do not appear to form any regular axis-associated signal (Fig. 5.17, C-D). We would therefore suggest that these foci are most likely background. Thus, we may conclude that the strong, axis-associated signal detected in *asy4-1* and *asy4-2* by Kim Osman (University of Birmingham) was likely due to the presence of the truncated protein. Furthermore, we conclude that the ASY4 antibody raised is indeed recognising ASY4, as it does not give a discernible axis-associated signal in the null-mutant presented in this chapter.

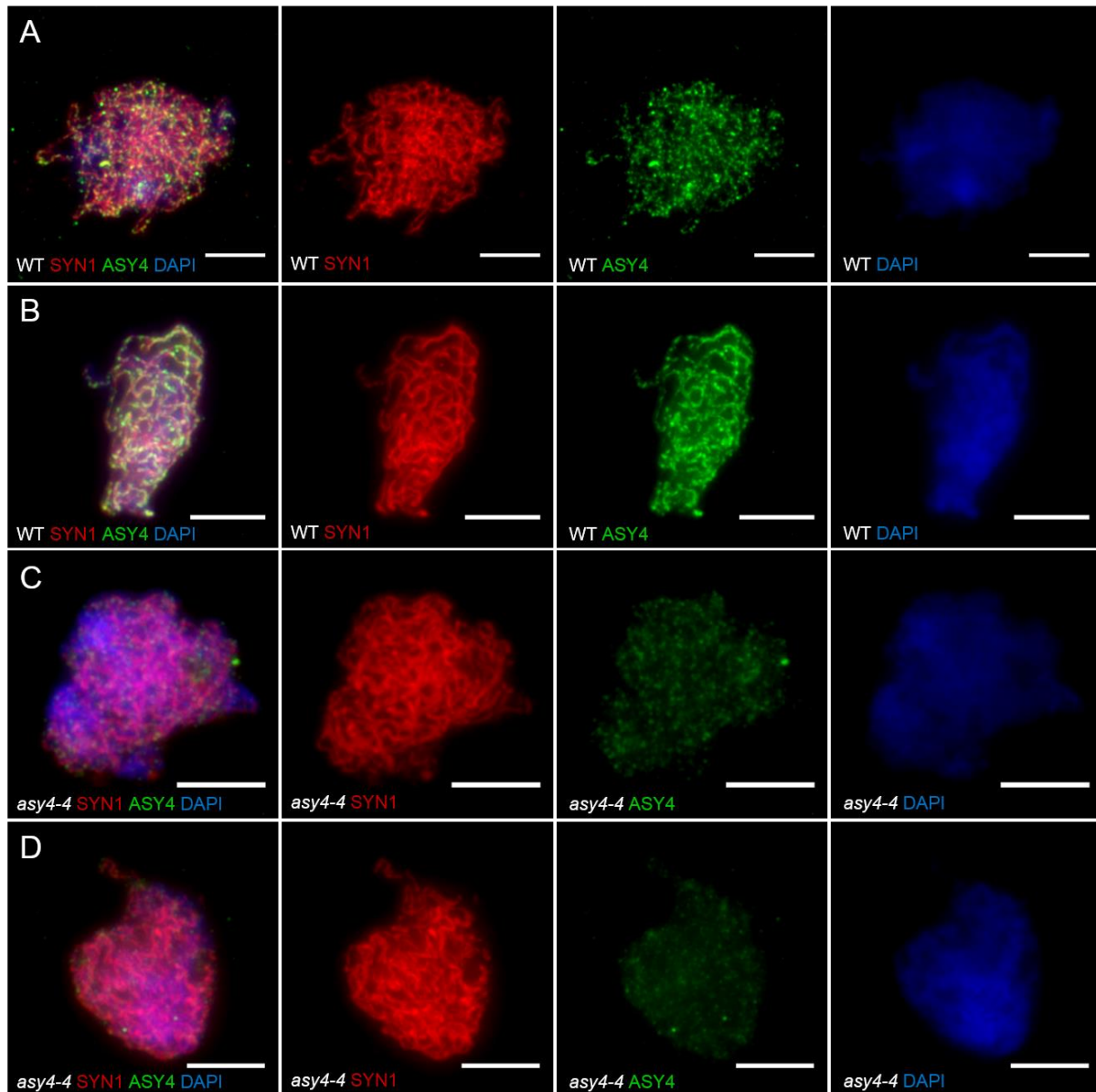


Figure 5.17 Immunolocalisation of the chromosome axis with SYN1 and ASY4 in WT and *asy4-4*. Early-mid prophase I PMCs. (A,B) WT. (C,D) *asy4-4*. SYN1 in Texas Red. ASY4 in FITC. FITC channels captured at the same exposure between cells. Chromatin stained with DAPI. Bar = 5 μ m.

5.6 Discussion

In this chapter, we describe *asy4-4*: a novel, null mutant of ASY4 in *A. thaliana*, generated via CRISPR-Cas9 gene editing. We show that the 1.7 kb deletion as described in **Chapter 4** is sufficient to prevent ASY4 expression, and that total absence of ASY4 results in a significant reduction in fertility and crossovers, disruption of the chromosome axis structure, and a reduction in synapsis. In contrast to *asy4-1* and *asy4-2* presented by Chambon *et al.* (2018) and in **Chapter 3**, *asy4-4* is not hypomorphic, and therefore can be used in future studies on the roles and dynamics of the chromosome axis during meiosis. We also show that the phenotypes observed in *asy4-4* are unlikely to be due to an off-target effect, given that WT plants descended from *asy4-4* heterozygous lines did not have fertility defects, and that the *asy4-1/asy4-4* double mutant is indistinguishable from the single mutants.

We also present an antibody raised against ASY4 that successfully recognises ASY4 in immunolocalization, and along with work conducted in **Chapter 3**, confirms that ASY4 is an essential component of the chromosome axis in *Arabidopsis thaliana*.

Here, we will directly compare the *asy4-1*, *asy4-2* and *asy4-4* mutants to begin to explore whether the presence of a truncated protein can shed insight on possible roles for ASY4. A full discussion combining all results presented in this thesis can be found in **Chapter 6**.

5.6.1 ASY4 is required for normal fertility

As in *asy4-1* and *asy4-2*, fertility is significantly reduced in *asy4-4*. That no significant difference was found between the fertility levels of *asy4-1* and *asy4-4* suggests that the probable truncated protein present in the T-DNA insertion lines is not, at the level of fertility, causing any problems specific to having a non- or partly functional version

of the protein still present. This same conclusion may not have been reached if data only from the Grelon group (as presented in Chambon *et al.*, 2018) for *asy4-1* fertility had been used; the Grelon group reported *asy4-1* to have only a 42% reduction in fertility. Thus, we must not rule out the possibility of these phenotypes becoming more pronounced in different environmental conditions; it is well documented that temperature has a variety of effects on meiosis (Dion *et al.*, 2007).

The only significant difference was in the number of viable pollen, with *asy4-4* seeming to produce slightly more inviable pollen than *asy4-1*. This was only significant at the 5% level, however, so is possibly not a robust conclusion to make.

5.6.2 Crossover number is reduced in all *asy4* mutants

Between the three *asy4* mutants, CO number is relatively consistent; no significant difference in CO number was detected between *asy4-1* and *asy4-4*. Once again, this would suggest that the truncated protein does not disrupt recombination in a detectably different way compared to having no ASY4 at all.

Comparing DAPI spreads of PMCs from the three mutants did reveal a key difference, however. In the T-DNA insertion mutants *asy4-1* and *asy4-2*, a key phenotype was the presence of connections and fragments, but neither of these were observed in *asy4-4* at metaphase I. Fragments at metaphase I would suggest that some DSBs remain unrepaired in the T-DNA lines, which does not appear to be the case in *asy4-4*. We were not able to attribute an origin to the connections observed in the T-DNA lines due to technical issues with the FISH experiments, yet given that most of them appear to be thin threads of chromatin, perhaps the simplest explanation is that they are likely entangled chromosomes. This could fit with a theory of a disorganised axis structure in *asy4*, as perhaps the chromatin loops are more prone to becoming caught in each

other. However, if this were true, it would then stand to reason that in *asy4-4*, we should also see connections, as it also has a disorganised axis. The connections could therefore be attributed to an issue with the T-DNA itself (FISH could reveal if the same chromosomes were the ones entangled, with particular focus on chromosome 2 as this is where the T-DNA is carried), or that the truncated protein itself has another adverse effect on the axis that prevents these entanglements from being resolved. For example, axis component TOPII is required for resolution of interlocks and entanglements (Martinez-Garcia *et al.*, 2018). With the current information available, however, we cannot currently conclude the origins of the connections, and how their formation/persistence may have been impacted by the presence of a partial ASY4 protein.

It is also worth noting that these phenotypes were not reported by the Grelon group in Chambon *et al.* (2018). Yet, as discussed in **Chapter 3**, we believe that at least the connections are likely genuine, given that connections were also observed in the third T-DNA allele, *asy4-3* (Osman *et al.*, 2018). Thus, to determine if this is a genuine phenotype or not, we would need to analyse plants grown fresh seed-stocks of *asy4-1* and *asy4-2*. Ideally, these would also be grown in a constant temperature growth cabinet to mitigate the possibility of environmental effects. Nonetheless, in terms of fertility and CO number, the T-DNA insertion mutants *asy4-1* and *asy4-2* appear to be as affected as the true null-mutant.

5.6.3 ASY4 and the chromosome axis

Both *asy4-1* and *asy4-4* have no obvious defect in sister cohesion; perhaps based on this, we would expect that in *asy4-4*, like in *asy4-1*, a normal, underlying axis structure would be present. This was shown in Chambon *et al.* (2018) via silver staining. However, the other axis proteins, ASY1 and ASY3, are affected by a lack of ASY4;

both appear patchy and diffuse in both *asy4* mutants. This was highlighted in the SIM images, where the co-localisation of SMC3 and ASY3 was disrupted in *asy4-4*. Therefore, to conclude if *asy4-1* is similarly affected, SIM would need to be conducted on this line. These experiments were not conducted as part of this thesis due to questions presented in **Chapter 3** about whether the *asy4-1* line had accrued mutations and re-arrangements since its propagation here at Birmingham, given the discrepancies in the severity of particular phenotypes. Once a fresh batch of seed is obtained, however, the experiments performed in *asy4-4* can be repeated in *asy4-1* to continue to determine if this truncated protein causes any unique phenotypes.

Another shared phenotype between the mutants is that both *asy4-1* and *asy4-4* fail to reach pachytene. For *asy4-4*, the maximum SC length observed was still only 46% of that of the maximum SC length observed for WT. This data is not available for *asy4-1*, though in the future, it would be interesting to determine whether *asy4-1* is more or less severely impacted in terms of synapsis than *asy4-4*. This would be of particular interest due to the similarity of *asy4-1* to *pch2* in that neither successfully deplete ASY1 from the axis at sites where the ZYP1 signal has polymerised (Lambing *et al.*, 2015; Chambon *et al.*, 2018). However, *asy4-4* that lacks this truncated protein, shows evidence of axis remodelling. In *asy4-4*, we show that PCH2 localisation is unaffected, with the antibody co-localising with the ZYP1 signal as in WT. It would therefore be interesting to see whether this is also the case for *asy4-1* to determine whether the truncated protein causes a noticeable effect on PCH2 localisation and loading itself, or if it is more likely related to an effect on PCH2 function. Given that we have now verified the ASY4 antibody, it would also be worthwhile looking at the ASY4 signal in the *pch2* mutant, and whether it corroborates what we have observed of ASY4eYFP in the *pch2* background. This difference in remodelling is perhaps the most crucial

difference between the alleles, and its implications, as well as potential relationships with PCH2, will be discussed in **Chapter 6** for clarity.

5.6.4 ASY4 is required for CO maturation

In this chapter, we also explored whether the reduction in CO number could be attributed to defects in the recombination pathway itself. Thus, as for *asy4-1*, immunolocalisation was conducted using antibodies to DMC1, MSH4, and HEI10, to investigate at which point the recombination process might be encountering problems. From this data, it also appears that *asy4-1* and *asy4-4* are similarly affected. DMC1 foci counts in *asy4-1* and *asy4-4* both show no significant difference compared to WT, and therefore we can conclude that ASY4 is dispensable for DSB production. The data could not be compared for significance between *asy4-1* and *asy4-4*, however, as the Grelon group use a different DMC1 antibody, and appear to observe a higher number of DMC1 foci than we do at Birmingham (Grelon *asy4-1* DMC1: $\bar{x} = 222$; WT $\bar{x} = 240$).

Similarly, we conclude that proto-dHJs are likely being produced, as no difference was detected between the number of MSH4 foci in either *asy4-1* or *asy4-4* compared to WT. As a significance test comparing the WT values obtained for the number of MSH4 foci revealed that the Col-0 controls were significantly different, it was not possible to compare the values obtained for *asy4-1* and *asy4-4* to each other (Grelon *asy4-1* MSH4: $\bar{x} = 121$; WT $\bar{x} = 110$) (Chambon *et al.*, 2018). Nonetheless, between both experiments, the conclusion is the same: *asy4* does not affect the number of Holliday junctions forming.

For both alleles, a reduction in the number of HEI10 foci was observed at late prophase I. Data for HEI10 was not presented by the Grelon lab in Chambon *et al.* (2018), and thus once again, we cannot compare it to our data. They did, however, present the

number of MLH1 foci: another component of the Class I CO complex known to mark Class I COs during late prophase I, overlapping with HEI10 on the SC (Chambon *et al.*, 2018; Chelysheva *et al.*, 2010; Higgins *et al.*, 2005; Lhuissier *et al.*, 2007; Lloyd *et al.*, 2018). Based on this, we see very similar results when comparing the number of HEI10 foci in *asy4-4* to the number of MLH1 foci in *asy4-1* (Grelon MLH1: *asy4-1* $\bar{x} = 8.6$; WT $\bar{x} = 11$). Thus we conclude that in both mutants, the later stages of recombination are similarly affected. Therefore, a lack of functional ASY4 results in failure of a proportion of later-stage recombination intermediates to resolve into COs.

Given that the remaining HEI10 foci in *asy4* are all SC associated, perhaps the reduction in CO number could be attributed to the SC (or at least, ZYP1) itself being required for successful resolution of dHJs into CO products. As such, the remainder of CO-designated intermediates in *asy4* could be in the regions where the SC had not extended, and thus end up being processed as an NCO. The co-localisation of HEI10 foci and ZYP1 was also noted for *asy4-1*, and in *Atasy3*, the residual MSH4 and MLH1 also co-localised with the ZYP1 signal, so this observation is not unexpected (Chambon *et al.*, 2018; Ferdous *et al.*, 2012a).

It has been noted in other organisms including budding yeast and *S. macrospora*, that COs are ‘embedded’ in the SC, which could suggest that it is necessary for the CO to be SC associated during its repair (Dubois *et al.*, 2019; Voelkel-Meiman *et al.*, 2019). Recent work in *S. macrospora* reveals that this transition of COs from axis association to SC association may be facilitated by the formation of inter-axis bridges, evidence for which in *A. thaliana* are presented in this thesis (Dubois *et al.*, 2019). Furthermore, evidence from budding yeast shows that the ZMMs are needed for the stabilisation of recombination intermediates, with particular emphasis on the SC TF protein Zip1 which has since been suggested to physically connect to both factors that promote

synapsis initiation, as well as those in the recombination machinery (Voelkel-Meiman *et al.*, 2019, 2015). This is in light of separation of function mutants developed for Zip1. Knocking out the Zip1 gene entirely resulted in asynapsis and an inability to produce MutSy-dependent COs (Börner *et al.*, 2004). Deleting residues 21-163 resulted in no SC assembly, but the persistence of MutSy COs. Deleting only residues 2-9 or 2-14, however, resulted in assembly of the SC, but a reduction in the number of MutSy COs. Thus it was concluded Zip1 likely has a role in promoting COs before, and independent of, its role in SC assembly (Voelkel-Meiman *et al.*, 2019). It was also suggested that this was related to a potential interaction between Zip1 and the SUMO E3 ligase Zip3, which is required for formation of MutSy-dependent COs in yeast, and is related to *Arabidopsis* HEI10 (Chelysheva *et al.*, 2012; Voelkel-Meiman *et al.*, 2019).

In contrast to these other organisms, however, in *A. thaliana*, evidence may suggest that ZYP1 is not absolutely required for CO maturation. Higgins *et al.* (2005) generated a *zyp1* mutant line where the duplicate copies of ZYP1a/ZYP1b had been knocked-out by a T-DNA insertion and by RNAi, respectively. It was found that CO frequency in this line was ~80% of that of WT despite it having no synapsis. Furthermore, there was a mild reduction in the number of MLH1 foci at late prophase I, again suggesting that ZYP1 was largely expendable for the later stages of recombination (Higgins *et al.*, 2005b). It is nonetheless possible that given the positioning of the T-DNA in the seventh exon of ZYP1a, and that it cannot be absolutely guaranteed that the RNAi targeting of ZYP1b completely silenced the gene, that a low level of ZYP1 protein was still produced in these lines, confounding analysis.

Nonetheless, it could be suggested that we see MLH1 and HEI10 foci associated with the ZYP1 signal as perhaps COs are merely more readily processed within a CO-specific environment. This may fit with observations in *C. elegans*, where it has been

suggested that COs are repaired in a ‘CO-specific environment’, where recombination intermediates are encased in a SC ‘bubble’, and that this is required for these intermediates to repair as a CO (Woglar and Villeneuve, 2018). This work therefore suggests that further exploration of the potential function of ZYP1 in CO maturation in *Arabidopsis* is worthwhile.

A final interesting point is that both the CO number and number of HEI10 foci in *asy4-4* were significantly reduced compared to WT, yet the number of HEI10 foci observed in both WT and *asy4-4* were slightly higher than the ultimate CO number. If HEI10 indeed only denotes Class I CO sites, then this is somewhat surprising. It is possible, of course, that the cells merely were not counted late enough in prophase I, and thus a few of the foci observed were not late-stage CO sites. However, another explanation is that perhaps HEI10 also marks something else, such as other recombination intermediates that may not necessarily end up as a CO. This would fit with data obtained in wheat and other *Arabidopsis* lines, where consistently, the HEI10 signal appears to outweigh the final number of COs observed (K. Osman, University of Birmingham, personal communication; C. Nibau, University of Aberystwyth, personal communication).

As the number of HEI10 foci is significantly reduced compared to WT, we can also conclude that, if indeed HEI10 only marks Class I COs, that the formation of interference sensitive COs has been affected by a loss of ASY4. Given that the number of HEI10 foci observed would fully account for the final number of COs observed at metaphase I, it is of course also possible that the residual COs in *asy4-4* could all be interference sensitive, and the Class II pathway has also been affected. It is also true that as we counted using the MCN, our estimate of CO number is a little conservative. Thus, were we to attempt FISH once more and potentially identify more than two COs

per ring bivalent, it is possible the numbers would be higher, and thus match the number of HEI10 foci.

For future studies, therefore, it would be interesting to investigate whether Class II COs have been affected in any way. Crossing *asy4-4* to a ZMM needed for the Class I CO pathway such as *msh5* would help clarify this point; if the *asy4-4/msh5* double mutant had a CO number reduced beyond that of the single *msh5* mutant, then we could conclude that both interference sensitive and insensitive pathways are affected by loss of *asy4-4*.

Chapter 6

General Discussion

6 General Discussion

In this thesis, we describe the novel chromosome axis protein, ASY4. This initially encompassed cytological analysis of two hypomorphic T-DNA insertion lines, and later, development and characterisation of a true ASY4-null mutant, generated by CRISPR-Cas9. This allowed for a thorough investigation into its potential roles at the chromosome axis during meiosis in *A. thaliana*. In this chapter, the results obtained from the three mutants are fully discussed, as well as future lines of investigation, and how this research may contribute toward our goal of improving the plant breeding process.

6.1 ASY4 as a chromosome axis component

6.1.1 ASY4 and axis organisation

Experiments in all three *asy4* mutants suggest that ASY4 is essential for normal axis structure; immunolocalisation studies show that axis morphology in *asy4* is abnormal, with patchy and apparently disorganised ASY1 and ASY3 signals. ASY4 does not appear to be required for loading of the proteins, however.

It is therefore possible that, whilst ASY1 and ASY3 can indeed localise to the axis, their positioning is incorrect; perhaps in the absence of ASY4, they are less regularly spaced within the axis-meshwork, or that their positioning may have changed in relation to the loop bases. The best evidence we have that this may be a plausible explanation is found in the SIM images of the axis in *asy4-4*, presented in **Chapter 5**. In WT, we observe near co-localisation of ASY3 and SMC3 along the axis (Fig. 5.10, D1), with this relationship appearing more pronounced in later cells, perhaps due to the overall condensation that occurs as chromosomes synapse (Fig. 5.10, A1). This is in-keeping with data presented in yeast where the cohesins also co-localise with the

axis protein Red1 (Sun *et al.*, 2015). In *asy4-4*, overall, there appears to be more ASY3 that is not co-localising with SMC3; much of it appears further out from the cohesin signal (Fig. 5.10, G1). Perhaps, therefore, ASY3 is farther out into the loop than in WT, rather than localised more completely at the loop base with SMC3. This could explain why ASY3 has an overall ‘fuzzy’ appearance in *asy4*. Given that ASY1 requires ASY3 for normal loading and extension along the axis, perhaps this is also the case for ASY1. Indeed, it is possible that the altered appearance of ASY1 in *asy4* is a consequence of the improper organisation of ASY3 on the axis, rather than a direct effect of the lack of ASY4 itself. Y2H results from Osman *et al.* (2018) and Chambon *et al.* (2018) show no interaction between ASY1 and ASY4; thus it is perhaps more likely that issues with ASY3 are more likely to cause an effect on ASY1 (Ferdous *et al.*, 2012; Chambon *et al.*, 2018).

It may also be interesting to determine their relative intensities to WT, as it is also possible that they appear patchy simply because the proteins are less abundant; in this case, ASY4 could be necessary for maintenance of the normal stoichiometry of the axis proteins. That ASY1 is perhaps less abundant is thought to possibly be the case for *pch2*, where the axis appears unaffected, until the relative intensity of ASY1 at leptotene in *pch2* was compared to WT. This fits with observations in yeast suggesting that Pch2 is required for organisation of Hop1 into hyper-abundant domains (West, A., 2015; Lambing *et al.*, 2015; Börner *et al.*, 2008).

This fuzzy appearance of ASY1 and ASY3 was also reported in *asy4-1* (Chambon *et al.*, 2018). In *asy4-1*, we believe a truncated protein is present, given data presented showing there is still expression of some ASY4 transcript, and also, given that the antibody gives a strong axis-associated signal in both T-DNA mutants. Based on the Y2H results presented in **Chapter 3**, we would expect that this truncated protein could

no longer interact with ASY3. Nonetheless, it appears on the chromosome axis in *asy4-1*. These data together would suggest that ASY4 does not need ASY3 to localise onto the chromosome axis, as in theory, this truncated protein would not be able to interact with ASY3.

In *asy3:ASY4eYFP*, however, we do not see any extension of the ASY4eYFP signal, with it instead appearing as foci. These foci do not, however, appear to be associated with the axis, instead appearing out into the chromatin. This confirms that ASY4 requires ASY3 for its localisation on the axis, but that this relationship is not equally interdependent, with ASY3 able to assemble onto the axis in absence of functional ASY4. As previously discussed, however, the Y2H system is prone to both false negatives and false positives, and the result provided by the system can change due to many factors; it has been observed that merely changing the brand of media can alter the result obtained, for example (Liu *et al.*, 2011). Thus to be certain of these interactions, other, more robust PPI methodologies would need to be used, such as pull-down experiments. Therefore, it is more likely that ASY4 does indeed require ASY3 to localise onto the axis, and that the truncated protein present in *asy4-1* can perhaps still recognise ASY3, given that we cannot exclude the possibility of the result obtained from Y2H being a false negative.

6.1.2 ASY3 and ASY4 as functional homologues of mammalian SYCP2 and SYCP3

Since ASY3 was first described by Ferdous *et al.* (2012), it has been considered the functional homolog of the yeast coiled-coil containing protein, Red1. BLAST searches with the sequence of ASY4 did not find any homologues in yeast. Similarly, in mammals, the core axis protein SYCP2 has been considered a functional homolog of yeast Red1, and therefore, also potentially of ASY3 (Ferdous *et al.*, 2012a; Yang *et*

al., 2006). Mammals, like plants, also possess a second coiled-coil containing axis component, namely, SYCP3 (Kouznetsova *et al.*, 2005). Furthermore, like ASY4, SYCP3 also appears to have no obvious homologues in *S. cerevisiae* (Offenberg *et al.*, 1998).

In *Mus musculus*, the axial element proteins SYCP2 and SYCP3 also appear to be analogous to ASY3 and ASY4 respectively in terms of size and structure. SYCP2 is comprised of 1500 amino acid residues, and SYCP3 contains just 254 (West *et al.*, 2019). ASY3 is comprised of 793 amino acid residues, and ASY4 of 212 (Ferdous *et al.*, 2012; Chambon *et al.*, 2018; Osman *et al.*, 2018). In both systems, ASY3/ASY4 and SYCP2/SYCP3 have homology to each other, with ASY4 and SYCP3 both having homology to the C-terminal ends of ASY3 and SYCP2 respectively (Ferdous *et al.*, 2012; Chambon *et al.*, 2018; West *et al.*, 2019).

SYCP2 and SYCP3 also appear to require each other for localisation onto the axis, but more obviously so than ASY3 and ASY4; both *sycp2*^{-/-} and *sycp3*^{-/-} mutants fail to form the axial element and SC (Pelttari *et al.*, 2001; Yang *et al.*, 2006; Yuan *et al.*, 2000). Furthermore, it has been demonstrated that merely removing the coiled-coil domain of SYCP2 is sufficient to prevent SYPC3 loading onto the axis (Yang *et al.*, 2006). In *A. thaliana*, it appears that ASY3 is absolutely required for ASY4 extension on the axis, but ASY3 can still linearise to some extent along the axis in absence of ASY4 (Chambon *et al.*, 2018; this thesis).

West *et al.* (2019) show that the coiled-coil protein SYCP3 is capable of self-assembling into a homotetramer in the absence of SYCP2, but that its structure is much less stable. SYCP3 is also required for normal bundling of the SYCP2:SYCP3 filaments. Given that ASY3 is also a coiled-coil protein shown to assemble with ASY4

into heterotetramers, perhaps it is possible that in *asy4-4*, ASY3 can self-polymerise, but its structure is unstable and inadequately organised. Furthermore, SYCP3 is known to act as a ‘molecular spacer’ required for regular patterning of the axis proteins (Syrjänen *et al.*, 2014). Thus, with the data obtained from the SIM presented in this thesis, we would suggest ASY4 to be acting in a manner akin to SYCP3, functioning as a key organisational component of the chromosome axis.

Thus, both in this thesis and in Chambon *et al.* (2018), we propose that it is possible that plants and mammals have analogous axis systems, more closely related to each other than is obvious in *S. cerevisiae*.

6.2 ASY4 and CO maturation

Lack of ASY4 results in an inability to assure the obligate CO, as is demonstrated by the presence of univalents in this mutant. There are two possible explanations for this. As discussed in 1.3.3.2.2, the Beam-Film (BF) model of CO patterning stipulates that mechanical stress builds along the meiotic chromosomes, and that for this stress to be relieved, a CO must be designated. Thus, a mechanical explanation fitting with the BF model could be that due to the disorganised axis structure in *asy4*, the mechanical stress required to designate the obligate CO was not sufficiently strong on all chromosomes. Another may relate to the SC itself potentially being required for CO maturation, and thus these chromosomes could have remained asynaptic. However, there is evidence suggesting that the SC may not absolutely be required for normal CO levels, and that COs may not be required for its initiation in *A. thaliana*. This comes from both the previously discussed *zyp1a^{T-DNA}/zyp1b^{RNAi}* lines showing near WT levels of COs, and that *Arabidopsis* ZMM mutants still have normal SC extension, despite a lack of Class I COs (Chelysheva *et al.*, 2007; Higgins *et al.*, 2008b, 2005a, 2004a; Macaisne *et al.*, 2011, 2008; Wijeratne *et al.*, 2006). Thus, the SC in of itself may not

be required for normal CO maturation, but merely provides a stable scaffold for the recombinases. The recombination complexes we see associated with the SC signal in *asy4* and other mutants perhaps were CO-designated sites that were more stable, and thus resolved more efficiently than any that may have been generated in asynaptic regions.

It is of course possible, given data presented by Kurzbauer *et al.* (2018) on *fancd2* mutants, that some class II COs are required to maintain the obligate CO. Thus, if ASY4, like PCH2, is required for normal levels of both CI and CII COs, it could be that these univalents arise due to CII CO issues. To clarify this, we could cross *asy4-4* and *asy4-1* to a ZMM mutant such as *msh5*; if the CO level is reduced beyond that of the *msh5* single mutant, then ASY4 influences both the CI and CII pathways.

6.3 ASY4 and PCH2

As shown in both this thesis and in Chambon *et al.* (2018), absence/defective ASY4 results in a partially asynaptic phenotype and an abnormal axis structure. Perhaps the most striking thing about the *asy4* mutants is their apparent similarity to *pch2*, rather than to mutants of the other structural axis components, *asy1* and *asy3*. A table illustrating this point is presented in Table 6.1.

Table 6. 1 Comparison of several axis mutants in *Arabidopsis thaliana*.

| | <i>asy1</i> | <i>asy3</i> | <i>pch2</i> | <i>asy4-1</i> | <i>asy4-4</i> |
|-----------------|--|----------------------|--|---|---|
| Fertility | 'Reduced' | 75% reduction | 49% reduction | 43% reduction | 57% reduction |
| Chiasmata | 1.64 | 3.3 | 6.9 | 5.9 (Chambon et al., 2018) 6.5 (this thesis) | 6.3 |
| DMC1 foci | Reduced | Reduced | Normal | Normal | Normal |
| MSH4/MSH5 | - | Reduced | Normal | Normal | Normal |
| Axis appearance | ASY3 normal | ASY1 foci | ASY3 normal ASY1 dimmer ASY1 not remodelled off SC | ASY1/ASY3 patchy ASY1 not remodelled off SC | ASY1/ASY3 patchy ASY1 is remodelled off SC |
| SC | Foci | Foci | 32% of WT | Short stretches | 39% of WT |
| References | Armstrong et al., 2002 Caryl et al., 2002 Sanchez-Moran et al., 2007 Ferdous et al., 2012 | Ferdous et al., 2012 | Lambing et al., 2015 West A., 2015 | Chambon et al., 2018 Osman et al., 2018 This thesis | This thesis |

A defining characteristic of the *pch2* mutant is the persistence of ASY1 on the lateral element of the SC; this led to the conclusion that in WT, ASY1 is depleted from the axis as the SC extends by the ATP-catalysed action of PCH2 (Lambing *et al.*, 2015). This was supported by evidence from other organisms showing that PCH2 homologues (and other proteins such as p31^{comet}) are required for opening of the HORMAD closure motif, allowing for dissociation of HORMADs from their interactors (Brulotte *et al.*, 2017; Rosenberg and Corbett, 2015; Ye *et al.*, 2017, 2015).

As is evident in Table 6.1, in terms of a lack of effects on early steps in recombination, CO number, fertility, and SC extension, *asy4* and *pch2* are indeed very similar. When comparing *asy4-1* and *pch2*, this is more pronounced, given that a defining feature of both mutants is that ASY1 is not depleted from the axis where the SC has extended. This is not the case in *asy4-4*, however. Possible explanations for this include that the truncated protein present in *asy4-1* and *asy4-2* cannot be regulated normally; perhaps ASY4 itself needs to be remodelled or post-translationally modified in some way to accommodate SC extension. Indeed, in mammalian systems, axis protein SYCP3 has

been found to be phosphorylated, SUMOylated, and associates with Ubc9: an ubiquitin-conjugation enzyme (Eichinger and Jentsch, 2010; Fukuda *et al.*, 2012; Rao *et al.*, 2017; Tarsounas *et al.*, 1997). Furthermore, disruption of the SUMO-ubiquitin relay has been shown to result in aggregations of SYCP3 in mouse spermatocytes, thus suggesting that these modifications are essential for its regulation (Rao *et al.*, 2017).

That ASY4 has some role during synapsis initiation could be suggested by the cells presented in **3.2.2.4** where a bright ASY4eYFP signal is seen flanking synapsis initiation sites. Whilst it could be argued that this is merely due to some issue with the eYFP tag, it is also possible that, potentially due to a delay in SC extension or an over-aggregation of ASY4eYFP, we see this in a more pronounced manner than we might do with the ASY4 antibody. Indeed, getting many cells with these foci of ZYP1 are comparatively rare, which may be due to this process proceeding quickly.

However, if ASY4 were necessary for axis remodelling itself, we would expect to see ASY1 persisting on the axis in *asy4-4*. Taken with the fact that the chromosome axis organisation prior to synapsis is unaffected in *pch2*, but significantly impacted in *asy4*, it is clear these proteins, despite their similarities, are conducting distinct roles. They are possibly, however, either functionally or temporally related in some way. We would therefore propose that ASY4 is likely dispensable for axis remodelling, but that having a truncated version of ASY4 present disrupts this process. That is, ASY4 is also not required for normal PCH2 function, given that PCH2 both localises to the SC successfully in *asy4-4*, and that it appears to be able to remodel ASY1 from the axis as zygotene progresses. West *et al.* (2019) propose that ASY3 and ASY4 form antiparallel heterotetramers along the axis, and that ASY3 recruits ASY1 via a closure motif. Later, it is thought that PCH2 opens up the closure motif, thus allowing removal

of ASY1 from the lateral elements. Based on this, it is possible that the truncated ASY4 protein causes some topological issue that may prevent normal dissociation of the ASY3 closure motif from ASY1, thus enabling ASY1 to persist on the axis.

This work also gives insight into whether it is the presence of ASY1 itself in *asy4-1* and *pch2* that prevents normal SC extension. If this were the case, then we would expect to see an obvious difference in the level of SC extension between *asy4-1* and *asy4-4*, given that in *asy4-4*, ASY1 is successfully depleted from the axis. As this was not observed, perhaps not the persistence of ASY1 on the axis *per se* that prevents SC extension, put potentially a wider issue with axis organisation or signalling in these mutants.

To try and pick apart any potential relationship between ASY4 and PCH2, crosses between *pch2* and both *asy4-1* and *asy4-4* would be useful. It would also be interesting to explore the dynamics of PCH2 in *asy4-1*, as we do not yet know if the protein is able to localise to the SC in *asy4-1* as it does in WT and *asy4-4*. In the reverse, we also need to confirm whether a lack of PCH2 influences the amount or organisation of ASY4 on the axis, given that in the *pch2:ASY4eYFP*, ASY4eYFP is co-localising with the axis, but presents an abnormal structure of many high intensity foci, with some short linear stretches.

6.4 CRISPR-Cas9 is an effective way to produce novel mutations in meiotic genes

One aim of this thesis was to successfully generate an *asy4* null mutant, given that other available mutants were determined to be hypomorphic (Chambon *et al.*, 2018; Osman *et al.*, 2018; this thesis). CRISPR-Cas9 has already been widely used in many systems to integrate targeted mutations in genes of interest, and in this thesis, we

present a novel mutant with a 1.7 kb deletion in ASY4, proving CRISPR-Cas9 to be an effective way of quickly producing mutants to overcome limitations with T-DNA insertions: the main manner in which *A. thaliana* mutants are generated. We also present evidence that the phenotype observed in *asy4-4* is likely not due to an off-target effect. Of course, we cannot unequivocally determine whether or not our construct did cause edits in other parts of the genome, but given that the phenotypes of *asy4-1/asy4-4* and the respective single mutants are so similar, it would seem these would be meiotically neutral and therefore inconsequential in this study. Therefore, *asy4-4* can be established as a useful mutant line available to the community for future research. To our knowledge, *asy4-4* is also the first fully described CRISPR-Cas9-generated meiotic mutant in *A. thaliana*.

6.5 Future Research and Applications

Future interesting lines of research could include determining the precise PPIs between the axis-associated proteins including PCH2, and ZYP1. In mouse, it has been demonstrated that the axis protein SYCP2, but not SYCP3, can interact with SYCP1, thus directly linking the axis to the SC (Syrjänen *et al.*, 2014). To our knowledge, thus far, only ASY1 has been tested for an interaction with ZYP1, which proved to be negative (Osman *et al.*, 2018). Therefore, it would be interesting to determine whether ASY3 or ASY4 has the capability to interact with ZYP1, further enlightening us on the direct relationships between these key SC components. Given the interesting similarities between PCH2 and ASY4 in terms of their mutant phenotypes, it may also be worthwhile determining if these proteins can interact. Though, it is worth noting that this interaction would potentially be biochemically complex, given that Pch2 in yeast is only seen to interact with other proteins in the presence of ATPyS (Chen *et al.*, 2014). This is because ATPyS cannot be turned over,

and thus the transient interactions between Pch2 and its targets are sustained for longer, and thus at detectable levels.

Indeed, for future research prospects, it would also be interesting to follow on from the research conducted by West *et al.* (2019) and investigate how tightly these proteins interact with each other. This could give us some indication about the importance of axis stoichiometry, and how tensile strengths could vary across the axis in different mutants, and at different temperatures: a key area of research given the global impacts of climate change. Topics for translatable research into crops could, therefore, focus on influencing the stoichiometry of the axis and thus its mechanical properties, which may allow for redistribution of COs. This could include, for example, knocking-down levels of protein, rather than knocking them out which could be both transiently administered (i.e., within one generation), and potentially minimise any fertility defect.

As ASY1 and ZYP1 homologues have already been identified in several crop species including barley and wheat, it would also be interesting to explore whether ASY4 is also a key player in these systems, and whether there is any functional divergence. Functional divergence of meiotic proteins across plant species has already been observed; for example, mutants of the rice AtPCH2 homologue *Oscrc1* revealed that, contrary to what is observed for *Arabidopsis*, OsCRC1 is required for DSB formation and recruitment of PAIR2, a rice HORMAD, to the axis (Miao *et al.*, 2013). Though, it is interesting to note that rice repeatedly appears to differ even from other monocots, a notable example being the function of OsZEP1 vs HvZYP1, where *Oszep1* mutants show an increase in CO number, and *Hvzyp1* mutants show a decrease (Barakate *et al.*, 2014; Wang *et al.*, 2010). Thus investigating the axis further in individual species of interest is crucial if we are to successfully manipulate meiosis in crops.

6.6 Summary

Combined, the work in this thesis characterises a previously unknown component of the chromosome axis in plants. It suggests that ASY4 is an essential organisational unit of the chromosome axis in *Arabidopsis thaliana*, and that disrupting it results in defects in axis organisation, SC extension, and CO maturation, culminating in an overall reduction in fertility less severe than is observed for *asy1*, *asy3*, and *syn1*. We also describe a novel, CRISPR-Cas9 generated mutant of *asy4* that will be available for use by other groups, and suggest further avenues of research to continue to deepen our understanding of the meiotic chromosome axis.

A diagrammatic summary of the results described in this thesis is presented in Figure 6.1.

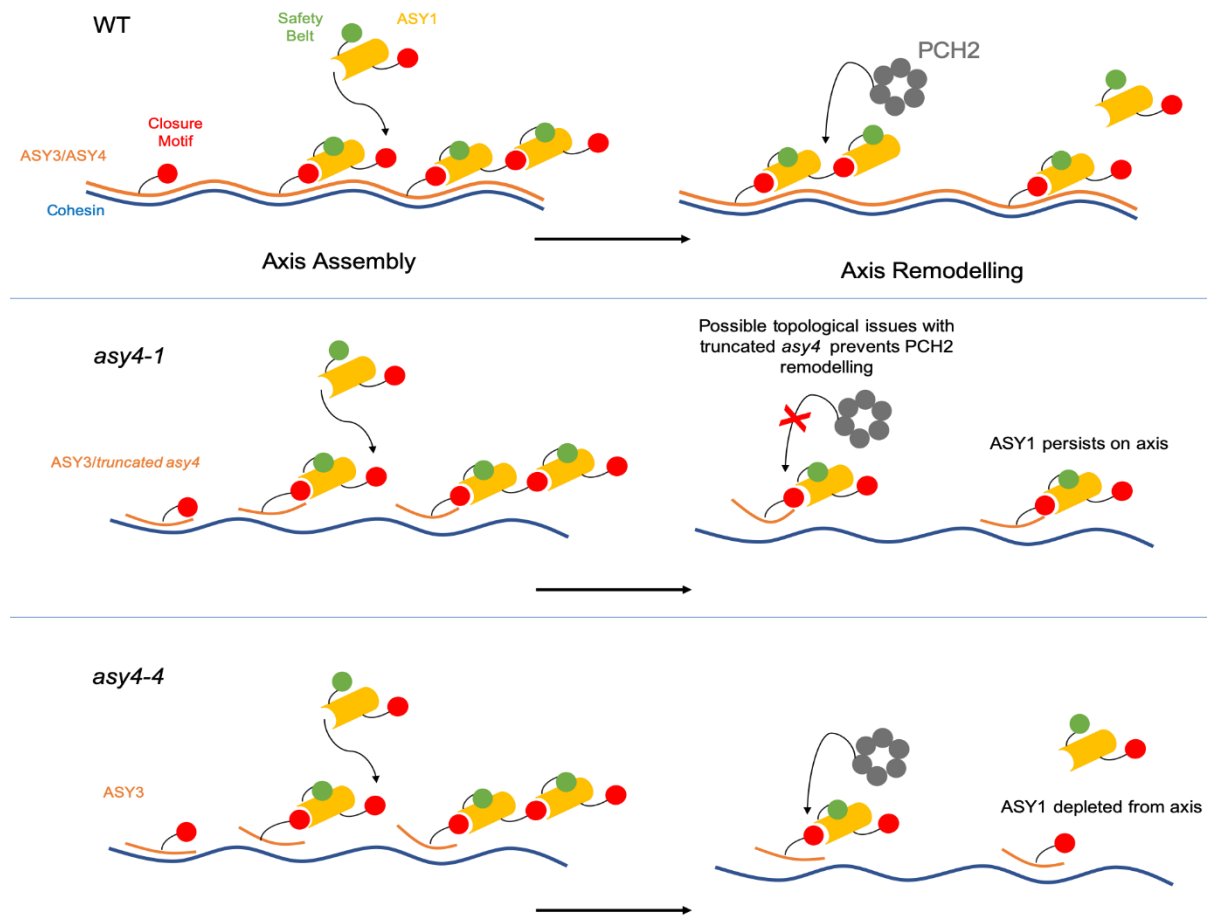


Figure 6.1 Chromosome axis assembly and remodelling in WT and two *asy4* mutants. In WT, the chromosome axis is organised with ASY3/ASY4 arranged into antiparallel heterotetramers which are closely associated with the cohesins. ASY1 is recruited to the axis by the ASY3 closure motif. As the axis is remodelled by PCH2, the ASY1 HORMA domain is successfully opened, allowing for ASY1 depletion. In both *asy4* mutants, ASY3 appears disorganized and farther away from the loop bases, but is still able to recruit ASY1 to the axis. In *asy4-1*, the truncated *asy4* protein may prevent normal dissociation of the ASY1 HORMA domain from the ASY3 closure motif, and thus ASY1 persists on the axis. In *asy4-4*, ASY1 is depleted from the axis as in WT. Adapted from Rosenberg and Corbett, 2015; West *et al.*, 2019; and Morgan, 2016.

References

- Aklilu, B.B., Soderquist, R.S., Culligan, K.M., 2014. Genetic analysis of the Replication Protein A large subunit family in *Arabidopsis* reveals unique and overlapping roles in DNA repair, meiosis and DNA replication. *Nucleic Acids Res.* 42, 3104–3118. <https://doi.org/10.1093/nar/gkt1292>
- Alberts, B., Bray, D., Lewis, J., Raff, M., Roberts, K., Watson, J.D., 1983. *Molecular Biology of the Cell*, 1st ed. Garland Publishing, London.
- Albini, S.M., Jones, G.H., 1987. Synaptonemal complex spreading in *Allium cepa* and *A. fistulosum*. *Chromosoma* 95, 324–338. <https://doi.org/10.1007/BF00293179>
- Alexander, M.P., 1969. Differential staining of aborted and nonaborted pollen. *Stain Technol.* 44, 117–122.
- Allers, T., Lichten, M., 2001. Differential Timing and Control of Noncrossover and Crossover Recombination during Meiosis. *Cell* 106, 47–57. [https://doi.org/10.1016/S0092-8674\(01\)00416-0](https://doi.org/10.1016/S0092-8674(01)00416-0)
- Al-Sweel, N., Raghavan, V., Dutta, A., Ajith, V.P., Di Vietro, L., Khondakar, N., Manhart, C.M., Surtees, J.A., Nishant, K.T., Alani, E., 2017. *mlh3* mutations in baker's yeast alter meiotic recombination outcomes by increasing noncrossover events genome-wide. *PLoS Genet.* 13, e1006974. <https://doi.org/10.1371/journal.pgen.1006974>
- Anderson, L.K., Hooker, K.D., Stack, S.M., 2001. The distribution of early recombination nodules on zygotene bivalents from plants. *Genetics* 159, 1259–1269.
- Anderson, L.K., Offenberg, H.H., Verkuijlen, W.M., Heyting, C., 1997. RecA-like proteins are components of early meiotic nodules in lily. *Proc. Natl. Acad. Sci. U. S. A.* 94, 6868–6873. <https://doi.org/10.1073/pnas.94.13.6868>
- Armstrong, S.J., Caryl, A.P., Jones, G.H., Franklin, F.C.H., 2002. Asy1, a protein required for meiotic chromosome synapsis, localizes to axis-associated chromatin in *Arabidopsis* and *Brassica*. *J. Cell Sci.* 115, 3645–3655.
- Armstrong, S.J., Franklin, F.C.H., Jones, G.H., 2003. A meiotic time-course for *Arabidopsis thaliana*. *Sex. Plant Reprod.* 16, 141–149. <https://doi.org/10.1007/s00497-003-0186-4>
- Arora, K., Corbett, K.D., 2019. The conserved XPF:ERCC1-like Zip2:Spo16 complex controls meiotic crossover formation through structure-specific DNA binding. *Nucleic Acids Res.* 47, 2365–2376. <https://doi.org/10.1093/nar/gky1273>
- Atcheson, C.L., DiDomenico, B., Frackman, S., Esposito, R.E., Elder, R.T., 1987. Isolation, DNA sequence, and regulation of a meiosis-specific eukaryotic recombination gene. *Proc. Natl. Acad. Sci. U. S. A.* 84, 8035–8039.
- Awika, J.M., 2011. Major Cereal Grains Production and Use around the World, in: Awika, J.M., Piironen, V., Bean, S. (Eds.), *Advances in Cereal Science: Implications to Food Processing and Health Promotion*. American Chemical Society, Washington, DC, pp. 1–13. <https://doi.org/10.1021/bk-2011-1089.ch001>
- Bai, X., Peirson, B.N., Dong, F., Xue, C., Makaroff, C.A., 1999. Isolation and characterization of SYN1, a RAD21-like gene essential for meiosis in *Arabidopsis*. *Plant Cell* 11, 417–430.
- Baltes, N.J., Gil-Humanes, J., Cermak, T., Atkins, P.A., Voytas, D.F., 2014. DNA replicons for plant genome engineering. *Plant Cell* 26, 151–163. <https://doi.org/10.1105/tpc.113.119792>
- Barakate, A., Higgins, J.D., Vivera, S., Stephens, J., Perry, R.M., Ramsay, L., Colas, I., Oakey, H., Waugh, R., Franklin, F.C.H., Armstrong, S.J., Halpin, C., 2014. The synaptonemal complex protein ZYP1 is required for imposition of meiotic crossovers in barley. *Plant Cell* 26, 729–740. <https://doi.org/10.1105/tpc.113.121269>
- Barrangou, R., Fremaux, C., Deveau, H., Richards, M., Boyaval, P., Moineau, S., Romero, D.A., Horvath, P., 2007. CRISPR provides acquired resistance against viruses in prokaryotes. *Science* 315, 1709–1712. <https://doi.org/10.1126/science.1138140>

- Baudat, F., Buard, J., Grey, C., Fledel-Alon, A., Ober, C., Przeworski, M., Coop, G., de Massy, B., 2010. PRDM9 is a major determinant of meiotic recombination hotspots in humans and mice. *Science* 327, 836–840. <https://doi.org/10.1126/science.1183439>
- Bell, L., Byers, B., 1983. Separation of branched from linear DNA by two-dimensional gel electrophoresis. *Anal. Biochem.* 130, 527–535. [https://doi.org/10.1016/0003-2697\(83\)90628-0](https://doi.org/10.1016/0003-2697(83)90628-0)
- Berchowitz, L.E., Hanlon, S.E., Lieb, J.D., Copenhaver, G.P., 2009. A positive but complex association between meiotic double-strand break hotspots and open chromatin in *Saccharomyces cerevisiae*. *Genome Res.* 19, 2245–2257. <https://doi.org/10.1101/gr.096297.109>
- Bergerat, A., de Massy, B., Gadelle, D., Varoutas, P.C., Nicolas, A., Forterre, P., 1997. An atypical topoisomerase II from Archaea with implications for meiotic recombination. *Nature* 386, 414–417. <https://doi.org/10.1038/386414a0>
- Berr, A., McCallum, E.J., Ménard, R., Meyer, D., Fuchs, J., Dong, A., Shen, W.-H., 2010. Arabidopsis SET DOMAIN GROUP2 is required for H3K4 trimethylation and is crucial for both sporophyte and gametophyte development. *Plant Cell* 22, 3232–3248. <https://doi.org/10.1105/tpc.110.079962>
- Bhatt, A.M., Lister, C., Page, T., Fransz, P., Findlay, K., Jones, G.H., Dickinson, H.G., Dean, C., 1999. The DIF1 gene of Arabidopsis is required for meiotic chromosome segregation and belongs to the REC8/RAD21 cohesin gene family. *Plant J. Cell Mol. Biol.* 19, 463–472.
- Bhaya, D., Davison, M., Barrangou, R., 2011. CRISPR-Cas systems in bacteria and archaea: versatile small RNAs for adaptive defense and regulation. *Annu. Rev. Genet.* 45, 273–297. <https://doi.org/10.1146/annurev-genet-110410-132430>
- Bishop, D.K., 1994. RecA homologs Dmc1 and Rad51 interact to form multiple nuclear complexes prior to meiotic chromosome synapsis. *Cell* 79, 1081–1092.
- Boer, E. de, Dietrich, A.J.J., Höög, C., Stam, P., Heyting, C., 2007. Meiotic interference among MLH1 foci requires neither an intact axial element structure nor full synapsis. *J. Cell Sci.* 120, 731–736. <https://doi.org/10.1242/jcs.003186>
- Bomblies, K., Higgins, J.D., Yant, L., 2015. Meiosis evolves: adaptation to external and internal environments. *New Phytol.* 208, 306–323. <https://doi.org/10.1111/nph.13499>
- Borde, V., de Massy, B., 2013. Programmed induction of DNA double strand breaks during meiosis: setting up communication between DNA and the chromosome structure. *Curr. Opin. Genet. Dev.* 23, 147–155. <https://doi.org/10.1016/j.gde.2012.12.002>
- Borde, V., Goldman, A.S., Lichten, M., 2000. Direct coupling between meiotic DNA replication and recombination initiation. *Science* 290, 806–809.
- Borde, V., Robine, N., Lin, W., Bonfils, S., Géli, V., Nicolas, A., 2009. Histone H3 lysine 4 trimethylation marks meiotic recombination initiation sites. *EMBO J.* 28, 99–111. <https://doi.org/10.1038/emboj.2008.257>
- Börner, G.V., Barot, A., Kleckner, N., 2008. Yeast Pch2 promotes domainal axis organization, timely recombination progression, and arrest of defective recombinosomes during meiosis. *Proc. Natl. Acad. Sci. U. S. A.* 105, 3327–3332. <https://doi.org/10.1073/pnas.0711864105>
- Börner, G.V., Kleckner, N., Hunter, N., 2004. Crossover/noncrossover differentiation, synaptonemal complex formation, and regulatory surveillance at the leptotene/zygotene transition of meiosis. *Cell* 117, 29–45.
- Bortesi, L., Fischer, R., 2015. The CRISPR/Cas9 system for plant genome editing and beyond. *Biotechnol. Adv.* 33, 41–52. <https://doi.org/10.1016/j.biotechadv.2014.12.006>
- Brulotte, M.L., Jeong, B.-C., Li, F., Li, B., Yu, E.B., Wu, Q., Brautigam, C.A., Yu, H., Luo, X., 2017. Mechanistic insight into TRIP13-catalyzed Mad2 structural transition and spindle checkpoint silencing. *Nat. Commun.* 8, 1956. <https://doi.org/10.1038/s41467-017-02012-2>
- Cai, X., Dong, F., Edelmann, R.E., Makaroff, C.A., 2003. The Arabidopsis SYN1 cohesin protein is required for sister chromatid arm cohesion and homologous chromosome pairing. *J. Cell Sci.* 116, 2999–3007. <https://doi.org/10.1242/jcs.00601>

- Callender, T.L., Laureau, R., Wan, L., Chen, X., Sandhu, R., Laljee, S., Zhou, S., Suhandynata, R.T., Prugar, E., Gaines, W.A., Kwon, Y., Börner, G.V., Nicolas, A., Neiman, A.M., Hollingsworth, N.M., 2016. Mek1 Down Regulates Rad51 Activity during Yeast Meiosis by Phosphorylation of Hed1. *PLoS Genet.* 12, e1006226. <https://doi.org/10.1371/journal.pgen.1006226>
- Carballo, J.A., Johnson, A.L., Sedgwick, S.G., Cha, R.S., 2008. Phosphorylation of the axial element protein Hop1 by Mec1/Tel1 ensures meiotic interhomolog recombination. *Cell* 132, 758–770. <https://doi.org/10.1016/j.cell.2008.01.035>
- Carballo, J.A., Panizza, S., Serrentino, M.E., Johnson, A.L., Geymonat, M., Borde, V., Klein, F., Cha, R.S., 2013. Budding Yeast ATM/ATR Control Meiotic Double-Strand Break (DSB) Levels by Down-Regulating Rec114, an Essential Component of the DSB-machinery. *PLOS Genet.* 9, e1003545. <https://doi.org/10.1371/journal.pgen.1003545>
- Carpenter, A.T.C., 1975. Electron microscopy of meiosis in *Drosophila melanogaster* females: II: The recombination nodule—a recombination-associated structure at pachytene? *Proc. Natl. Acad. Sci. U. S. A.* 72, 3186–3189.
- Caryl, A.P., Armstrong, S.J., Jones, G.H., Franklin, F.C., 2000. A homologue of the yeast HOP1 gene is inactivated in the *Arabidopsis* meiotic mutant *asy1*. *Chromosoma* 109, 62–71.
- Chambon, A., West, A., Vezon, D., Horlow, C., Muyt, A.D., Chelysheva, L., Ronceret, A., Darbyshire, A., Osman, K., Heckmann, S., Franklin, F.C.H., Grelon, M., 2018. Identification of ASYNAAPTIC4, a Component of the Meiotic Chromosome Axis. *Plant Physiol.* 178, 233–246. <https://doi.org/10.1104/pp.17.01725>
- Chan, Y.-L., Brown, M.S., Qin, D., Handa, N., Bishop, D.K., 2014. The third exon of the budding yeast meiotic recombination gene HOP2 is required for calcium-dependent and recombinase Dmc1-specific stimulation of homologous strand assimilation. *J. Biol. Chem.* 289, 18076–18086. <https://doi.org/10.1074/jbc.M114.558601>
- Chelysheva, L., Diallo, S., Vezon, D., Gendrot, G., Vrielynck, N., Belcram, K., Rocques, N., Márquez-Lema, A., Bhatt, A.M., Horlow, C., Mercier, R., Mézard, C., Grelon, M., 2005. AtREC8 and AtSCC3 are essential to the monopolar orientation of the kinetochores during meiosis. *J. Cell Sci.* 118, 4621–4632. <https://doi.org/10.1242/jcs.02583>
- Chelysheva, L., Gendrot, G., Vezon, D., Doutriaux, M.-P., Mercier, R., Grelon, M., 2007. Zip4/Spo22 Is Required for Class I CO Formation but Not for Synapsis Completion in *Arabidopsis thaliana*. *PLOS Genet.* 3, e83. <https://doi.org/10.1371/journal.pgen.0030083>
- Chelysheva, L., Grandont, L., Vrielynck, N., le Guin, S., Mercier, R., Grelon, M., 2010. An easy protocol for studying chromatin and recombination protein dynamics during *Arabidopsis thaliana* meiosis: immunodetection of cohesins, histones and MLH1. *Cytogenet. Genome Res.* 129, 143–153. <https://doi.org/10.1159/000314096>
- Chelysheva, L., Vezon, D., Belcram, K., Gendrot, G., Grelon, M., 2008. The *Arabidopsis* BLAP75/Rmi1 homologue plays crucial roles in meiotic double-strand break repair. *PLoS Genet.* 4, e1000309. <https://doi.org/10.1371/journal.pgen.1000309>
- Chelysheva, L., Vezon, D., Chambon, A., Gendrot, G., Pereira, L., Lemhemdi, A., Vrielynck, N., Le Guin, S., Novatchkova, M., Grelon, M., 2012. The *Arabidopsis* HEI10 Is a New ZMM Protein Related to Zip3. *PLoS Genet* 8, e1002799. <https://doi.org/10.1371/journal.pgen.1002799>
- Chen, C., Jomaa, A., Ortega, J., Alani, E.E., 2014. Pch2 is a hexameric ring ATPase that remodels the chromosome axis protein Hop1. *Proc. Natl. Acad. Sci. U. S. A.* 111, E44–53. <https://doi.org/10.1073/pnas.1310755111>
- Chen, X., Suhandynata, R.T., Sandhu, R., Rockmill, B., Mohibullah, N., Niu, H., Liang, J., Lo, H.-C., Miller, D.E., Zhou, H., Börner, G.V., Hollingsworth, N.M., 2015. Phosphorylation of the Synaptonemal Complex Protein Zip1 Regulates the Crossover/Noncrossover Decision during Yeast Meiosis. *PLOS Biol.* 13, e1002329. <https://doi.org/10.1371/journal.pbio.1002329>

- Cheng, C.-H., Lo, Y.-H., Liang, S.-S., Ti, S.-C., Lin, F.-M., Yeh, C.-H., Huang, H.-Y., Wang, T.-F., 2006. SUMO modifications control assembly of synaptonemal complex and polycomplex in meiosis of *Saccharomyces cerevisiae*. *Genes Dev.* 20, 2067–2081. <https://doi.org/10.1101/gad.1430406>
- Choi, K., Henderson, I.R., 2015. Meiotic recombination hotspots - a comparative view. *Plant J. Cell Mol. Biol.* 83, 52–61. <https://doi.org/10.1111/tpj.12870>
- Choi, K., Zhao, X., Kelly, K.A., Venn, O., Higgins, J.D., Yelina, N.E., Hardcastle, T.J., Ziolkowski, P.A., Copenhaver, G.P., Franklin, F.C.H., McVean, G., Henderson, I.R., 2013. Arabidopsis meiotic crossover hot spots overlap with H2A.Z nucleosomes at gene promoters. *Nat. Genet.* 45, 1327–1336. <https://doi.org/10.1038/ng.2766>
- Choi, K., Zhao, X., Tock, A.J., Lambing, C., Underwood, C.J., Hardcastle, T.J., Serra, H., Kim, Juhyun, Cho, H.S., Kim, Jaeil, Ziolkowski, P.A., Yelina, N.E., Hwang, I., Martienssen, R.A., Henderson, I.R., 2018. Nucleosomes and DNA methylation shape meiotic DSB frequency in *Arabidopsis thaliana* transposons and gene regulatory regions. *Genome Res.* 28, 532–546. <https://doi.org/10.1101/gr.225599.117>
- Choulet, F., Alberti, A., Theil, S., Glover, N., Barbe, V., Daron, J., Pingault, L., Sourdille, P., Couloux, A., Paux, E., Leroy, P., Mangenot, S., Guilhot, N., Le Gouis, J., Balfourier, F., Alaux, M., Jamilloux, V., Poulain, J., Durand, C., Bellec, A., Gaspin, C., Safar, J., Dolezel, J., Rogers, J., Vandepoele, K., Aury, J.-M., Mayer, K., Berges, H., Quesneville, H., Wincker, P., Feuillet, C., 2014. Structural and functional partitioning of bread wheat chromosome 3B. *Science* 345, 1249721. <https://doi.org/10.1126/science.1249721>
- Chua, P.R., Roeder, G.S., 1998. Zip2, a meiosis-specific protein required for the initiation of chromosome synapsis. *Cell* 93, 349–359. [https://doi.org/10.1016/s0092-8674\(00\)81164-2](https://doi.org/10.1016/s0092-8674(00)81164-2)
- Chuang, C.-N., Cheng, Y.-H., Wang, T.-F., 2012. Mek1 stabilizes Hop1-Thr318 phosphorylation to promote interhomolog recombination and checkpoint responses during yeast meiosis. *Nucleic Acids Res.* 40, 11416–11427. <https://doi.org/10.1093/nar/gks920>
- Cloud, V., Chan, Y.-L., Grubb, J., Budke, B., Bishop, D.K., 2012. Rad51 is an accessory factor for Dmc1-mediated joint molecule formation during meiosis. *Science* 337, 1222–1225. <https://doi.org/10.1126/science.1219379>
- Clough, S.J., Bent, A.F., 1998. Floral dip: a simplified method for *Agrobacterium*-mediated transformation of *Arabidopsis thaliana*. *Plant J. Cell Mol. Biol.* 16, 735–743.
- Cole, F., Kauppi, L., Lange, J., Roig, I., Wang, R., Keeney, S., Jasin, M., 2012. Homeostatic control of recombination is implemented progressively in mouse meiosis. *Nat. Cell Biol.* 14, 424–430. <https://doi.org/10.1038/ncb2451>
- Costa, Y., Speed, R., Ollinger, R., Alsheimer, M., Semple, C.A., Gautier, P., Maratou, K., Novak, I., Höög, C., Benavente, R., Cooke, H.J., 2005. Two novel proteins recruited by synaptonemal complex protein 1 (SYCP1) are at the centre of meiosis. *J. Cell Sci.* 118, 2755–2762. <https://doi.org/10.1242/jcs.02402>
- Couteau, F., Belzile, F., Horlow, C., Grandjean, O., Vezon, D., Doutriaux, M.-P., 1999. Random Chromosome Segregation without Meiotic Arrest in Both Male and Female Meiocytes of a dmc1 Mutant of *Arabidopsis*. *Plant Cell* 11, 1623–1634. <https://doi.org/10.1105/tpc.11.9.1623>
- Crismani, W., Girard, C., Froger, N., Pradillo, M., Santos, J.L., Chelysheva, L., Copenhaver, G.P., Horlow, C., Mercier, R., 2012. FANCM limits meiotic crossovers. *Science* 336, 1588–1590. <https://doi.org/10.1126/science.1220381>
- Crismani, W., Portemer, V., Froger, N., Chelysheva, L., Horlow, C., Vrielynck, N., Mercier, R., 2013. MCM8 Is Required for a Pathway of Meiotic Double-Strand Break Repair Independent of DMC1 in *Arabidopsis thaliana*. *PLOS Genet.* 9, e1003165. <https://doi.org/10.1371/journal.pgen.1003165>
- Day, R.N., Davidson, M.W., 2009. The fluorescent protein palette: tools for cellular imaging. *Chem. Soc. Rev.* 38, 2887–2921. <https://doi.org/10.1039/b901966a>

- de los Santos, T., Hunter, N., Lee, C., Larkin, B., Loidl, J., Hollingsworth, N.M., 2003. The Mus81/Mms4 endonuclease acts independently of double-Holliday junction resolution to promote a distinct subset of crossovers during meiosis in budding yeast. *Genetics* 164, 81–94.
- De Muyt, A., Jessop, L., Kolar, E., Sourirajan, A., Chen, J., Dayani, Y., Lichten, M., 2012. BLM helicase ortholog Sgs1 is a central regulator of meiotic recombination intermediate metabolism. *Mol. Cell* 46, 43–53. <https://doi.org/10.1016/j.molcel.2012.02.020>
- De Muyt, A., Vezon, D., Gendrot, G., Gallois, J.-L., Stevens, R., Grelon, M., 2007. AtPRD1 is required for meiotic double strand break formation in *Arabidopsis thaliana*. *EMBO J.* 26, 4126–4137. <https://doi.org/10.1038/sj.emboj.7601815>
- Dernburg, A.F., McDonald, K., Moulder, G., Barstead, R., Dresser, M., Villeneuve, A.M., 1998. Meiotic recombination in *C. elegans* initiates by a conserved mechanism and is dispensable for homologous chromosome synapsis. *Cell* 94, 387–398.
- Deshong, A.J., Ye, A.L., Lamelza, P., Bhalla, N., 2014. A Quality Control Mechanism Coordinates Meiotic Prophase Events to Promote Crossover Assurance. *PLOS Genet.* 10, e1004291. <https://doi.org/10.1371/journal.pgen.1004291>
- Dickinson, D.J., Ward, J.D., Reiner, D.J., Goldstein, B., 2013. Engineering the *Caenorhabditis elegans* genome using Cas9-triggered homologous recombination. *Nat. Methods* 10, 1028–1034. <https://doi.org/10.1038/nmeth.2641>
- Dion, E., Li, L., Jean, M., Belzile, F., 2007. An *Arabidopsis* MLH1 mutant exhibits reproductive defects and reveals a dual role for this gene in mitotic recombination. *Plant J. Cell Mol. Biol.* 51, 431–440. <https://doi.org/10.1111/j.1365-313X.2007.03145.x>
- Dong, H., Roeder, G.S., 2000. Organization of the yeast Zip1 protein within the central region of the synaptonemal complex. *J. Cell Biol.* 148, 417–426. <https://doi.org/10.1083/jcb.148.3.417>
- Doutriaux, M.P., Couteau, F., Bergounioux, C., White, C., 1998. Isolation and characterisation of the RAD51 and DMC1 homologs from *Arabidopsis thaliana*. *Mol. Gen. Genet. MGG* 257, 283–291.
- Drouaud, J., Khademian, H., Giraut, L., Zanni, V., Bellalou, S., Henderson, I.R., Falque, M., Mézard, C., 2013. Contrasted Patterns of Crossover and Non-crossover at *Arabidopsis thaliana* Meiotic Recombination Hotspots. *PLOS Genet.* 9, e1003922. <https://doi.org/10.1371/journal.pgen.1003922>
- Drouaud, J., Mercier, R., Chelysheva, L., Bérard, A., Falque, M., Martin, O., Zanni, V., Brunel, D., Mézard, C., 2007. Sex-Specific Crossover Distributions and Variations in Interference Level along *Arabidopsis thaliana* Chromosome 4. *PLOS Genet.* 3, e106. <https://doi.org/10.1371/journal.pgen.0030106>
- Dubois, E., Muyt, A.D., Soyer, J.L., Budin, K., Legras, M., Piolot, T., Debuchy, R., Kleckner, N., Zickler, D., Espagne, E., 2019. Building bridges to move recombination complexes. *Proc. Natl. Acad. Sci.* 116, 12400–12409. <https://doi.org/10.1073/pnas.1901237116>
- Duroc, Y., Kumar, R., Ranjha, L., Adam, C., Guérois, R., Md Muntaz, K., Marsolier-Kergoat, M.-C., Dingli, F., Laureau, R., Loew, D., Llorente, B., Charbonnier, J.-B., Cejka, P., Börde, V., 2017. Concerted action of the MutL β heterodimer and Mer3 helicase regulates the global extent of meiotic gene conversion. *eLife* 6, e21900. <https://doi.org/10.7554/eLife.21900>
- Eichinger, C.S., Jentsch, S., 2010. Synaptonemal complex formation and meiotic checkpoint signaling are linked to the lateral element protein Red1. *Proc. Natl. Acad. Sci. U. S. A.* 107, 11370–11375. <https://doi.org/10.1073/pnas.1004248107>
- Engebrecht, J.A., Voelkel-Meiman, K., Roeder, G.S., 1991. Meiosis-specific RNA splicing in yeast. *Cell* 66, 1257–1268.
- Erayman, M., Sandhu, D., Sidhu, D., Dilbirligi, M., Baenziger, P.S., Gill, K.S., 2004. Demarcating the gene-rich regions of the wheat genome. *Nucleic Acids Res.* 32, 3546–3565. <https://doi.org/10.1093/nar/gkh639>

- Fauser, F., Schiml, S., Puchta, H., 2014. Both CRISPR/Cas-based nucleases and nickases can be used efficiently for genome engineering in *Arabidopsis thaliana*. *Plant J. Cell Mol. Biol.* 79, 348–359. <https://doi.org/10.1111/tpj.12554>
- Feng, Z., Mao, Y., Xu, N., Zhang, B., Wei, P., Yang, D.-L., Wang, Z., Zhang, Z., Zheng, R., Yang, L., Zeng, L., Liu, X., Zhu, J.-K., 2014. Multigeneration analysis reveals the inheritance, specificity, and patterns of CRISPR/Cas-induced gene modifications in *Arabidopsis*. *Proc. Natl. Acad. Sci.* 111, 4632–4637. <https://doi.org/10.1073/pnas.1400822111>
- Ferdous, M., Higgins, J.D., Osman, K., Lambing, C., Roitinger, E., Mechtler, K., Armstrong, S.J., Perry, R., Pradillo, M., Cuñado, N., Franklin, F.C.H., 2012a. Inter-homolog crossing-over and synapsis in *Arabidopsis* meiosis are dependent on the chromosome axis protein AtASY3. *PLoS Genet.* 8, e1002507. <https://doi.org/10.1371/journal.pgen.1002507>
- Ferdous, M., Higgins, J.D., Osman, K., Lambing, C., Roitinger, E., Mechtler, K., Armstrong, S.J., Perry, R., Pradillo, M., Cuñado, N., Franklin, F.C.H., 2012b. Inter-homolog crossing-over and synapsis in *Arabidopsis* meiosis are dependent on the chromosome axis protein AtASY3. *PLoS Genet.* 8, e1002507. <https://doi.org/10.1371/journal.pgen.1002507>
- Fernandes, J.B., Duhamel, M., Seguéla-Arnaud, M., Froger, N., Girard, C., Choinard, S., Solier, V., Winne, N.D., Jaeger, G.D., Gevaert, K., Andrey, P., Grelon, M., Guerois, R., Kumar, R., Mercier, R., 2018. FIGL1 and its novel partner FLIP form a conserved complex that regulates homologous recombination. *PLOS Genet.* 14, e1007317. <https://doi.org/10.1371/journal.pgen.1007317>
- Ferrari, S.R., Grubb, J., Bishop, D.K., 2009. The Mei5-Sae3 protein complex mediates Dmc1 activity in *Saccharomyces cerevisiae*. *J. Biol. Chem.* 284, 11766–11770. <https://doi.org/10.1074/jbc.C900023200>
- Food and Agriculture Organisation of the United Nations, 2009. How to Feed the World in 2050.
- Food and Agriculture Organisation of the United Nations, 2001. The State of Food Insecurity in the World [WWW Document]. URL <http://www.fao.org/3/y1500e/y1500e00.htm> (accessed 7.3.19).
- Food Security Information Network (FSIN) -Global Report [WWW Document], n.d. URL <http://www.fsincop.net/global-network/global-report/en/> (accessed 7.14.18).
- Forejt, J., 2001. Nondisjunction, in: Brenner, S., Miller, J.H. (Eds.), *Encyclopedia of Genetics*. Academic Press, New York, pp. 1345–1347. <https://doi.org/10.1006/rwgn.2001.0903>
- Foss, E., Lande, R., Stahl, F.W., Steinberg, C.M., 1993. Chiasma interference as a function of genetic distance. *Genetics* 133, 681–691.
- Franklin, F.C.H., Higgins, J.D., Sanchez-Moran, E., Armstrong, S.J., Osman, K.E., Jackson, N., Jones, G.H., 2006. Control of meiotic recombination in *Arabidopsis*: role of the MutL and MutS homologues. *Biochem. Soc. Trans.* 34, 542–544. <https://doi.org/10.1042/BST0340542>
- Friedland, A.E., Tzur, Y.B., Esvelt, K.M., Colaiácovo, M.P., Church, G.M., Calarco, J.A., 2013. Heritable genome editing in *C. elegans* via a CRISPR-Cas9 system. *Nat. Methods* 10, 741–743. <https://doi.org/10.1038/nmeth.2532>
- Fu, H., Park, W., Yan, X., Zheng, Z., Shen, B., Dooner, H.K., 2001. The highly recombinogenic bz locus lies in an unusually gene-rich region of the maize genome. *Proc. Natl. Acad. Sci. U. S. A.* 98, 8903–8908. <https://doi.org/10.1073/pnas.141221898>
- Fukuda, T., Fukuda, N., Agostinho, A., Hernández-Hernández, A., Kouzenetsova, A., Höög, C., 2014. STAG3-mediated stabilization of REC8 cohesin complexes promotes chromosome synapsis during meiosis. *EMBO J.* 33, 1243–1255. <https://doi.org/10.1002/embj.201387329>
- Fukuda, T., Pratto, F., Schimenti, J.C., Turner, J.M.A., Camerini-Otero, R.D., Höög, C., 2012. Phosphorylation of chromosome core components may serve as axis marks

- for the status of chromosomal events during mammalian meiosis. *PLoS Genet.* 8, e1002485. <https://doi.org/10.1371/journal.pgen.1002485>
- Fung, J.C., Rockmill, B., Odell, M., Roeder, G.S., 2004. Imposition of crossover interference through the nonrandom distribution of synapsis initiation complexes. *Cell* 116, 795–802. [https://doi.org/10.1016/s0092-8674\(04\)00249-1](https://doi.org/10.1016/s0092-8674(04)00249-1)
- Gasior, S.L., Wong, A.K., Kora, Y., Shinohara, A., Bishop, D.K., 1998. Rad52 associates with RPA and functions with rad55 and rad57 to assemble meiotic recombination complexes. *Genes Dev.* 12, 2208–2221.
- Gilbertson, L.A., Stahl, F.W., 1996. A Test of the Double-Strand Break Repair Model for Meiotic Recombination in *Saccharomyces Cerevisiae*. *Genetics* 144, 27–41.
- Girard, C., Chelysheva, L., Choinard, S., Frogé, N., Macaisne, N., Lemhemdi, A., Lehmemdi, A., Mazel, J., Crismani, W., Mercier, R., 2015. AAA-ATPase FIDGETIN-LIKE 1 and Helicase FANCM Antagonize Meiotic Crossovers by Distinct Mechanisms. *PLoS Genet.* 11, e1005369. <https://doi.org/10.1371/journal.pgen.1005369>
- Girard, C., Crismani, W., Frogé, N., Mazel, J., Lemhemdi, A., Horlow, C., Mercier, R., 2014. FANCM-associated proteins MHF1 and MHF2, but not the other Fanconi anemia factors, limit meiotic crossovers. *Nucleic Acids Res.* 42, 9087–9095. <https://doi.org/10.1093/nar/gku614>
- Global Partnership Initiative for Plant Breeding Capacity Building (FAO), n.d. Plant Breeding Impacts and Current Challenges.
- Grabarz, A., Guirouilh-Barbat, J., Barascu, A., Pennarun, G., Genet, D., Rass, E., Germann, S.M., Bertrand, P., Hickson, I.D., Lopez, B.S., 2013. A Role for BLM in Double-Strand Break Repair Pathway Choice: Prevention of CtIP/Mre11-Mediated Alternative Nonhomologous End-Joining. *Cell Rep.* 5, 21–28. <https://doi.org/10.1016/j.celrep.2013.08.034>
- Grelon, M., Vezon, D., Gendrot, G., Pelletier, G., 2001. AtSPO11-1 is necessary for efficient meiotic recombination in plants. *EMBO J.* 20, 589–600. <https://doi.org/10.1093/emboj/20.3.589>
- Guiraldelli, M.F., Eyster, C., Wilkerson, J.L., Dresser, M.E., Pezza, R.J., 2013. Mouse HFM1/Mer3 is required for crossover formation and complete synapsis of homologous chromosomes during meiosis. *PLoS Genet.* 9, e1003383. <https://doi.org/10.1371/journal.pgen.1003383>
- Guirouilh-Barbat, J., Huck, S., Bertrand, P., Pirzio, L., Desmaze, C., Sabatier, L., Lopez, B.S., 2004. Impact of the KU80 Pathway on NHEJ-Induced Genome Rearrangements in Mammalian Cells. *Mol. Cell* 14, 611–623. <https://doi.org/10.1016/j.molcel.2004.05.008>
- Hamer, G., Gell, K., Kouznetsova, A., Novak, I., Benavente, R., Höög, C., 2006. Characterization of a novel meiosis-specific protein within the central element of the synaptonemal complex. *J. Cell Sci.* 119, 4025–4032. <https://doi.org/10.1242/jcs.03182>
- Hara, K., Hashimoto, H., Murakumo, Y., Kobayashi, S., Kogame, T., Unzai, S., Akashi, S., Takeda, S., Shimizu, T., Sato, M., 2010. Crystal structure of human REV7 in complex with a human REV3 fragment and structural implication of the interaction between DNA polymerase zeta and REV1. *J. Biol. Chem.* 285, 12299–12307. <https://doi.org/10.1074/jbc.M109.092403>
- Hartung, F., Puchta, H., 2000. Molecular characterisation of two paralogous SPO11 homologues in *Arabidopsis thaliana*. *Nucleic Acids Res.* 28, 1548–1554.
- Hartung, F., Suer, S., Knoll, A., Wurz-Wildersinn, R., Puchta, H., 2008. Topoisomerase 3 α and RMI1 Suppress Somatic Crossovers and Are Essential for Resolution of Meiotic Recombination Intermediates in *Arabidopsis thaliana*. *PLOS Genet.* 4, e1000285. <https://doi.org/10.1371/journal.pgen.1000285>
- Hartung, F., Suer, S., Puchta, H., 2007a. Two closely related RecQ helicases have antagonistic roles in homologous recombination and DNA repair in *Arabidopsis*

- thaliana. Proc. Natl. Acad. Sci. U. S. A. 104, 18836–18841.
<https://doi.org/10.1073/pnas.0705998104>
- Hartung, F., Wurz-Wildersinn, R., Fuchs, J., Schubert, I., Suer, S., Puchta, H., 2007b. The catalytically active tyrosine residues of both SPO11-1 and SPO11-2 are required for meiotic double-strand break induction in Arabidopsis. Plant Cell 19, 3090–3099.
<https://doi.org/10.1105/tpc.107.054817>
- Hayase, A., Takagi, M., Miyazaki, T., Oshiumi, H., Shinohara, M., Shinohara, A., 2004. A protein complex containing Mei5 and Sae3 promotes the assembly of the meiosis-specific RecA homolog Dmc1. Cell 119, 927–940.
<https://doi.org/10.1016/j.cell.2004.10.031>
- He, W., Rao, H.B.D.P., Tang, S., Bhagwat, N., Kulkarni, D.S., Chang, M.A.W., Hall, C., Singh, L., Chen, X., Hollingsworth, N.M., Cejka, P., Hunter, N., 2018. The crossover function of MutSy is activated via Cdc7-dependent stabilization of Msh4. bioRxiv 386458. <https://doi.org/10.1101/386458>
- He, Y., Wang, M., Dukowic-Schulze, S., Zhou, A., Tiang, C.-L., Shilo, S., Sidhu, G.K., Eichten, S., Bradbury, P., Springer, N.M., Buckler, E.S., Levy, A.A., Sun, Q., Pillardy, J., Kianian, P.M.A., Kianian, S.F., Chen, C., Pawlowski, W.P., 2017. Genomic features shaping the landscape of meiotic double-strand-break hotspots in maize. Proc. Natl. Acad. Sci. 114, 12231–12236. <https://doi.org/10.1073/pnas.1713225114>
- Hermans, P.W., van Soelingen, D., Bik, E.M., de Haas, P.E., Dale, J.W., van Embden, J.D., 1991. Insertion element IS987 from Mycobacterium bovis BCG is located in a hot-spot integration region for insertion elements in Mycobacterium tuberculosis complex strains. Infect. Immun. 59, 2695–2705.
- Higgins, J.D., Armstrong, S.J., Franklin, F.C.H., Jones, G.H., 2004. The Arabidopsis MutS homolog AtMSH4 functions at an early step in recombination: evidence for two classes of recombination in Arabidopsis. Genes Dev. 18, 2557–2570.
<https://doi.org/10.1101/gad.317504>
- Higgins, J.D., Buckling, E.F., Franklin, F.C.H., Jones, G.H., 2008a. Expression and functional analysis of AtMUS81 in Arabidopsis meiosis reveals a role in the second pathway of crossing-over. Plant J. Cell Mol. Biol. 54, 152–162.
<https://doi.org/10.1111/j.1365-313X.2008.03403.x>
- Higgins, J.D., Ferdous, M., Osman, K., Franklin, F.C.H., 2011. The RecQ helicase AtRECQL is required to remove inter-chromosomal telomeric connections that arise during meiotic recombination in Arabidopsis. Plant J. Cell Mol. Biol. 65, 492–502.
<https://doi.org/10.1111/j.1365-313X.2010.04438.x>
- Higgins, J.D., Perry, R.M., Barakate, A., Ramsay, L., Waugh, R., Halpin, C., Armstrong, S.J., Franklin, F.C.H., 2012. Spatiotemporal asymmetry of the meiotic program underlies the predominantly distal distribution of meiotic crossovers in barley. Plant Cell 24, 4096–4109. <https://doi.org/10.1105/tpc.112.102483>
- Higgins, J.D., Sanchez-Moran, E., Armstrong, S.J., Jones, G.H., Franklin, F.C.H., 2005. The Arabidopsis synaptonemal complex protein ZYP1 is required for chromosome synapsis and normal fidelity of crossing over. Genes Dev. 19, 2488–2500.
<https://doi.org/10.1101/gad.354705>
- Higgins, J.D., Vignard, J., Mercier, R., Pugh, A.G., Franklin, F.C.H., Jones, G.H., 2008b. AtMSH5 partners AtMSH4 in the class I meiotic crossover pathway in Arabidopsis thaliana, but is not required for synapsis. Plant J. Cell Mol. Biol. 55, 28–39.
<https://doi.org/10.1111/j.1365-313X.2008.03470.x>
- Ho, H.-C., Burgess, S.M., 2011. Pch2 Acts through Xrs2 and Tel1/ATM to Modulate Interhomolog Bias and Checkpoint Function during Meiosis. PLOS Genet. 7, e1002351. <https://doi.org/10.1371/journal.pgen.1002351>
- Holliday, R., 1964. A mechanism for gene conversion in fungi. Genet. Res. 5, 282–304.
<https://doi.org/10.1017/S0016672300001233>
- Hollingsworth, N.M., Ponte, L., 1997. Genetic interactions between HOP1, RED1 and MEK1 suggest that MEK1 regulates assembly of axial element components during meiosis in the yeast *Saccharomyces cerevisiae*. Genetics 147, 33–42.

- Hou, Y., Fan, W., Yan, L., Li, R., Lian, Y., Huang, J., Li, J., Xu, L., Tang, F., Xie, X.S., Qiao, J., 2013. Genome analyses of single human oocytes. *Cell* 155, 1492–1506. <https://doi.org/10.1016/j.cell.2013.11.040>
- Hunter, N., Kleckner, N., 2001. The single-end invasion: an asymmetric intermediate at the double-strand break to double-holliday junction transition of meiotic recombination. *Cell* 106, 59–70. [https://doi.org/10.1016/s0092-8674\(01\)00430-5](https://doi.org/10.1016/s0092-8674(01)00430-5)
- Hyppa, R.W., Smith, G.R., 2010. Crossover Invariance Determined by Partner Choice for Meiotic DNA Break Repair. *Cell* 142, 243–255. <https://doi.org/10.1016/j.cell.2010.05.041>
- Hyun, Y., Kim, J., Cho, S.W., Choi, Y., Kim, J.-S., Coupland, G., 2015. Site-directed mutagenesis in *Arabidopsis thaliana* using dividing tissue-targeted RGEN of the CRISPR/Cas system to generate heritable null alleles. *Planta* 241, 271–284. <https://doi.org/10.1007/s00425-014-2180-5>
- Ines, O.D., Degroote, F., Goubely, C., Amiard, S., Gallego, M.E., White, C.I., 2013. Meiotic Recombination in *Arabidopsis* Is Catalysed by DMC1, with RAD51 Playing a Supporting Role. *PLOS Genet.* 9, e1003787. <https://doi.org/10.1371/journal.pgen.1003787>
- Ishino, Y., Shinagawa, H., Makino, K., Amemura, M., Nakata, A., 1987. Nucleotide sequence of the iap gene, responsible for alkaline phosphatase isozyme conversion in *Escherichia coli*, and identification of the gene product. *J. Bacteriol.* 169, 5429–5433. <https://doi.org/10.1128/jb.169.12.5429-5433.1987>
- Jackson, N., Sanchez-Moran, E., Buckling, E., Armstrong, S.J., Jones, G.H., Franklin, F.C.H., 2006. Reduced meiotic crossovers and delayed prophase I progression in AtMLH3-deficient *Arabidopsis*. *EMBO J.* 25, 1315–1323. <https://doi.org/10.1038/sj.emboj.7600992>
- Jahns, M.T., Vezon, D., Chambon, A., Pereira, L., Falque, M., Martin, O.C., Chelysheva, L., Grelon, M., 2014. Crossover Localisation Is Regulated by the Neddylation Posttranslational Regulatory Pathway. *PLOS Biol.* 12, e1001930. <https://doi.org/10.1371/journal.pbio.1001930>
- Jansen, R., Embden, J.D.A. van, Gaastraa, W., Schouls, L.M., 2002. Identification of genes that are associated with DNA repeats in prokaryotes. *Mol. Microbiol.* 43, 1565–1575. <https://doi.org/10.1046/j.1365-2958.2002.02839.x>
- Jinek, M., Chylinski, K., Fonfara, I., Hauer, M., Doudna, J.A., Charpentier, E., 2012. A programmable dual-RNA-guided DNA endonuclease in adaptive bacterial immunity. *Science* 337, 816–821. <https://doi.org/10.1126/science.1225829>
- Jolivet, S., Vezon, D., Froger, N., Mercier, R., 2006. Non conservation of the meiotic function of the Ski8/Rec103 homolog in *Arabidopsis*. *Genes Cells* 11, 615–622. <https://doi.org/10.1111/j.1365-2443.2006.00972.x>
- Jones, G.H., Franklin, F.C.H., 2006. Meiotic Crossing-over: Obligation and Interference. *Cell* 126, 246–248. <https://doi.org/10.1016/j.cell.2006.07.010>
- Joshi, N., Barot, A., Jamison, C., Börner, G.V., 2009. Pch2 Links Chromosome Axis Remodeling at Future Crossover Sites and Crossover Distribution during Yeast Meiosis. *PLOS Genet* 5, e1000557. <https://doi.org/10.1371/journal.pgen.1000557>
- Joyce, E.F., Pedersen, M., Tiong, S., White-Brown, S.K., Paul, A., Campbell, S.D., McKim, K.S., 2011. *Drosophila* ATM and ATR have distinct activities in the regulation of meiotic DNA damage and repair. *J Cell Biol* 195, 359–367. <https://doi.org/10.1083/jcb.201104121>
- Kaur, H., De Muyt, A., Lichten, M., 2015. Top3-Rmi1 DNA Single-Strand Decatenase Is Integral to the Formation and Resolution of Meiotic Recombination Intermediates. *Mol. Cell* 57, 583–594. <https://doi.org/10.1016/j.molcel.2015.01.020>
- Keeney, S., Giroux, C.N., Kleckner, N., 1997. Meiosis-specific DNA double-strand breaks are catalyzed by Spo11, a member of a widely conserved protein family. *Cell* 88, 375–384.

- Kerr, G.W., Sarkar, S., Arumugam, P., 2012. How to halve ploidy: lessons from budding yeast meiosis. *Cell. Mol. Life Sci.* CMLS 69, 3037–3051. <https://doi.org/10.1007/s00018-012-0974-9>
- Kim, K.P., Weiner, B.M., Zhang, L., Jordan, A., Dekker, J., Kleckner, N., 2010. Sister cohesion and structural axis components mediate homolog bias of meiotic recombination. *Cell* 143, 924–937. <https://doi.org/10.1016/j.cell.2010.11.015>
- Kim, Y., Rosenberg, S.C., Kugel, C.L., Kostow, N., Rog, O., Davydov, V., Su, T.Y., Dernburg, A.F., Corbett, K.D., 2014. The Chromosome Axis Controls Meiotic Events through a Hierarchical Assembly of HORMA Domain Proteins. *Dev. Cell* 31, 487–502. <https://doi.org/10.1016/j.devcel.2014.09.013>
- Kim, Y.G., Cha, J., Chandrasegaran, S., 1996. Hybrid restriction enzymes: zinc finger fusions to Fok I cleavage domain. *Proc. Natl. Acad. Sci. U. S. A.* 93, 1156–1160.
- King, J.S., Mortimer, R.K., 1990. A polymerization model of chiasma interference and corresponding computer simulation. *Genetics* 126, 1127–1138.
- Kleckner, N., Zickler, D., Jones, G.H., Dekker, J., Padmore, R., Henle, J., Hutchinson, J., 2004. A mechanical basis for chromosome function. *Proc. Natl. Acad. Sci. U. S. A.* 101, 12592–12597. <https://doi.org/10.1073/pnas.0402724101>
- Knoll, A., Higgins, J.D., Seeliger, K., Reha, S.J., Dangel, N.J., Bauknecht, M., Schröpfer, S., Franklin, F.C.H., Puchta, H., 2012. The Fanconi Anemia Ortholog FANCM Ensures Ordered Homologous Recombination in Both Somatic and Meiotic Cells in *Arabidopsis*[W]. *Plant Cell* 24, 1448–1464. <https://doi.org/10.1105/tpc.112.096644>
- Koonin, E.V., Makarova, K.S., Zhang, F., 2017. Diversity, classification and evolution of CRISPR-Cas systems. *Curr. Opin. Microbiol.* 37, 67–78. <https://doi.org/10.1016/j.mib.2017.05.008>
- Kouznetsova, A., Novak, I., Jessberger, R., Höög, C., 2005. SYCP2 and SYCP3 are required for cohesin core integrity at diplotene but not for centromere cohesion at the first meiotic division. *J. Cell Sci.* 118, 2271–2278. <https://doi.org/10.1242/jcs.02362>
- Künzel, G., Korzun, L., Meister, A., 2000. Cytologically integrated physical restriction fragment length polymorphism maps for the barley genome based on translocation breakpoints. *Genetics* 154, 397–412.
- Künzel, G., Waugh, R., 2002. Integration of microsatellite markers into the translocation-based physical RFLP map of barley chromosome 3H. *TAG Theor. Appl. Genet. Theor. Angew. Genet.* 105, 660–665. <https://doi.org/10.1007/s00122-002-0913-5>
- Kurzbauer, M.-T., Pradillo, M., Kerzendorfer, C., Sims, J., Ladurner, R., Oliver, C., Janisiw, M.P., Mosiolek, M., Schweizer, D., Copenhaver, G.P., Schlögelhofer, P., 2018. *Arabidopsis thaliana* FANCD2 Promotes Meiotic Crossover Formation. *Plant Cell* 30, 415–428. <https://doi.org/10.1105/tpc.17.00745>
- Kurzbauer, M.-T., Uanschou, C., Chen, D., Schlögelhofer, P., 2012. The Recombinases DMC1 and RAD51 Are Functionally and Spatially Separated during Meiosis in *Arabidopsis*. *Plant Cell* 24, 2058–2070. <https://doi.org/10.1105/tpc.112.098459>
- Lake, C.M., Nielsen, R.J., Guo, F., Unruh, J.R., Slaughter, B.D., Hawley, R.S., 2015. Vilya, a component of the recombination nodule, is required for meiotic double-strand break formation in *Drosophila*. *eLife* 4, e08287. <https://doi.org/10.7554/eLife.08287>
- Lam, I., Keeney, S., 2014. Mechanism and regulation of meiotic recombination initiation. *Cold Spring Harb. Perspect. Biol.* 7, a016634. <https://doi.org/10.1101/cspperspect.a016634>
- Lam, W.S., Yang, X., Makaroff, C.A., 2005. Characterization of *Arabidopsis thaliana* SMC1 and SMC3: evidence that AtSMC3 may function beyond chromosome cohesion. *J. Cell Sci.* 118, 3037–3048. <https://doi.org/10.1242/jcs.02443>
- Lambing, C., Franklin, F.C.H., Wang, C.-J.R., 2017. Understanding and Manipulating Meiotic Recombination in Plants[OPEN]. *Plant Physiol.* 173, 1530–1542. <https://doi.org/10.1104/pp.16.01530>
- Lambing, C., Osman, K., Nuntasoontorn, K., West, A., Higgins, J.D., Copenhaver, G.P., Yang, J., Armstrong, S.J., Mechtler, K., Roitinger, E., Franklin, F.C.H., 2015. *Arabidopsis PCH2* Mediates Meiotic Chromosome Remodeling and Maturation of

- Crossovers. PLoS Genet. 11, e1005372.
<https://doi.org/10.1371/journal.pgen.1005372>
- Lambing, C., Tock, A.J., Choi, K., Topp, S.D., Kuo, P.C., Blackwell, A.R., Zhao, X., Osman, K., Higgins, J.D., Franklin, F.C.H., Henderson, I.R., 2019. REC8-cohesin, chromatin and transcription orchestrate meiotic recombination in the *Arabidopsis* genome. bioRxiv 512400. <https://doi.org/10.1101/512400>
- Lampson, M.A., Cheeseman, I.M., 2011. Sensing centromere tension: Aurora B and the regulation of kinetochore function. Trends Cell Biol. 21, 133–140.
<https://doi.org/10.1016/j.tcb.2010.10.007>
- Lange, J., Pan, J., Cole, F., Thelen, M.P., Jasen, M., Keeney, S., 2011. ATM controls meiotic double-strand-break formation. Nature 479, 237–240.
<https://doi.org/10.1038/nature10508>
- Lange, J., Yamada, S., Tischfield, S.E., Pan, J., Kim, S., Zhu, X., Socci, N.D., Jasen, M., Keeney, S., 2016. The Landscape of Mouse Meiotic Double-Strand Break Formation, Processing, and Repair. Cell 167, 695-708.e16.
<https://doi.org/10.1016/j.cell.2016.09.035>
- Lawrenson, T., Shorinola, O., Stacey, N., Li, C., Østergaard, L., Patron, N., Uauy, C., Harwood, W., 2015. Induction of targeted, heritable mutations in barley and *Brassica oleracea* using RNA-guided Cas9 nuclease. Genome Biol. 16, 258.
<https://doi.org/10.1186/s13059-015-0826-7>
- Lee, K., Lee, S.E., 2007. *Saccharomyces cerevisiae* Sae2- and Tel1-Dependent Single-Strand DNA Formation at DNA Break Promotes Microhomology-Mediated End Joining. Genetics 176, 2003–2014. <https://doi.org/10.1534/genetics.107.076539>
- Lhuissier, F.G.P., Offenberg, H.H., Wittich, P.E., Vischer, N.O.E., Heyting, C., 2007. The Mismatch Repair Protein MLH1 Marks a Subset of Strongly Interfering Crossovers in Tomato. Plant Cell 19, 862–876. <https://doi.org/10.1105/tpc.106.049106>
- Li, J., Hooker, G.W., Roeder, G.S., 2006. *Saccharomyces cerevisiae* Mer2, Mei4 and Rec114 form a complex required for meiotic double-strand break formation. Genetics 173, 1969–1981. <https://doi.org/10.1534/genetics.106.058768>
- Li, J.-F., Norville, J.E., Aach, J., McCormack, M., Zhang, D., Bush, J., Church, G.M., Sheen, J., 2013. Multiplex and homologous recombination-mediated genome editing in *Arabidopsis* and *Nicotiana benthamiana* using guide RNA and Cas9 [WWW Document]. Nat. Biotechnol. <https://doi.org/10.1038/nbt.2654>
- Li, W., Chen, C., Markmann-Mulisch, U., Timofejeva, L., Schmelzer, E., Ma, H., Reiss, B., 2004. The *Arabidopsis* AtRAD51 gene is dispensable for vegetative development but required for meiosis. Proc. Natl. Acad. Sci. U. S. A. 101, 10596–10601.
<https://doi.org/10.1073/pnas.0404110101>
- Li, X., Li, L., Yan, J., 2015. Dissecting meiotic recombination based on tetrad analysis by single-micropore sequencing in maize. Nat. Commun. 6, 6648.
<https://doi.org/10.1038/ncomms7648>
- Li, Y., Qin, B., Shen, Y., Zhang, F., Liu, C., You, H., Du, G., Tang, D., Cheng, Z., 2018. HEIP1 regulates crossover formation during meiosis in rice. Proc. Natl. Acad. Sci. U. S. A. 115, 10810–10815. <https://doi.org/10.1073/pnas.1807871115>
- Liang, F., Romanienko, P.J., Weaver, D.T., Jeggo, P.A., Jasen, M., 1996. Chromosomal double-strand break repair in Ku80-deficient cells. Proc. Natl. Acad. Sci. 93, 8929–8933. <https://doi.org/10.1073/pnas.93.17.8929>
- Lin, F.-M., Lai, Y.-J., Shen, H.-J., Cheng, Y.-H., Wang, T.-F., 2010. Yeast axial-element protein, Red1, binds SUMO chains to promote meiotic interhomologue recombination and chromosome synapsis. EMBO J. 29, 586–596.
<https://doi.org/10.1038/emboj.2009.362>
- Lin, Y., Smith, G.R., 1994. Transient, meiosis-induced expression of the rec6 and rec12 genes of *Schizosaccharomyces pombe*. Genetics 136, 769–779.
- Liu, J.G., Yuan, L., Brundell, E., Björkroth, B., Daneholt, B., Höög, C., 1996. Localization of the N-terminus of SCP1 to the central element of the synaptonemal complex and

- evidence for direct interactions between the N-termini of SCP1 molecules organized head-to-head. *Exp. Cell Res.* 226, 11–19. <https://doi.org/10.1006/excr.1996.0197>
- Liu, Y., Merchant, Z., Hsiao, H.-C., Gonzalez, K.L., Matthews, K.S., Bondos, S.E., 2011. Media composition influences yeast one- and two-hybrid results. *Biol. Proced. Online* 13, 6. <https://doi.org/10.1186/1480-9222-13-6>
- Lloyd, A., Morgan, C., Franklin, F.C.H., Bomblies, K., 2018. Plasticity of Meiotic Recombination Rates in Response to Temperature in *Arabidopsis*. *Genetics* 208, 1409–1420. <https://doi.org/10.1534/genetics.117.300588>
- Lu, P., Wijeratne, A.J., Wang, Z., Copenhaver, G.P., Ma, H., 2014. *Arabidopsis* PTD Is Required for Type I Crossover Formation and Affects Recombination Frequency in Two Different Chromosomal Regions. *J. Genet. Genomics, Special Issue: Meiosis* 41, 165–175. <https://doi.org/10.1016/j.jgg.2014.02.001>
- Luo, X., Tang, Z., Rizo, J., Yu, H., 2002. The Mad2 spindle checkpoint protein undergoes similar major conformational changes upon binding to either Mad1 or Cdc20. *Mol. Cell* 9, 59–71.
- Ma, X., Zhu, Q., Chen, Y., Liu, Y.-G., 2016. CRISPR/Cas9 Platforms for Genome Editing in Plants: Developments and Applications. *Mol. Plant* 9, 961–974. <https://doi.org/10.1016/j.molp.2016.04.009>
- Macaisne, N., Novatchkova, M., Peirera, L., Vezon, D., Jolivet, S., Froger, N., Chelysheva, L., Grelon, M., Mercier, R., 2008. SHOC1, an XPF Endonuclease-Related Protein, Is Essential for the Formation of Class I Meiotic Crossovers. *Curr. Biol.* 18, 1432–1437. <https://doi.org/10.1016/j.cub.2008.08.041>
- Macaisne, N., Vignard, J., Mercier, R., 2011. SHOC1 and PTD form an XPF–ERCC1-like complex that is required for formation of class I crossovers. *J. Cell Sci.* 124, 2687–2691. <https://doi.org/10.1242/jcs.088229>
- Macqueen, A.J., Roeder, G.S., 2009. Fpr3 and Zip3 ensure that initiation of meiotic recombination precedes chromosome synapsis in budding yeast. *Curr. Biol. CB* 19, 1519–1526. <https://doi.org/10.1016/j.cub.2009.08.048>
- Malapeira, J., Moldón, A., Hidalgo, E., Smith, G.R., Nurse, P., Ayté, J., 2005. A meiosis-specific cyclin regulated by splicing is required for proper progression through meiosis. *Mol. Cell. Biol.* 25, 6330–6337. <https://doi.org/10.1128/MCB.25.15.6330-6337.2005>
- Mao-Draayer, Y., Galbraith, A.M., Pittman, D.L., Cool, M., Malone, R.E., 1996. Analysis of meiotic recombination pathways in the yeast *Saccharomyces cerevisiae*. *Genetics* 144, 71–86.
- Marand, A.P., Jansky, S.H., Zhao, H., Leisner, C.P., Zhu, X., Zeng, Z., Crisovan, E., Newton, L., Hamernik, A.J., Veilleux, R.E., Buell, C.R., Jiang, J., 2017. Meiotic crossovers are associated with open chromatin and enriched with Stowaway transposons in potato. *Genome Biol.* 18, 203. <https://doi.org/10.1186/s13059-017-1326-8>
- Marand, A.P., Zhao, H., Zhang, W., Zeng, Z., Fang, C., Jiang, J., 2019. Historical Meiotic Crossover Hotspots Fueled Patterns of Evolutionary Divergence in Rice. *Plant Cell* 31, 645–662. <https://doi.org/10.1105/tpc.18.00750>
- Martinez-Garcia, M., Schubert, V., Osman, K., Darbyshire, A., Sanchez-Moran, E., Franklin, F.C.H., 2018. TOPII and chromosome movement help remove interlocks between entangled chromosomes during meiosis. *J Cell Biol* 217, 4070–4079. <https://doi.org/10.1083/jcb.201803019>
- Martini, E., Diaz, R.L., Hunter, N., Keeney, S., 2006. Crossover homeostasis in yeast meiosis. *Cell* 126, 285–295. <https://doi.org/10.1016/j.cell.2006.05.044>
- Mayer, K.F.X., Martis, M., Hedley, P.E., Simková, H., Liu, H., Morris, J.A., Steuernagel, B., Taudien, S., Roessner, S., Gundlach, H., Kubaláková, M., Suchánková, P., Murat, F., Felder, M., Nussbaumer, T., Graner, A., Salse, J., Endo, T., Sakai, H., Tanaka, T., Itoh, T., Sato, K., Platzer, M., Matsumoto, T., Scholz, U., Dolezel, J., Waugh, R., Stein, N., 2011. Unlocking the barley genome by chromosomal and comparative genomics. *Plant Cell* 23, 1249–1263. <https://doi.org/10.1105/tpc.110.082537>

- Mazina, O.M., Mazin, A.V., Nakagawa, T., Kolodner, R.D., Kowalczykowski, S.C., 2004. *Saccharomyces cerevisiae* Mer3 helicase stimulates 3'-5' heteroduplex extension by Rad51; implications for crossover control in meiotic recombination. *Cell* 117, 47–56. [https://doi.org/10.1016/s0092-8674\(04\)00294-6](https://doi.org/10.1016/s0092-8674(04)00294-6)
- Mazón, G., Symington, L.S., 2013. Mph1 and Mus81-Mms4 prevent aberrant processing of mitotic recombination intermediates. *Mol. Cell* 52, 63–74. <https://doi.org/10.1016/j.molcel.2013.09.007>
- McIntosh, J.R., 2016. Mitosis. *Cold Spring Harb. Perspect. Biol.* 8. <https://doi.org/10.1101/cshperspect.a023218>
- McMahill, M.S., Sham, C.W., Bishop, D.K., 2007. Synthesis-Dependent Strand Annealing in Meiosis. *PLOS Biol.* 5, e299. <https://doi.org/10.1371/journal.pbio.0050299>
- Mehla, J., Caufield, J.H., Uetz, P., 2015. The yeast two-hybrid system: a tool for mapping protein-protein interactions. *Cold Spring Harb. Protoc.* 2015, 425–430. <https://doi.org/10.1101/pdb.top083345>
- Mehrrotra, S., McKim, K.S., 2006. Temporal Analysis of Meiotic DNA Double-Strand Break Formation and Repair in *Drosophila* Females. *PLOS Genet.* 2, e200. <https://doi.org/10.1371/journal.pgen.0020200>
- Mercier, R., Jolivet, S., Vezon, D., Huppe, E., Chelysheva, L., Giovanni, M., Nogué, F., Doutriaux, M.-P., Horlow, C., Grelon, M., Mézard, C., 2005. Two Meiotic Crossover Classes Cohabit in *Arabidopsis*: One Is Dependent on MER3, whereas the Other One Is Not. *Curr. Biol.* 15, 692–701. <https://doi.org/10.1016/j.cub.2005.02.056>
- Mercier, R., Vezon, D., Bullier, E., Motamayor, J.C., Sellier, A., Lefèvre, F., Pelletier, G., Horlow, C., 2001. SWITCH1 (SWI1): a novel protein required for the establishment of sister chromatid cohesion and for bivalent formation at meiosis. *Genes Dev.* 15, 1859–1871. <https://doi.org/10.1101/gad.203201>
- Miao, C., Tang, D., Zhang, H., Wang, M., Li, Y., Tang, S., Yu, H., Gu, M., Cheng, Z., 2013. Central region component1, a novel synaptonemal complex component, is essential for meiotic recombination initiation in rice. *Plant Cell* 25, 2998–3009. <https://doi.org/10.1105/tpc.113.113175>
- Miller, J.C., Tan, S., Qiao, G., Barlow, K.A., Wang, J., Xia, D.F., Meng, X., Paschon, D.E., Leung, E., Hinkley, S.J., Dulay, G.P., Hua, K.L., Ankoudinova, I., Cost, G.J., Urnov, F.D., Zhang, H.S., Holmes, M.C., Zhang, L., Gregory, P.D., Rebar, E.J., 2011. A TALE nuclease architecture for efficient genome editing. *Nat. Biotechnol.* 29, 143–148. <https://doi.org/10.1038/nbt.1755>
- Mimitou, E.P., Symington, L.S., 2009. DNA end resection: many nucleases make light work. *DNA Repair* 8, 983–995. <https://doi.org/10.1016/j.dnarep.2009.04.017>
- Miné-Hattab, J., Rothstein, R., 2012. Increased chromosome mobility facilitates homology search during recombination. *Nat. Cell Biol.* 14, 510–517. <https://doi.org/10.1038/ncb2472>
- Mitchel, K., Lehner, K., Jinks-Robertson, S., 2013. Heteroduplex DNA position defines the roles of the Sgs1, Srs2, and Mph1 helicases in promoting distinct recombination outcomes. *PLoS Genet.* 9, e1003340. <https://doi.org/10.1371/journal.pgen.1003340>
- Mojica, F.J., Juez, G., Rodríguez-Valera, F., 1993. Transcription at different salinities of *Haloferax mediterranei* sequences adjacent to partially modified PstI sites. *Mol. Microbiol.* 9, 613–621.
- Mojica, F.J.M., Díez-Villaseñor, C., García-Martínez, J., Soria, E., 2005. Intervening sequences of regularly spaced prokaryotic repeats derive from foreign genetic elements. *J. Mol. Evol.* 60, 174–182. <https://doi.org/10.1007/s00239-004-0046-3>
- Moses, M.J., 1956. Chromosomal structures in crayfish spermatocytes. *J. Biophys. Biochem. Cytol.* 2, 215–218. <https://doi.org/10.1083/jcb.2.2.215>
- Muller, H.J., 1916. The Mechanism of Crossing-Over. *Am. Nat.* 50, 193–221.
- Murashige, T., Skoog, F., 1962. A Revised Medium for Rapid Growth and Bio Assays with Tobacco Tissue Cultures. *Physiol. Plant.* 15, 473–497. <https://doi.org/10.1111/j.1399-3054.1962.tb08052.x>

- Muyt, A.D., Pereira, L., Vezon, D., Chelysheva, L., Gendrot, G., Chambon, A., Lainé-Choinard, S., Pelletier, G., Mercier, R., Nogué, F., Grelon, M., 2009. A High Throughput Genetic Screen Identifies New Early Meiotic Recombination Functions in *Arabidopsis thaliana*. *PLOS Genet.* 5, e1000654. <https://doi.org/10.1371/journal.pgen.1000654>
- Muyt, A.D., Pyatnitskaya, A., Andréani, J., Ranjha, L., Ramus, C., Laureau, R., Fernandez-Vega, A., Holoch, D., Girard, E., Govin, J., Margueron, R., Couté, Y., Cejka, P., Guérois, R., Borde, V., 2018. A meiotic XPF–ERCC1-like complex recognizes joint molecule recombination intermediates to promote crossover formation. *Genes Dev.* 32, 1085–1097. <https://doi.org/10.1101/gad.308510.117>
- Muyt, A.D., Zhang, L., Pirola, T., Kleckner, N., Espagne, E., Zickler, D., 2014. E3 ligase Hei10: a multifaceted structure-based signaling molecule with roles within and beyond meiosis. *Genes Dev.* 28, 1111–1123. <https://doi.org/10.1101/gad.240408.114>
- Nassif, N., Penney, J., Pal, S., Engels, W.R., Gloor, G.B., 1994. Efficient copying of nonhomologous sequences from ectopic sites via P-element-induced gap repair. *Mol. Cell. Biol.* 14, 1613–1625. <https://doi.org/10.1128/mcb.14.3.1613>
- Neale, M.J., Pan, J., Keeney, S., 2005. Endonucleolytic processing of covalent protein-linked DNA double-strand breaks. *Nature* 436, 1053–1057. <https://doi.org/10.1038/nature03872>
- Nimonkar, A.V., Dombrowski, C.C., Siino, J.S., Stasiak, A.Z., Stasiak, A., Kowalczykowski, S.C., 2012. *Saccharomyces cerevisiae* Dmc1 and Rad51 proteins preferentially function with Tid1 and Rad54 proteins, respectively, to promote DNA strand invasion during genetic recombination. *J. Biol. Chem.* 287, 28727–28737. <https://doi.org/10.1074/jbc.M112.373290>
- Nishant, K.T., Plys, A.J., Alani, E., 2008. A mutation in the putative MLH3 endonuclease domain confers a defect in both mismatch repair and meiosis in *Saccharomyces cerevisiae*. *Genetics* 179, 747–755. <https://doi.org/10.1534/genetics.108.086645>
- Nonomura, K.-I., Nakano, M., Fukuda, T., Eiguchi, M., Miyao, A., Hirochika, H., Kurata, N., 2004. The Novel Gene HOMOLOGOUS PAIRING ABERRATION IN RICE MEIOSIS1 of Rice Encodes a Putative Coiled-Coil Protein Required for Homologous Chromosome Pairing in Meiosis. *Plant Cell* 16, 1008–1020. <https://doi.org/10.1105/tpc.020701>
- Novak, I., Wang, H., Revenkova, E., Jessberger, R., Scherthan, H., Höög, C., 2008. Cohesin Smc1β determines meiotic chromatin axis loop organization. *J. Cell Biol.* 180, 83–90. <https://doi.org/10.1083/jcb.200706136>
- Offenberg, H.H., Schalk, J.A., Meuwissen, R.L., van Aalderen, M., Kester, H.A., Dietrich, A.J., Heyting, C., 1998. SCP2: a major protein component of the axial elements of synaptonemal complexes of the rat. *Nucleic Acids Res.* 26, 2572–2579.
- Oh, S.D., Lao, J.P., Taylor, A.F., Smith, G.R., Hunter, N., 2008. RecQ helicase, Sgs1, and XPF family endonuclease, Mus81-Mms4, resolve aberrant joint molecules during meiotic recombination. *Mol. Cell* 31, 324–336. <https://doi.org/10.1016/j.molcel.2008.07.006>
- Ollinger, R., Alsheimer, M., Benavente, R., 2005. Mammalian protein SCP1 forms synaptonemal complex-like structures in the absence of meiotic chromosomes. *Mol. Biol. Cell* 16, 212–217. <https://doi.org/10.1091/mbc.e04-09-0771>
- Osman, K., Higgins, J.D., Sanchez-Moran, E., Armstrong, S.J., Franklin, F.C.H., 2011. Pathways to meiotic recombination in *Arabidopsis thaliana*. *New Phytol.* 190, 523–544. <https://doi.org/10.1111/j.1469-8137.2011.03665.x>
- Osman, K., Yang, J., Roitinger, E., Lambing, C., Heckmann, S., Howell, E., Cuacos, M., Imre, R., Dürnberger, G., Mechtler, K., Armstrong, S., Franklin, F.C.H., 2018. Affinity proteomics reveals extensive phosphorylation of the *Brassica* chromosome axis protein ASY1 and a network of associated proteins at prophase I of meiosis. *Plant J. Cell Mol. Biol.* 93, 17–33. <https://doi.org/10.1111/tpj.13752>

- Østergaard, L., Yanofsky, M.F., 2004. Establishing gene function by mutagenesis in *Arabidopsis thaliana*. *Plant J. Cell Mol. Biol.* 39, 682–696.
<https://doi.org/10.1111/j.1365-313X.2004.02149.x>
- Page, S.L., Hawley, R.S., 2004. The genetics and molecular biology of the synaptonemal complex. *Annu. Rev. Cell Dev. Biol.* 20, 525–558.
<https://doi.org/10.1146/annurev.cellbio.19.111301.155141>
- Pan, J., Sasaki, M., Kniewel, R., Murakami, H., Blitzblau, H.G., Tischfield, S.E., Zhu, X., Neale, M.J., Jasin, M., Socci, N.D., Hochwagen, A., Keeney, S., 2011. A hierarchical combination of factors shapes the genome-wide topography of yeast meiotic recombination initiation. *Cell* 144, 719–731. <https://doi.org/10.1016/j.cell.2011.02.009>
- Panizza, S., Mendoza, M.A., Berlinger, M., Huang, L., Nicolas, A., Shirahige, K., Klein, F., 2011. Spo11-Accessory Proteins Link Double-Strand Break Sites to the Chromosome Axis in Early Meiotic Recombination. *Cell* 146, 372–383.
<https://doi.org/10.1016/j.cell.2011.07.003>
- Pelttari, J., Hoja, M.R., Yuan, L., Liu, J.G., Brundell, E., Moens, P., Santucci-Darmanin, S., Jessberger, R., Barbero, J.L., Heyting, C., Höög, C., 2001. A meiotic chromosomal core consisting of cohesin complex proteins recruits DNA recombination proteins and promotes synapsis in the absence of an axial element in mammalian meiotic cells. *Mol. Cell. Biol.* 21, 5667–5677. <https://doi.org/10.1128/MCB.21.16.5667-5677.2001>
- Peterson, B.A., Haak, D.C., Nishimura, M.T., Teixeira, P.J.P.L., James, S.R., Dangl, J.L., Nimchuk, Z.L., 2016. Genome-Wide Assessment of Efficiency and Specificity in CRISPR/Cas9 Mediated Multiple Site Targeting in *Arabidopsis*. *PLOS ONE* 11, e0162169. <https://doi.org/10.1371/journal.pone.0162169>
- Petes, T.D., 2001. Meiotic recombination hot spots and cold spots. *Nat. Rev. Genet.* 2, 360–369. <https://doi.org/10.1038/35072078>
- Petkov, P.M., Broman, K.W., Szatkiewicz, J.P., Paigen, K., 2007. Crossover interference underlies sex differences in recombination rates. *Trends Genet. TIG* 23, 539–542.
<https://doi.org/10.1016/j.tig.2007.08.015>
- Piazza, A., Shah, S.S., Wright, W.D., Gore, S.K., Koszul, R., Heyer, W.-D., 2019. Dynamic Processing of Displacement Loops during Recombinational DNA Repair. *Mol. Cell* 73, 1255–1266.e4. <https://doi.org/10.1016/j.molcel.2019.01.005>
- Porter, S.E., White, M.A., Petes, T.D., 1993. Genetic evidence that the meiotic recombination hotspot at the HIS4 locus of *Saccharomyces cerevisiae* does not represent a site for a symmetrically processed double-strand break. *Genetics* 134, 5–19.
- Pradillo, M., López, E., Linacero, R., Romero, C., Cuñado, N., Sánchez-Morán, E., Santos, J.L., 2012. Together yes, but not coupled: new insights into the roles of RAD51 and DMC1 in plant meiotic recombination. *Plant J. Cell Mol. Biol.* 69, 921–933.
<https://doi.org/10.1111/j.1365-313X.2011.04845.x>
- Prakash, R., Satory, D., Dray, E., Papusha, A., Scheller, J., Kramer, W., Krejci, L., Klein, H., Haber, J.E., Sung, P., Ira, G., 2009. Yeast Mph1 helicase dissociates Rad51-made D-loops: implications for crossover control in mitotic recombination. *Genes Dev.* 23, 67–79. <https://doi.org/10.1101/gad.1737809>
- Qiao, H., Prasada Rao, H.B.D., Yang, Y., Fong, J.H., Cloutier, J.M., Deacon, D.C., Nagel, K.E., Swartz, R.K., Strong, E., Holloway, J.K., Cohen, P.E., Schimenti, J., Ward, J., Hunter, N., 2014. Antagonistic roles of ubiquitin ligase HEI10 and SUMO ligase RNF212 regulate meiotic recombination. *Nat. Genet.* 46, 194–199.
<https://doi.org/10.1038/ng.2858>
- R. Mercier, Mézard, C., Jenczewski, E., Macaisne, N., Grelon, M., 2015. The Molecular Biology of Meiosis in Plants. *Annu. Rev. Plant Biol.* 66, 297–327.
<https://doi.org/10.1146/annurev-arplant-050213-035923>
- Rajagopala, S.V., Hughes, K.T., Uetz, P., 2009. Benchmarking yeast two-hybrid systems using the interactions of bacterial motility proteins. *Proteomics* 9, 5296–5302.
<https://doi.org/10.1002/pmic.200900282>

- Ranjha, L., Anand, R., Cejka, P., 2014. The *Saccharomyces cerevisiae* Mlh1-Mlh3 heterodimer is an endonuclease that preferentially binds to Holliday junctions. *J. Biol. Chem.* 289, 5674–5686. <https://doi.org/10.1074/jbc.M113.533810>
- Rao, H.B.D.P., Qiao, H., Bhatt, S.K., Bailey, L.R.J., Tran, H.D., Bourne, S.L., Qiu, W., Deshpande, A., Sharma, A.N., Beebout, C.J., Pezza, R.J., Hunter, N., 2017. A SUMO-ubiquitin relay recruits proteasomes to chromosome axes to regulate meiotic recombination. *Science* 355, 403–407. <https://doi.org/10.1126/science.aaf6407>
- Rass, E., Grabarz, A., Plo, I., Gautier, J., Bertrand, P., Lopez, B.S., 2009. Role of Mre11 in chromosomal nonhomologous end joining in mammalian cells. *Nat. Struct. Mol. Biol.* 16, 819–824. <https://doi.org/10.1038/nsmb.1641>
- Rath, D., Amlinger, L., Rath, A., Lundgren, M., 2015. The CRISPR-Cas immune system: Biology, mechanisms and applications. *Biochimie, Special Issue: Regulatory RNAs* 117, 119–128. <https://doi.org/10.1016/j.biochi.2015.03.025>
- Resnick, M.A., Martin, P., 1976. The repair of double-strand breaks in the nuclear DNA of *Saccharomyces cerevisiae* and its genetic control. *Mol. Gen. Genet. MGG* 143, 119–129.
- Robert, T., Nore, A., Brun, C., Maffre, C., Crimi, B., Bourbon, H.-M., de Massy, B., 2016. The TopoVIB-Like protein family is required for meiotic DNA double-strand break formation. *Science* 351, 943–949. <https://doi.org/10.1126/science.aad5309>
- Roeder, G.S., Bailis, J.M., 2000. The pachytene checkpoint. *Trends Genet. TIG* 16, 395–403.
- Rogacheva, M.V., Manhart, C.M., Chen, C., Guarne, A., Surtees, J., Alani, E., 2014. Mlh1-Mlh3, a Meiotic Crossover and DNA Mismatch Repair Factor, Is a Msh2-Msh3-stimulated Endonuclease. *J. Biol. Chem.* 289, 5664–5673. <https://doi.org/10.1074/jbc.M113.534644>
- Ronceret, A., Doutriaux, M.-P., Golubovskaya, I.N., Pawlowski, W.P., 2009. PHS1 regulates meiotic recombination and homologous chromosome pairing by controlling the transport of RAD50 to the nucleus. *Proc. Natl. Acad. Sci. U. S. A.* 106, 20121–20126. <https://doi.org/10.1073/pnas.0906273106>
- Rong, M., Matsuda, A., Hiraoka, Y., Lee, J., 2016. Meiotic cohesin subunits RAD21L and REC8 are positioned at distinct regions between lateral elements and transverse filaments in the synaptonemal complex of mouse spermatocytes. *J. Reprod. Dev.* 62, 623–630. <https://doi.org/10.1262/jrd.2016-127>
- Rosenberg, S.C., Corbett, K.D., 2015. The multifaceted roles of the HORMA domain in cellular signaling. *J. Cell Biol.* 211, 745–755. <https://doi.org/10.1083/jcb.201509076>
- Ross, K.J., Fransz, P., Armstrong, S.J., Vizir, I., Mulligan, B., Franklin, F.C., Jones, G.H., 1997. Cytological characterization of four meiotic mutants of *Arabidopsis* isolated from T-DNA-transformed lines. *Chromosome Res. Int. J. Mol. Supramol. Evol. Asp. Chromosome Biol.* 5, 551–559.
- Saintenac, C., Falque, M., Martin, O.C., Paux, E., Feuillet, C., Sourdille, P., 2009. Detailed recombination studies along chromosome 3B provide new insights on crossover distribution in wheat (*Triticum aestivum* L.). *Genetics* 181, 393–403. <https://doi.org/10.1534/genetics.108.097469>
- Samach, A., Melamed-Bessudo, C., Avivi-Ragolski, N., Pietrovski, S., Levy, A.A., 2011. Identification of plant RAD52 homologs and characterization of the *Arabidopsis thaliana* RAD52-like genes. *Plant Cell* 23, 4266–4279. <https://doi.org/10.1105/tpc.111.091744>
- Sanchez Moran, E., Armstrong, S.J., Santos, J.L., Franklin, F.C., Jones, G.H., 2001. Chiasma formation in *Arabidopsis thaliana* accession Wassileskija and in two meiotic mutants. *Chromosome Res. Int. J. Mol. Supramol. Evol. Asp. Chromosome Biol.* 9, 121–128.
- Sanchez-Moran, E., Armstrong, S.J., Santos, J.L., Franklin, F.C.H., Jones, G.H., 2002. Variation in chiasma frequency among eight accessions of *Arabidopsis thaliana*. *Genetics* 162, 1415–1422.

- Sanchez-Moran, E., Santos, J.-L., Jones, G.H., Franklin, F.C.H., 2007. ASY1 mediates AtDMC1-dependent interhomolog recombination during meiosis in *Arabidopsis*. *Genes Dev.* 21, 2220–2233. <https://doi.org/10.1101/gad.439007>
- San-Segundo, P.A., Roeder, G.S., 1999. Pch2 links chromatin silencing to meiotic checkpoint control. *Cell* 97, 313–324. [https://doi.org/10.1016/s0092-8674\(00\)80741-2](https://doi.org/10.1016/s0092-8674(00)80741-2)
- Sasanuma, H., Murakami, H., Fukuda, T., Shibata, T., Nicolas, A., Ohta, K., 2007. Meiotic association between Spo11 regulated by Rec102, Rec104 and Rec114. *Nucleic Acids Res.* 35, 1119–1133. <https://doi.org/10.1093/nar/gkl1162>
- Schiml, S., Fauser, F., Puchta, H., 2016. CRISPR/Cas-Mediated Site-Specific Mutagenesis in *Arabidopsis thaliana* Using Cas9 Nucleases and Paired Nickases, in: Murata, M. (Ed.), *Chromosome and Genomic Engineering in Plants, Methods in Molecular Biology*. Springer New York, pp. 111–122. https://doi.org/10.1007/978-1-4939-4931-1_8
- Schmid, R., Grellscheid, S.N., Ehrmann, I., Dalgliesh, C., Danilenko, M., Paronetto, M.P., Pedrotti, S., Grellscheid, D., Dixon, R.J., Sette, C., Eperon, I.C., Elliott, D.J., 2013. The splicing landscape is globally reprogrammed during male meiosis. *Nucleic Acids Res.* 41, 10170–10184. <https://doi.org/10.1093/nar/gkt811>
- Schramm, S., Fraune, J., Naumann, R., Hernandez-Hernandez, A., Höög, C., Cooke, H.J., Alsheimer, M., Benavente, R., 2011. A Novel Mouse Synaptonemal Complex Protein Is Essential for Loading of Central Element Proteins, Recombination, and Fertility. *PLOS Genet.* 7, e1002088. <https://doi.org/10.1371/journal.pgen.1002088>
- Seeliger, K., Dukowic-Schulze, S., Wurz-Wildersinn, R., Pacher, M., Puchta, H., 2012. BRCA2 is a mediator of RAD51- and DMC1-facilitated homologous recombination in *Arabidopsis thaliana*. *New Phytol.* 193, 364–375. <https://doi.org/10.1111/j.1469-8137.2011.03947.x>
- Séguéla-Arnaud, M., Choinard, S., Larchevêque, C., Girard, C., Froger, N., Crismani, W., Mercier, R., 2017. RMI1 and TOP3 α limit meiotic CO formation through their C-terminal domains. *Nucleic Acids Res.* 45, 1860–1871. <https://doi.org/10.1093/nar/gkw1210>
- Séguéla-Arnaud, M., Crismani, W., Larchevêque, C., Mazel, J., Froger, N., Choinard, S., Lemhemdi, A., Macaisne, N., Van Leene, J., Gevaert, K., De Jaeger, G., Chelysheva, L., Mercier, R., 2015. Multiple mechanisms limit meiotic crossovers: TOP3 α and two BLM homologs antagonize crossovers in parallel to FANCM. *Proc. Natl. Acad. Sci. U. S. A.* 112, 4713–4718. <https://doi.org/10.1073/pnas.1423107112>
- Serrentino, M.-E., Borde, V., 2012. The spatial regulation of meiotic recombination hotspots: are all DSB hotspots crossover hotspots? *Exp. Cell Res.* 318, 1347–1352. <https://doi.org/10.1016/j.yexcr.2012.03.025>
- Serrentino, M.-E., Chaplain, E., Sommermeyer, V., Borde, V., 2013. Differential Association of the Conserved SUMO Ligase Zip3 with Meiotic Double-Strand Break Sites Reveals Regional Variations in the Outcome of Meiotic Recombination. *PLOS Genet.* 9, e1003416. <https://doi.org/10.1371/journal.pgen.1003416>
- Shan, Q., Wang, Y., Li, J., Zhang, Y., Chen, K., Liang, Z., Zhang, K., Liu, J., Xi, J.J., Qiu, J.-L., Gao, C., 2013. Targeted genome modification of crop plants using a CRISPR-Cas system. *Nat. Biotechnol.* 31, 686–688. <https://doi.org/10.1038/nbt.2650>
- Shen, B., Zhang, J., Wu, H., Wang, J., Ma, K., Li, Z., Zhang, X., Zhang, P., Huang, X., 2013. Generation of gene-modified mice via Cas9/RNA-mediated gene targeting. *Cell Res.* 23, 720–723. <https://doi.org/10.1038/cr.2013.46>
- Shilo, S., Melamed-Bessudo, C., Dorone, Y., Barkai, N., Levy, A.A., 2015. DNA Crossover Motifs Associated with Epigenetic Modifications Delineate Open Chromatin Regions in *Arabidopsis*. *Plant Cell* 27, 2427–2436. <https://doi.org/10.1105/tpc.15.00391>
- Shin, H.Y., Wang, C., Lee, H.K., Yoo, K.H., Zeng, X., Kuhns, T., Yang, C.M., Mohr, T., Liu, C., Hennighausen, L., 2017. CRISPR/Cas9 targeting events cause complex deletions and insertions at 17 sites in the mouse genome. *Nat. Commun.* 8, 15464. <https://doi.org/10.1038/ncomms15464>

- Shin, Y.-H., Choi, Y., Erdin, S.U., Yatsenko, S.A., Kloc, M., Yang, F., Wang, P.J., Meistrich, M.L., Rajkovic, A., 2010. Hormad1 mutation disrupts synaptonemal complex formation, recombination, and chromosome segregation in mammalian meiosis. *PLoS Genet.* 6, e1001190. <https://doi.org/10.1371/journal.pgen.1001190>
- Shinohara, M., Hayashihara, K., Grubb, J.T., Bishop, D.K., Shinohara, A., 2015. DNA damage response clamp 9-1-1 promotes assembly of ZMM proteins for formation of crossovers and synaptonemal complex. *J. Cell Sci.* 128, 1494–1506. <https://doi.org/10.1242/jcs.161554>
- Shinohara, M., Oh, S.D., Hunter, N., Shinohara, A., 2008. Crossover assurance and crossover interference are distinctly regulated by the ZMM proteins during yeast meiosis. *Nat. Genet.* 40, 299–309. <https://doi.org/10.1038/ng.83>
- Shultz, R.W., Tatineni, V.M., Hanley-Bowdoin, L., Thompson, W.F., 2007. Genome-wide analysis of the core DNA replication machinery in the higher plants *Arabidopsis* and rice. *Plant Physiol.* 144, 1697–1714. <https://doi.org/10.1104/pp.107.101105>
- Siaud, N., Dray, E., Gy, I., Gérard, E., Takvorian, N., Doutriaux, M.-P., 2004. Brca2 is involved in meiosis in *Arabidopsis thaliana* as suggested by its interaction with Dmc1. *EMBO J.* 23, 1392–1401. <https://doi.org/10.1038/sj.emboj.7600146>
- Sironi, L., Mapelli, M., Knapp, S., Antoni, A.D., Jeang, K.-T., Musacchio, A., 2002. Crystal structure of the tetrameric Mad1–Mad2 core complex: implications of a ‘safety belt’ binding mechanism for the spindle checkpoint. *EMBO J.* 21, 2496–2506. <https://doi.org/10.1093/emboj/21.10.2496>
- Smagulova, F., Brick, K., Pu, Y., Camerini-Otero, R.D., Petukhova, G.V., 2016. The evolutionary turnover of recombination hot spots contributes to speciation in mice. *Genes Dev.* 30, 266–280. <https://doi.org/10.1101/gad.270009.115>
- Snowden, T., Acharya, S., Butz, C., Berardini, M., Fishel, R., 2004. hMSH4-hMSH5 recognizes Holliday Junctions and forms a meiosis-specific sliding clamp that embraces homologous chromosomes. *Mol. Cell* 15, 437–451. <https://doi.org/10.1016/j.molcel.2004.06.040>
- Sommermeyer, V., Béneut, C., Chaplais, E., Serrentino, M.E., Borde, V., 2013. Spp1, a member of the Set1 Complex, promotes meiotic DSB formation in promoters by tethering histone H3K4 methylation sites to chromosome axes. *Mol. Cell* 49, 43–54. <https://doi.org/10.1016/j.molcel.2012.11.008>
- Soustelle, C., Vedel, M., Kolodner, R., Nicolas, A., 2002. Replication protein A is required for meiotic recombination in *Saccharomyces cerevisiae*. *Genetics* 161, 535–547.
- Sprink, T., Hartung, F., 2014. The splicing fate of plant SPO11 genes. *Front. Plant Sci.* 5. <https://doi.org/10.3389/fpls.2014.00214>
- Stacey, N.J., Kuromori, T., Azumi, Y., Roberts, G., Breuer, C., Wada, T., Maxwell, A., Roberts, K., Sugimoto-Shirasu, K., 2006. *Arabidopsis SPO11-2* functions with SPO11-1 in meiotic recombination. *Plant J. Cell Mol. Biol.* 48, 206–216. <https://doi.org/10.1111/j.1365-313X.2006.02867.x>
- Storlazzi, A., Gargano, S., Ruprich-Robert, G., Falque, M., David, M., Kleckner, N., Zickler, D., 2010. Recombination proteins mediate meiotic spatial chromosome organization and pairing. *Cell* 141, 94–106. <https://doi.org/10.1016/j.cell.2010.02.041>
- Strunnikov, A.V., Larionov, V.L., Koshland, D., 1993. SMC1: an essential yeast gene encoding a putative head-rod-tail protein is required for nuclear division and defines a new ubiquitous protein family. *J. Cell Biol.* 123, 1635–1648.
- Sturtevant, A.H., 1915. The behavior of the chromosomes as studied through linkage. *Z. Für Indukt. Abstamm.- Vererbungslehre* 13, 234–287. <https://doi.org/10.1007/BF01792906>
- Sun, W., Nandi, S., Osman, F., Ahn, J.S., Jakovleska, J., Lorenz, A., Whitby, M.C., 2008. The FANCM ortholog Fml1 promotes recombination at stalled replication forks and limits crossing over during DNA double-strand break repair. *Mol. Cell* 32, 118–128. <https://doi.org/10.1016/j.molcel.2008.08.024>

- Sun, X., Huang, L., Markowitz, T.E., Blitzblau, H.G., Chen, D., Klein, F., Hochwagen, A., 2015. Transcription dynamically patterns the meiotic chromosome-axis interface. *eLife* 4. <https://doi.org/10.7554/eLife.07424>
- Sym, M., Engebrecht, J.A., Roeder, G.S., 1993. ZIP1 is a synaptonemal complex protein required for meiotic chromosome synapsis. *Cell* 72, 365–378.
- Syrjänen, J.L., Pellegrini, L., Davies, O.R., 2014. A molecular model for the role of SYCP3 in meiotic chromosome organisation. *eLife* 3, e02963. <https://doi.org/10.7554/eLife.02963>
- Szostak, J.W., Orr-Weaver, T.L., Rothstein, R.J., Stahl, F.W., 1983. The double-strand-break repair model for recombination. *Cell* 33, 25–35. [https://doi.org/10.1016/0092-8674\(83\)90331-8](https://doi.org/10.1016/0092-8674(83)90331-8)
- Tang, S., Wu, M.K.Y., Zhang, R., Hunter, N., 2015. Pervasive and essential roles of the top3-rmi1 decatenase orchestrate recombination and facilitate chromosome segregation in meiosis. *Mol. Cell* 57, 607–621. <https://doi.org/10.1016/j.molcel.2015.01.021>
- Tarsounas, M., Pearlman, R.E., Gasser, P.J., Park, M.S., Moens, P.B., 1997. Protein-protein interactions in the synaptonemal complex. *Mol. Biol. Cell* 8, 1405–1414.
- Tay, Y.D., Sidebotham, J.M., Wu, L., 2010. Mph1 requires mismatch repair-independent and -dependent functions of MutS α to regulate crossover formation during homologous recombination repair. *Nucleic Acids Res.* 38, 1889–1901. <https://doi.org/10.1093/nar/gkp1199>
- Tian, G.-W., Mohanty, A., Chary, S.N., Li, S., Paap, B., Drakakaki, G., Kopec, C.D., Li, J., Ehrhardt, D., Jackson, D., Rhee, S.Y., Raikhel, N.V., Citovsky, V., 2004. High-throughput fluorescent tagging of full-length *Arabidopsis* gene products in planta. *Plant Physiol.* 135, 25–38. <https://doi.org/10.1104/pp.104.040139>
- Tiang, C.L., 2011. The role of SYN1 in early *Arabidopsis* meiosis (d_ph). University of Birmingham.
- Tsai, S.Q., Zheng, Z., Nguyen, N.T., Liebers, M., Topkar, V.V., Thapar, V., Wyveldens, N., Khayter, C., Iafrate, A.J., Le, L.P., Aryee, M.J., Joung, J.K., 2015. GUIDE-Seq enables genome-wide profiling of off-target cleavage by CRISPR-Cas nucleases. *Nat. Biotechnol.* 33, 187–197. <https://doi.org/10.1038/nbt.3117>
- Tsubouchi, T., Macqueen, A.J., Roeder, G.S., 2008. Initiation of meiotic chromosome synapsis at centromeres in budding yeast. *Genes Dev.* 22, 3217–3226. <https://doi.org/10.1101/gad.1709408>
- Tung, K.S., Roeder, G.S., 1998. Meiotic chromosome morphology and behavior in zip1 mutants of *Saccharomyces cerevisiae*. *Genetics* 149, 817–832.
- United Nations, 2017. World Population Prospects: The 2017 Revision.
- Voelkel-Meiman, K., Cheng, S.-Y., Parziale, M., Morehouse, S.J., Feil, A., Davies, O.R., Muyt, A. de, Borde, V., MacQueen, A.J., 2019. Crossover recombination and synapsis are linked by adjacent regions within the N terminus of the Zip1 synaptonemal complex protein. *PLOS Genet.* 15, e1008201. <https://doi.org/10.1371/journal.pgen.1008201>
- Voelkel-Meiman, K., Johnston, C., Thappeta, Y., Subramanian, V.V., Hochwagen, A., MacQueen, A.J., 2015. Separable Crossover-Promoting and Crossover-Constraining Aspects of Zip1 Activity during Budding Yeast Meiosis. *PLOS Genet.* 11, e1005335. <https://doi.org/10.1371/journal.pgen.1005335>
- Vrielynck, N., Chambon, A., Vezon, D., Pereira, L., Chelysheva, L., De Muyt, A., Mézard, C., Mayer, C., Grelon, M., 2016. A DNA topoisomerase VI-like complex initiates meiotic recombination. *Science* 351, 939–943. <https://doi.org/10.1126/science.aad5196>
- Wan, L., Niu, H., Futcher, B., Zhang, C., Shokat, K.M., Boulton, S.J., Hollingsworth, N.M., 2008. Cdc28–Clb5 (CDK-S) and Cdc7–Dbf4 (DDK) collaborate to initiate meiotic recombination in yeast. *Genes Dev.* 22, 386–397. <https://doi.org/10.1101/gad.1626408>

- Wang, H., La Russa, M., Qi, L.S., 2016. CRISPR/Cas9 in Genome Editing and Beyond. *Annu. Rev. Biochem.* 85, 227–264. <https://doi.org/10.1146/annurev-biochem-060815-014607>
- Wang, K., Tang, D., Wang, M., Lu, J., Yu, H., Liu, J., Qian, B., Gong, Z., Wang, X., Chen, J., Gu, M., Cheng, Z., 2009. MER3 is required for normal meiotic crossover formation, but not for presynaptic alignment in rice. *J. Cell Sci.* 122, 2055–2063. <https://doi.org/10.1242/jcs.049080>
- Wang, M., Wang, K., Tang, D., Wei, C., Li, M., Shen, Y., Chi, Z., Gu, M., Cheng, Z., 2010. The central element protein ZEP1 of the synaptonemal complex regulates the number of crossovers during meiosis in rice. *Plant Cell* 22, 417–430. <https://doi.org/10.1105/tpc.109.070789>
- Wang, S., Zickler, D., Kleckner, N., Zhang, L., 2015. Meiotic crossover patterns: Obligatory crossover, interference and homeostasis in a single process. *Cell Cycle* 14, 305–314. <https://doi.org/10.4161/15384101.2014.991185>
- Wang, T.-F., Kleckner, N., Hunter, N., 1999. Functional specificity of MutL homologs in yeast: Evidence for three Mlh1-based heterocomplexes with distinct roles during meiosis in recombination and mismatch correction. *Proc. Natl. Acad. Sci. U. S. A.* 96, 13914–13919.
- Wang, Z.-P., Xing, H.-L., Dong, L., Zhang, H.-Y., Han, C.-Y., Wang, X.-C., Chen, Q.-J., 2015. Egg cell-specific promoter-controlled CRISPR/Cas9 efficiently generates homozygous mutants for multiple target genes in *Arabidopsis* in a single generation. *Genome Biol.* 16, 144. <https://doi.org/10.1186/s13059-015-0715-0>
- Ward, A., Hopkins, J., Mckay, M., Murray, S., Jordan, P.W., 2016. Genetic Interactions Between the Meiosis-Specific Cohesin Components, STAG3, REC8, and RAD21L. *G3 Bethesda Md* 6, 1713–1724. <https://doi.org/10.1534/g3.116.029462>
- West, A., 2015. Investigating the Links Between Meiotic Chromosome Structure and Homologous Recombination in *Arabidopsis thaliana*. The University of Birmingham, Birmingham, UK.
- West, A.M., Rosenberg, S.C., Ur, S.N., Lehmer, M.K., Ye, Q., Hagemann, G., Caballero, I., Usón, I., MacQueen, A.J., Herzog, F., Corbett, K.D., 2019. A conserved filamentous assembly underlies the structure of the meiotic chromosome axis. *eLife* 8, e40372. <https://doi.org/10.7554/eLife.40372>
- Wijeratne, A.J., Chen, C., Zhang, W., Timofejeva, L., Ma, H., 2006. The *Arabidopsis thaliana* PARTING DANCERS Gene Encoding a Novel Protein Is Required for Normal Meiotic Homologous Recombination. *Mol. Biol. Cell* 17, 1331–1343. <https://doi.org/10.1091/mbc.e05-09-0902>
- Wijnker, E., Velikkakam James, G., Ding, J., Becker, F., Klasen, J.R., Rawat, V., Rowan, B.A., de Jong, D.F., de Snoo, C.B., Zapata, L., Huettel, B., de Jong, H., Ossowski, S., Weigel, D., Koornneef, M., Keurentjes, J.J., Schneeberger, K., 2013. The genomic landscape of meiotic crossovers and gene conversions in *Arabidopsis thaliana*. *eLife* 2, e01426. <https://doi.org/10.7554/eLife.01426>
- Woglar, A., Villeneuve, A.M., 2018. Dynamic Architecture of DNA Repair Complexes and the Synaptonemal Complex at Sites of Meiotic Recombination. *Cell* 173, 1678–1691.e16. <https://doi.org/10.1016/j.cell.2018.03.066>
- Woltering, D., Baumgartner, B., Bagchi, S., Larkin, B., Loidl, J., de los Santos, T., Hollingsworth, N.M., 2000. Meiotic segregation, synapsis, and recombination checkpoint functions require physical interaction between the chromosomal proteins Red1p and Hop1p. *Mol. Cell. Biol.* 20, 6646–6658. <https://doi.org/10.1128/mcb.20.18.6646-6658.2000>
- Woo, J.W., Kim, J., Kwon, S.I., Corvalán, C., Cho, S.W., Kim, H., Kim, S.-G., Kim, S.-T., Choe, S., Kim, J.-S., 2015. DNA-free genome editing in plants with preassembled CRISPR-Cas9 ribonucleoproteins. *Nat. Biotechnol.* 33, 1162–1164. <https://doi.org/10.1038/nbt.3389>
- Wyatt, H.D.M., West, S.C., 2014. Holliday Junction Resolvases. *Cold Spring Harb. Perspect. Biol.* 6. <https://doi.org/10.1101/cshperspect.a023192>

- Xie, K., Yang, Y., 2013. RNA-guided genome editing in plants using a CRISPR-Cas system. *Mol. Plant* 6, 1975–1983. <https://doi.org/10.1093/mp/sst119>
- Xu, L., Weiner, B.M., Kleckner, N., 1997. Meiotic cells monitor the status of the interhomolog recombination complex. *Genes Dev.* 11, 106–118. <https://doi.org/10.1101/gad.11.1.106>
- Yamada, S., Ohta, K., Yamada, T., 2013. Acetylated Histone H3K9 is associated with meiotic recombination hotspots, and plays a role in recombination redundantly with other factors including the H3K4 methylase Set1 in fission yeast. *Nucleic Acids Res.* 41, 3504–3517. <https://doi.org/10.1093/nar/gkt049>
- Yang, F., De La Fuente, R., Leu, N.A., Baumann, C., McLaughlin, K.J., Wang, P.J., 2006. Mouse SYCP2 is required for synaptonemal complex assembly and chromosomal synapsis during male meiosis. *J. Cell Biol.* 173, 497–507. <https://doi.org/10.1083/jcb.200603063>
- Ye, Q., Kim, D.H., Dereli, I., Rosenberg, S.C., Hagemann, G., Herzog, F., Tóth, A., Cleveland, D.W., Corbett, K.D., 2017. The AAA+ ATPase TRIP13 remodels HORMA domains through N-terminal engagement and unfolding. *EMBO J.* 36, 2419–2434. <https://doi.org/10.15252/embj.201797291>
- Ye, Q., Rosenberg, S.C., Moeller, A., Speir, J.A., Su, T.Y., Corbett, K.D., 2015. TRIP13 is a protein-remodeling AAA+ ATPase that catalyzes MAD2 conformation switching. *eLife* 4, e07367. <https://doi.org/10.7554/eLife.07367>
- Yelina, N.E., Choi, K., Chelysheva, L., Macaulay, M., de Snoo, B., Wijnker, E., Miller, N., Drouaud, J., Grelon, M., Copenhaver, G.P., Mezard, C., Kelly, K.A., Henderson, I.R., 2012. Epigenetic remodeling of meiotic crossover frequency in *Arabidopsis thaliana* DNA methyltransferase mutants. *PLoS Genet.* 8, e1002844. <https://doi.org/10.1371/journal.pgen.1002844>
- Yokoo, R., Zawadzki, K.A., Nabeshima, K., Drake, M., Arur, S., Villeneuve, A.M., 2012. COSA-1 reveals robust homeostasis and separable licensing and reinforcement steps governing meiotic crossovers. *Cell* 149, 75–87. <https://doi.org/10.1016/j.cell.2012.01.052>
- Yu, Z., Kim, Y., Dernburg, A.F., 2016. Meiotic Recombination and the Crossover Assurance Checkpoint in *Caenorhabditis elegans*. *Semin. Cell Dev. Biol.* 54, 106–116. <https://doi.org/10.1016/j.semcdb.2016.03.014>
- Yuan, L., Liu, J.-G., Hoja, M.-R., Wilbertz, J., Nordqvist, K., Höög, C., 2002. Female germ cell aneuploidy and embryo death in mice lacking the meiosis-specific protein SCP3. *Science* 296, 1115–1118. <https://doi.org/10.1126/science.1070594>
- Yuan, L., Liu, J.G., Zhao, J., Brundell, E., Daneholt, B., Höög, C., 2000. The murine SCP3 gene is required for synaptonemal complex assembly, chromosome synapsis, and male fertility. *Mol. Cell* 5, 73–83.
- Zakharyevich, K., Tang, S., Ma, Y., Hunter, N., 2012. Delineation of joint molecule resolution pathways in meiosis identifies a crossover-specific resolvase. *Cell* 149, 334–347. <https://doi.org/10.1016/j.cell.2012.03.023>
- Zanders, S., Brown, M.S., Chen, C., Alani, E., 2011. Pch2 Modulates Chromatid Partner Choice During Meiotic Double-Strand Break Repair in *Saccharomyces cerevisiae*. *Genetics* 188, 511–521. <https://doi.org/10.1534/genetics.111.129031>
- Zhang, C., Song, Y., Cheng, Z., Wang, Y., Zhu, J., Ma, H., Xu, L., Yang, Z.-N., 2012. The *Arabidopsis thaliana* DSB formation (AtDFO) gene is required for meiotic double-strand break formation. *Plant J. Cell Mol. Biol.* 72, 271–281. <https://doi.org/10.1111/j.1365-313X.2012.05075.x>
- Zhang, H., Zhang, J., Wei, P., Zhang, B., Gou, F., Feng, Z., Mao, Y., Yang, L., Zhang, Heng, Xu, N., Zhu, J.-K., 2014. The CRISPR/Cas9 system produces specific and homozygous targeted gene editing in rice in one generation. *Plant Biotechnol. J.* 12, 797–807. <https://doi.org/10.1111/pbi.12200>
- Zhang, J., Pawlowski, W.P., Han, F., 2013. Centromere pairing in early meiotic prophase requires active centromeres and precedes installation of the synaptonemal complex in maize. *Plant Cell* 25, 3900–3909. <https://doi.org/10.1105/tpc.113.117846>

- Zhang, L., Liang, Z., Hutchinson, J., Kleckner, N., 2014a. Crossover Patterning by the Beam-Film Model: Analysis and Implications. *PLoS Genet.* 10. <https://doi.org/10.1371/journal.pgen.1004042>
- Zhang, L., Wang, S., Yin, S., Hong, S., Kim, K.P., Kleckner, N., 2014b. Topoisomerase II Mediates Meiotic Crossover Interference. *Nature* 511, 551–556. <https://doi.org/10.1038/nature13442>
- Zhang, Q., Xing, H.-L., Wang, Z.-P., Zhang, H.-Y., Yang, F., Wang, X.-C., Chen, Q.-J., 2018. Potential high-frequency off-target mutagenesis induced by CRISPR/Cas9 in *<Emphasis Type="Italic">Arabidopsis</Emphasis>* and its prevention. *Plant Mol. Biol.* 96, 445–456. <https://doi.org/10.1007/s11103-018-0709-x>
- Zickler, D., Kleckner, N., 2015. Recombination, Pairing, and Synapsis of Homologs during Meiosis. *Cold Spring Harb. Perspect. Biol.* 7. <https://doi.org/10.1101/cshperspect.a016626>
- Zickler, D., Kleckner, N., 1999. Meiotic chromosomes: integrating structure and function. *Annu. Rev. Genet.* 33, 603–754. <https://doi.org/10.1146/annurev.genet.33.1.603>

Appendix

Appendix

Appendix for Chapter 2: Materials and Methods

Table A 1. T-DNA insertion lines used in this study

| Gene | AGI Code | T-DNA Line | Allele(s) | Reference |
|------|-----------|--------------------------|-----------|--|
| ASY1 | AT1G67370 | SALK_046272 | asy1-4 | Crismani <i>et al.</i> , 2013 |
| ASY3 | AT2G46980 | SALK_143676 | asy3-1 | Ferdous <i>et al.</i> , 2012 |
| ASY4 | AT2G33973 | SK22114 | asy4-1 | This thesis, and Chambon et.al, (2018) |
| | | 65433 (Koncz Collection) | asy4-2 | |
| PCH2 | AT4G24710 | SAIL_1187_C06 | pch2-1 | Lambing <i>et al.</i> , 2015 |
| SYN1 | AT5G05490 | SALK_091193 | syn1 | (Cai <i>et al.</i> , 2003) |

Table A 2. List of primers used for genotyping T-DNA lines

| Allele | Primer Name | Sequence (5'-3') |
|--------|---------------|------------------------|
| asy1-4 | ASY1-4-F | CTATGGACGCTGAATCTCGC |
| | ASY1-4-R | GAACCATTGCAAGCTGAACTCC |
| asy3-1 | ASY3-1-F1 | AGGAGATGCTTCTGGAGAAC |
| | ASY3-1-R1 | CTGGTGCCAACCTAGGTCGC |
| asy4-1 | ASY4-1F | CTATGGACGCTGAATCTCGC |
| | ASY4-1R | GAACCATTGCAAGCTGAACTCC |
| asy4-2 | At2g33793-P7R | TCCTCATCAGAAGCCTCGTT |
| | At2g33793-P4R | TCCACTGAGGTGAAGTCAAA |

| | | |
|---------------|---------------|-----------------------------------|
| <i>pch2-1</i> | PCH2-1 Fv | CAGTGCAAATAGCCGTCGCTGAG |
| | PCH2-1 Rv | CTCACATGGTCCTTCTTCAATGAGC |
| <i>syn1</i> | SYN1F | CTTCTTAAGGATGGCCGCTAC |
| | SYN1R | CCACTTTATGGGCAATGAAG |
| T-DNA | GABIKat | ATATTGACCATCATACTCATTGC |
| | LB2 (SAIL) | GCTTCCTATTATATCTTCCAAATTACCAATACA |
| | LBb1.3 (SALK) | ATTTTGCCGATTCGGAAC |
| | RBSKI015 | AGATCCGAAACTATCAGTG |

Table A 3. Primers used in RT-PCR

| Gene Target | Primer Name | Sequence (5'-3') |
|-------------|----------------|------------------------|
| Actin 2 | RTPCR Actin2 F | CGTACAACCGGTATTGTGCTG |
| | RTPCR Actin2 R | AGGTTTCCATCTCCTGCTCGT |
| ASY3 | RTPCR ASY3 F | ACATCAGCCCCGAAGAAAGAG |
| | RTPCR ASY3 R | ATCTCCTCGGAGACTGATGCT |
| ASY4 | ASY4 RTPCR F | ACACCGAAAGCAAAACTCCC |
| | ASY4 RTPCR R | CAAGTTTGACTTCAGCTCGTC |
| | ASY4 FL F1 | ATGTCGTCTACCAGAAGAGGGC |
| | ASY4 Y2H R1 | TCACTCATCAGGTGGGAATTC |

Table A 4. Primers used in the Yeast-2-Hybrid experiments

| Gene Target | Primer Name | Sequence (5'-3') |
|--------------------|---------------------------------|------------------------------|
| ASY1 | ASY1 Y2H F1 | CACCATGGTGATGGCTCAGAAGCT |
| | ASY1 Y2H R1 | TCAATTAGCTTGAGAGTTCTGACG |
| ASY3 | ASY3 Y2H F1 | CACCATGAGCGACTATAGAAGCTTCGG |
| | ASY3 Y2H R1 | TCAATCATCCCTCAAACATTCTG |
| | ASY3 N-TERM F | CACCATGAGCGACTATAGAAGCT |
| | ASY3 N-TERM R | TTCATCCTCATCCATCTCTGAA |
| | ASY3 COIL Y2H F1 (OUT OF FRAME) | CACCATGAAGGCTTGGGAAGGG |
| | ASY3COIL IN-FRAME Y2H | CACCGATGAAGGCTTGGGAAGGG |
| | ASY3 HALF1 COIL R1 | CATTCTCATTTCCTCTTGTCTT |
| | ASY3 HALF 2 COIL F1 | CACCATCCATGAAAAGTTCAAGGACG |
| ASY4 | ASY4 Y2H F1 | CACCATGTCGTCTACCAGAAGAGGC |
| | ASY4 Y2H R1 | TCACTCATCAGGTGGGAATTC |
| | ASY4 HALF 1 R1 | CTCCTTGAACTCTTGAAAGTGC |
| | ASY4 HALF 2 F1 | CACCTGTGAGAATATTTGAAGGATGAAG |
| pENTR/D-TOPO™ | M13(-20)F (Invitrogen) | GTAAAACGACGCCAG |
| | M13 R (Invitrogen) | CAGGAAACAGCTATGAC |
| pDEST-22/pDEST-32 | pDEST22-F1 | TATAACGCGTTGGAATCACT |

Table A 5. Concentrations for antibodies used in Western Blotting

| Antibody | Raised in | Concentration | Reference |
|---------------------------|------------------|----------------------|---|
| α-ASY1 | Rat | 1:500 | (Armstrong <i>et al.</i> , 2002a) |
| α-GAL4 AD [14-7E10G10] | Mouse | 1:5000 | AbCam, Catalogue No. ab135398 |
| α-GAL4 DBD (RK5C1) | Mouse | 1:1000 | Santa Cruz Biotechnology, Catalogue No. sc-510 |

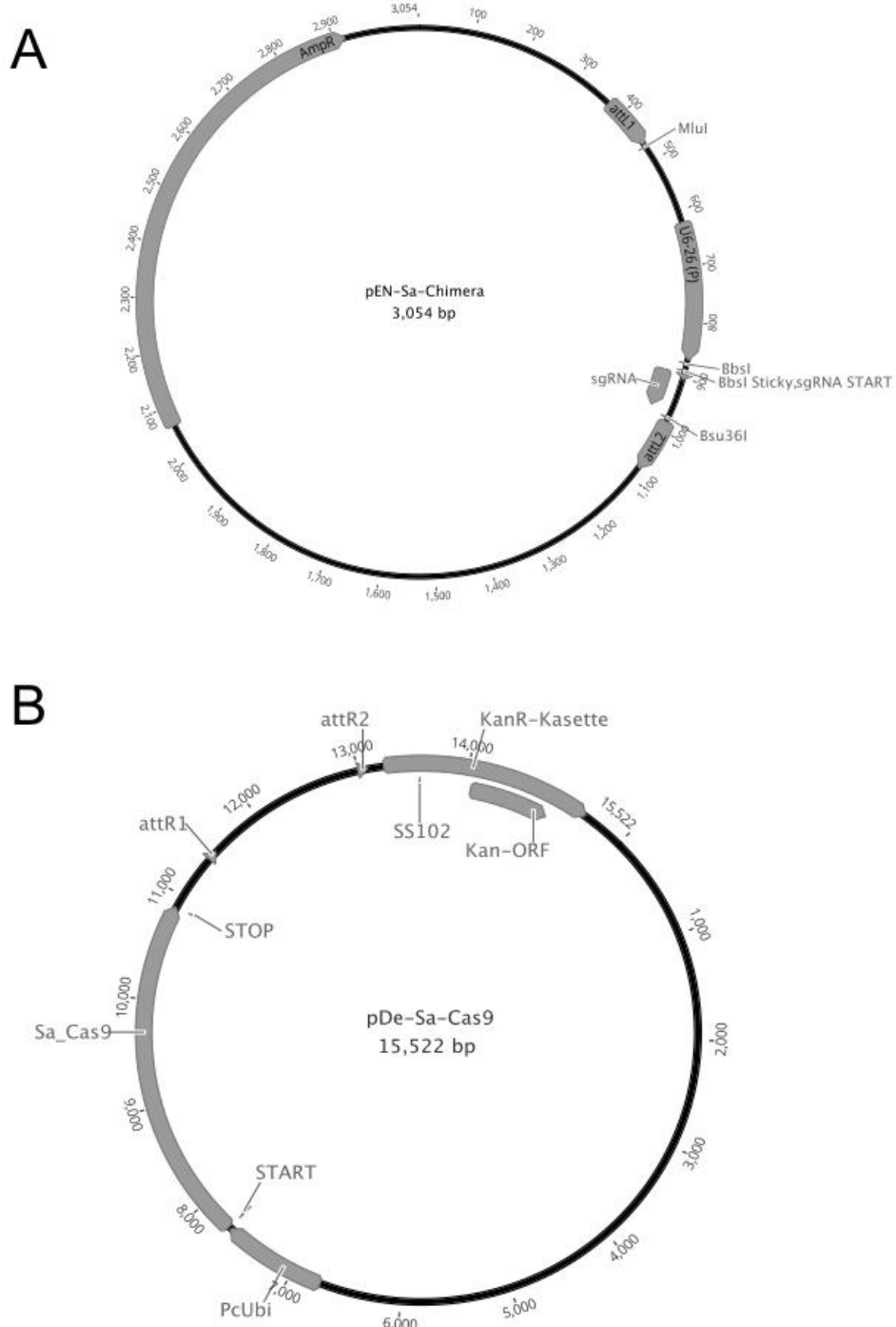


Figure A 1 Vector maps for pEn-Sa-Chimera (A) and pDe-Sa-Cas9 (B). Maps produced within Geneious R9. Sequence data available at: <http://www.botanik.kit.edu/molbio/983.php>

Table A 6. Oligonucleotide pairs and primers used in CRISPR/Cas9

| Primer Name | Sequence (5'-3') |
|----------------------|---------------------------|
| ASY4Pair1F | ATTGACCGAAAGCAAAACTCCGG |
| ASY4Pair1R | AAACCCGGGAGTTTGCTTCGGT |
| ASY4Pair2F | ATTGAGCGATTGC GGCGGCTCTGG |
| ASY4Pair2R | AAACCCAGAGCCGCCGCAATCGCT |
| ASY4Pair3F | ATTGCATCTTGTGCGCTTCTCT |
| ASY4Pair3R | AAACAGAGAAAGCGCACGAAGATG |
| SS129 | CACAGGAAACAGCTATGAC |
| SS42 | TCCCAGGATTAGAATGATTAGG |
| SS102 | CACCATGTTATCACATCAATCC |
| SS61 | GAGCTCCAGGCCTCCCAGCTTCG |
| ASY4 CRISPR CHECK F2 | CCATGAGGCCAATGATGTT |
| ASY4 CRISPR CHECK R2 | AAGCGATA CATGAGCATACCA |
| A4_WHOLE_F1 | ATTAGTCATGAGTTTCATTATGT |
| A4_WHOLE_R2 | CTTCTAGCGTCAAGTAAAAAGAC |
| A4 CR F2 | TGCGGCTTCAACACATTACA |
| A4 CR R1 | TGGACACACTGCCAGAAAGA |

Table A 7. Concentrations for antibodies used in immunolocalisation

| Antibody | Raised in | Concentration | Reference |
|--|----------------|---------------|---|
| α-ASY1 | Rabbit and Rat | 1:5000 | (Armstrong <i>et al.</i> , 2002a) |
| α-ASY3 | Rabbit | 1:200 | Ferdous <i>et al.</i> , 2012 |
| α-ASY4 | Rat | 1:200-1:500 | This thesis, and Osman and Franklin, unpublished. |
| α-MSH4 | Rabbit | 1:200 | (Higgins <i>et al.</i> , 2004b) |
| α-MSH5 | Rabbit | 1:200 | Higgins <i>et al.</i> , 2008 |
| α-SYN1 | Rabbit | 1:500 | Tiang, 2011 |
| α-PCH2 | Rabbit | 1:200 | Lambing <i>et al.</i> , 2015 |
| α-ZYP1 | Rabbit and Rat | 1:500 | Higgins <i>et al.</i> , 2005 |
| α-GFP (Living Colours A.v. Peptide Antibody) | Rabbit | 1:500 | Clontech, Catalogue No. 632376. |
| α-GFP | Goat | 1:2000 | AbCam, Catalogue No. ab5450 |

Table A 8.. Primers used to PCR screen for ASY4 over-expression lines

| Primer Name | Sequence (5'-3') |
|------------------|--------------------------|
| pLH9000 F1 | TGTGTGAGTAGTTCCCAGATAAGG |
| ASY4 Promoter R1 | AACATCATTGGGCCTCATGG |

Appendix for Chapter 3: ASYNAPTIC 4 is a novel component of the meiotic chromosome axis in *Arabidopsis thaliana*

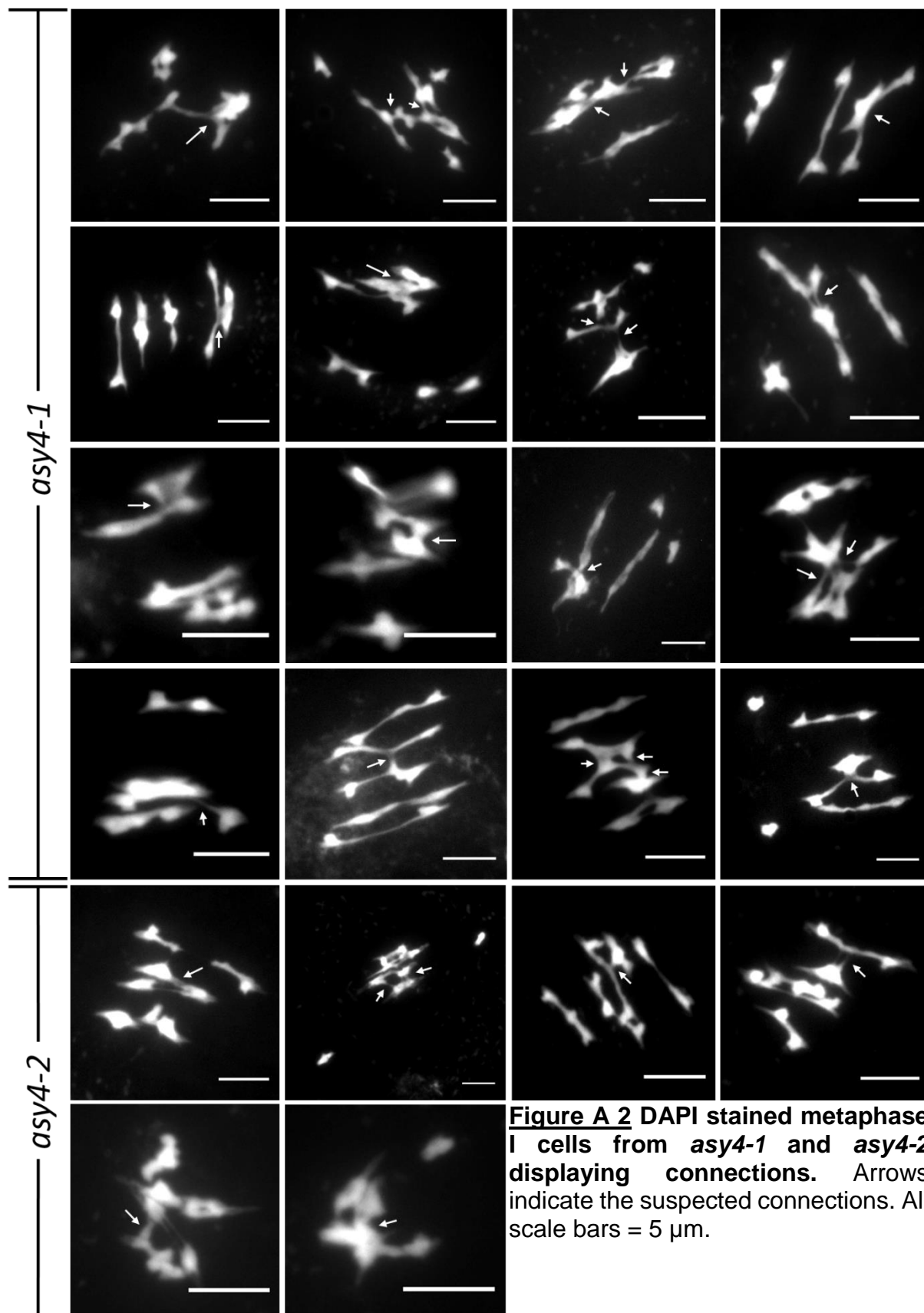


Figure A 2 DAPI stained metaphase I cells from *asy4-1* and *asy4-2* displaying connections. Arrows indicate the suspected connections. All scale bars = 5 μ m.

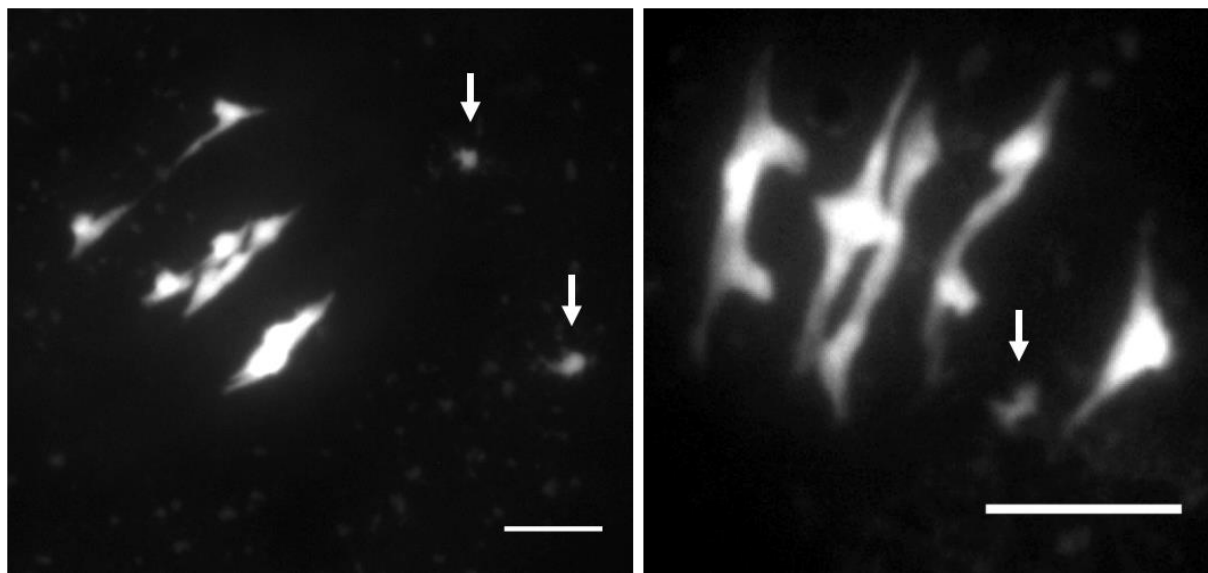


Figure A 3 DAPI stained metaphase I cells from *asy4-1* displaying chromosome fragments. Arrows indicate the fragments. All scale bars = 5 μ m.

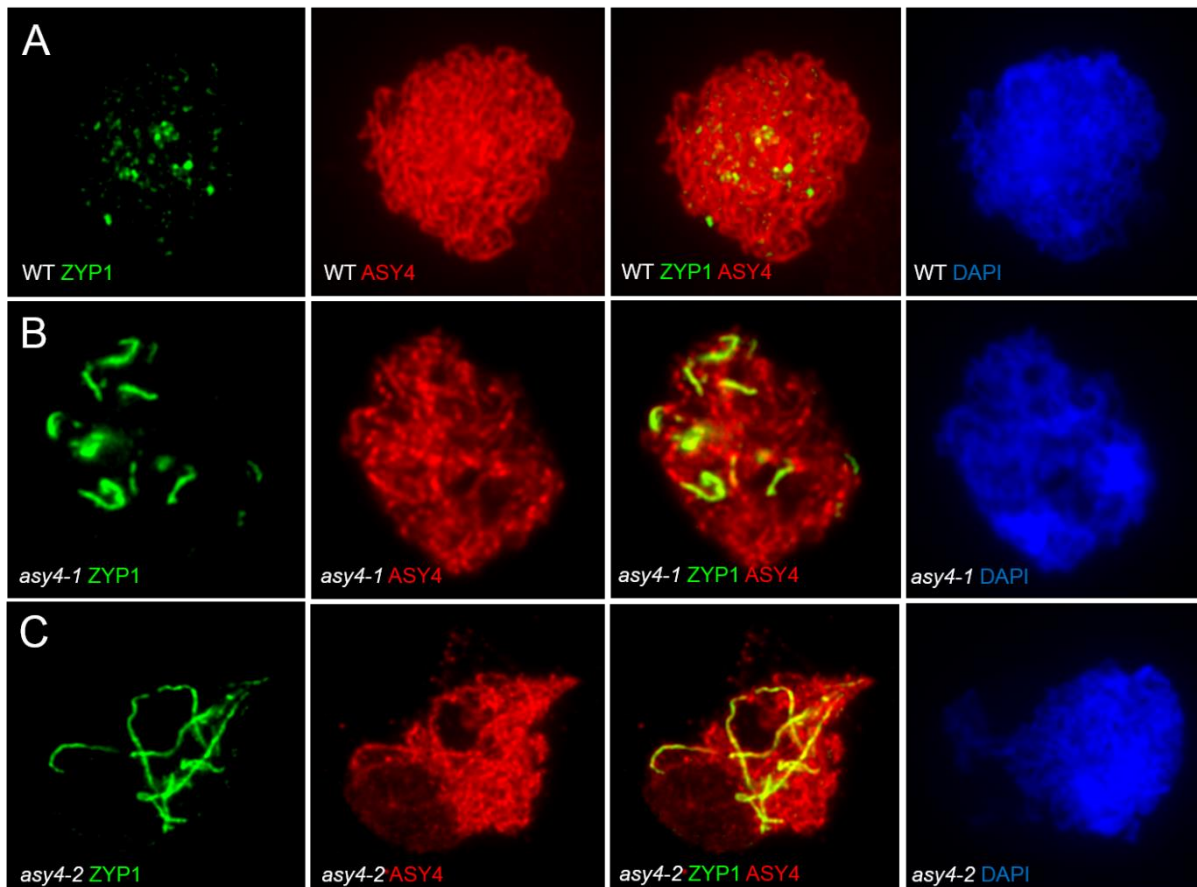


Figure A 4 Immunolocalisation with ASY4 antibody in two T-DNA insertion mutants for *asy4* gives a strong axis-associated signal. Image provided by Dr Kim Osman (University of Birmingham). ASY4 in Texas Red. ZYP1 in FITC. Chromatin in DAPI.

Table A 9. Counts of MSH4/MSH5 foci on *asy4-1*. Counts were performed using the NIS Elements software.

| Col-0 MSH5 | <i>asy4-1</i> MSH5 | Col-0 MSH4 | <i>asy4-1</i> MSH4 |
|---------------|-----------------------|---------------|-----------------------|
| 74 | 73 | 111 | 96 |
| 107 | 108 | 142 | 105 |
| 99 | 72 | 142 | 79 |
| 164 | 123 | 106 | 94 |
| 161 | 158 | 96 | 108 |
| 85 | 158 | 117 | 141 |
| 145 | 165 | 92 | 126 |
| 202 | 136 | 132 | 82 |
| 65 | 157 | 116 | 103 |
| 87 | 98 | 154 | 97 |
| 141 | 123 | 152 | 97 |
| 70 | 106 | 88 | 119 |
| 110 | 103 | 124 | 117 |
| 66 | 124 | 121 | 152 |
| 109 | 113 | 112 | 121 |

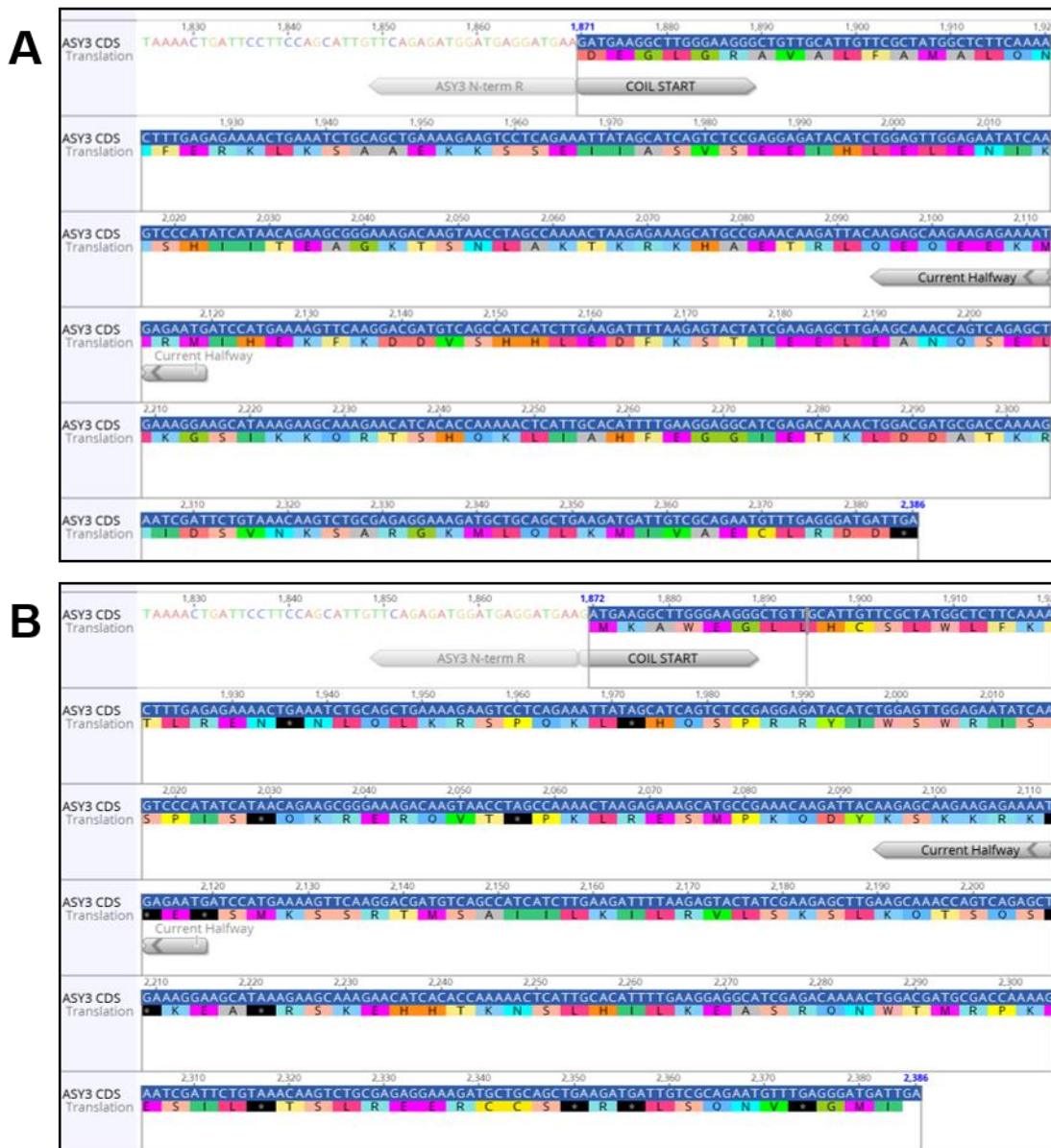
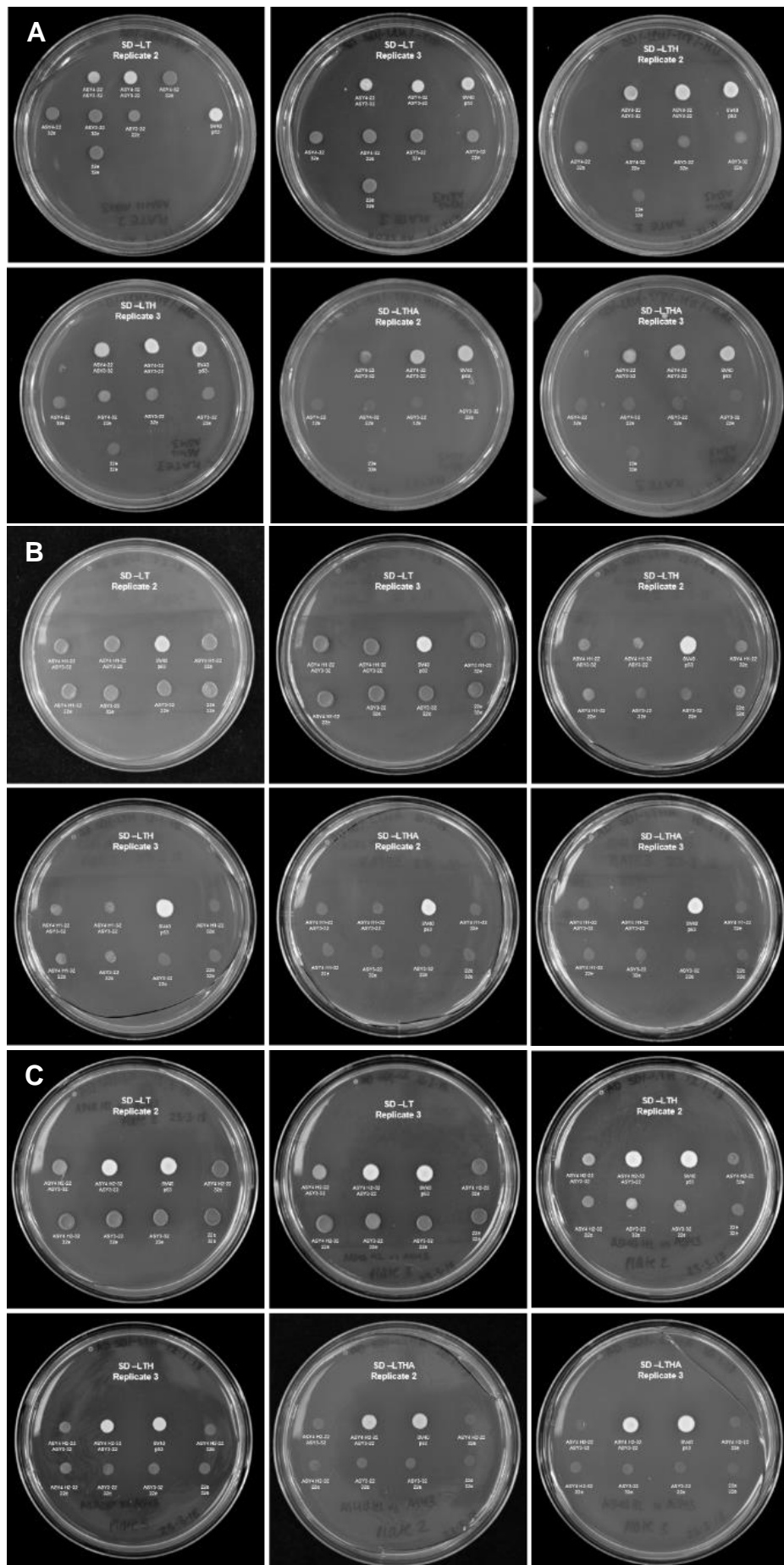


Figure A 3 Locations of Y2H primer sets for the ASY3 coiled-coil domain. (A) C2 is the ‘in-frame’ protein used in this thesis. **(B) C1 ASY3** is the proposed ‘out-of-frame’ protein as designed and used in Ferdous *et al.*, 2012. In colour under each sequence is the proposed amino acid sequence, showing that the coiled-coil described in Ferdous *et al.*, (2012) is predicted to produce a short nonsense protein. Translation completed within Geneious R9.



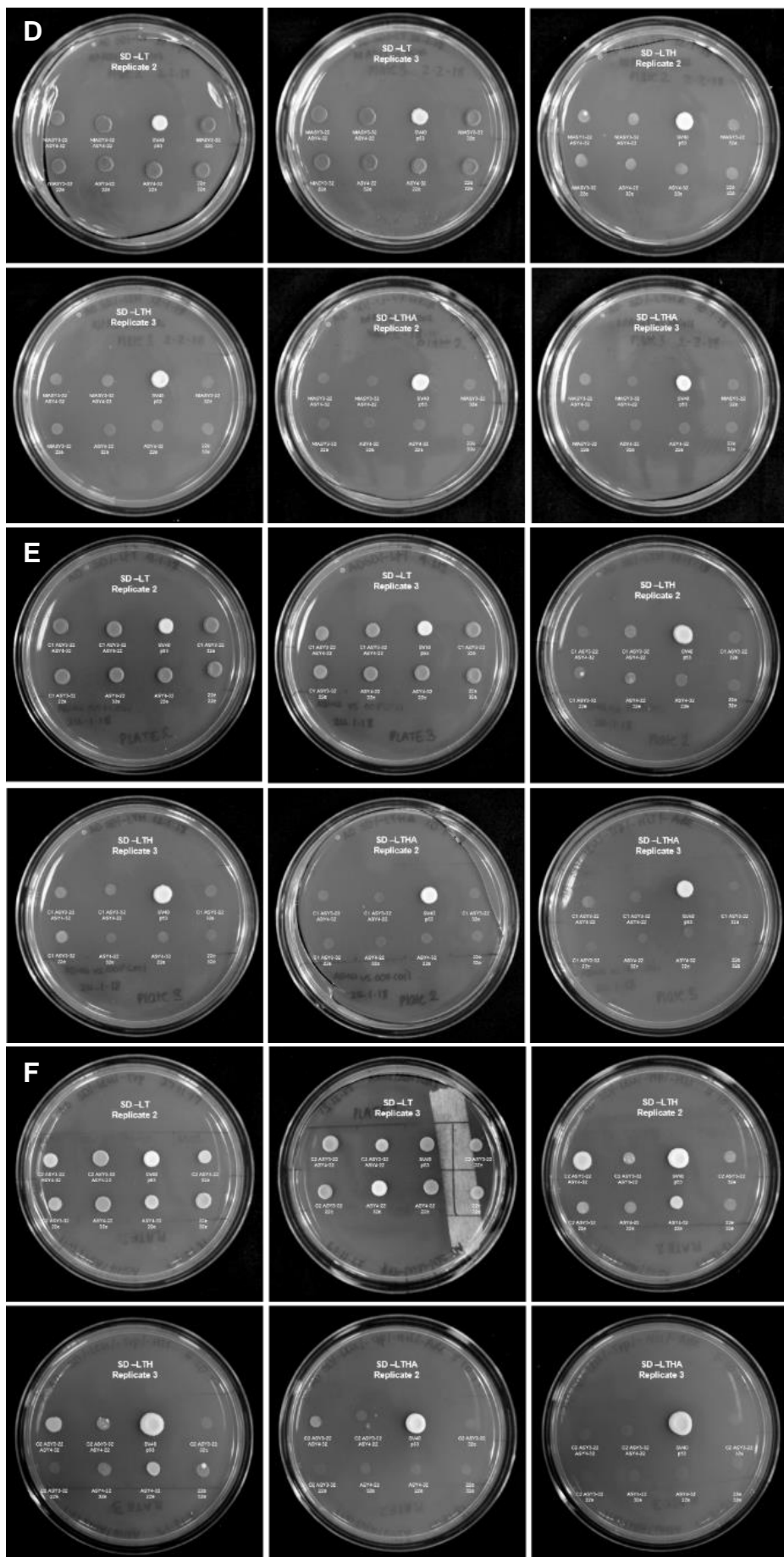


Figure A4
Replicate plates
from the Y2H
experiments.

(A) ASY4 vs ASY3.

(B) H1ASY4 vs ASY3.

(C) H2ASY4 vs ASY3

(D) NtASY3 vs ASY4

(E) C1ASY3 vs ASY4

(F) C2ASY3 vs ASY4.

Appendix for Chapter 4: Generation of ASY4 mutant lines using the CRISPR/Cas9 gene editing system

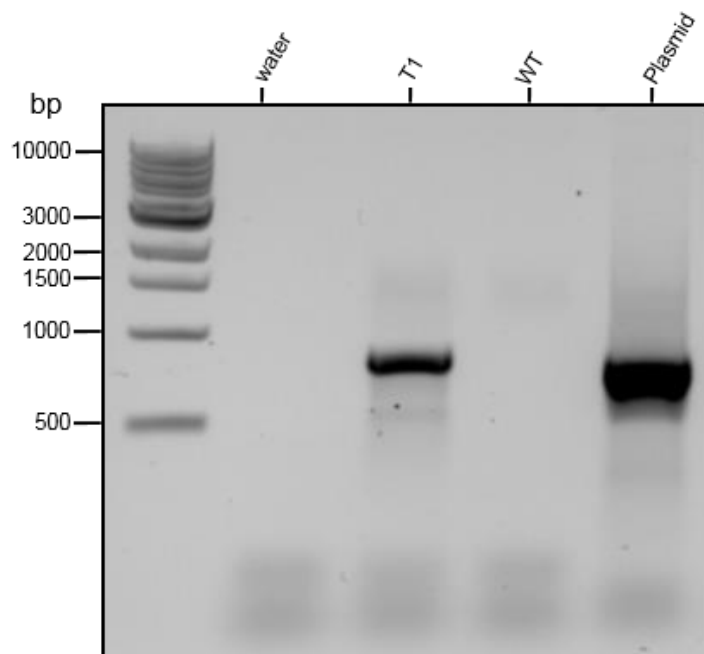


Figure A 5 Detection of the CRISPR/Cas9 construct *in planta* via PCR. PCR products imaged on an ethidium bromide agarose gel. T1 plant was selected as a transformant on MS media with kanamycin, and the presence of the plasmid confirmed by PCR. CRISPR/Cas9 is absent in the WT control. Positive plasmid control confirms the band obtained from T1 PCR is of the correct size.

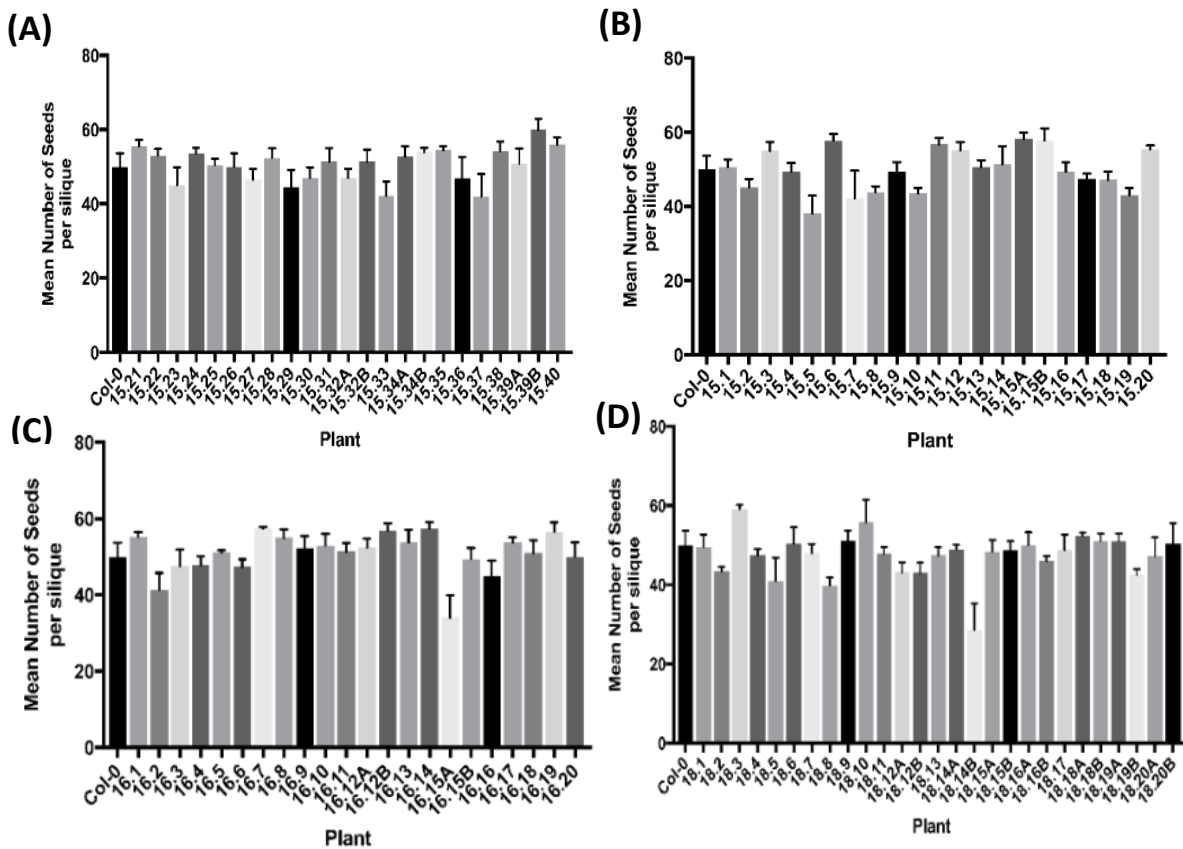


Figure A 6 Seed count data from T2 ASY4 CRISPR-Cas9 lines. **(A)** Seed count data from Line 15 (7.2). **(B)** Seed count data from Line 15 (7.3). **(C)** Seed count data from Line 16. **(D)** Seed count data from Line 18. Each column represents average data from 5 siliques. Bars represent SEM. All plants were compared in a Kruskal-Wallis test at the 5% level (with Dunn's correction) to WT (Col-0). All plants were not significantly different compared to WT.

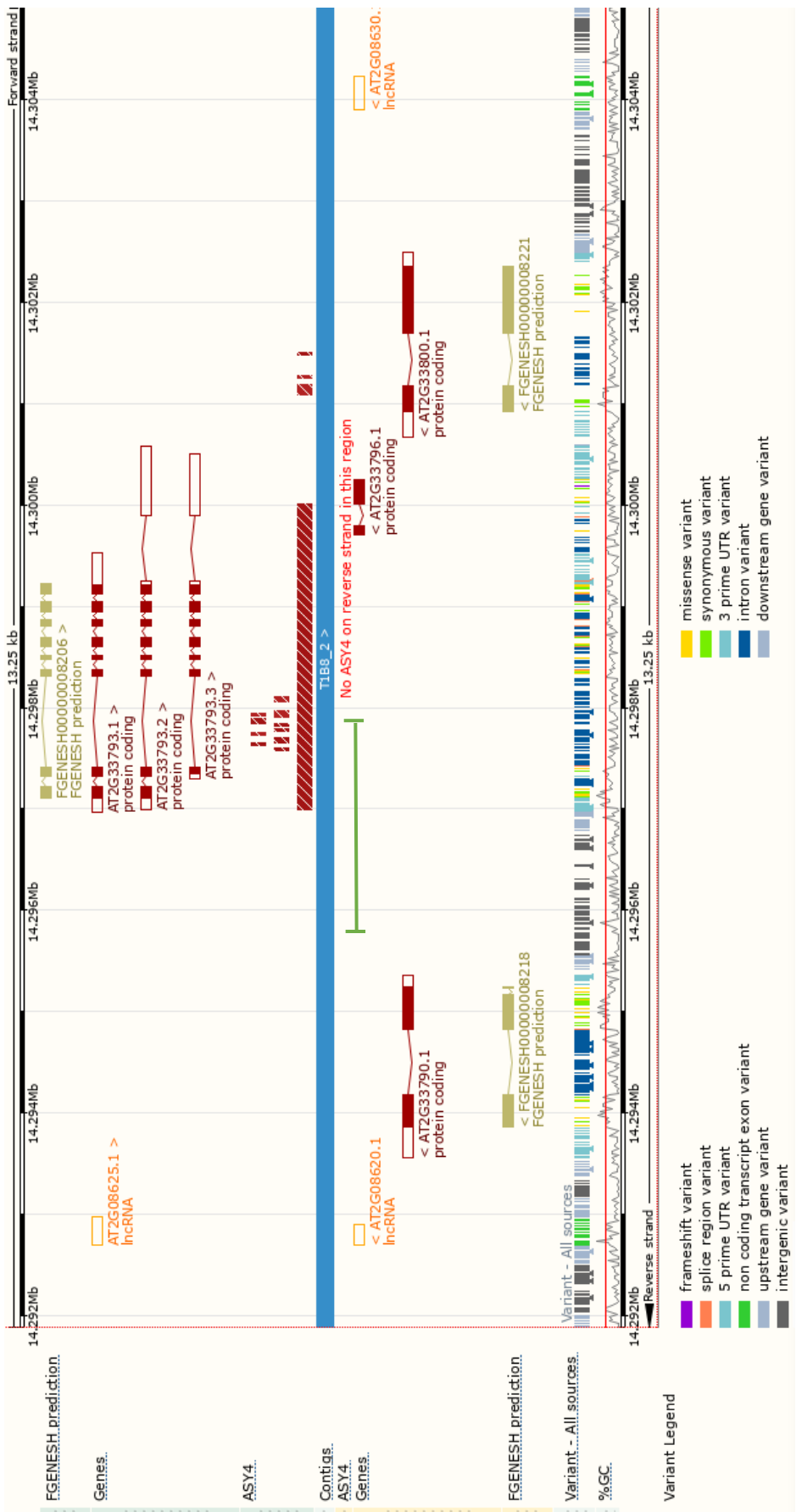


Figure A7 The ~1.7 kb deletion in ASY4 should not interfere with genes on the reverse strand. Green bar indicates the approximate span of the deletion. The deletion does not extend into any genes on the antisense strand. Alignment conducted within Ensembl Plants (available at: <https://plants.ensembl.org/index.html>).

Appendix for Chapter 5: Characterisation of a null-mutant of *asy4* generated by CRISPR-Cas9

Table A 10. Total SC length data for Col-0 (WT) and *asy4-4*

| Col-0 | <i>asy4-4</i> |
|----------|---------------|
| 133.0349 | 156.7809 |
| 126.9668 | 88.8819 |
| 268.4133 | 114.5217 |
| 340.2426 | 54.4345 |
| 208.6795 | 16.4815 |
| 141.0573 | 96.5421 |
| 79.4107 | 43.8093 |
| 225.6380 | 57.6943 |
| | 40.5149 |

Table A 11. DMC1 foci data for Col-0 (WT) and *asy4-4*

| Col-0 | <i>asy4-4</i> |
|-------|---------------|
| 220 | 242 |
| 206 | 163 |
| 227 | 202 |
| 221 | 214 |
| 151 | 207 |
| 202 | 183 |
| 163 | 170 |
| 146 | 221 |

| | |
|-----|-----|
| 177 | 232 |
| 189 | 204 |
| 182 | 224 |
| 190 | 150 |
| 220 | 227 |
| 200 | 143 |
| 172 | 146 |
| 182 | 155 |
| 197 | 227 |
| 157 | 212 |
| 183 | 154 |
| 163 | 209 |
| 175 | 215 |
| 163 | 160 |
| 176 | 135 |
| | 171 |
| | 144 |
| | 159 |
| | 204 |

Table A 12. MSH4 foci data for Col-0 (WT) and *asy4-4*

| Col-0 | <i>asy4-4</i> |
|-------|---------------|
| 133 | 158 |
| 157 | 139 |
| 174 | 137 |
| 160 | 128 |
| 158 | 140 |
| 163 | 176 |
| 146 | 148 |
| 155 | 150 |
| 119 | 163 |
| 143 | 170 |
| 177 | 145 |
| 161 | 180 |
| 161 | 138 |
| 147 | 158 |
| 171 | 166 |
| | 137 |
| | 170 |
| | 127 |

Table A 13. HEI10 foci data for Col-0 (WT) and *asy4-4*

| Col-0 | <i>asy4-4</i> |
|--------------|----------------------|
| 10 | 7 |
| 12 | 5 |
| 12 | 5 |
| 11 | 8 |
| 12 | 10 |
| 13 | 7 |
| 18 | 9 |
| 9 | 15 |
| 10 | 8 |
| 12 | 5 |
| 14 | 10 |
| 10 | 8 |
| 8 | 9 |
| 9 | 6 |
| 8 | 8 |
| 9 | 7 |
| 13 | 8 |
| 11 | 8 |
| 10 | 7 |
| | 7 |
| | 13 |
| | 12 |

General Appendix: Presentations, Publications, Outreach, Teaching, and Awards

List of Oral Presentations

Darbyshire A., Franklin F.C.H., Sanchez-Moran E. Investigating the roles of the chromosome axis during meiosis using gene editing. University of Bristol, March 2019. **Invited Speaker by Prof. Keith Edwards.**

Darbyshire A., West A., Osman K., Lambing C., Grelon M., Franklin F.C.H., Sanchez-Moran E. ASY4: A novel axis protein essential for meiotic recombination in *Arabidopsis thaliana*. British Meiosis Meeting, University of Sussex. May 2018.

Darbyshire A., West A., Osman K., Franklin F.C.H., Sanchez-Moran E. The Chromosome Axis and its role in Meiosis in *Arabidopsis thaliana*. MIBTP Symposium, University of Leicester, April 2018.

Darbyshire A., West A., Osman K., Franklin F.C.H., Sanchez-Moran E. The Chromosome Axis and its role in Meiosis in *Arabidopsis thaliana*. MIBTP Symposium, University of Leicester, April 2017.

List of Poster Presentations

Darbyshire A., Osman K., Franklin F.C.H., Sanchez-Moran E. Analysis of a null allele of the chromosome axis protein ASY1 generated by CRISPR-Cas9 using super-resolution microscopy. British Meiosis Meeting, University of Aberystwyth. April 2019.

Darbyshire A., West A., Osman K., Lambing C., Grelon M., Franklin F.C.H., Sanchez-Moran E. ASY4: A novel axis protein essential for meiotic recombination in *Arabidopsis thaliana*. Biosciences Graduate Research School Symposium, University of Birmingham. June 2018. **Awarded 1st Prize for Best Poster.**

Darbyshire A., West A., Osman K., Lambing C., Franklin F.C.H., Sanchez-Moran E. Characterisation of a Novel Chromosome Axis Associated Protein in *Arabidopsis thaliana*. Spanish Meiosis Meeting, Complutense University of Madrid. June 2017.

List of Publications

Martinez-Garcia, M., Schubert, V., Osman, K., **Darbyshire, A.**, Sanchez-Moran, E., Franklin, F.C.H., 2018. TOPII and chromosome movement help remove interlocks between entangled chromosomes during meiosis. *Journal of Cell Biology* 217, 4070–4079.

I provided RT-PCR data and conducted some cytology to analyse the prevalence of bridging in these mutants.

Chambon, A., West, A., Vezon, D., Horlow, C., Muyt, A.D., Chelysheva, L., Ronceret, A., **Darbyshire, A.**, Osman, K., Heckmann, S., Franklin, F.C.H., Grelon, M., 2018. Identification of ASYNTAPIC4, a Component of the Meiotic Chromosome Axis. *Plant Physiology* 178, 233–246.

I independently analysed the *asy4-1* and *asy4-2* lines, and analysed the ASY4eYFP lines. This paper is presented at the end of this thesis.

In Preparation:

Darbyshire A., Osman K., Price S., Franklin F.C.H., Sanchez-Moran E. Working title: Analysis of a null-allele of ASY4 generated by CRISPR-Cas9.

Aloufi S., **Darbyshire A.**, Sanchez-Moran E. Working title: Manipulating the meiotic pathway with CRISPR/Cas9.

List of Teaching Experience

2015-2019

Laboratory Demonstrator to second year undergraduates: Molecular Biology and its Applications: *Cloning the XylE gene*.

Roles included demonstrating protocols and marking submissions.

2018

Laboratory Demonstrator to second year undergraduates: Genetics II: *Genetic Mapping*.

Demonstrating protocols.

List of Outreach Actions

2019, 2017 & 2015

'Meet the Scientist'

Think Tank, Millennium Point, Birmingham, UK.

- 2015: Event organised with the Brownies highlighting some of the important contributions of women in STEM.
- 2017: Co-ordinated two events with fellow lab members, focused on introducing children to meiosis, food security, and genetically modified foods.
- 2019: Assisted in demonstrations to the public on the topic of DNA in plants, as part of a wider event organised by COMREC on meiosis in food security.

2017

'The Joy of Plant Sex: Meiosis and Food Security'

University of the Third Age, Birmingham Science Branch, UK.

Organised a talk at the U3A local meeting to discuss how our research at Birmingham hopes to alleviate present and future food security issues. Made meiosis-themed biscuits.

A-Level Science Resources: 'Laboratory Confessions'.

University of Birmingham, UK.

Approached by the University to conduct a series of podcasts as a resource for A-Level students and teachers to better understand various topics in biology from a researcher's perspective.

2016

'Meiosis and Food Security'

University of Birmingham School, Birmingham, UK.

Presented my thesis research topic to A-Level students, highlighting the importance of research in plants.

2015

'Improving the Sex Lives of Plants... and saving the world!'

Biosciences PhD Forum (<https://biosciencephdforum.wordpress.com>)

Invited to write a blog post on my research topic, explaining the importance of understanding meiosis to improving plant breeding.

Awards

2019

Postgraduate Certificate in Advanced Research Methods & Skills (PGCARMs)

For my extra-PhD activities, I qualified for the PGCARMs certificate, which has taken into account my outreach and teaching work, along with other academic activities such as successfully completing a computer programming, statistics, and maths course.

2017

Pass Certificate for completing Module 1 of SysMIC: Quantitative Skills for Bioscience.

Included programming in MATLAB and R.



Identification of ASYNAPTIC4, a Component of the Meiotic Chromosome Axis¹

Aurélie Chambon,^a Allan West,^{b,2} Daniel Vezon,^a Christine Horlow,^a Arnaud De Muyt,^{a,3} Liudmila Chelysheva,^a Arnaud Ronceret,^{a,4} Alice Darbyshire,^b Kim Osman,^b Stefan Heckmann,^{b,5} F. Chris H. Franklin,^b and Mathilde Grelon^{a,6,7}

^aInstitut Jean-Pierre Bourgin, Institut National de la Recherche Agronomique, AgroParisTech, Centre National de la Recherche Scientifique, Université Paris-Saclay, RD10, 78026 Versailles cedex, France

^bSchool of Biosciences, University of Birmingham, Edgbaston, Birmingham B15 2TT, United Kingdom

ORCID IDs: 0000-0003-2984-2108 (A.C.); 0000-0003-3473-9957 (A.W.); 0000-0002-1379-5709 (A.D.M.); 0000-0002-7538-2184 (L.C.); 0000-0002-1319-4006 (A.R.); 0000-0003-3391-328X (A.D.); 0000-0002-0282-4148 (K.O.); 0000-0002-0189-8428 (S.H.); 0000-0003-3507-722X (F.C.H.F.); 0000-0003-3695-4984 (M.G.)

During the leptotene stage of prophase I of meiosis, chromatids become organized into a linear looped array via a protein axis that forms along the loop bases. Establishment of the axis is essential for the subsequent synapsis of the homologous chromosome pairs and the progression of recombination to form genetic crossovers. Here, we describe ASYNAPTIC4 (ASY4), a meiotic axis protein in Arabidopsis (*Arabidopsis thaliana*). ASY4 is a small coiled-coil protein that exhibits limited sequence similarity with the carboxyl-terminal region of the axis protein ASY3. We used enhanced yellow fluorescent protein-tagged ASY4 to show that ASY4 localizes to the chromosome axis throughout prophase I. Bimolecular fluorescence complementation revealed that ASY4 interacts with ASY1 and ASY3, and yeast two-hybrid analysis confirmed a direct interaction between ASY4 and ASY3. Mutants lacking full-length ASY4 exhibited defective axis formation and were unable to complete synapsis. Although the initiation of recombination appeared to be unaffected in the *asy4* mutant, the number of crossovers was reduced significantly, and crossovers tended to group in the distal parts of the chromosomes. We conclude that ASY4 is required for normal axis and crossover formation. Furthermore, our data suggest that ASY3/ASY4 are the functional homologs of the mammalian SYCP2/SYCP3 axial components.

Meiosis is the specialized cell division that produces the haploid cells from which the gametes will be generated. In most organisms, this reduction in ploidy is

achieved by first segregating the homologous chromosomes from each other (meiosis I), then by separating the sister chromatids at meiosis II. The correct meiotic course relies on a series of coordinated mechanisms that take place during meiotic prophase I. They include the organization of sister chromatids along a common proteinaceous axis (the axial element [AE]), the pairing and the synapsis of these axes, recombination, and the formation of at least one crossover (CO) per homologous pair (Zickler and Kleckner, 1999).

The AEs are assembled early during meiotic prophase I, defining the leptotene stage. Then, axes from the homologous chromosomes become connected by the polymerization of the central element of the synaptonemal complex (SC), forming the lateral elements of the SC. The polymerization of the SC is complete by pachytene, a stage at which the maturation of recombination intermediates into COs is achieved, at least in *Saccharomyces cerevisiae* (Zickler and Kleckner, 1999). Next, the central element of the SC is disassembled while the chromosome axis participates in the dramatic chromosome condensation that occurs during the remaining steps of meiotic prophase I (diplotene, diakinesis).

Therefore, a defining feature of meiotic chromosomes is that sister chromatids share a chromosome axis to which they are anchored, forming regular arrays of chromatin loops. Because most of the recombination proteins are axis associated, it has been proposed that

¹Work in F.C.H.F.'s lab was supported by Biotechnology and Biological Sciences Research Council Grants ERA-Caps-13 BB/M004902/1 and MIBTP GBGB GAM2526. The Institut Jean-Pierre Bourgin benefits from the support of the LabEx Saclay Plant Sciences SPS (ANR-10-LABX-0040-SPS).

²Current address: Central European Institute of Technology, Masaryk University, Kamenice 753/5, 62500, Czech Republic.

³Current address: Institut Curie, PSL Research University, Centre National de la Recherche Scientifique, Unité Mixte de Recherche 3664, F-75005 Paris, France.

⁴Current address: Instituto de Biotecnología/UNAM, Av. Universidad #2001, Col. Chamilpa C.P. 62210, Cuernavaca, Morelos, Mexico.

⁵Current address: Leibniz Institute of Plant Genetics and Crop Plant Research, D-06466, Stadt Seeland, Germany.

⁶Author for contact: mathilde.grelon@inra.fr.

⁷Senior author: mathilde.grelon@inra.fr.

The author responsible for distribution of materials integral to the findings presented in this article in accordance with the policy described in the Instructions for Authors (www.plantphysiol.org) is: Mathilde Grelon (mathilde.grelon@inra.fr).

A.C., A.D., K.O., and A.W. performed most of the experiments; D.V., C.H., L.C., A.R., and S.H. provided technical assistance; A.D.M., F.C.H.F., and M.G. conceived the experiments; F.C.H.F. and M.G. supervised the writing.

www.plantphysiol.org/cgi/doi/10.1104/pp.17.01725

meiotic chromosome axes form a scaffold on which meiotic recombination takes place (Blat et al., 2002; Panizza et al., 2011). Notwithstanding these structural roles, chromosome axes also appear highly flexible and dynamic. Their physical association with the chromosomes depends on and is responsive to underlying transcriptional activity (Sun et al., 2015). Some of their components are displaced upon synapsis and during recombination, where there is a requirement for localized axis exchange at CO sites.

Chromosome axes are composed of various protein families (Zickler and Kleckner, 1999). Cohesins (and notably the meiosis-specific Rec8 protein) as well as cohesin-associated factors such as the condensins are key components of the AEs. Cohesins form ring-shaped complexes that associate sister chromatids together after replication and that, in *S. cerevisiae*, anchor the other AE proteins to chromatin (Sun et al., 2015). The HORMA domain proteins (Hop1 in *S. cerevisiae*, Hormad1 and Hormad2 in mammals, ASY1 [ASYNAPTIC1]/PAIR2 [HOMOLOGOUS PAIRING ABERRATION IN RICE MEIOSIS2] in plants, and HIM-3 [HIGH INCIDENCE OF XO MALES-3], HTP-1, HTP-2, and HTP-3 [HIM THREE PARALOG-1, -2, and -3] in *Caenorhabditis elegans*) also represent major components of the meiotic chromosomal axes that, in *C. elegans*, constitute the linker between the cohesins and the SC central element (Pattabiraman et al., 2017). In several organisms, including Arabidopsis (*Arabidopsis thaliana*), their axis association is negatively regulated by synapsis (Börner et al., 2008; Wojtasz et al., 2009; Lambing et al., 2015). The last class of known AE proteins contains the *S. cerevisiae* Red1 (REDUCTIONAL DIVISION1), the mouse SYCP2 and SYCP3 (SCP2 and SCP3 in rat; SYNAPTONEMAL COMPLEX PROTEINS2 and -3), and the plant ASY3/PAIR3/DSY2 (DESYNAPTIC2; Wangetal., 2011; Ferdous et al., 2012; Lee et al., 2015). All these proteins are meiosis-specific components of the AE. Red1, SYCP2/SCP2, and ASY3/PAIR3 are large proteins that show limited sequence similarities, suggesting that they could be distantly related (Offenberg et al., 1998; Ferdous et al., 2012). Concerning the mammalian SYCP3/SCP3, they are small proteins that show sequence similarities with SYCP2/SCP2, with which they interact through their coiled-coil regions. They are thought to represent key structural components of the mammalian meiotic chromosome axes, since, notably, they form multistranded fibers that mimic the AEs when expressed ectopically in somatic cells (Yuan et al., 1998; Pelttari et al., 2001). In addition, structural resolution of human SYCP3 revealed that it forms elongated helical tetrameric structures that self-assemble into AE-like fibers that possess the intrinsic capacity of mediating double-stranded DNA compaction (Syrijänen et al., 2014, 2017).

Mutants defective in any component of the AE exhibit substantial perturbation of the meiotic recombination process. The plant HORMA domain-containing protein ASY1 is not required for normal double-strand break (DSB) formation but for DMC1 stabilization on recombination sites (Armstrong et al., 2002;

Sanchez-Moran et al., 2007). In consequence, in *asy1* mutants, meiotic DSBs are repaired predominantly using a sister chromatid as template, as is the case in a *dmc1* mutant, provoking a shortage in CO formation (Sanchez-Moran et al., 2007). The axial protein ASY3/PAIR3/DSY2, on the other hand, is required for normal levels of DSB formation in Arabidopsis and in maize (*Zea mays*; Ferdous et al., 2012; Lee et al., 2015). It is also required for normal ASY1 assembly onto the chromosome axis, and it interacts with ASY1 (Ferdous et al., 2012; Lee et al., 2015) and with ZYP1 (Lee et al., 2015).

In this article, we identify ASY4, a short coiled coil-containing protein showing similarity with the ASY3 C-terminal coiled-coil region. We show that ASY4 is an axis-associated protein that interacts with ASY1 and ASY3. We also found that ASY4 is required for normal ASY1 and ASY3 localization, for full synapsis, and for CO formation.

RESULTS

Identification of ASY4, a Meiotic Gene with Similarity to ASY3

A BLASTP search against the Arabidopsis genome using ASY3 (At2G46980) as a query identified the uncharacterized At2g33793 protein (hereafter called ASY4) as showing 29% identity and 45% similarity with 142 amino acids of the C-terminal region of ASY3 (Fig. 1). While ASY3 is a large protein (793 amino acids, 88 kD), ASY4 is only 212 amino acids long (25 kD). Its sequence does not contain any known functional domains, and most of ASY4 is predicted to form coiled coils (amino acids 71–183; Fig. 1). Homologs of ASY4 can be identified in Tracheophyta sequenced genomes (which include flowering plant genomes and *Sellaginella moellendorffii*). Outside Tracheophyta, an ASY4 homolog is found in *Marchantia polymorpha* but not in mosses. Reverse transcription PCR on Arabidopsis cDNAs isolated from different organs from wild-type plants showed that ASY4 is expressed predominantly in flower buds (Supplemental Fig. S1).

To analyze ASY4 function, we characterized two independent mutant lines in At2g33793. One was available in the public databases: line SK22114 (stock CS1006148, later referred to as *asy4-1*). The second one (*asy4-2*) was isolated by PCR screening of Max Planck Institute for Plant Breeding Research Arabidopsis T-DNA insertion mutants (Ríos et al., 2002). Insertions in the *asy4-1* and *asy4-2* mutants are located in the fourth and fifth exons of ASY4, respectively, and are associated with deletions of 17 and 19 bp, respectively (Fig. 1; Supplemental Fig. S2). Residual transcription corresponding to the 5' end of the gene can be detected in both mutants (Supplemental Fig. S1). They could potentially generate a C-terminally truncated protein of 92 or 106 amino acids, respectively.

Both *asy4* mutants investigated in this study showed normal vegetative growth (data not shown) but fertility

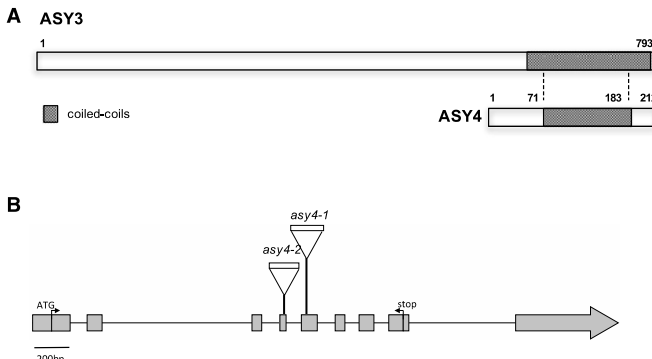


Figure 1. Schematic representation of the ASY4 protein and the ASY4 gene. A, The ASY4 protein shows similarities with the ASY3 C-terminal region (dashed lines). Predicted coiled coils of both proteins are indicated by gray boxes. Numbers refer to amino acids. B, The ASY4 open reading frame and the positions of the T-DNA insertion in *asy4-1* and *asy4-2* mutants. Exons are shown as gray boxes.

defects (Supplemental Fig. S3) that correlated with meiotic defects (Fig. 2). During prophase I in wild-type meiosis, the 10 *Arabidopsis* chromosomes condense and recombine, resulting in the formation of five bivalents, each consisting of two homologous chromosomes attached to each other by sister chromatid cohesion and chiasmata (the cytological manifestation of COs), which become visible at diakinesis. Synapsis (the close association of two chromosomes mediated by the SC) begins at zygote and is complete by pachytene. At metaphase I, the five bivalents are easily distinguishable and aligned on the metaphase plate. During anaphase I, each chromosome separates from its homolog, leading to the formation of dyads corresponding to two pools of five chromosomes. The second meiotic division then separates the sister chromatids, generating four pools of five chromosomes, which gives rise to tetrads of four haploid daughter cells. In *asy4* mutants, each of these meiotic stages can be identified, although full synapsis was not detected. Moreover, the presence of univalent chromosomes at diakinesis and unbalanced tetrads (illustrated for the *asy4-1* mutant in Fig. 2) indicates a defect in CO formation.

The reduction in chiasma number observed in *asy4* meiocytes was quantified at the transition between metaphase I and anaphase I by estimating the number of chiasma based on bivalent shape. Rod bivalents reflect the occurrence of a minimum of one chiasma on a single chromosome arm pair, whereas ring bivalents reflect the occurrence of at least one chiasma per chromosome arm. This estimation provides a minimum chiasma number (MCN; as defined by Jahns et al. [2014]), because multiple chiasmata on a single bivalent arm cannot generally be discriminated from single chiasma. In both *asy4* mutants, the MCN is decreased significantly in comparison with the wild type, with the *asy4-1* allele being the most affected, showing an average of 5.9 ± 1.5 MCN per cell (in the wild type, the mean number of MCN per cell is 8.9 ± 0.89 ; Student's *t* test, $P < 0.0001$; Fig. 2; Supplemental Fig. S4). Therefore, all subsequent analyses were conducted with the *asy4-1* mutant.

This phenotype of a decrease in chiasma formation associated with abnormal synapsis has been described previously for mutants defective in axis formation typified by the *asy1* and *asy3* mutants (Armstrong et al., 2002; Ferdous et al., 2012). Therefore, we analyzed the epistatic relationships between these various mutations. This revealed that, in terms of chiasma level, the *asy1* mutation is epistatic to the *asy3* and *asy4* mutations, with *asy1 asy3* and *asy1 asy4* double mutant combinations showing only 2 MCN per cell (Fig. 2; Supplemental Fig. S4). When analyzing the double mutation *asy3 asy4*, however, we found that the average number of chiasmata per cell is intermediate between the *asy3* and *asy4* mutations (4.1 ± 1.3 MCN per cell) and significantly different from each single mutant (one-way ANOVA, $P < 0.0005$).

asy4 Mutants Are Defective in Meiotic Recombination

In order to understand the origin of the reduced chiasma formation observed in the *asy4* mutants, we investigated meiotic recombination in further detail. First, we immunolocalized DMC1, a meiosis-specific recombinase that forms foci at recombination sites. In the wild type, DMC1 foci appear at late leptotene/early zygote, reaching an average of 240 foci per nucleus (Chelysheva et al., 2007). In the *asy4-1* mutant, we counted an average of 222 ± 107 ($n = 15$) foci per cell, suggesting that early recombination events are not affected in *asy4* (Supplemental Fig. S5). We then immunolocalized the ZMM protein MSH5, a MUTATOR S homolog, that is involved in the stabilization of progenitor double-Holliday Junctions and HEI10 (ENHANCER OF CELL INVASION NO. 10), which has been shown to mark a subset of recombination intermediates that are channeled into the ZMM pathway (Snowden et al., 2004; Higgins et al., 2008; Chelysheva et al., 2012). MSH5 foci were detected in the wild type and the *asy4-1* mutant at late leptotene/early zygote (Fig. 3, A and B). No significant difference in the number of foci was observed (wild type = 110.9 ± 38.61 , $n = 15$; *asy4-1* = 121.1 ± 29.55 , $n = 15$; Mann-Whitney

Chambon et al.

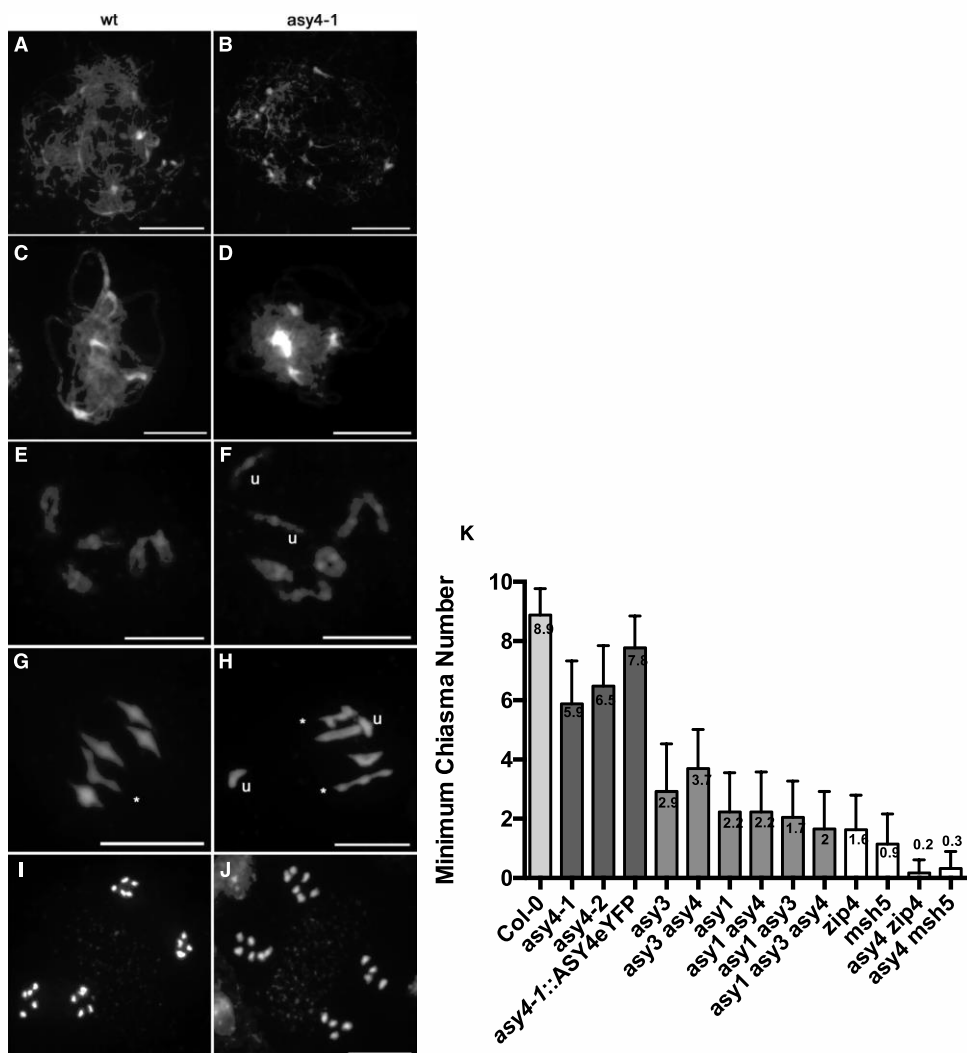


Figure 2. ASY4 is required for normal meiosis. A to J, 4',6-Diamino-phenylindole (DAPI) staining of meiotic chromosomes in the wild type (A, C, E, G, and I) and the *asy4-1* mutant (B, D, F, H, and J). A and B, Leptotene. C, Pachytene. D, Partial synapsis typical of the defects of synapsis observed in *asy4* mutants. E and F, Diakinesis. G and H, Metaphase I. I and J, End of anaphase II. u, Univalent; *, rod bivalent. Bars = 5 μ m. K, Quantification of the number of chiasma that can be identified at metaphase I (MCN) in both *asy4* mutants as well as in a series of mutants and multimers. Numbers give the average MCN per cell. The detailed data set can be found in Supplemental Figure S4.

U test, $P = 0.3835$). This implies that recombination in the *asy4-1* mutant progresses beyond DMC1-catalyzed strand invasion. HEI10 is loaded early during prophase I on a large number of recombination sites, forming foci of different sizes on chromosomes. As

meiosis progresses, HEI10 foci become brighter and associated with the central element of the SC (ZYP1; Fig. 3C). During pachytene, a limited number of these foci remain at sites that correspond to class I COs, where they colocalize with MLH1 until the end of prophase

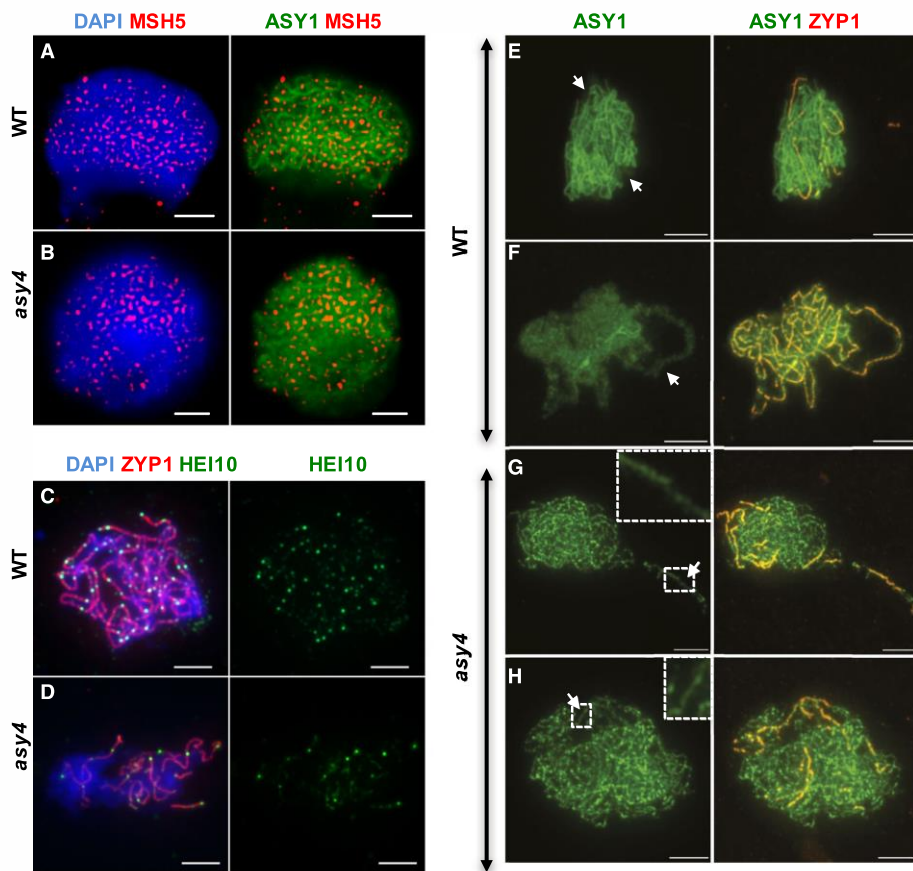


Figure 3. The *asy4* mutant is defective in recombination, axis biogenesis, and synapsis. A and B, Dual ASY1 and MSH5 immunodetection. Colors are as follows: ASY1 (green), MSH5 (red), and DAPI (blue). Images are single frames from mid Z-stack. Bars = 2 μ m. C and D, Dual ZYP1 and HEI10 immunodetection together with DAPI (blue) on male meiocytes at a similar stage. Bars = 2 μ m. E to H, Dual ASY1 (green) and ZYP1 (red) immunodetection. Arrows indicate synapsed regions where ASY1 is depleted in the wild type (WT) but not in the *asy4-1* mutant. Bars = 2 μ m.

(data not shown). In the *asy4-1* mutant, the HEI10 dynamics were similar to those in the wild type, with foci of mixed sizes colocalizing with ZYP1 while synapsis progresses (Fig. 3D). However, ZYP1 staining was very limited, never progressing to full synapsis, confirming the chromosome synapsis defects detected after DAPI staining of the chromosomes (Fig. 2). In consequence, the pachytene-like HEI10 foci observed on the partially synapsed nuclei were decreased strongly in comparison with the wild type (Fig. 3D).

We then estimated the average number of the class I COs (which rely on the ZMM pathway and are sensitive to interference from neighboring COs) in the *asy4* mutant by immunolabeling chromosomes with

antibodies directed against MLH1, a marker of class I COs (Fig. 4). We found that the *asy4-1* mutant shows a limited but significant decrease in MLH1 foci from 11 ± 1.5 (mean \pm SD; $n = 60$) in the wild type to 8.6 ± 2.2 ($n = 147$) in the *asy4-1* mutant (Student's *t* test, $P < 0.05$). We then analyzed the distribution of these foci within bivalents. We kept in our analysis all pairs of chromosome arms where at least one MLH1 foci can be observed at diakinesis. In wild-type meiocytes, the mean number of MLH1 foci per chromosome arm is 1.4 ± 0.52 ($n = 180$; range, 1–3), whereas in the *asy4-1* mutant, it increased significantly ($P < 0.0001$, Student's *t* test) to a mean of 1.8 ± 0.85 ($n = 134$), with a much greater range of values than in the wild type (1–6 compared with

1–3 in the wild type; Fig. 4B). In order to confirm these results, we analyzed the level of recombination in four genetic intervals located on chromosome 5 using the Fluorescent Tagged Lines (FTL) tool (Berchowitz and Copenhaver, 2008). For most intervals (three out of four), recombination rates decreased significantly but moderately in the *asy4* mutant, reaching, on average, 75% of the wild-type level of recombination (Table 1). This effect is comparable to the decrease in chiasma number observed in *asy4* mutants (Fig. 2). However, the I5b interval, which is distally located on chromosome 5, appears differentially affected, since meiotic recombination increases slightly but significantly in *asy4* mutants (from 16 to 20 cM; Table 1). In conclusion, the *asy4* mutation provokes a decrease in meiotic recombination, but this effect appears to vary according to the chromosomal intervals considered.

In *Arabidopsis*, most COs are under the control of the ZMM pathway and exhibit interference (Mercier et al., 2015). We analyzed *asy4 zip4* and *asy4 msh5* double mutants and found that the level of bivalent formation was reduced dramatically by more than 95% (Fig. 2), showing that, in mutants as in the wild type, most of the COs were dependent on the ZMM pathway. We then estimated the level of interference between COs in each FTL interval by calculating the ratio between the observed number of double COs and the expected number of double COs under the hypothesis of no interference (NPD ratio as defined by Snow [1979]). We observed that, in most intervals considered, in the *asy4* mutants as in the wild type, the NPD ratio is smaller than 1, revealing the presence of interference between adjacent COs.

Then, the interference between COs occurring in adjacent intervals (I5a/I5b or I5c/I5d) was estimated by calculating the IR as defined by Malkova et al. (2004). The IR compares the genetic length of one interval with and without the presence of a simultaneous event in the neighboring interval. When the occurrence of a CO in one interval reduces the probability of a CO occurring in the adjacent interval, the IR is less than 1, indicating CO interference. When COs in the two adjacent intervals are independent of each other, the IR is 1, and if the presence of one CO in an interval increases the probability of an additional CO in the adjacent interval, the IR is greater than 1, indicating negative interference. IRs revealed the presence of interference between COs in the wild type (for both pairs of intervals) and for the *asy4* mutants for the I5c/I5d pair of intervals (Table 1). However, for the I5a/I5b pair of intervals, the IR in *asy4* mutants is above 1, suggesting that, in that chromosomal region, adjacent COs occur more frequently than in the wild type. Taken together, these data show that the *asy4* mutation perturbs meiotic recombination quantitatively (by decreasing it) and qualitatively (by altering CO location).

The *asy4* Mutation Is Associated with Axis Defects

We investigated the behavior of several components of the meiotic chromosome axis (ASY1, ASY3, REC8, and SCC3) in the *asy4* mutant in comparison with the

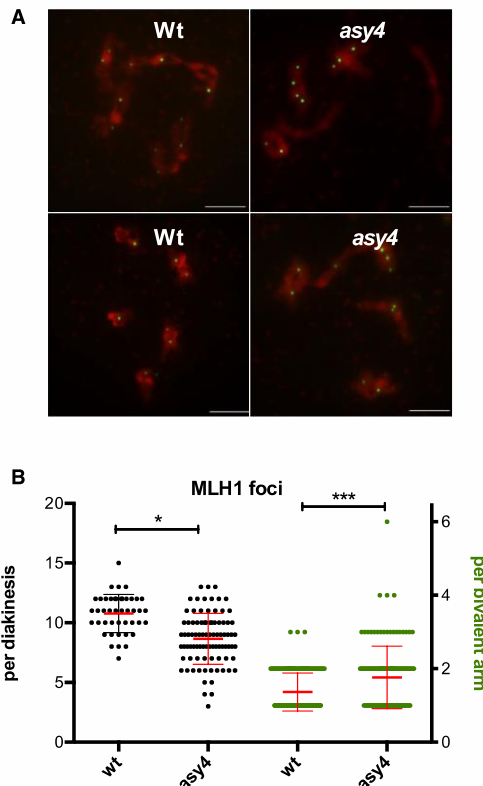


Figure 4. MLH1 detection and quantification. **A**, MLH1 was immunolocalized (green) on diakinesis chromosomes from the wild type (Wt) or the *asy4-1* mutant (*asy4*). Chromosomes were stained by DAPI (red). Bars = 5 μ m. **B**, Left side of the graph (black dots), number of MLH1 foci per cell at diakinesis in the wild type and the *asy4-1* mutant. Right side of the graph (green dots), number of MLH1 foci per chromosome arm, measured among the pairs of chromosome arms where at least one MLH1 foci can be observed at diakinesis. Asterisks indicate significant differences between the wild type and the mutant in both cases (*, $P < 0.05$ and ***, $P < 0.0001$).

wild type (Figs. 3 and 5; Supplemental Fig. S6). ASY1, ASY3, REC8, and SCC3 are detected during meiotic prophase I and exhibit different dynamics as meiosis progresses (Armstrong et al., 2002; Cai et al., 2003; Chelysheva et al., 2005; Ferdous et al., 2012). At leptotene, immunodetection showed that all these proteins decorate meiotic chromosomes, revealing signals all along the typical thread-like chromosomal axis. As synapsis proceeds and the central element connects the AEs of the homologous chromosomes, ASY1 is depleted from the axis and, consequently, the ASY1 signal appears faint and fuzzy (Fig. 3, arrows; Supplemental Fig. S6). ASY3, REC8, and SCC3 also mark the chromosome

Table 1. Recombination rates and interference

Recombination rates were measured in four chromosome 5 intervals (I5a–I5d). For each interval, the map distance in centimorgan (cM) was calculated using the Perkins genetic map equation (PMID 17247336). The distance ratio compares the recombination rates between the wild type and *asy4-1*. The nonparental ditype (NPD) ratio and the interference ratio (IR) give the strength of interference either within the considered interval or among two adjacent intervals (no interference if the ratios are equal to 1, absolute interference if the ratios are equal to 0). Asterisks indicate significant differences between ratios and 1 (*, significant at 5% and **, significant at 1%).

| Plant | Interval | No. of Tetads | Map Distance | Distance Ratio (<i>asy4</i> /Wild Type) | NPD Ratio | IR |
|---------------|----------|---------------|--------------|---|-----------|-------|
| Wild type | I5a | 10,303 | 27 | — | 0.3** | 0.4** |
| | I5b | 10,303 | 16.1 | — | 0.2** | |
| | I5c | 14,590 | 7.7 | — | 0.3** | 0.3** |
| | I5d | 14,590 | 7.4 | — | 0.3** | |
| <i>asy4-1</i> | I5a | 7,462 | 15.5 | 0.6 | 0.9 | 1.2** |
| | I5b | 7,462 | 20 | 1.2 | 0.6** | |
| | I5c | 13,753 | 6.8 | 0.9 | 0.4** | 0.7** |
| | I5d | 13,753 | 5.6 | 0.8 | 0.5* | |

axes, but contrary to ASY1, they are not removed during synapsis (Fig. 5; Supplemental Fig. S6). In the case of the cohesins REC8 and SCC3, no obvious modification in their pattern could be detected (Fig. 5; Supplemental Fig. S6). The two axis-associated proteins ASY1 and ASY3 are loaded onto the chromosome axis, and chromosome threads typical of leptotene stages can be seen. However, ASY1 and ASY3 signals adopt an abnormally patchy and lumpy aspect (Figs. 3 and 5) that is very unlikely to originate from the synapsis defect of *asy4* mutants; instead, it suggests that ASY4 is required for normal chromosome axis structure. In addition, we observed no displacement of ASY1 from the synapsed chromosome axes (Fig. 3, zoom), revealing abnormal axis dynamics. We investigated the chromosome axis further by silver staining of chromosome spreads and wide-field microscopy observation as described by Armstrong and Jones (2001). This chromatin staining permits the detection of the meiotic chromosome axis from leptotene to the end of meiosis. In the *asy4* mutant as well as in *asy3 asy4* and *asy1 asy3 asy4* multiple mutants, no modification of the silver-stained axis could be detected (Fig. 5), suggesting that, even if axis composition and/or dynamics is affected in *asy4*, at this level of resolution, the overall structure of the axis appears physically intact.

ASY4 Is an Axis-Associated Protein

To examine the cellular localization of ASY4, we used fluorescent protein tagging. An ASY4-eYFP construct was produced and introduced into homozygous *asy4-1* plants, the most severely affected mutant background. Seed counts were performed on siliques from T2 generation plants (Supplemental Fig. S7). Fertility levels across the transformant lines were wide ranging, from those similar to the *asy4-1* mutant to a line that was not significantly different from the wild type (line 165.15, subsequently referred to as *asy4-1::ASY4eYFP*; Supplemental Fig. S7). Analysis of DAPI-stained chromosome spreads of *asy4-1::ASY4eYFP* male meiocytes from T3 plants at metaphase I revealed a chiasma frequency of 7.7 ± 1.1 ($n = 75$). This was significantly higher than in

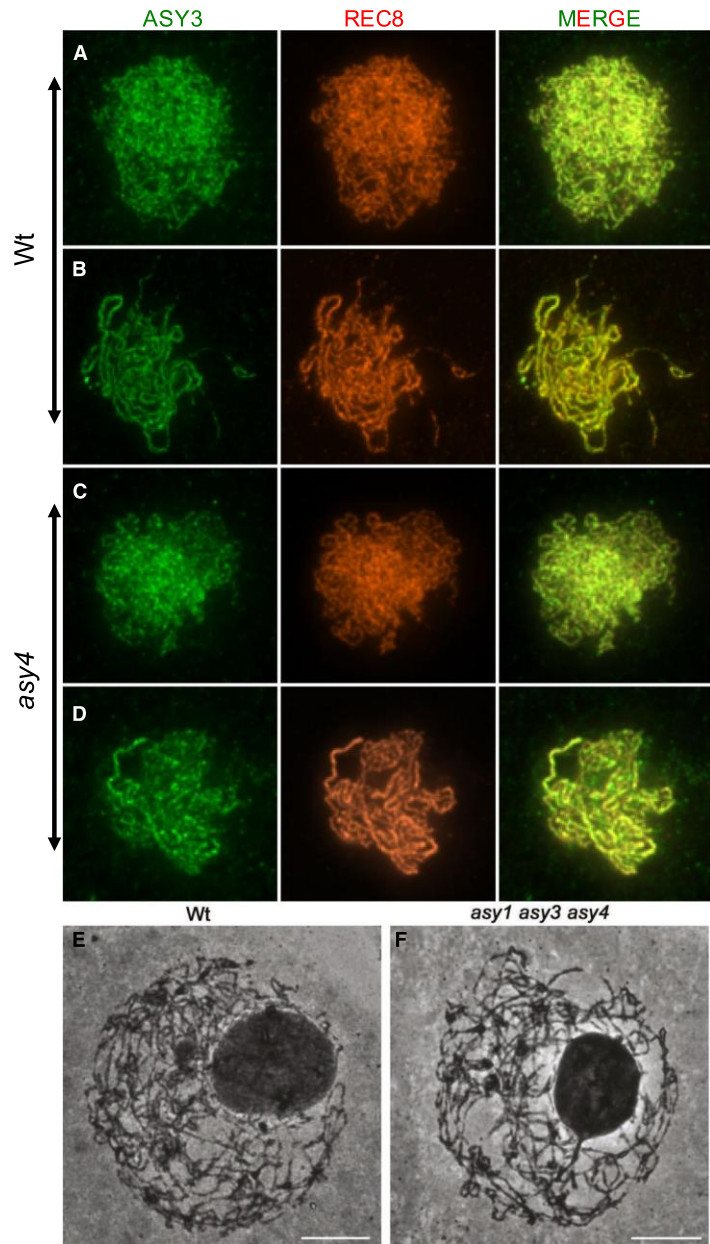
the *asy4-1* mutant (5.9 ± 1.43 [$n = 64$]; Mann-Whitney *U* test, $P < 0.01$). However, it was slightly lower than in the wild type (8.6 ± 0.83 [$n = 28$]; Mann-Whitney *U* test, $P < 0.01$; Fig. 2; Supplemental Fig. S7). In addition, occasional seed gaps in its siliques were apparent, suggesting that fertility was not restored completely (Supplemental Fig. S7).

Examination of the anthers from *asy4-1::ASY4eYFP* plants using epifluorescence microscopy confirmed the expression of the tagged gene within male meiocytes (Supplemental Fig. S7). Localization of ASY4eYFP was then investigated in prophase I chromosome spread preparations by direct fluorescence combined with immunostaining of the chromosome axis protein, ASY1, and the SC protein, ZYP1. This revealed that ASY4 localizes as a linear, axis-associated signal at leptotene, where it follows the localization pattern of ASY1 with alternating regions of high and low intensity (Fig. 6). However, in contrast to ASY1, which becomes depleted from the axes as zygote progresses, it persists on synapsed regions of the chromosomes (Fig. 6). In this respect, its behavior is similar to that of ASY3, REC8, and SCC3.

Considering the similarity between the ASY3 and ASY4 protein sequences, the axial association of these two proteins (Ferdous et al., 2012; this study), and the perturbed ASY1 and ASY3 signals observed in the *asy4* mutant, we investigated whether these proteins interact physically. An interaction between ASY1 and ASY3 has already been demonstrated for *Brassica oleracea* and *Arabidopsis* proteins either in planta by coimmunoprecipitation of ASY3 from anthers by antibodies directed against ASY1 or in yeast two-hybrid experiments using the *Arabidopsis* proteins (Ferdous et al., 2012). Here, we used bimolecular fluorescence complementation (BiFC) assays in leaf epidermal cells of *Nicotiana benthamiana* plants (Hu et al., 2002). Fusion proteins with complementary YFP truncations (YFP^N + YFP^C) were coinfiltrated in *N. benthamiana* leaves expressing a cyan fluorescent protein (CFP) nuclear marker. As shown in Figure 7 and Supplemental Figure S8, this assay revealed interactions among the three ASY proteins and also self-interaction of these three

Chambon et al.

Figure 5. Chromosome axis investigation. A to D, Dual ASY3 (green) and REC8 (orange) immunolocalization on wild-type (Wt; A and B) or *asy4-1* mutant (*asy4*; C and D) male meiocytes. E and F, Silver staining of wild-type and triple *asy1 asy3 asy4* mutant male meiocytes. Bars = 2 μ m.



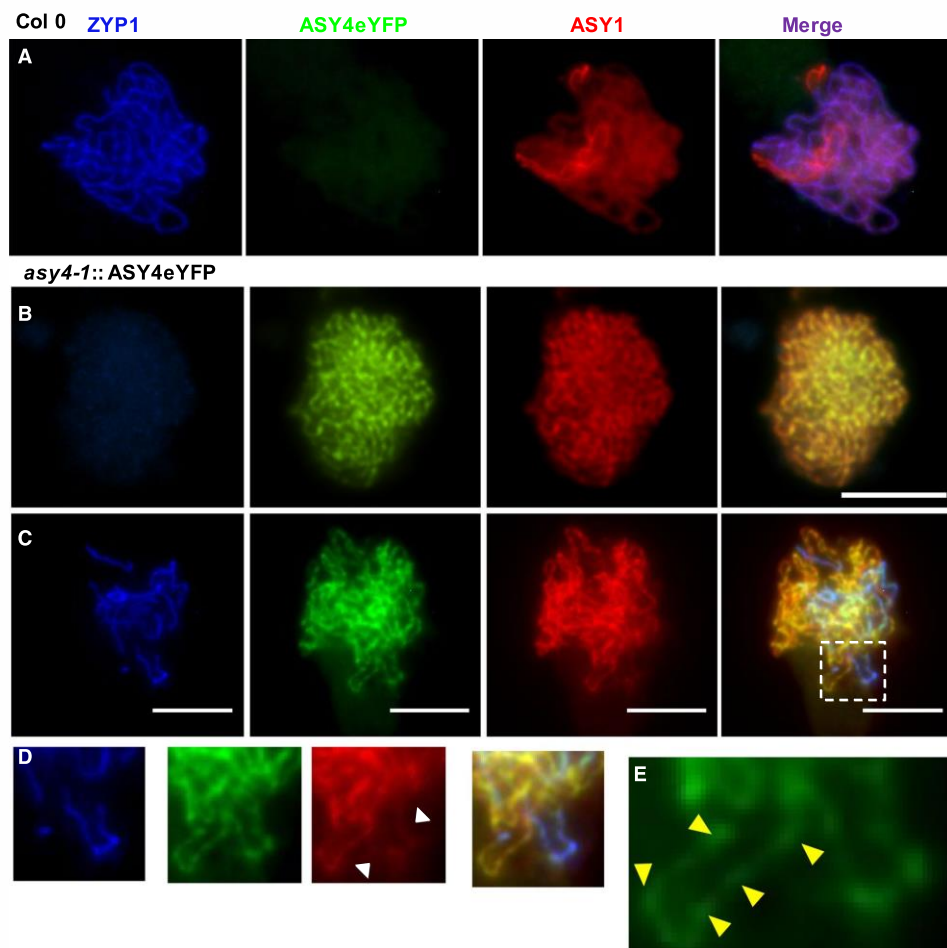


Figure 6. Localization of ASY4eYFP in prophase I chromosome spreads of *asy4-1::ASY4eYFP* plants. A, Wild-type (Col 0) zygote showing the absence of eYFP fluorescence. B and C, *asy4-1::ASY4eYFP* leptotene (B) and *asy4-1::ASY4eYFP* zygote (C). D, Details of the ASY4eYFP fluorescence present on the axis in regions of intense ASY1 staining (unsynapsed) and ZYP1 staining (synapsed). Note the reduction in intensity of ASY1 signal in synapsed regions (white arrowheads). E, ASY4eYFP fluorescence is nonuniform and alternates between regions of high (yellow arrowheads) and low intensity. Colors are as follows: ZYP1 (blue) and ASY1 (red) immunostaining with ASY4-eYFP fluorescence (green). Bars = 5 μ m.

proteins. The YFP signal recovered in these experiments using ASY3 or ASY4 fusion proteins revealed nonuniform nucleus-targeted signals, suggesting that these proteins when overexpressed in plant cells form nuclear aggregates. Yeast two-hybrid experiments confirmed ASY3-ASY4 interactions as well as ASY3-ASY3 and ASY4-ASY4 self-interactions (Supplemental Fig. S9).

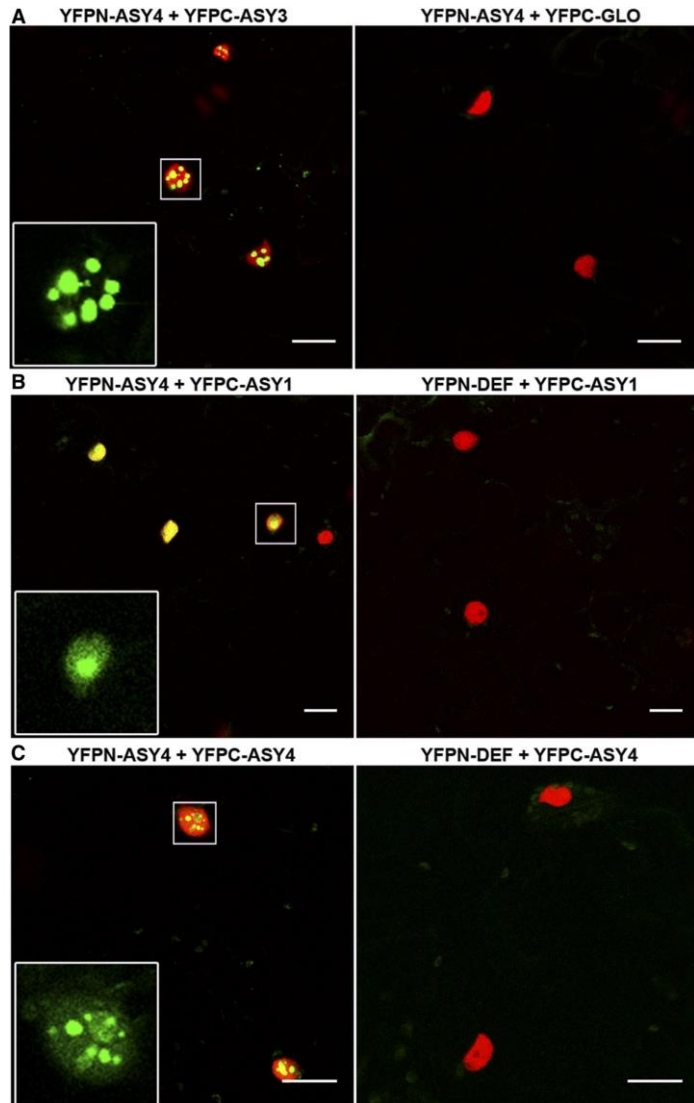
DISCUSSION

Conserved Composition of the Meiotic Axial Element in Spite of Poor Primary Protein Sequence Conservation

We identified ASY4, which shows sequence similarity with the ASY3 C-terminal region and is closely related with two of the known plant axial components, ASY1/PAIR2 and ASY3/PAIR3/DSY2. The three

Chambon et al.

Figure 7. Split-YFP assays in *N. benthamiana* epidermal cells. *N. benthamiana* epidermal cells were coinfiltrated with *Agrobacterium tumefaciens* cultures expressing two complementary YFP fusions (N- or C-terminal truncations, YFPN or YFPC). Nuclei are identified by a constitutively expressed fluorescent nuclear protein (H2B-CFP, here shown in red). The interaction between the two tested proteins revealed a YFP signal (green). For each interaction tested, a negative control corresponding to the coinfiltration of one of the fusion proteins of interest with the complementary YFP moiety fused with an unrelated protein (*Antirrhinum majus* MADS box transcription factor DEFICIENS [DEF] or GLOBOSA [GLO]). The complete set of split-YFP data can be found in Supplemental Figure S8. Bars = 25 μ m.



proteins interact together, and ASY4 is required for normal loading and/or stabilization of ASY1 and ASY3 onto chromosomes. We also found that an ASY4-eYFP fusion protein is axis associated, leading us to conclude that ASY4 is a component of the meiotic chromosome axis.

The link between ASY3 and ASY4 can be viewed as a parallel with those existing between the mammalian SYCP2/SCP2 and SYCP3/SCP3: ASY3 and SYCP2/

SCP2 are large proteins that show limited sequence similarities with the small coiled-coil proteins ASY4 and SYCP3/SCP3, respectively (as an example, SCP3 shows 19% amino acid identity and 47% amino acid similarity with the last 163 amino acids of SCP2); ASY3 and ASY4 interact together (this study) as well as the mammalian SYCP3 and SYCP2 (Yang et al., 2006); all these proteins are axis-associated proteins (Offenberg et al., 1998; Schalk et al., 1998; Yang et al., 2006; Ferdous

et al., 2012; this study). In addition, limited sequence similarities can be detected between ASY3/SYCP2 and the *S. cerevisiae* Red1 axial component (Offenberg et al., 1998; Ferdous et al., 2012). The close interconnection between these proteins and the HORMA domain-containing protein ASY1 in plants (Wang et al., 2011; Ferdous et al., 2012; Lee et al., 2015; this study) and HormaD1 and HormaD2 in mammals (Wojtasz et al., 2009) suggest that, altogether, they form a protein complex crucial for the biogenesis of the meiotic chromosome axis scaffold. Taken together, these data suggest that ASY3/ASY4 are the functional homologs of the mammalian SYCP2/SYCP3. It is interesting that these proteins of the AE as well as those that form the CE of the SC are very poorly conserved at the sequence level but that all show the same structure and assembly characteristics (Fraune et al., 2016). This limited sequence conservation among SC proteins from different species probably is due to rapid sequence divergence, as has been observed for plant and mammalian SC proteins (Ferdous et al., 2012; Fraune et al., 2016).

ASY4 Is Required for Normal Meiotic Recombination

According to chiasma and MLH1 foci counting and to genetic measurement of recombination using FTL lines, CO formation is reduced by a factor of 1.5 in *asy4* mutants. This occurred with a clear decrease in HEI10 and MLH1 foci at late prophase I and diakinesis, showing that ASY4 is required for normal recombination. It should be noted that the CO decrease observed in *asy4* is lower than the one associated with disruption of either of the two ASY4 partners, ASY1 and ASY3. In terms of chiasma level, the *asy1* mutation is the most affected and is epistatic to *asy3* and *asy4*. This suggests that, among the three axis components ASY1, ASY3, and ASY4, the HORMA domain-containing protein ASY1 is a key player, while ASY3 and ASY4 could be seen as accessory proteins. Nevertheless, we cannot exclude the possibility that the partially penetrant phenotype of *asy4* is due to leaky mutations, since we could detect the transcription of the 5' end of the gene in both mutants.

Interestingly, we observed that the decrease in recombination observed in *asy4* mutants is differentially distributed within the genome, since we found that one interval out of four tested (I5b) revealed an increase in CO level (from 16 to 20 cM). This could be related to the distal location of this interval on chromosome 5 and to the observation that the vast majority of chiasma are terminally located in *asy3* and *asy1* mutants (Ross et al., 1997; Ferdous et al., 2012). Two other findings of our study confirm that CO location is modified in *asy4*. First, despite the average decrease in MLH1 foci in *asy4* mutants, we detected an increased number of MLH1 foci per chromosome arm in comparison with the wild type, with up to six foci in the same arm in the *asy4* mutant, while we never observed more than three per chromosome arm in the wild type. Second, we found an IR greater than

1 for one pair of intervals tested by FTL (I5a/I5b). This latter result involves the I5b terminally located interval on chromosome 5, suggesting that the two phenomena may be connected and that, in the *asy4* mutants, COs are not only decreased but also tend to group in the distal parts of the chromosomes. In this regard, it is interesting that we reported recently that, in Arabidopsis as in most species, synapsis is initiated preferentially from the distal parts of the chromosomes (Hurel et al., 2018). If this also is the case in the *asy4* mutants, the limited number of ZYP1-labeled central elements on which recombination events appear to be restricted (according to HEI10 labeling; Fig. 3) are expected to be predominantly distally located. This could explain why we observed a bias in the location of the COs in the *asy4* mutants. Further studies will be required to confirm these observations on a genome-wide scale and to understand the mechanisms involved.

According to our study, the decrease in CO formation measured in *asy4* is not correlated with a decrease in the overall number of early initiation events, since the number of DMC1 and MSH5 foci was unchanged in the *asy4-1* mutant in comparison with the wild type. It is interesting that the role in recombination of the three ASY proteins can be differentiated: ASY1, like ASY4, is not required for normal DSB formation but, contrary to ASY4, is mandatory for the formation of stable DMC1 nucleofilaments (Sanchez-Moran et al., 2007), while ASY3 is required at the step of DSB formation (Ferdous et al., 2012). Chromosome fragmentation was not detected in *asy4*, showing that the DMC1-labeled recombination events are eventually repaired, using either the sister chromatid or the homologous chromosome as a template. Since the number of MSH5 foci at early/mid prophase I appeared normal in the *asy4-1* mutant, it would seem likely that recombination proceeds beyond the initial strand invasion stage. This would imply that CO designation, which occurs in early prophase I (Lambing et al., 2017), is normal in the mutant but that a proportion of the designated intermediates fail to mature into COs, consistent with the observed reduction in MLH1 and HEI10 foci. The defect in SC polymerization observed in *asy4* may result in CO designated recombination intermediates that lie within regions of the homologs that remain asynaptic failing to form COs. Establishing the exact relationship between the loss of ASY4 and the defect in SC formation will be the target of future investigation.

MATERIALS AND METHODS

Plant Materials and Growth Conditions

The *asy4-1* mutant (SK22114, CS1006148) was available in public databases and was provided by the Nottingham Arabidopsis Stock Centre (<http://arabidopsis.info/>; Scholl et al., 2000). The *asy4-2* mutant (line 65433) was identified through a PCR-based screen of the Koncz collection (Rios et al., 2002). Other mutant alleles used in this study are *asy1* (SALK_046272, N546272), *asy3*

Chambon et al.

(SALK_143676, N643676), *dmc1* (SAU_170_F08, N871769), *mer3* (SALK_091560, N591560), *mlh1* (SK25975, N1008089), *msh5* (SALK_026553, N526553), *rad51* (GABI_134A01), and *zip4* (SALK_068052, N568052). Genotyping conditions and primer sequences are given in Supplemental Tables S1 and S2.

Arabidopsis (*Arabidopsis thaliana*) and *Nicotiana benthamiana* plants were grown in the greenhouse (photoperiod of 16-h day/8-h night, temperature of 20°C day and night, and humidity of 70%; photoperiod of 13-h day/11-h night and temperature of 25°C day and 17°C night, respectively).

Clone Construction

ASY4 cDNA was amplified from flower bud cDNA (Columbia-0) after two rounds of nested PCR (PCRI, AtASY4RTF and AtASY4RTR; PCRII, AtASY4attB1 and AtASY4attB2; Supplemental Table S1) and cloned into pDONR207 (Invitrogen) following the manufacturer's instructions. The generated entry vector was sequenced and used to transfer *ASY4* cDNA into the yeast two-hybrid expression vectors pDEST-GADT7 and pDEST-GBK7 (Rossignol et al., 2007). To generate the C-terminal split-YFP clones (Azimzadeh et al., 2008), a version of the cDNA without a stop codon was amplified beforehand using primers AtASY4attB1 and AtASY4-attB2wstop (Supplemental Table S1). Similar approaches were undertaken for *ASY1* and *ASY3* cDNAs except using primers AtASY1-attB1, AtASY3-attB1, AtASY3-attB2, AtASY3-attB2wstop, and AtASY1-attB2 (Supplemental Table S1).

Yeast Two-Hybrid Assays

Yeast two-hybrid assays were carried out using the GAL4-based system (Clontech). SV40 Antigen T and p53 protein were used as positive controls. Yeast plasmids were introduced into AH109 or Y187 strains by lithium acetate transformation following the protocol in the MATCHMAKER GAL4 Two Hybrid System 3 manual (Clontech). After mating in appropriate pairwise combinations, the resulting diploid cells were selected on synthetic dropout (SD) medium lacking a combination of amino acids, driven by the auxotrophy genes carried by the cloning vectors. Protein interactions were assayed by growing diploid cells on SD-LWH and SD-LWA.

BiFC

Protein interactions were tested in planta using BiFC assays (Hu et al., 2002) in leaf epidermal cells of *N. benthamiana* plants expressing a nuclear CFP fused to histone 2B (Martin et al., 2009). For each protein, four expression vectors were produced, generating inactive N and C termini of the YFP (YFP^N and YFP^C) fused with the target sequence in N or C termini. Combinations bringing together the two YFP complementary regions (YFP^N + YFP^C) were coinfiltrated in *N. benthamiana* leaves as described (Azimzadeh et al., 2008; Vrielynck et al., 2016).

Bioinformatics

PSI BLAST on the nonredundant protein sequences database using *ASY3* as a query picked up At2g33793 at the first round of iteration with its C-terminal region (amino acids 636–777), where coiled coils lie (amino acids 625–785, according to Ferdous et al. [2012]). BLASTP and TBLASTN on plant sequenced genomes present in the phytozome 12 database (Blosum45) were conducted to identify homologs.

Recombination Measurement

We used the FTIs described by Berchowitz and Copenhaver (2008) to estimate recombination rates in four different genomic intervals (I5a, I5b, I5c, and I5d). We generated plants that were homozygous for the *quartet* mutation, heterozygous for pairs of linked fluorescent markers RY/+ (I5a and i5d) or YC/+ (I5b and I5c; R = red, Y = yellow, and C = cyan) and either wild type or homozygous for the *asy4-1* mutation. Tetrad analyses were carried out as described by Berchowitz and Copenhaver (2008) on tetrads where each fluorescent marker segregated correctly.

Fluorescent Protein Tagging

The *ASY4* genomic locus, comprising 1,835 bp upstream of the start codon to 502 bp downstream of the stop codon and including all introns and

untranslated regions, was amplified with the primers At2g33793-P9 and At2g33793-P10 (Supplemental Table S1). The eYFP sequence was inserted in frame at amino acid position 202, downstream of the predicted coiled-coil region and close to the C terminus. The construct was inserted into the p35-Nos-BM cloning vector using *Sfi*I sites incorporated into the primers. The resulting expression cassette was subcloned via *Sfi*I into the pLH9000 binary vector and used for *Agrobacterium tumefaciens*-mediated transformation of plants using the floral dip method. Transformants were selected on kanamycin (50 µg mL⁻¹) Murashige and Skoog medium (Murashige and Skoog, 1962).

Cytological Procedures

Meiotic chromosome spreads were DAPI stained as described previously (Ross et al., 1996) or silver nitrate stained as described by Armstrong et al. [2001]. Immunostaining of male meiotic spreads was carried out as described (Armstrong and Osman, 2013; Chelysheva et al., 2013). Antibodies used for immunolocalization were anti-*ASY1* (rat, 1:1,000 dilution; Armstrong et al., 2002), anti-*ATZYP1* (rabbit, N-terminal antibody amino acid residues 1–415, 1:500 dilution; Higgins et al., 2005), anti-*ASY3* (rabbit, 1:250 dilution; Ferdous et al., 2012), anti-*REC8* (rat, 1:250 dilution; Cromer et al., 2013), anti-*DMC1* (rat, 1:20 dilution; Vignard et al., 2007), anti-*MSH5* (rabbit, 1:200 dilution; Higgins et al., 2008), anti-*MLH1* (rabbit, 1:200 dilution; Chelysheva et al., 2013), and anti-*HEI10* (rabbit, 1:250 dilution; Chelysheva et al., 2012).

Image Analysis

asy4-1::ASY4:eYFP zygote male meiocyte nucleus images were captured with a Nikon 90i, 100× objective as a Z-stack. The green channel (eYFP) was processed as an average intensity projection using Fiji, due to more rapid bleaching of eYFP relative to the red (Tx red-*ASY1*) and blue (Alexa350-ZYP1) channels, which were processed as maximum intensity projections. Columbia-0 was imaged using the same exposure times and processed in the same way. MSH5 foci were scored using Z-stack images and Mexican Hat deconvolution as described (Ferdous et al., 2012).

Accession Numbers

Sequence data from this article can be found in the GenBank/EMBL libraries under accession numbers At2G46980 (*ASY3*) and At2g33793 (*ASY4*).

Supplemental Data

The following supplemental materials are available.

Supplemental Figure S1. *ASY4* expression.

Supplemental Figure S2. *ASY4* coding sequence and mutations.

Supplemental Figure S3. A decrease in fertility is associated with *asy4* mutations.

Supplemental Figure S4. Average MCN measured in metaphase I cells.

Supplemental Figure S5. *DMC1* foci formation.

Supplemental Figure S6. *ASY1*, *REC8*, and *SCC3* immunolocalization.

Supplemental Figure S7. *asy4-1* complementation with an *ASY4::eYFP* fusion.

Supplemental Figure S8. BiFC results.

Supplemental Figure S9. Yeast two-hybrid assay results.

Supplemental Table S1. Primer sequences.

Supplemental Table S2. Mutant lines and genotyping conditions.

ACKNOWLEDGMENTS

We thank Christine Mézard for critical reading of the article. We also thank Csaba Koncz and Sabine Schäfer for giving access to the Max Planck Institute for Plant Breeding Research T-DNA insertion mutant collection.

Received December 4, 2017; accepted June 27, 2018; published July 12, 2018.

LITERATURE CITED

- Armstrong SJ, Jones GH (2001) Female meiosis in wild-type *Arabidopsis thaliana* and in two meiotic mutants. *Sex Plant Reprod* 13: 177–183
- Armstrong S, Osman K (2013) Immunolocalization of meiotic proteins in *Arabidopsis thaliana*: method 2. *Methods Mol Biol* 990: 103–107
- Armstrong SJ, Franklin FCH, Jones GH (2001) Nucleolus-associated telomere clustering and pairing precede meiotic chromosome synapsis in *Arabidopsis thaliana*. *J Cell Sci* 114: 4207–4217
- Armstrong SJ, Caryl AP, Jones GH, Franklin FCH (2002) ASY1, a protein required for meiotic chromosome synapsis, localizes to axis-associated chromatin in *Arabidopsis* and *Brassica*. *J Cell Sci* 115: 3645–3655
- Azimzadeh J, Naury P, Christodoulidou A, Drevensek S, Camilleri C, Amouri N, Parcy F, Pastuglia M, Bouchez D (2008) *Arabidopsis TON-NEAU1* proteins are essential for preprophase band formation and interact with centrin. *Plant Cell* 20: 2146–2159
- Berchowitz LE, Copenhaver GP (2008) Fluorescent *Arabidopsis* tetrads: a visual assay for quickly developing large crossover and crossover interference data sets. *Nat Protoc* 3: 41–50
- Blat Y, Protacio RU, Hunter N, Kleckner N (2002) Physical and functional interactions among basic chromosome organizational features govern early steps of meiotic chiasma formation. *Cell* 111: 791–802
- Börner GV, Barot A, Kleckner N (2008) Yeast Pch2 promotes domainal axis organization, timely recombination progression, and arrest of defective recombinosomes during meiosis. *Proc Natl Acad Sci USA* 105: 3327–3332
- Cai X, Dong F, Edelmann RE, Makaroff CA (2003) The *Arabidopsis* SYN1 cohesin protein is required for sister chromatid arm cohesion and homologous chromosome pairing. *J Cell Sci* 116: 2999–3007
- Chelysheva L, Diallo S, Vezon D, Gendrot G, Vrielynck N, Belcram K, Rocques N, Márquez-Lema A, Bhatt AM, Horlow C, (2005) AtREC8 and AtSCC3 are essential to the monopolar orientation of the kinetochores during meiosis. *J Cell Sci* 118: 4621–4632
- Chelysheva L, Gendrot G, Vezon D, Doutriaux MP, Mercier R, Grelon M (2007) Zip4/Spo22 is required for class I CO formation but not for synapsis completion in *Arabidopsis thaliana*. *PLoS Genet* 3: e83
- Chelysheva L, Vezon D, Chambon A, Gendrot G, Pereira L, Lemhemdi A, Vrielynck N, Le Guin S, Novatchkova M, Grelon M (2012) The *Arabidopsis* HEI10 is a new ZMM protein related to Zip3. *PLoS Genet* 8: e1002799
- Chelysheva LA, Grandont L, Grelon M (2013) Immunolocalization of meiotic proteins in Brassicaceae: method 1. *Methods Mol Biol* 990: 93–101
- Cromer L, Jolivet S, Horlow C, Chelysheva L, Heyman J, De Jaeger G, Koncz C, De Veylder L, Mercier R (2013) Centromeric cohesion is protected twice at meiosis, by SHUGOSHins at anaphase I and by PATRONUS at interkinetics. *Curr Biol* 23: 2090–2099
- Ferdous M, Higgins JD, Osman K, Lambing C, Roitinger E, Mechtlar K, Armstrong SJ, Perry R, Pradillo M, Cunado N, (2012) Inter-homolog crossing-over and synapsis in *Arabidopsis* meiosis are dependent on the chromosome axis protein ATASY3. *PLoS Genet* 8: e1002507
- Fraune J, Brochier-Armanet C, Alsheimer M, Volff JN, Schücker K, Benavente R (2016) Evolutionary history of the mammalian synaptonemal complex. *Chromosoma* 125: 355–360
- Higgins JD, Sanchez-Moran E, Armstrong SJ, Jones GH, Franklin FCH (2005) The *Arabidopsis* synaptonemal complex protein ZYP1 is required for chromosome synapsis and normal fidelity of crossing over. *Genes Dev* 19: 2488–2500
- Higgins JD, Vignard J, Mercier R, Pugh AG, Franklin FCH, Jones GH (2008) AtMSH5 partners ATMH4 in the class I meiotic crossover pathway in *Arabidopsis thaliana*, but is not required for synapsis. *Plant J* 55: 28–39
- Hu CD, Chinenov Y, Kerppola TK (2002) Visualization of interactions among bZIP and Rel family proteins in living cells using bimolecular fluorescence complementation. *Mol Cell* 9: 789–798
- Hurel A, Phillips D, Vrielynck N, Mézard C, Grelon M, Christopherou N (2018) A cytological approach to studying meiotic recombination and chromosome dynamics in *Arabidopsis thaliana* male meiocytes in three dimensions. *Plant J* 95: 385–396 10.1111/tpj.1394229681056
- Jahns MT, Vezon D, Chambon A, Pereira L, Falque M, Martin OC, Chelysheva L, Grelon M (2014) Crossover localisation is regulated by the neddylation posttranslational regulatory pathway. *PLoS Biol* 12: e1001930
- Lambing C, Osman K, Nuntasoontorn K, West A, Higgins JD, Copenhaver GP, Yang J, Armstrong SJ, Mechtlar K, Roitinger E, (2015) *Arabidopsis* PCH2 mediates meiotic chromosome remodeling and maturation of crossovers. *PLoS Genet* 11: e1005372
- Lambing C, Franklin FCH, Wang CR (2017) Understanding and manipulating meiotic recombination in plants. *Plant Physiol* 173: 1530–1542
- Lee DH, Kao YH, Ku JC, Lin CY, Meeley R, Jan YS, Wang CJR (2015) The axial element protein DESYNAPTIC2 mediates meiotic double-strand break formation and synaptonemal complex assembly in maize. *Plant Cell* 27: 2516–2529
- Malkova A, Swanson J, German M, McCusker JH, Housworth EA, Stahl FW, Haber JE (2004) Gene conversion and crossing over along the 405-kb left arm of *Saccharomyces cerevisiae* chromosome VII. *Genetics* 168: 49–63
- Martin K, Kopperud K, Chakrabarty R, Banerjee R, Brooks R, Goodin MM (2009) Transient expression in *Nicotiana benthamiana* fluorescent marker lines provides enhanced definition of protein localization, movement and interactions in planta. *Plant J* 59: 150–162
- Mercier R, Mézard C, Jenczewski E, Macaisne N, Grelon M (2015) The molecular biology of meiosis in plants. *Annu Rev Plant Biol* 66: 297–327
- Murashige T, Skoog F (1962) A revised medium for rapid growth and bioassays with tobacco tissue cultures. *Physiol Plant* 15: 473–497
- Offenberg HH, Schalk JA, Meuwissen RL, van Aalderen M, Kester HA, Dietrich AJ, Heyting C (1998) SCP2: a major protein component of the axial elements of synaptonemal complexes of the rat. *Nucleic Acids Res* 26: 2572–2579
- Panizza S, Mendoza MA, Berlinger M, Huang L, Nicolas A, Shirahige K, Klein F (2011) Spo11-accessory proteins link double-strand break sites to the chromosome axis in early meiotic recombination. *Cell* 146: 372–383
- Pattabiraman D, Roelens B, Woglar A, Villeneuve AM (2017) Meiotic recombination modulates the structure and dynamics of the synaptonemal complex during *C. elegans* meiosis. *PLoS Genet* 13: e1006670
- Peltari J, Hoja MR, Yuan L, Liu JG, Brundell E, Moens P, Santucci-Darmanin S, Jessberger R, Barbero JL, Heyting C, (2001) A meiotic chromosomal core consisting of cohesion complex proteins recruits DNA recombination proteins and promotes synapsis in the absence of an axial element in mammalian meiotic cells. *Mol Cell Biol* 21: 5667–5677
- Rios G, Lossow A, Hertel B, Breuer F, Schaefer S, Broich M, Kleinow T, Jásik J, Winter J, Ferrando A, (2002) Rapid identification of *Arabidopsis* insertion mutants by non-radioactive detection of T-DNA tagged genes. *Plant J* 32: 243–253
- Ross KJ, Fransz P, Jones GH (1996) A light microscopic atlas of meiosis in *Arabidopsis thaliana*. *Chromosome Res* 4: 507–516
- Ross KJ, Fransz P, Armstrong SJ, Vizir I, Mulligan B, Franklin FCH, Jones GH (1997) Cytological characterization of four meiotic mutants of *Arabidopsis* isolated from T-DNA-transformed lines. *Chromosome Res* 5: 551–559
- Rossignol P, Collier S, Bush M, Shaw P, Doonan JH (2007) *Arabidopsis POT1A* interacts with TERT-V(18), an N-terminal splicing variant of telomerase. *J Cell Sci* 120: 3678–3687
- Sanchez-Moran E, Santos JL, Jones GH, Franklin FCH (2007) ASY1 mediates AtDMC1-dependent interhomolog recombination during meiosis in *Arabidopsis*. *Genes Dev* 21: 2220–2233
- Schalk JA, Dietrich AJ, Vink AC, Offenberg HH, van Aalderen M, Heyting C (1998) Localization of SCP2 and SCP3 protein molecules within synaptonemal complexes of the rat. *Chromosoma* 107: 540–548
- Scholl RL, May ST, Ware DH (2000) Seed and molecular resources for *Arabidopsis*. *Plant Physiol* 124: 1477–1480
- Snow R (1979) Maximum likelihood estimation of linkage and interference from tetrad data. *Genetics* 92: 231–245
- Snowden T, Acharya S, Butz C, Berardini M, Fishel R (2004) hMSH4-hMSH5 recognizes Holliday Junctions and forms a meiosis-specific sliding clamp that embraces homologous chromosomes. *Mol Cell* 15: 437–451
- Sun X, Huang L, Markowitz TE, Blitzblau HG, Chen D, Klein F, Hochwagen A (2015) Transcription dynamically patterns the meiotic chromosome-axis interface. *eLife* 4: 1–23
- Syrjänen JL, Pellegrini L, Davies OR (2014) A molecular model for the role of SYCP3 in meiotic chromosome organisation. *eLife* 3: 1–18
- Vignard J, Heller I, Candelli A, Davies OR, Peterman EJG, Wuite GJL, Pellegrini L (2017) Single-molecule observation of DNA compaction by meiotic protein SYCP3. *eLife* 6: 1–14
- Vignard J, Siwiec T, Chelysheva L, Vrielynck N, Gonord F, Armstrong SJ, Schöglhofer P, Mercier R (2007) The interplay of RecA-related proteins and the MND1-HOP2 complex during meiosis in *Arabidopsis thaliana*. *PLoS Genet* 3: 1894–1906

Chambon et al.

- Vrielynck N, Chambon A, Vezon D, Pereira I, Chelysheva L, De Muyt A, Mézard C, Mayer C, Grelon M (2016) A DNA topoisomerase VI-like complex initiates meiotic recombination. *Science* **351**: 939–943
- Wang K, Wang M, Tang D, Shen Y, Qin B, Li M, Cheng Z (2011) PAIR3, an axis-associated protein, is essential for the recruitment of recombination elements onto meiotic chromosomes in rice. *Mol Biol Cell* **22**: 12–19
- Wojtasz L, Daniel K, Roig I, Bolcun-Filas E, Xu H, Boonsanay V, Eckmann CR, Cooke HJ, Jasin M, Keeney S, (2009) Mouse HORMAD1 and HORMAD2, two conserved meiotic chromosomal proteins, are depleted from synapsed chromosome axes with the help of TRIP13 AAA-ATPase. *PLoS Genet* **5**: e1000702
- Yang F, De La Fuente R, Leu NA, Baumann C, McLaughlin KJ, Wang PJ (2006) Mouse SYCP2 is required for synaptonemal complex assembly and chromosomal synapsis during male meiosis. *J Cell Biol* **173**: 497–507
- Yuan L, Pelttari J, Brundell E, Björkroth B, Zhao J, Liu JG, Brismar H, Daneholt B, Höög C (1998) The synaptonemal complex protein SCP3 can form multistranded, cross-striated fibers in vivo. *J Cell Biol* **142**: 331–339
- Zickler D, Kleckner N (1999) Meiotic chromosomes: integrating structure and function. *Annu Rev Genet* **33**: 603–754